THE FLOW OF HUMAN BLOOD THROUGH CAPILLARY TUBES WITH INSIDE DIAMETERS BETWEEN 8.7 AND 221 MICRONS

Thesis by

James Henry Barbee

In Partial Fulfillment of the Requirements

For the Degree of

Doctor of Philosophy

California Institute of Technology

Pasadena, California

1971

(Submitted December 11, 1970)

ACKNOWLEDGMENT

Even before I entered Caltech, Professor Cokelet was assisting me by answering my questions concerning placement exams, course work, etc. Since then, he has always been helpful and patient. Special thanks are due to Professor Cokelet for suggesting the subject matter for my thesis and for his help through all phases of the research. Special thanks are also due to each one of my committee members for their instruction in course work as well as suggestions for improving the quality and presentation of my research results. Professor C. J. Pings, my committee chairman, has been of invaluable help in smoothing the path that led to Montana State University. Without his constant attention to the red tape that interfered with an efficient transition, I would probably never have been able to explain why a student at Caltech was living in Bozeman, Montana.

Thanks are also due to the students of Montana State for the never ending flow of blood, and to V. W. Steele, M.D., for removing said blood from its native environment. Radiologist C. E. Taylor, M.D., provided interesting discussions concerning the flow of particulate dyes, used for X-ray purposes, through the human body.

And thanks, of course, to Judy, Minx, Whidby, Bird, Noel, and Buzz. Also JK or KJ, as the case may be.

The government supported the research via Public Health Service Grant HE 12723 from the National Heart Institute, and me, for a time, through an NDEA fellowship.

ABSTRACT

The purpose of this study was to investigate the pressure drop-flow rate behavior of normal human blood flowing through small capillary tubes. A sensitive pressure transducer was used to measure the pressure gradient along an experimental tube when various red cell suspensions passed through glass and plastic capillary tubes. In particular, the effect of capillary tube diameter on the rheological properties of blood was observed for capillary tube diameters from 8 to 221 microns.

For tubes of 221 microns and smaller, it was found that the hematocrit (volume fraction of red cells in a blood sample) of the blood flowing through a capillary tube is less than the hematocrit of the blood in the feed reservoir. The tube hematocrit decreases linearly with the logarithm of the tube diameter at constant feed reservoir hematocrit and for a given diameter tube, increases linearly with the feed reservoir hematocrit.

An equation was developed from data taken in an 811-micron ID tube that allows the shear stress-shear rate relation to be predicted from the tube diameter, tube hematocrit, and the temperature.

It was found that the rheological properties of blood can be accurately predicted from the equation developed if the average hematocrit inside the capillary tube is used as the correct hemato-

crit parameter. A surprising result found is that fluid properties can be predicted for blood flow through a 29-micron ID tube; in such a tube, the equation of motion may not be valid because the "continuous fluid" assumption is not valid. Blood flow data were taken at 98.6°F as well as 73.5°F. Blood heated to 111°F and then cooled to 98.6°F was also investigated.

Blood flow through 15- and 9-micron ID capillaries was investigated. Blood exhibits no yield stress in a 15-micron ID tube because rouleaux formation cannot restrict the flow as it does in larger tubes.

An increased yield stress was found in a 9-micron ID tube. The measured shear stress was only slightly larger (for a given $\bar{U}$) than predicted by the continuum model in both the 15- and 9-micron ID capillary tubes.

TABLE OF CONTENTS

Page

LIST OF TABLES

LIST OF FIGURES

Figure Page

Figure Page

Figure Page

TABLE OF NOMENCLATURE

a	Constant, slope of yield stress-hematocrit correlation
A	Constant in Eqns. (24) and (25), dynes/cm ^{2}
b	Length of a rouleaux, cm
B	Constant in Eqns. (24), (26), and (27), dim.
C	Constant in Eqns. (27), (28), and Table VI, $\bar{U}$ in sec^{-1}
d	Radius of a particle, cm
D	Tube diameter, cm.
e	Exponential function
exp	Exponential function
E	Exponential constant in Eqn. (30)
f	Function
F	Force, dynes
g	Acceleration of gravity, cm /sec^2
G	Constant in Eqn. (30), $\bar{U}$ in sec $^{-1}$
H	Hematocrit (volume fraction of suspended particles)
H_c	Hematocrit below which blood cannot have a yield stress
H_{core}	Hematocrit in the core of a capillary tube
H_d	Hematocrit of the blood discharged from a capillary tube
H_f	Hematocrit of the blood in the feed reservoir
H_r	Tube relative hematocrit, H_t/H_f
H_t	Hematocrit of the blood inside the capillary tube
K	Power law viscosity constant

L	Length of a tube, cm
M	Compliance of a pressure transducer, ml/mm of Hg
n	Exponent in the power law fluid model
n_t	Total number of particles in a suspension
n_o	Number of rouleaux
n_r	Number of red cells in a rouleaux
ΔP	Pressure drop, mm of Hg
Q	Volumetric flow rate, ml/min
r	Length variable in the radial direction, cm
r_y	Radius of a core of packed red cells, cm
R	Radius of a tube, cm
s	Slope of a Casson plot, $(\text{dynes-sec/cm}^2)^{1/2}$
t	Time; sec, min
(U)	Average velocity, cm/sec
$\bar{U}$	Reduced average velocity, tubes diameters per sec, sec^{-1}
V	Internal volume of a pressure transducer, ml
V_a	Axial slip velocity, cm/sec
V_m	Centerline velocity, cm/sec
α	Slope of ln $_w$ vs H plot, dynes/cm^2
β	Intercept of ln $_w$ vs H plot, dynes cm^2
γ	Shear rate, sec^{-1}
γ_w	Shear rate at the tube wall, sec^{-1}
δ	Plasma layer thickness, microns

Ω	Angular velocity of a particle, sec^{-1}
μ	Newtonian viscosity coefficient, centipoise
μ_p	Newtonian viscosity coefficient of pure plasma, centipoise
ρ	Density, gm/cm^3
τ	Shear stress, $dynes/cm^2$
τ_w	Shear stress at the tube wall, $dynes/cm^2$
τ_w^*	Excess wall shear stress, $\tau_w - 8\mu \bar{U}$, $dynes/cm^2$
τ_y	Yield shear stress, $dynes/cm^2$

INTRODUCTION

Physiology of Human Blood and Blood Flow

The primary function of the human circulatory system is to provide the various tissues of the body with nourishment (oxygen, metabolic materials such as sugar and water) and to remove waste materials (carbon dioxide, urea, metabolic by-products). This is accomplished by circulating blood through a closed system of vessels with the heart acting as the pump. The flow of blood is not necessarily constant to all areas of the body, and in fact, the total volume of blood circulated need not be constant.

The ultimate objective of this study was to gain insight into the interactions between human red blood cells in their normal suspending media (plasma) and the relation to blood flow in the human circulatory system. It is expected that the conclusions drawn from the experimental data will be of value to medical science in two areas. First, it is anticipated that the data taken in a capillary viscometer can be correlated with the data taken in the actual human circulatory system. Secondly, the information presented can be used to determine the engineering design of specialized surgical equipment, such as the heart-lung machine, artificial kidneys and artificial hearts.

The research objective of this study was to investigate the rheological properties of normal human blood with a capillary vis-

cometer. The capillary tube diameter range was from the same size as the suspended particles (red blood cells) to approximately twenty-five times the size of the suspended particles. The assumption of a homogeneous, single-phase fluid was expected to fail somewhere within this tube diameter range.

From an engineering point of view, blood can be considered as a suspension of non-spherical, non-rigid particles in a Newtonian liquid. The resulting suspension is non-Newtonian and exhibits a measurable yield shear stress at zero shear rate. The yield shear stress is caused by the interaction between suspended particles. The concentration of the particles is high enough so that interaction among the particles is the same order of magnitude as the hydrodynamic forces acting on the particles.

Composition of Normal Human Blood (10,33,32,108)

Normal human blood consists of three types of suspended particles in a complex aqueous solution (plasma) of inorganic salts and organic macromolecules. The red cells normally occupy about 45% of the blood volume and the other particles together occupy less than 1% of the total blood volume. The three types of particles are the erythrocytes (red cells), the leukocytes (white cells), and the platelets. When considering only momentum transport, the importance of the white cells and the platelets is negligible compared to the red cell, and for engineering measurements, blood can be considered to be a suspension of red cells in plasma.

The Red Blood Cell

The normal human red blood cell (at rest) has the shape of a bi-concave disk with a mean diameter of approximately eight microns, a maximum thickness of two microns, and a minimum thickness of one micron (106). The average volume is about 107.5 cubic microns, and the average surface area is 138 square microns (23). The shape of the undeformed normal human red blood cell is shown in Figure 1.

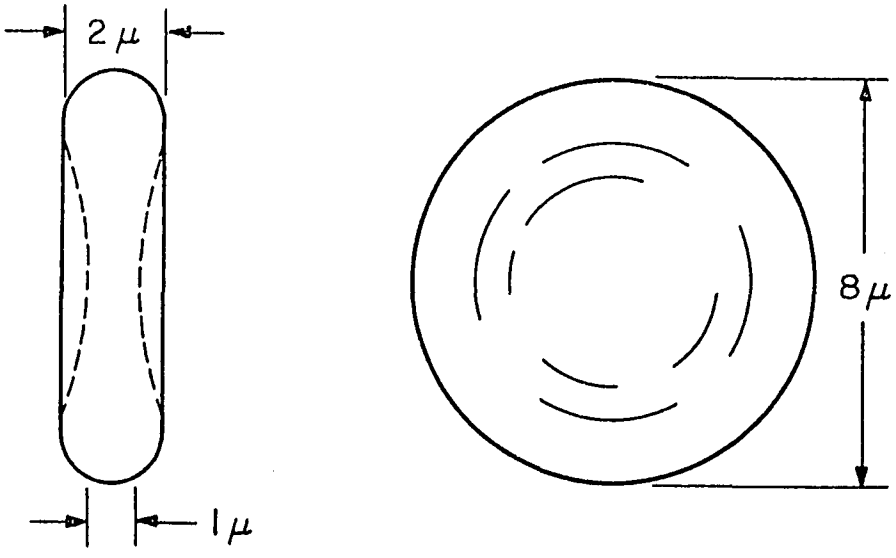

Figure 1. The Human Red Cell.

The human red cell is very flexible, and Figure 1 shows the unstressed red blood cell as found, for example, in stationary blood. During flow it is easily deformed into almost every possible shape, especially in the smaller blood vessels (17,20). The flexibility arises because the red cell is essentially a thin membrane container filled with a fluid.

At sea level, normal blood contains about 5.4 million red blood cells per cubic millimeter in the male and about 4.6 million red cells per cubic millimeter in the female. Thus, the red cells occupy about 47% of the blood by volume in the male, and about 42% by volume in the female. The volume fraction of red cells in blood is called the 'hematocrit', and does not include the volume occupied by the white cells or the platelets. Changes in the hematocrit can occur as the result of external causes (loss of blood due to accidents) and through disease. Low hematocrit, called anemia, can be caused by 1) blood loss due to bleeding, 2) lack of functioning bone marrow, 3) failure of the red cells to mature, and 4) destruction of the red cells, as in sickle cell anemia. High hematocrit, known as polycythemia, can develop in persons living at high altitudes as well as in persons suffering from abnormal red cell forming organs. In disease conditions the hematocrit can vary from 0.10 to 0.75.

The red blood cell is a 'living' cell in that metabolism takes place in the interior and that it does age. The red cell survives for about 110 to 120 days in the normal human. During its lifetime, the red cell is reported to undergo changes in its dimensions, shape, volume, density, osmotic fragility, metabolism, and composition.

At the physiological pH of 7.46, the red cell has a net negative charge (1). Attempts to determine the isoelectric point have been inconclusive, with pH values between 3.6 and 4.7 being reported as well as no measurable neutral point (93). The net negative charge

has been attributed to organic and inorganic components of the red cell membrane. The negative charge is not strong enough to prevent the red cells from sticking together, and in stationary blood the red cells aggregate face to face and form stacks called 'rouleaux'. The red cells in rouleaux are only weakly held together and when the blood is sheared, the rouleaux decrease in length or break up completely. The rouleaux are not rigid and can bend around obstacles without breaking. In stationary blood the rouleaux may contain as many as 30 red blood cells.

An important aspect of the red cell is its ability to respond rapidly to osmotic pressure changes in the suspending media. The red cell membrane acts as a semipermeable barrier to material of high molecular weight and permits the diffusion of low molecular weight substances into and out of the cell. The process is not always one of simple diffusion since the red cell, at equilibrium with plasma at 98.6°F, has a sodium ion concentration about one-tenth that of the plasma and a potassium ion concentration about thirty times that of plasma. Red cells which have been kept at 4°C have an ionic distribution more like the plasma, but when the temperature is raised back up to 98.6°F, the original ionic distribution is again achieved. It seems that some metabolic process is responsible for the rejection of one ion from the red cell and the accumulation of another ion.

The rate of water permeation through the red cell membrane is very rapid, and the lack of osmotic equilibrium between the cell and its environment is corrected within a few seconds. Red cells placed in distilled water burst in about two seconds, and shrinkage can be observed immediately when they are placed in a concentrated salt solution.

Random fluctuation or flickering of the red cell membrane has been reported and this motion has been attributed to either Brownian motion of the molecules in the cell or to metabolic activity of the cell. Neither cause has been specifically demonstrated to be completely responsible, and both sources may contribute to the motion.

The contents of the red cell interior are dissolved in an aqueous medium and include materials which cannot diffuse through the membrane, as well as materials which diffuse easily. Estimates based on the response of the red cell to osmotic pressure changes indicate that the red cell contents are 70% water (62). More recent measurements indicate that the contents are less than 70% water (36). The non-diffusible substances are responsible for many important functions of blood. For example, the hemoglobin molecule is responsible for transporting oxygen. The viscosity of the contents of the red cell has been measured and found to be 6.0 cp at 37°C (36). The hemoglobin solution was Newtonian and this reported viscosity suggests that, contrary to popular belief, blood viscosity is not lowered by packaging the hemoglobin into red cells as compared to a solution of

hemoglobin in plasma capable of transporting the same amount of O_2 or CO_2 as whole blood. The hemoglobin concentration in the red cell is high enough to make its physical state somewhere between a liquid and a crystal (66). Some of the remaining main chemicals inside the red cell and their concentrations are listed in Table I.

TABLE I. LIST OF THE CONTENTS OF THE RED CELL INTERIOR

Reduced Glututhione	1.1 gm/liter of H_2O
Chloride Ion	73 gm/liter of H_2O
Bicarbonate Ion	25 gm/liter of H_2O
Phosphate Ion	0.04 gm/liter of H_2O
Ester Phosphate	0.69 gm as P/liter of H_2O
Sodium Ion	15 gm/liter of H_2O
Potassium Ion	150 gm/liter of H_2O
Water	69 wt.%

These species represent only the most abundant chemicals inside the red cell; many other chemicals are present in trace amounts.

The White Blood Cell

The white cells, or leukocytes, are of five types, including three types of polymorphonuclear cells, monocytes, and lymphocytes. Unlike the red cells, they contain discrete nucleoli. The white cell concentration in an adult is usually about 7,000 per cubic millimeter. The concentration and distribution of white cells can vary

considerably and also rapidly. Hard exercise and even deep breathing can increase the concentration by a factor of six or seven. Tissue damage and certain diseases such as leukemia may cause a 50-fold increase in the white cell count.

The general description of the white cells is that they are easily deformed spheres, approximately 8 to 15 microns in diameter. They are extremely flexible, since they not only squeeze through capillaries which have a smaller diameter than the white cell, but also pass through the pores of the blood vessel walls themselves.

The interior of the white cell is more complex than the red cell interior. The white cell contains a nucleous, ingested particles, and cytoplasm. The inorganic chemical composition of a leucocyte (in millimoles per liter) is: sodium - 113; potassium - 22; calcium - 2; chloride - 70; inorganic phosphorus - 10; bicarbonate - 1.8. The white cell also contains a high concentration of various enzymes. The contents of the white cell have an ionic composition close to that of plasma.

The white cell membrane is even more elastic than the red cell membrane and the white cell can increase in volume up to 1000 cubic microns without any irreversible change in shape. These expanded cells account for the spherical white cells seen rolling along the blood vessel walls in motion pictures of the microcirculation (53). The white cell membrane is hydrophilic (unlike the red cell, which is hydrophobic), and will stick to wettable surfaces.

The Platelets

The third type of particle, the platelet, is an incomplete cell lacking both a nucleus and a clearly defined boundary. The platelets are the smallest of the particles, ranging in size from about one to three microns, and are normally present in the blood in a concentration of about 400,000 per cubic millimeter.

Using phase contrast microscopy, it has been shown that the platelet has many fibrils or spikes projecting from its surface. The formation and destruction of these fibrils is reversible and is dependent on the dissolved carbon dioxide and oxygen content of the platelet environment; high carbon dioxide-low oxygen conditions result in fibril formation, while the reverse conditions cause fibril destruction.

Blood Plasma

When the particles in the blood are removed (as by centrifugation), the remaining liquid is plasma. Blood plasma is usually a clear, straw-amber colored fluid with a pH of 7.46 and a specific gravity of about 1.03. (Note that the red cell specific gravity, 1.10, is larger than that of the plasma, and the red cells have a tendency toward sedimentation). Even though plasma is an extremely complex solution of organic and inorganic substances in an aqueous solvent, it has been found to be Newtonian with a viscosity of about 1.2 cp at 37°C (61,55). Table II lists the more abundant substances in plasma and their normal concentrations.

TABLE II. LIST OF THE MAIN CONSTITUENTS OF BLOOD PLASMA AND THEIR NORMAL CONCENTRATIONS

Proteins - 6.8% by weight

Albumin	3.5 wt %
α-globulins	0.83 wt %
β-globulins	0.89 wt %
γ-globulins	0.70 wt %
Fibrinogen	0.49 wt %

Other Organic Substances (in mg/100 ml of plasma)

Sugar	123	
Urea	22	
Cholesterol	107-320	(194 average)

Inorganic Ions (in mg/100 ml of plasma)

Na^{+}	311-334
K^{+}	13.7-19.5
Ca^{+2}	9.2-11.2
Mg^{+2}	1.22-2.43
Cl^{-}	352-373
SO_4^{-2}	22.1
PO_4^{-2}	13.3
HCO_3^{-}	170

The proteins are large molecules composed of various amino acids. The rate of plasma protein formation by the liver can be extremely high, as great as 100 grams per day. Protein loss can also be large, through severe burns or through kidney disease. Of all the proteins present in plasma, only albumin and fibrinogen have been obtained as pure substances. The other proteins are obtained in groups by fractionation (based on solubility or mobility).

The molecular weights of the plasma proteins range from about 44,000 to over one million. The number average molecular weight (obtained by osmotic pressure measurements) is approximately 85,000 to 90,000 (117). This is because the most abundant protein, albumin, has a molecular weight of about 69,000. Fibrinogen has a molecular weight of about 340,000.

With the exception of fibrinogen, most of the proteins are roughly spherical in shape. The size and shape of the fibrinogen molecule, as determined in the dry state, is unique for plasma proteins and is shown in Figure 2. Electron microscopic studies indicate that fibrinogen has a double-dumbbell shape, with the middle sphere being smaller than the two outer spheres (65).

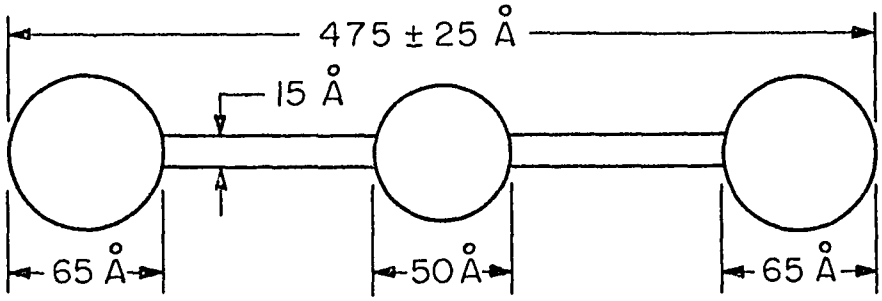

Figure 2. The Fibrinogen Molecule.

An important and sometimes undesirable property of the plasma proteins is their ability to act as surface active agents. Upon reaching a liquid-gas interface, the proteins change their configuration irreversibly, thus changing their physical and chemical properties. This irreversible change (called denaturing) can be detrimental to the human body, for example in the operation of a heart-lung machine, and the free surface must be eliminated in order to preserve the integrity of the blood plasma. When the plasma proteins denature at a liquid-gas free surface, the resulting interfacial film has considerable mechanical strength. Thus, exposing plasma or blood to the air can lead to experimental artifacts in the operation of a capillary or couette type viscometer.

An important physiological function of the plasma is its role in controlling the total volume of blood in the circulatory system (2). The vessels, especially the small capillaries, are highly permeable to water and small ions, and any changes in either colloid or hydrostatic pressure can cause a shift of liquid from the intravascular to extra-vascular compartments. The "law of the capillaries" formulated by Starling (also called "Starling's hypothesis") states that along a length of capillary tubing, the upstream pressure is greater than the total osmotic pressure, thus forcing liquid out of the vessel, but the downstream pressure is usually much lower than the total osmotic pressure, allowing liquid and ions to flow into the vessel. Thus, under normal conditions, the forces tending to

move fluids out of the capillaries equal the forces tending to move fluids inwards; thus a dynamic exchange of fluid between capillary vessel and the surrounding tissue is established.

Behavior of Blood in the Human Body

In the human circulatory system, blood is pumped from the heart through a branching network of vessels; first through the large arteries, then through smaller arterioles, and finally to the capillaries where transfer of material between blood and the other parts of the body takes place. From the capillaries, blood returns to the heart through vessels similar to those on the arterial side, the venules and veins. The arterioles, venules, and capillaries comprise the 'microcirculation'.

The various blood vessels vary greatly in size and construction. In the human circulatory system, the diameter ranges from about 2.5 cm for the aorta to about 5-10 microns for the capillaries. The large vessels are very muscular and are in a constant state of tension, while in the true capillaries elastic tissue is absent from the vessel wall. Except possibly in the venules, flow in the microcirculation is not steady but appears to be continually stopping and starting as valves called precapillary sphincters divert the flow through those capillaries located in areas of highest tissue nourishment demand (144).

Estimates based on microphotography indicate that less than twenty percent of the total capillary system is involved in flow, under resting conditions, at any given time (139). Flow can bypass the capillaries completely and return to the venous blood vessels through shunts.

Flow leaving the heart is highly periodic, and the arteries can be seen to flex in response to pressure changes. The pulsing is damped out when the small arterioles are reached, and periodicity is usually not detectable in the venules. Small pulsations can be found in the arterioles (141,79). Reynolds Numbers based on apparent blood viscosity are much smaller than required to maintain turbulent flow (25).

The pressure drop across the entire human circulation is about 100 mm of Hg, most of which occurs across the arterioles and capillaries (about 80%). The venules and small veins have a pressure drop of about 5-7 mm of Hg. A phenomenon known as 'critical closing pressure' has been observed in the human circulation (63). That is, if the arterial pressure drops below a certain critical value, the flow of blood will stop entirely and remain so until the pressure rises above this value.

Our understanding of the mechanisms of blood flow in the human circulation has been greatly increased by the use of cine-microphotography of anesthetized animal tissue. The motion pictures of the hamster cheek pouch show that there is a great difference between

the type of flow in the capillaries and that in the larger vessels (53). The flow in the capillaries, where the vessel diameter is just slightly greater than the diameter of the red cell, is a 'plug flow' with the red cells passing through in single file. The flow is seen to completely stop at times, and the rouleaux aggregations are easily seen. In the arterioles and venules, on the other hand, a rapidly flowing stream of blood is observed with the individual cells not being distinguishable to the eye. The high-speed motion pictures of Bloch (12), showing this type of flow, reveal that the cells travel as individuals rather than as aggregates, and that the cells tumble about randomly without being oriented in any particular way. The red cells are definitely not seen to remain on streamlines parallel to the vessel wall.

The films of Fulton (50,51,52) also show a phenomenon known as 'plasma skimming'. This effect is sometimes observed when a small vessel branches away from a larger one. The cells, possibly carried by their inertial momentum, will all flow past the junction and remain in the larger vessel, while only plasma, and occasionally platelets, will pass into the smaller side vessel.

A further physiological effect, quite relevant to blood rheology, is also apparent in Fulton's films. If a vessel wall is injured, platelets will aggregate at the point of injury and form a large cohesive mass within a matter of seconds. In fact, such adverse reactions have been observed by merely stroking the tissue

with a micro-needle (145). Such observations suggest that valid pressure measurements cannot be made in the living micro-circulation by the insertion of cannulae. However, advanced techniques have allowed the insertion of 1-5 micron micropipettes into the capillary system. Pressure measurements can be made for a short time, then the capillary tube plugs the micropipette (141,79).

Coagulation

As long as blood remains in the normal circulatory system, there is no tendency for coagulation to occur except at sites of injury. Coagulation is the result of a complex irreversible mechanism. When a substance foreign to blood is present, the platelets burst, releasing chemicals that start a series of chemical reactions which finally convert the protein prothrombin to the enzyme thrombin. The presence of thrombin causes irreversible polymerization of the plasma protein fibrinogen to a solid structural network of fibrin. It has been demonstrated that calcium ions must be present in order for the coagulation mechanism to proceed. Platelets can also cohere and form aggregates. Both types of 'clots', fibrin and platelet, can occur in the living circulation under abnormal circumstances.

The steps involved in coagulation are (33):

1) damage to the blood vessel wall;
2) contraction of the blood vessel;
3) adhesion of platelets to the damaged vessel wall to form a platelet clot (thrombus);

4) formation of a fibrin clot from fibrinogen;

5) shrinkage of the fibrin clot;

6) relaxation of the blood vessel; and

7) final destruction of the fibrin clot after blood vessel repair.

This mechanism is a simplification of the actual situation. Over thirty different substances have been found in blood and related tissues which have an effect on blood coagulation.

When blood is taken from a person or animal, the nature of the surface of the container into which the fresh whole blood is placed considerably influences the rate at which coagulation proceeds. Some evidence exists indicating a non-migratable negative charge on the surface of many materials, including glass (78). This is thought to create a high concentration of calcium ions at the surface and cause coagulation to occur at an increased rate. Siliconized surfaces have been found to be relatively inert toward blood.

Platelet adhesion will occur on any wettable surface but can be prevented by treating surfaces that come in contact with blood in order to make them hydrophobic (by siliconizing). However, when platelets do stick to a surface, they burst and release their contents into the blood.

In order to make valid measurements in experimental apparatus, the clotting tendency must be eliminated. This can be done in three

ways: 1) add one of the various anti-coagulating agents to the whole blood; 2) remove the calcium ions; or 3) remove the fibrin clot after it has formed. When a fibrin clot is allowed to form and then is removed, the physical properties of blood change. Also, the rheological properties of blood change when the fibrinogen is removed (98).

Aggregation of Red Cells

An important property of the red cells is their ability to aggregate in stationary or slowly flowing human blood (33,87,134). Fåhraeus (44) was the first to study this phenomenon and he observed that the red cells aggregate with their flat faces together to form the analogy of a stack of poker chips. Secondary aggregation is also possible, with both rouleaux and single cells combining to produce a three-dimensional network. Normally, in stationary healthy blood the rouleaux may contain from eight to thirty cells, with an average of about fifteen. Their formation is reversible, and they can be broken up under conditions of high shear rate and reformed when flow is stopped (46). Fåhraeus found that albumin acted to prevent aggregation while fibrinogen acted to increase aggregation.

Two important properties of rouleaux formation should be remembered:

1) They occur normally in the living circulatory system and also in experimental apparatus.

2) Unlike coagulation, their formation is reversible and they may be broken up into individual red cells at high shear rate and then reformed at low shear rate.

The Rheology of Human Blood

Early Experimental Work

Possibly the first work done with blood was performed in the 1830's when the French physician Poiseuille considered the flow of blood in the narrow parts of the vascular system (21). As he encountered experimental difficulties with blood, he examined in detail the flow of liquids through small glass tubes (105). Working with aqueous solutions, he developed the famous 'Poiseuille equation' relating flow rate, tube diameter and length, and the pressure drop along the tube. Poiseuille's law can be derived mathematically from the laws of fluid mechanics if Newtonian behavior and steady, laminar flow with no slip at the wall are assumed. Many fluids show excellent agreement with the Poiseuille equation but Poiseuille himself discovered that complex fluids such as blood do not necessarily obey the law that he developed (38).

When workers began to investigate blood with the intention of determining its viscosity, anomalous behavior was found. They used the Poiseuille equation and found that the viscosity was not constant. The flow rate was not proportional to the pressure drop for

a given tube, the flow rate was not proportional to the fourth power of the tube diameter when the pressure drop was constant, and so on. The deviations were most pronounced in small tubes (below 300 microns), and Fåhraeus and Lindqvist (45) found it impossible to make blood flow at all through tubes less than 30 microns in diameter.

It is generally accepted that the non-Newtonian behavior of blood is due to the suspended erythrocytes. The suspending plasma is found to be Newtonian. Experimental artifacts that lead to the apparent non-Newtonian behavior of plasma are discussed by Joly (81) and Cokelet (33). It is also known that the 'apparent viscosity' of blood (defined as τ/γ) increases with hematocrit.

The concepts set forth by Bingham on plastic flow (37,120) raised the possibility that blood has a yield shear stress. The work of Haynes (72,92) has been reported to refute the yield-stress concept. Haynes worked with red cells suspended in a simple saline solution, and recent research has shown that suspensions of red cells in saline solutions do not behave the same as whole human blood (6,7). Bayliss (4) has presented an extensive review of much of the work prior to 1952. An excellent survey of the blood flow literature through 1962 has been published by Whitmore (140), and through 1969 by Fung (54).

Theoretical Models

The model used to interpret the rheological behavior of normal human blood, in the low shear rate region, consists of mutually attractive, flexible, disk-like particles (red cells) suspended in a Newtonian fluid (plasma) of slightly lower density than the particles. Inter-particle forces are hypothesized to exist, and the particles will reversibly aggregate at low shear rates. The aggregates are formed only by joining together the faces of the particles. Figure 3 shows the suggested model. The length of the aggregates

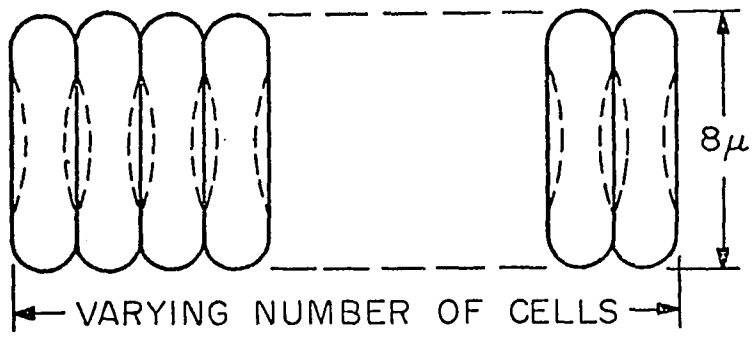

Figure 3. Red Cell Aggregate (Rouleaux).

(rouleaux) varies inversely with the shear rate. The rouleaux are not rigid, but bend with ease when flowing past obstacles. In flowing through a tube, the rouleaux tend to align their long axis parallel to the flow (33). Because of this tendency to align, any three-dimensional network formed when flowing blood is stopped will

differ from a network formed from blood which previously had been subjected to a sufficiently high shear field so that no aggregates could exist. In the first case, the network will be similar to a collection of fibers which are more or less parallel to each other, while the second case will be analogous to a mesh of fibers which are randomly interwoven. In addition, the length of the rouleaux formed while the blood was flowing (and hence the shear rate) will affect the nature of the network. Therefore, the rheological behavior of blood could depend on its prior history, predominantly shear rate, and the direction of stress. A hysteresis effect might be expected such that data taken in the direction of increasing shear rate might differ from data taken in the direction of decreasing shear rate. This has not been found to be the case, and in sufficiently large tubes the shear stress-shear rate relation for blood is unique.

As mentioned previously, the flow properties of blood seem to be a function of the tube diameter, at least in tubes less than 300 microns. Three mathematical models have been proposed to explain the behavior of blood in small tubes. One theory suggests that there is slip at the tube wall (80). A second theory, called the 'sigma effect', postulates a step velocity profile of unsheared laminae of finite thickness (41). The third theory, called the 'axial streaming' or 'radial migration' theory, suggests that the

red cells are drawn into a central core by some hydrodynamic force and are thus surrounded by an annulus of plasma. Maude and Whitmore (90) claim that radial migration can be the result of a mechanical effect, and base their theory on the earlier work of Vand (133). Rubinow and Keller (115) derived an equation for the magnitude of the hydrodynamic force on the particles and found that for a material such as blood, the force is always toward the axis when the blood flows through a horizontal tube. Saffman (116) also found theoretical evidence for a hydrodynamic force normal to the tube axis for the flow of particles in a tube. Goldsmith and Mason (58) predict that particles will migrate only if they are deformable, and found no migration for rigid polystyrene spheres at low Reynolds Numbers but did find migration at higher shear rates. Sutera and Seshadri (129), however, do find radial migration for rigid polyethylene spheres. Also, Segre and Silberberg (122,123) found radial migration using rigid spheres of polymethylmethacrylate, but the particles near the axis migrated away from the centerline while particles near the wall migrated toward the axis. An annulus of particles was eventually formed with clear fluid near the wall and at the tube center.

Axial streaming has also been used to explain the phenomenon called 'plasma skimming' (the decrease in hematocrit often observed in small vessels branching away from larger vessels) (103). It is

claimed that the plasma skimming effect in branching vessels is a direct result of radial migration.

Recent investigations have cast some doubt on the existence of any hydrodynamic radial migration of red cells. Bloch (12), using both regular and high speed microphotography, found that red cells often came into contact with the vessel walls. While regular speed photography indicated streamlined flow and an apparently lower concentration at the wall, Bloch suggests that this is an optical illusion caused by the averaging ability of the human eye. His high speed photography clearly shows that no marginal layer exists.

Bayliss (5) tried to relate changes in concentration with transmittance of light through the tube. Bayliss came to the conclusion that the light transmittance was not as large as would be expected if the red cells had entirely left the tube wall. Bennett (8) has recently reported an experiment in which he caused blood to flow through a rectangular channel and observed the proximity of the red cells to the lower wall by means of an interference microscope. He claims a resolution of 0.04 microns. In this geometry he finds a region near the wall with a reduced concentration but no cell-free plasma zone. He also finds that the majority of cells near the wall are oriented with the flat side parallel to the wall.

Bennett made his observations on the lower surface of a horizontal channel and sedimentation may have affected his results.

Interpretation of Rheological Data

From a force balance on an element of fluid flowing through a circular tube in steady, uniform flow, the shear stress at any point, for a continuous fluid, may be expressed as:

$$\tau_r = \frac{\Delta P r}{2L} \tag{1}$$

In particular, the shear stress at the wall may be expressed as:

$$\tau_w = \frac{\Delta P R}{2L} \tag{2}$$

Equations (1) and (2) are valid whether or not the fluid is Newtonian. Also, for a Newtonian fluid we can note the following relations:

1) $\tau = \mu\gamma$ at any point in the tube. (3)

2) The shear rate at the wall can be written:

$$\gamma_w = \frac{4Q}{\pi R^3} \tag{4}$$

3) Poiseuille's law holds.

4) Velocity profiles are geometrically similar and parabolic.

5) The viscosity coefficient can be written as:

$$\mu = \frac{\tau}{\gamma} = \frac{\tau_w}{\gamma_w} = \frac{\pi \Delta P R^4}{8QL} \tag{5}$$

and is a constant for all experimental values of ΔP, Q, R, and L.

If, for a given tube, the flow rate is not directly proportional to the pressure drop, Poiseuille's law is not being obeyed. The first possibility is that the fluid is non-Newtonian, but that a unique relation exists between the shear stress and the shear rate. That is, $\tau = f(\gamma)$. This can be checked in the following way. For a non-Newtonian fluid, Equation (2) is valid and the shear stress at the wall can be calculated. It can also be shown that if a fluid satisfies the relation $\gamma = f(\tau)$, then:

$$\frac{Q}{\pi R^3} = \frac{1}{\tau_w^3} \int_0^{\tau_w} \tau^2 \, f(\tau) \, d\tau \tag{6}$$

and from Equation (6), the shear rate at the wall can be written as:

$$\gamma_w = \frac{8Q}{\pi D^3} (3 + N) \tag{7}$$

where $N = \frac{d \ln Q}{d \ln \Delta P}$. Thus, if the fluid is indeed non-Newtonian in the sense that the shear rate is a unique function of the shear

stress, then plots of $\gamma_w = \frac{Q}{\pi R^3}(3 + N)$ versus $\tau_w = \frac{\Delta P R}{2L}$ must coincide for all values of the tube radius R; that is, different tube sizes. If the plots do not coincide, then there is no way to calculate the wall shear rate solely from pressure drop-flow rate data. It can also be shown that an equivalent method for testing the relation $\tau = f(\gamma)$ is to plot Q/R^3 versus τ_w, since the integral in Equation (6) is only a function of the limits for any fluid that obeys the relation $\gamma = f(\tau, \text{only})$. These plots should also coincide for tubes of various diameters and lengths (74,84).

If experimental flow curves, plotted as Q/R^3 versus τ_w, do not coincide for tubes of various sizes, and the fluid is a homogeneous fluid (not a suspension), there are two possible explanations for this behavior:

1) There is slip at the wall (112).
2) Thixotropy exists. That is, the shear rate is not only a function of shear stress but also a function of time.

If the Q/R^3 versus τ_w curves do not coincide and the fluid is a suspension, four possible explanations exist:

1) There is slip at the wall.
2) The shear rate is not only a function of shear stress but also a function of time.

3) An anisotropic condition exists due to a plasmatic zone caused by axial streaming. In this case, the shear rate is not only a function of shear stress but also a function of radial position.

4) The flow may be non-homogeneous and not strictly laminar. Due to the presence of solid particles, the idealized analysis of infinitesimal layers sliding over each other may not hold, and the shear stress may not be rigorously expressed by Eqn. (1).

The preceding analysis of capillary flow has assumed that end effects and kinetic energy effects are negligible. These phenomena have been investigated in detail for Newtonian flow (41,42,107) and the appropriate corrections can be made. The corrections that must be applied depend both on the nature of the fluid (127) and the shape of the ends of the capillary tube (9). Both the kinetic energy correction and the end effect correction are negligible if the length-to-diameter ratio of the capillary is greater than about 100. Thus, by making measurements using capillaries of the same diameter but different length-to-diameter ratios, the importance of these effects can be calculated. If plots of Q versus $\Delta P/L$ (or Q/R^3 versus τ_w) are the same for all L/D ratios, then the viscous pressure drop is much larger than losses due to other causes. It is important to remember that when the tube diameter approaches the diameter of the red

cell, the analysis for steady, homogeneous, laminar flow may not be valid. Thus, at some small tube diameter, deviations between Q/R^3 versus τ_w plots are likely to appear, but it can be a mistake to associate the deviation with kinetic energy or end effects.

Blood Suspension Stability

An important aspect of the behavior of human blood that is closely related to its rheological properties is its suspension stability under no-flow conditions. The erythrocyte sedimentation rate (ESR) is widely used in clinical applications and the results have generally been related to the diagnosis of disease or plasma abnormalities (102).

Fåhraeus (43) was the first to examine the factors active in the sedimentation of red cells in plasma. He determined that sedimentation is preceded by aggregation of the individual cells into rouleaux. He also concluded that the aggregation of red cells and the subsequent rate of sedimentation are affected by 1) hematocrit, 2) the type and amount of individual protein fractions in the plasma, 3) the fat content of the blood, 4) the temperature of the plasma, 5) the physical dimensions of the equipment (usually a hollow tube) used for the determination, 6) the degree of deviation of the tube from a vertical position, 7) the anti-coagulant used, and 8) the length of time between withdrawal of the sample and the determination.

In the Rourke-Ernstene method (114) of determining ESR, the sedimentation tube is closed at one end and has a length of 120 mm, and internal diameter of 4.0 mm and is graduated in 2 mm divisions from 0 to 100 mm. The volume of blood used is about 1.2 ml. Heparin solution is used as the anticoagulant, and the test is usually started within six hours after withdrawal from the patient. Observations of the red cell-plasma interfacial height are made at regular intervals during the first hour, and the rate of sedimentation is determined from the steady state slope of the curve relating the interfacial height with time. The normal range is from 3 to 21 mm per hour. Other methods used to measure ESR record the cell-plasma interfacial height only once, at the end of one hour, and thus do not give a true steady state rate of sedimentation.

The sedimentation curve appears to be divided into three sections:

1) An initiation period, where little or no settling is observed. Microscopically, the red cells observed during this period appear to be in the process of aggregation and rouleaux formation.
2) A steady state sedimentation period, when the interface drop per unit time is constant. Rouleaux and aggregates of rouleaux are seen to travel downward, usually with their long axes parallel to the tube. Plasma is

simultaneously displaced upward around the descending red cell structure (93).

3) A leveling-off period, where the sedimentation rate decreases. Here, the influence of the packed cells in the bottom of the tube becomes important, and the sedimentation eventually ceases.

Attempts made to obtain quantitative information on particle size from sedimentation tests usually involve the use of Stokes' equation for the behavior of a sphere in an infinite fluid (44). However, since the normal volume fraction of solids is about 0.45, this model must be modified. Hardwicke (69,70,71) has correlated the sedimentation rate with plasma composition. Using steady state sedimentation rates, he normalized them for differences in specific gravity between the red cell and plasma and also considered the viscosity of the plasma. Hematocrits were constant at 0.30. Using over two hundred separate samples under these controlled conditions, he was able to demonstrate that:

1) A linear relation exists between the steady state sedimentation rate and the concentration of macromolecules, especially fibrinogen.

2) Sedimentation can be positively correlated with plasma viscosity, since an increase in plasma viscosity is usually caused by an increase in

concentration of aggregating macromolecules.

3) The use of a single one-hour observation to measure rates is unreliable and does not correspond well with either the steady state sedimentation rate or protein concentration.

The third observation is most important to any rheological study, and casts doubts on the results of those workers who use the one-hour method to obtain their data.

Effect of Tube Diameter on Blood Rheology

Theoretical Considerations

Rigid Particles

As the diameter of a capillary tube containing flowing blood is decreased, the particulate nature of blood must be recognized. The assumption of a continuous fluid is no longer valid, and the apparent rheological properties of blood may become a function of the tube diameter. Any limiting process such as integration is no longer valid and in fact, the Navier-Stokes equation may not apply to flow in a tube containing particles the same order of magnitude in size as the tube diameter. Numerous investigators insist on solving the equation of motion, neglecting the inertial terms, for the case of spherical particles flowing in a circular tube.

Ladenburg (86), Faxen (47), Bohlin (14), Happel and Byrne (67), and Wakiya (135) have dealt with the case of a single sphere in a circular tube and obtained approximate formulas for the drag. Haberman and Sayre (64) obtained more accurate and extensive results for the drag in this case, and they developed an exact solution in the form of an infinite series of solutions of the slow viscous flow equations.

The interaction between two or more rigid spheres moving in an infinite medium has been treated in a general way by Kynch (85), and Brenner (18) has given some general formulas for drag in multiparticle systems. Happel and Brenner (68) have obtained approximate results for two spheres and also reviewed the work of other investigators. Stimson and Jeffery (126) obtained an exact solution to the problem of two spheres moving with constant velocities along their line of centers. Rubinow and Keller (115) considered the problem of a rotating-translating sphere in an infinite fluid. They derived an equation for the force normal to the direction of translation.

Wang and Skalak (136) considered the problem of an infinite row of rigid spheres moving in a viscous, incompressible fluid bounded by a fixed circular cylinder. Chen and Skalak (26) solved the problem for a line of spheroidal particles. The particles had their centers on the axis of the cylinder and were equally spaced.

It is assumed that the fluid is Newtonian and that the motion is sufficiently slow so that the inertial terms in the equation of motion can be neglected. They derived solutions in the form of infinite series whose rate of convergence depends on the ratio of the particle diameter to the tube diameter. Particle spacing, from adjacent particles touching to a maximum spacing of twenty tube diameters, was a parameter. They found that as the tube size approaches the size of the particle, the pressure drop along the tube becomes infinite.

Bloor (13) computed streamlines and pressure gradients for a line of axisymmetric disks. The disks almost completely filled the capillary tube cross-section. Numerical solutions were obtained for the flow between disks.

These models may apply to rigid particles but certainly do not describe the flow behavior of flexible red cells in a tube. The fact that the red cells can pass readily along capillaries whose diameters are smaller than the red cell's major diameter, and often enter these capillaries through openings even more restricted, shows that the red cells can be easily deformed. Actually, the red cells pass through the capillaries in single file and it seems probable that very little plasma is needed to lubricate their motion, so it should be possible for them to flow in such vessels with relatively little resistance even at quite high concentrations.

Flexible Particles

In photometric studies of red cell motion through capillaries in a cat mesentery, long trains of red cells are seen, with very little space between the cells for plasma (137). In other situations the red cells seem to be individuals with a volume of plasma at least equal to that of the red cell between each pair of red cells.

Benis (6) qualitatively investigated the flow of whole blood through tubes less than 100 microns by visual observation through a microscope. He found that in tubes with inside diameters of about 40 microns, some red cells adhere to the tube wall but the flow could be maintained for long periods of time without plugging. Velocity profiles were very flat for $\bar{U}$'s of the order of 1 sec^{-1}. In tubes with inside diameters of about 10 microns, the red cells passed through the tube in "convoys" separated by clear liquid. The red cell faces were perpendicular to the direction of flow. The "convoys" contained up to 30 cells and all cells in a "convoy" were deformed in the direction of flow, apparently due to viscous drag at the tube wall.

A theory was formulated by Whitmore (142) which applies to capillary tubes approximately 8 to 16 microns in diameter. The theory, based on the earlier work of Thomas (131), incorporates the idea of the red cells forming a semi-solid core when flowing in tubes above about 12 microns and forming an "axial train" when passing

through tubes whose diameter is comparable to the dimension of the cell. The theory predicts that blood should exhibit a minimum hematocrit (and therefore a minimum apparent viscosity) when flowing through a vessel with a diameter between 8 and 16 microns. One important implication of the theory is that the mean velocity of a red cell is inversely proportional to its diameter--large red cells move more slowly. In humans, 5% of the red cells vary in diameter by more than 1 micron (142) and there are also variations in flexibility. Thus, this mechanism may explain the fact that in small vessels the red cells usually travel as groups of 10 or more instead of as individuals. In a small vessel, explains Whitmore, large or rigid cells will travel more slowly than average cells. The small cells will try to travel faster than the average cells, so that groups of cells headed by a large or rigid cell and tailed by a small cell should break up into separate groups.

When blood flows through capillaries that have an inside diameter less than 8 microns, the red cells must be deformed in order to pass through the tube. In tubes with inside diameters between 8 and about 16 microns, the red cells will deform due to viscous stresses. In both cases the magnitude of the deformation of a red cell should depend on the magnitude of the viscous stresses, and therefore on the velocity or pressure gradient in the tube. The shape of a red cell will depend on the velocity in the tube, and

since the additional pressure drop due to the particle depends on its shape, the shear stress-shear rate relationship may depend on tube diameter as well as shear rate. Again, such a dependence does not clearly prove that the continuum model has failed.

A theory of flexible particles was developed by Lighthill (89), based on lubrication theory and a linear shear stress-strain relationship for the red cell membrane. The theory was improved quantitatively by Fitz-Gerald (48,49). In lubrication theory, the Reynolds Number based on film thickness is assumed small enough so that the inertial terms in the equation of motion can be neglected. The other approximations are those of boundary-layer theory. The pressure is taken to depend on the axial coordinate only and does not vary across the layer. Also, the lubrication film thickness is taken to be much smaller than the reference radius so that a two-dimensional cartesian coordinate system can be used.

The following results were found. The increased pressure per red cell varies as the square root of $\bar{U}$, not as $\bar{U}$ in the Stokes equation. Another result is that at very low velocity the clearance between the red blood cell and the capillary wall would become small enough so that the lubricating layer would break down and the red cell would come into direct contact with the wall. Any further motion of the red cell would be impeded by static or dynamic friction.

Fitz-Gerald (49) implies that the Fåhraeus-Lindqvist effect should occur down to capillary diameters of about 15 microns, then the viscosity should increase slightly from 15 down to 9 microns and then increase rapidly for capillaries less than 9 microns in diameter. Whitmore's theory (142) also predicts a decrease down to 15 microns ID, but then a very sharp increase below 15 microns.

Dintenfass (40) measured the apparent viscosity of blood flowing through a parallel plate viscometer and found that the viscosity decreased with decrease in plate spacing down to 12 microns. Then the viscosity increased gradually down to 10 microns and reached very large values below 8 microns. These results illustrate both Whitmore's and Fitz-Gerald's results and the effective seize-up below about 8 microns is also in accord with the predictions of lubrication theory. However, it is not at all clear that measurements made with a parallel plate viscometer concerning red cell deformations apply at all to the case of circular tube capillary flow. In fact, Prothero and Burton (111) found that the viscosity of blood in small capillaries is only slightly (30%) greater than that of plasma alone. Their capillaries were between 5.0 and 8.4 microns in ID. However, the flow velocities ($\bar{U} \approx 30{,}000$) were so large that red cell deformations may have been very large. In this case, the true ratio of tube diameter to red cell diameter may have been about 2.0 and this implies flow through tubes with a 16 micron ID.

These results are in agreement with Whitmore's theory for tubes of this size.

Although this analysis of lubrication breakdown is for tubes smaller than the red cell, any time a rouleaux or three-dimensional network is established that is larger than the tube diameter, lubrication could break down. It does not seem reasonable that this static friction could be responsible for the yield stress in, say, a 1000 micron tube, but in small tubes, 20-50 microns, perhaps this mechanism is involved in the magnitude of the yield stress.

The shapes of the deformed red cells predicted by lubrication theory are in agreement with those observed in small living capillaries (124). One main deficiency of the lubrication theory treatment of red cell motion in small capillaries is that the theory makes no attempt at conserving either the volume or the surface area of the red blood cell. These are known to be important constraints (23).

No theory more exact than lubrication theory (for 2 to 8 micron tubes) or Whitmore's "axial train" model (for about 9 to 12 micron tubes) is available for predicting shear stress-shear rate behavior for blood flow through small tubes.

When red cells flow in single file, with an appreciable plasma gap between them, the flow pattern in the plasma is probably in the form of a translating vortex, as shown in model experiments by

Prothero and Burton (109). Figure 4 shows a schematic drawing of vortex flow between two moving erythrocytes in a capillary.

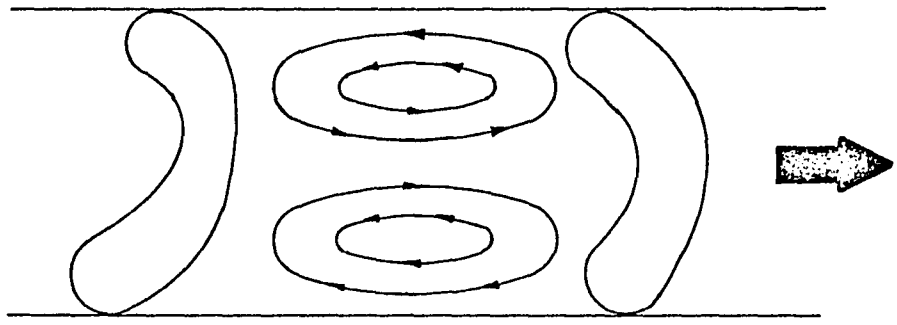

Figure 4. Vortex Flow Between Two Moving Erythrocytes.

In some situations the red cells appear to travel as essentially undeformed bi-concave disks with their axis of symmetry along the axis of the tube, while in other situations they assume various deformed shapes. Regardless of their deformed shape, there appears to be a thin film of plasma at the wall lubricating the moving cells. The plasma film between the red cell membrane and the vessel wall will be highly sheared and will probably account for most of the frictional resistance.

The intimacy of the contact between the vessel wall and the red cell membrane will be quite different in capillaries which are larger in diameter than the major diameter of the red cell, and those capillaries so small that the red cell must be deformed in order to pass at all.

The vortex flow between the cells is probably far more significant in heat and mass transfer processes than in flow resistance. The additional 'stirring' mechanism brings fluid from near the vessel wall to the red cell membrane, which will facilitate exchange. Prothero and Burton (109) have shown that diffusive exchange from the wall to the fluid can be significantly increased by the vortex flow between cells. Their work was done at fairly large Reynold's Number ($Re \approx 10$), and it has since been shown (3) that at the small Reynolds Numbers encountered in the microcirculation, ($Re \approx 10^{-3}$), plasma mixing is insignificant.

The various theories, both for solid and flexible particles, apply to tubes only about 7 to 10 microns in diameter. The theory of Whitmore (142) applies up to approximately 16 microns. There is very little work being done in the range between about 16 microns and where the continuum model fails. Brenner (19) has considered the rheology of two-phase systems in general, and has included the case of suspensions of solid particles in which there are sufficiently large numbers of particles so that it is reasonable to define macro continuum variables in terms of integrated averages over micro continuum variables. For example, the micro velocity field is the detailed velocity in the vicinity of a single particle. The macro velocity is an average velocity over a volume that contains many particles. It is shown that the mean speed of rotation of the

particles is the same as the local macroscopic fluid rotation. This is not true, however, if an external field exerts couples on the particles. This is the case for blood flow, and a micro rotation that is different from the macro rotation is incorporated into so-called micro polar fluid theories. A discussion of polar theories is given by Skalak (125) and the application to blood flow is included. Skalak points out that experimental findings and polar theory predictions do not agree.

Since it is believed that the measured yield stress of blood is due to reversible aggregation of the erythrocytes, there is almost certainly a tube diameter size below which the aggregates will have to be broken apart before the red cells enter the tube. Thus, it is quite possible that in capillary tubes below a certain diameter, the yield stress will depend more on the membrane-wall friction than on the formation of aggregates. In tubes just slightly larger than the red cell major diameter, the red cells will have to flow through the tube in single file. In such a tube the red cell membrane would not be touching the wall, but no red cell aggregates could form due to the small size of the tube. Thus, it is entirely possible that in a tube of this size, blood will not have a yield shear stress. However, the aggregates formed in the feed reservoir will have to be broken apart before the red cells can enter the tube and this will represent an increased pressure drop across the tube. At best, the

strength of the aggregate could be measured, but at worst, (and most likely), it would be impossible to correctly analyze the data.

Experimental Investigations

Large Scale Models

The only presently published works pertaining to flow through the capillaries has been performed on model experiments. Sutera and Hochmuth (128) considered the general problem of quantitative analysis of the dynamics of flow through the microcirculation, and performed the analysis on simplified, large scale hydrodynamic models.

When simulated red cells flowed through a tube only slightly larger than the cell, two distinct orientations of the cell were found.

1) The concave faces were normal to the direction of flow.
2) The concave faces were parallel to the direction of flow.

Orientation 1) was called 'normal' and 2) was called 'edge on'. The pressure drop measurements showed that a discoid moving 'edge on' through the tube involved an increase in pressure drop which was much less than that associated with 'normal' motion of the same discoid. The 'edge on' configuration was preferred, but as the con-

centration of cells increased, the 'normal' configuration was the only one possible. Closely packed groups of cells were found to cause 30 to 40% less additional pressure drop than the same number of cells widely spaced but all in the 'normal' orientation. Cells spaced more than approximately one tube diameter apart do not interact. The additional pressure drop due to a succession of non-interacting cells is equal to the sum of the additional pressure drop due to each individual cell. Lee and Fung (88), using 4.29 cm diameter, thin walled, bi-concave rubber cells filled with silicone oil, found that in tubes larger than the cell (4.37 and 5.03 cm diameter), the cell travels in an 'edge on' orientation and that the trailing edge of the model cell buckles inward at high velocity. In tubes of 2.54, 3.15, and 3.81 cm diameter, the deformation of the model cell resembles some of the deformation patterns observed in the living circulation. The additional pressure drop due to the presence of the cell is not a linear function of velocity as predicted by the Stokes creeping flow theory for rigid particles. The additional pressure is proportional to the square root of velocity as predicted by Lighthill's (89) theory. Skalak and Branemark (124) studied cell deformation in living tissue and both the above studies indicate that the red cell deforms in the 'edge on' orientation and not in the 'normal' orientation as previously supposed.

Blood Flow Through Small Tubes

Fåhraeus and Lindqvist found that the apparent viscosity of whole blood flowing through tubes less than about 300 microns in diameter is less than that for larger tubes, and the apparent viscosity continues to decrease as the tube diameter decreases. Later, Fåhraeus measured the hematocrit inside capillary tubes from 50 to over 250 microns in diameter and found that the hematocrit inside the tube was lower than in the feed reservoir; the smaller the tube, the lower the hematocrit inside the tube. Hochmuth and Davis (75) also measured the hematocrit inside experimental capillary tubes and found that the hematocrit inside the tubes was less than in the reservoir, but the decrease was not as large as Fåhraeus found.

It was supposed that the decrease in apparent viscosity could be due to the reduced hematocrit inside the capillary tube, and Cokelet (34), using Fåhraeus' and Fåhraeus and Lindqvists' data, demonstrated a direct correlation between the hematocrit inside the tube and the apparent viscosity.

APPARATUS AND PROCEDURE

Pressure Drop-Flow Rate Capillary Viscometer

Description

The apparatus used to measure the pressure drop-flow rate relations for various liquid samples is shown in Figure 5. The apparatus consists of two reservoirs interconnected in parallel by the experimental capillary fiber, and the pressure measuring device (Sanborn transducer-models 267BC and 268BC). A description of the components follows:

1) Experimental Fiber: The capillary fiber of interest was either mounted in 5/20 male standard taper ground-glass joints by using epoxy cement, or machine ground on both ends to make a 5/20 male standard taper.

   In order to use thin-walled, flexible glass fibers, it was necessary to mount them in specially constructed fittings. The fittings were prepared by cementing two 5/20 ground-glass male joints, each about five inches long, onto a 1x3-inch glass slide about 1 mm thick. A space of about one inch was left between the ends of the 5/20 fittings to allow a microscope objective to come into close

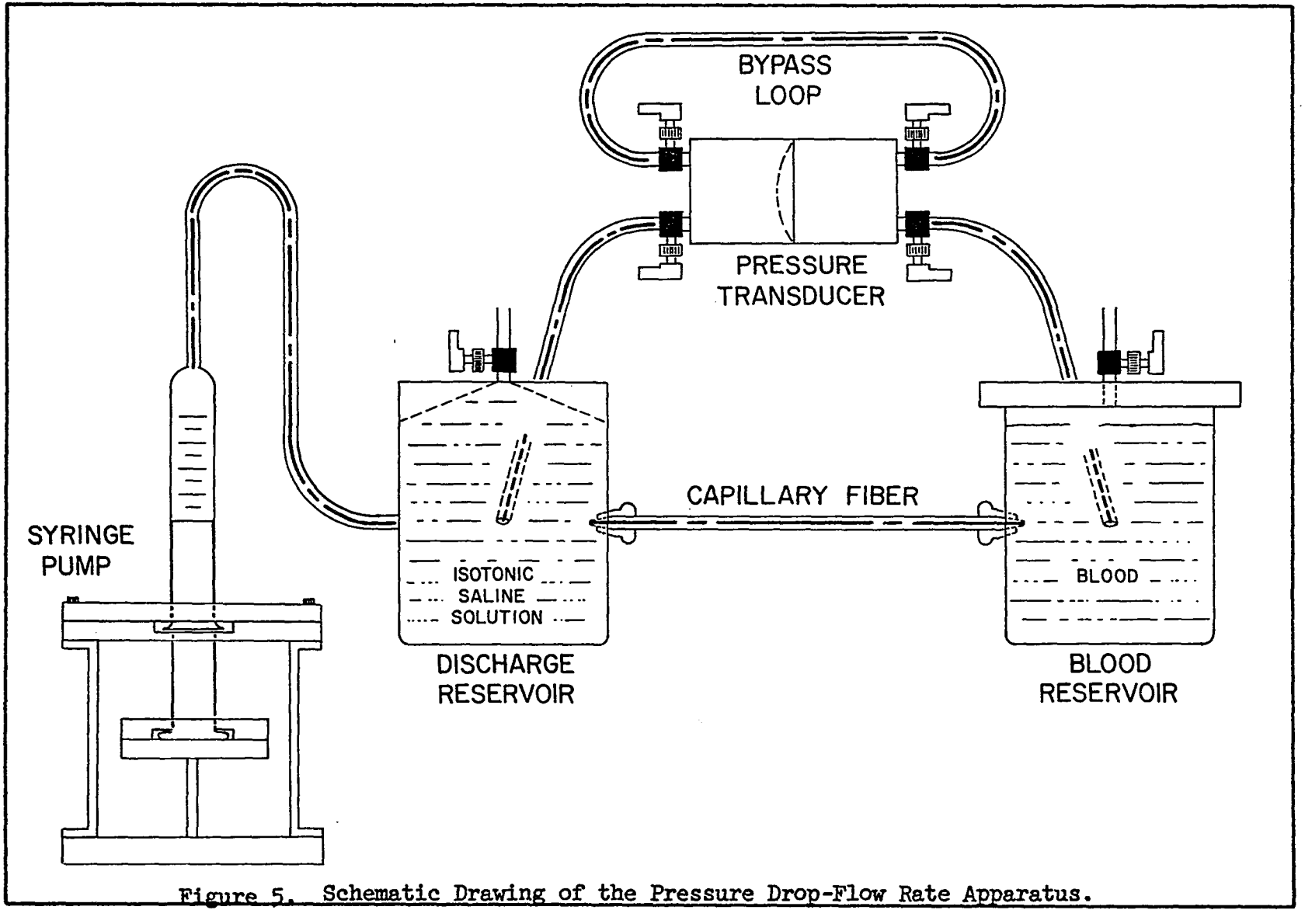

Figure 5. Schematic Drawing of the Pressure Drop-Flow Rate Apparatus.

proximity to the experimental fiber. The glass fiber was then placed in the special fitting and cemented at both ends. The ends of the capillary tubes were then squarely cut with a razor blade. It was found that the razor blade could only be used once. Using a dull blade results in tubes that are pinched closed at the end. After a sharp razor blade was used, the tube was carefully examined and it was noted that the ends were open, circular, and squarely cut. It appeared that the capillary tube was circular in cross-sections. The fiber was then placed across the microscope stage and held in place by 5/20 female standard taper ground-glass joints cemented in the blood and discharge reservoirs. The dimensions of the experimental fibers used in this study are shown in Appendix B.

2) Blood Reservoir: At the high pressure end of the capillary fiber is a machined Lucite reservoir of about 40 ml capacity. Connection to the fiber is accomplished by a 5/20 female ground-glass joint, positioned in such a fashion that the fiber tip extends well into the blood reservoir, thus assuring,

as much as possible, uniformity between the blood in the reservoir and that entering the fiber. A machined cap of Lucite fitted with a two-way valve (Hamilton Company) provides a cover for the blood in the reservoir.

3) Discharge Reservoir: At the low pressure discharge end of the capillary fiber is a machined Lucite reservoir of about 40 ml capacity. Connection to the fiber is accomplished by a 5/20 female ground-glass joint. The discharge reservoir is fitted with a two-way valve (Hamilton Company) and is designed to allow the removal of all air bubbles when filling with an isotonic saline solution. The discharge reservoir is also connected to the syringe pump via teflon tubing.

4) Transducers: Connections from the machined Lucite reservoirs to the transducer are made with 0.076 inch ID teflon tubing with female Luer fittings on both ends (Hamilton Company).

The transducers used (interchangeably) are Models 267BC and 268BC Sanborn bi-directional differential pressure transducers, both operating on a differential transformer principle. The use of

two transducers (one at a time) allows a larger range of experimental pressures to be measured with a minimum of uncertainty. The transducer being used for a given experiment is coupled with a Model 311A transducer amplifier/indicator (Sanborn Division/Hewlett Packard Company) which has an output to an external recorder. A V.O.M.-5 recorder (Bausch and Lomb Company) is used to make permanent pressure-time recordings. The 311A amplifier contains an eight-position attenuator: x 200, 100, 50, 20, 10, 5, 2, 1; and at x 1 gives a full scale meter reading of about 0.4 mm of Hg for the 268BC transducer.

The transducing element of both transducers is a hollow metal bellows, indicated in Figure 5 as a plane diaphram. The bellows is completely filled with, and immersed in, an isotonic saline solution, so that there is a gas-free liquid connection on both sides of the bellows. Since the connecting lines are also filled with isotonic saline solution, surface tension effects are eliminated, and there is a gas-free liquid connection

between both ends of the experimental capillary fiber and the transducing element.

An additional feature of the transducer circuit is a saline filled loop that can be used to connect both sides of the bellows. The loop is used to 1) balance the transducer to find the zero point, and 2) equalize the pressure in both reservoirs. When the saline-filled lines that connect the reservoirs to the transducer are disconnected by closing the appropriate valves, and the valves connecting the loop to the transducer are opened, saline will flow through the loop until the pressure on both sides of the bellows is the same. Thus, the zero point can be determined. Then, if while the loop is open, the valves connecting the reservoirs to the transducer are opened, and the loop closed, the transducer should still read zero; the discharge reservoir is completely closed and no liquid can leave or enter this reservoir until the syringe pump is activated.

Both the 267BC and the 268BC transducers were calibrated against a National Bureau of Standards secondary reference pressure measuring instrument

(Texas Instrument Company). The 267BC transducer was found to be nearly linear over the entire range of 0-400 mm of Hg. The 268BC transducer was also found to be nearly linear over its entire range of 0-40 mm of Hg. Using the calibrated transducers, and distilled water, the inside diameter of a number of experimental tubes was calculated from experimental data and Eqn. (8). The tube diameters varied from 59 microns to 811 microns. The values of the tube diameter calculated from Eqn. (8) were then used in Eqns. (12) and (13) to determine the $\tau_w - \bar{U}$ relation using water as the experimental fluid. The results are plotted on log-log paper and shown in Figure 6. The solid line is the theoretical relation for water at the experimental temperature. This plot gives an indication of the expected accuracy of the experimental apparatus. The pressure readings are considered accurate to within $\pm$ 0.5%. The rotation of the stirring bar had no effect on the pressure drop-flow rate relation for water.

An important point that has been ignored by other workers using capillary viscometers similar

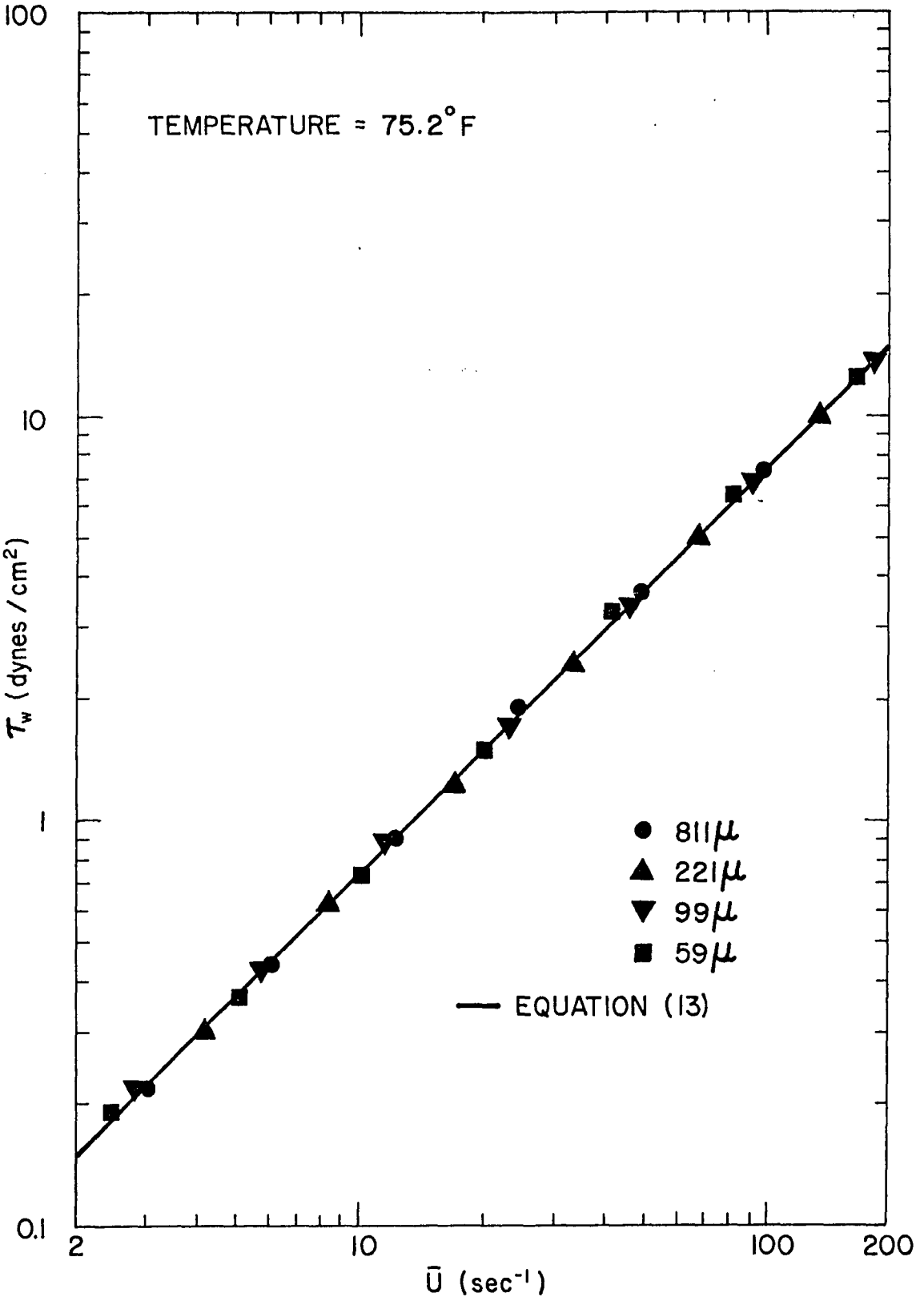

Figure 6. τ_w - $\bar{U}$ Plot for Distilled Water, Various Tube Diameters

to the one described here is that, since there is a blood-saline interface in the tube connecting the blood reservoir to the transducer, and since blood exhibits a yield stress (and therefore a yield pressure), the pressure drop measured by the transducer across the capillary fiber may be erroneous. When the flow is started, liquid goes through the connecting tubes in order to displace the transducer bellows until a steady state pressure is reached. Only after steady state is reached, will all the flow go through the capillary fiber. However, the pressure in the blood reservoir can be higher (by an amount equal to the yield pressure) than the pressure in the line connecting the blood reservoir to the transducer. A calculation shows that for the connecting tube used in the apparatus described above, the yield pressure, about 10^{-4} mm of Hg, is negligible compared to the pressure drop across a typical capillary tube (about 1 to 300 mm of Hg.)

5) Syringe Pump: The discharge reservoir is also connected, via a teflon tube, to a variable speed syringe pump of special design. The drive unit of the pump

consists of a precision-machined lead screw, which translates by means of a rotating nut assembly. The plunger of an appropriate syringe is firmly attached to the end of the lead screw.

The lead screw is driven, via the rotating nut assembly, by a reversible synchronous motor, through a gear train. A gear box knob allows the selection of ten steps of reduction covering a range of 512 to 1. Table III gives the ten steps of reduction.

TABLE III. GEAR TRAIN SPEED REDUCTIONS

1.0	0.25	0.0625	0.1562	0.00390
0.5	0.125	0.03125	0.00781	0.00195

A gear reduction of 1 corresponds to a linear velocity of 0.3214 in./min for the lead screw. Both infusion and withdrawal modes are possible, and numerous flow rates can be obtained by using the proper size syringe and lead screw velocity.

6) Syringes: Four syringes of different capacities are used interchangeably in the apparatus, with a volume range of 1 microliter to 20 milliliters. The syringe specifications are shown in Table IV.

TABLE IV. SYRINGES USED IN THE PRESSURE-FLOW APPARATUS

Syringe	Capacity	Flow rate at a gear train speed reduction of one
A	20 ml	2.447 ml/min
B	500 μl	6.90×10^{-2} ml/min
C	50 μl	6.90×10^{-3} ml/min
D	1 μl	1.44×10^{-4} ml/min

Syringes A and B were calibrated, at a reduction of one, by weighing the volume of mercury discharged during a given time interval. Syringes C and D were calibrated from the manufacturers' graduations. The flow rate range is from 2.447 ml/min. (Syringe A at a reduction of 1.0) to 2.8×10^{-7} ml/min. (Syringe D at a reduction of 0.00195). Note that the lowest flow rate is equivalent to about 3 drops per year!

7) Magnetic Stirring: Three different sizes of teflon-coated alnico magnets are used interchangeably and located at the bottom of the blood reservoir. The magnetic stirring bar in use is rotated by a Thomas Magnetic Stirring Motor located

underneath the blood reservoir. The rotational speed is controlled by a Variac variable voltage unit and was maintained at about 200 rpm.

8) Temperature Regulation: The entire apparatus is securely fastened to an aluminum plate, and the plate is bolted to a 4000-pound cement block. The block is supported by three neoprene rubber mounts, each loaded at 1000 pounds per square inch. The entire apparatus is also covered by a plexiglass enclosure. Located in the plexiglass enclosure is a Ronson Escort hairdryer of 345 watts capacity, which acts as a heater. The output of the heating unit is controlled by a Variac variable voltage unit, and the temperature inside the enclosure can be varied from room temperature (70°F) to over 110°F. The temperature can be regulated to within $\pm$ 0.2°F and determined by thermometers to within $\pm$ 0.05°F.

9) Microscopic Observations and Photography: An American Optical Series 10 microscope with a 35 mm camera is located between the reservoirs and allows direct observation of the experimental capillary fiber. The microscope is mounted such that both horizontal and vertical views of the fiber are possible. The micro-

scope stage serves as partial support for the experimental capillary fiber.

Operation

The apparatus described above normally requires a sample size of about 20 mls. Capillary fibers are easily interchanged, allowing several tubes to be used with a given sample of blood. The procedure for obtaining pressure drop-flow rate relations for a given blood sample is as follows:

1) The discharge reservoir, syringe pump and connecting line are filled with an isotonic saline solution. The transducer and lines connecting it to both reservoirs are also filled with isotonic saline. The blood reservoir is then filled with blood, and by manipulating an external syringe, a small portion of blood is drawn into the line connecting the blood reservoir to the transducer. The blood-saline interface in the connecting line is carefully checked to make certain that no air is in the connecting line. The magnetic stirring bar is then activated.

2) The transducer loop is then opened, and the output meter on the Sanborn 311A amplifier is zeroed together with the pen on the external recorder (V.O.M.-5).

3) The transducer loop is then closed, the lines connecting the reservoirs to the transducer opened, and the amplifier checked to be certain that the output is still zero. The syringe pump motor is then turned on, withdrawing blood from the blood reservoir through the experimental fiber, and into the discharge reservoir. When steady state is achieved, no flow occurs through the transducer circuit, and the meter reading (and chart recorder reading) represent the frictional pressure drop due to blood flow through the fiber.

4) This procedure is repeated for various pump speeds, hematocrits, and capillary fibers. After a run is completed, the sample is removed and the system washed in distilled water and air dried.

The experimentation is conducted at room temperature, and at normal body temperatures. The blood was analyzed by standard clinical methods and each sample of blood was found to be "normal" with respect to plasma composition, hematocrit, and red cell size and shape. The sodium chloride concentration of the salt solution was adjusted in order to insure that the osmotic pressure of the isotonic saline solution was the same as for the blood plasma.

The osmotic pressure of liquid samples (usually blood plasma or isotonic saline solution) was determined by measuring the freez-

ing point depression capability of the dissolved solute in an aqueous medium. The sample was placed in a special glass tube, supercooled to about 2°C below its freezing point, nucleated, and the equilibrium temperature of the ice-liquid mixture determined. The freezing point depression was determined with an "Osmette" precision osmometer (Precision Systems). It consisted of the following units:

1) A thermoelectric refrigeration unit which maintained an ethylene glycol-water mixture at approximately -6°C.
2) A thermistor probe unit which allowed measurement of the equilibrium freezing point of the sample to within $\pm$ 0.001°C.
3) A Wheatstone bridge and meter assembly. Coupled with the thermistor probe, this section allowed following the temperature decrease of the sample into a supercooled region and determination of the freezing point after nucleation.

The above units were assembled together with controls for calibration and mechanical means for stirring and nucleating the sample.

Approximately 2 ml of sample was required for each determination, and at least two samples were used to determine the osmotic pressure of the test liquid. The reproducibility was better

than ± 0.5 milliosmole; where a milliosmole is the change in ionic concentration required to cause a change of 0.001858°C in the freezing point of pure water.

The percent transmittance of 424 millimicron light that passed through hemolysed blood contained in special cuvettes was measured by a Coleman 6A Spectrophotometer (Coleman Instruments). The spectrophotometer incorporated a sensitive galvanometer that allowed precision to ± 0.5% of full scale. The spectrophotometer was calibrated at 610 millimicrons using a Didymium calibrating standard. The cuvettes required a sample volume of 1.8 mls and when a special adaptor was inserted in the cuvette, as little as 0.7 mls was required.

Measurement of Experimental Fibers

The ends of all capillary fibers are cut squarely, and their length measured with a steel rule to within ± 0.2 mm. The length of a typical fiber is about 12 inches. The fiber end is observed under the microscope to be certain that the end is not plugged with debris, and that the end is not pinched closed. The glass fibers were made by a high speed continuous drawing technique that can produce constant bore, cylindrical tubing to within ± 1%. The axial variation in internal diameter found by microscopic observation was at most 1 micron for the largest tube and probably much less, but it was impossible to measure closer than 1 micron through the microscope.

The average inside diameter of a fiber is calculated from Poiseuille's law, using distilled water as the calibrating liquid. Viscosity values for water at the various experimental temperatures are obtained from standard literature sources (77). Poiseuille's law, in terms of the units used in this study, is:

$$D^4 = 5.11 \times 10^{-6} \frac{Q\mu L}{\Delta P} \qquad (8)$$

where

D [=] cm
Q [=] ml/min
μ [=] centipoise
L [=] cm
ΔP [=] mm Hg

The value of D obtained from Equation (8) can be considered to be an average value, since the flow of a Newtonian fluid through a straight tube of elliptical cross-section also obeys Poiseuille's law (74).

The inside diameter of the 811 micron tube was also measured by filling the tube with mercury, then weighing the amount of mercury required to fill the tube. From the density of mercury, the average diameter by the mercury technique was calculated to be 811 microns.

For tubes less than 29 microns, it was found that the temperature could not be controlled closely enough to obtain a steady

state reading over a long period of time. With a very small tube, for instance, 10 microns, the return to steady state took so long that it was impossible to ever reach the true steady state before the pressure was again affected by some disturbance. Therefore, the pressure decay method described by Benis (6) was used. In order to measure the pressure drop along the experimental capillary tube, the membrane of the pressure transducer was deflected and a volume displacement inside the transducer occurred; i.e., $V = M \Delta P$, where ΔP is the pressure drop measured by the transducer, M is a constant, and V is the volume change inside the transducer. This volume change was used as a means for producing a flow rate (unsteady) through an experimental capillary tube. Measurements made by this method require only about fifteen minutes to obtain an entire shear stress-shear rate curve as compared to about one hour (for the 29 micron tube) to reach steady state for each experimental data point. However, the results are for unsteady flow and it is not known how unsteady results compare to those obtained for steady flow through tubes as small as 10 microns.

It was found, using the 0.05 ml syringe, that the volume displaced by the transducer membrane was directly proportional to the pressure drop measured by the transducer. That is,

$$V = M\Delta P \tag{9}$$

When using the pressure decay method, the syringe pump is removed from the system and the pressure transducer and experimental fiber become an isolated closed loop. Therefore, the flow rate through the capillary tube is equal to the flow rate emanating from the transducer:

$$Q = dV/dt = M\, d(\Delta P)/dt \qquad (10)$$

The value of M was calculated to be 8.5×10^{-5} ml/mm Hg for the 267BC transducer and was obtained from unsteady flow as follows:

1) The 0.05 ml syringe was placed in the syringe pump and attached directly to the low pressure side of the pressure transducer.
2) The high pressure side of the transducer was connected to a water source.
3) The entire system, syringe pump, transducer, and water reservoir, and connecting lines were filled with distilled water.
4) The by-pass loop was opened and the transducer was zeroed.
5) The by-pass loop was then disconnected and the syringe pump was operated in the withdrawal mode.
6) The flow rate was known; the slope of the pressure change as a function of time was measured (and found

to be linear) and from these data, M was calculated.

For actual use, either in calibrating the inside diameter of an experimental fiber or the measurement of shear stress-shear rate data, the pressure transducer-flow meter was used as follows:

1) The experimental equipment was modified such that the syringe pump was disconnected from the discharge reservoir.
2) The feed reservoir was filled with blood (or distilled water) and agitated as usual.
3) The by-pass loop was opened and the meter was zeroed. Then the by-pass loop was closed.
4) A pressure difference was imposed across the capillary tube by withdrawing isotonic saline from the discharge reservoir (thereby deflecting the transducer membrane). The transducer and capillary tube were an isolated unit and since a pressure difference had been imposed across the fiber, flow occurred and the deflected transducer membrane withdrew fluid from the feed reservoir through the capillary tube while seeking to return to its equilibrium position. The fluid level in the feed reservoir remained essentially unchanged during the process.

5) The original pressure drop along the capillary tube slowly decayed toward zero as flow through the fiber continued. Since the speed of the recorder chart paper travel was known, it was easy to calculate $d(\Delta P)/dt$ for a given ΔP. Thus Q and ΔP are known and from them, τ_w and $\bar{U}$ can be calculated.

6) This procedure was repeated at different attenuator settings and the entire shear stress-shear rate curve was obtained.

7) The hematocrit of the blood was changed and a new shear stress-shear rate curve was obtained.

As mentioned earlier, the measurements taken by the pressure decay method are not steady state measurements. The flow through the fiber is continually decreasing. However, if the rate of pressure decay is slow enough, then the difference between the values obtained and those that might be obtained by a steady state method may be very small. Benis (6) found excellent agreement between the pressure decay and syringe pump methods.

Observation and Microphotography

Observation

Observation of blood flow through the capillary fibers was made directly through a trinocular American Optical Microstar

Series 10 microscope. Magnification from 40 to 1000 x was possible. Illumination for both observation and photography was provided by a built-in light source, the intensity of which could be varied by a rheostat.

Microphotography

Still photographs were taken with a Kodak 35 mm camera adapted for use with the American Optical microscope via a special lens and shutter assembly. The entire microscope-camera assembly was mounted in a horizontal or vertical position. Usually, the microscope was mounted vertically. The microscope optics were designed such that it was possible to view the image being photographed, and therefore it was possible to observe the experimental capillary during the photographic sequence.

Preparation of Samples

The blood samples used in this study were obtained from donors in good health. The blood was drawn by venipuncture and collected in 500-ml Fenwal bags by routine blood bank procedure. When full, the bag contains 450 ml of whole blood and 67.5 mls of ACD anticoagulant. Each 100 ml of ACD anticoagulant contains 2.2 gms of sodium citrate, 0.73 gms of citric acid, and 2.45 gms of dextrose. The ability of the citrate ion to complex Ca^{+2} blocks the coagulation mechanism. The dextrose supplies nutrition for the red

cells. All blood samples were used within five days after withdrawal and samples were stored at 4°C until use.

The following procedure is used to prepare a suspension of red cells in plasma:

1) The sample is centrifuged for ten minutes at 3000 g to allow complete separation of the red cells from the plasma.
2) The plasma fraction is removed with a syringe having a large bore needle.
3) The buffy coat (white cells and platelets) is removed with a syringe having a large bore needle.
4) The red cell pack is washed with a few mls of plasma, and steps 1) through 3) repeated.
5) A suspension of the desired hematocrit is prepared by combining a known amount of final suspending media with the washed red cells.
6) The suspension is then filtered through a 14-micron neoprene filter (Millipore Corporation) directly into the feed reservoir.

Hematocrits are determined by filling small glass capillary tubes with blood sample, sealing the bottom with clay, and then centrifuging at 5500 g for five minutes. The hematocrit is the ratio of the red cell pack length divided by the total sample

length. At least two capillaries were used for each hematocrit determination, and usually agreed within ± 0.001 hematocrit units.

It was noted that the hematocrit of the blood used in this study dropped by about 0.002 hematocrit units as the blood was heated from about 15°C to about 20°C. At other times, the hematocrit would drop about 0.001 hematocrit units and this is suspected to be due to hemolysis. Thus, the hematocrits reported have an estimated accuracy of ± 0.001 hematocrit units. It is well known that the hematocrit increases as the body is cooled (11).

DISCUSSION OF EXPERIMENTAL RESULTS

Previously Reported Results

Theoretical Results

Human blood, a complex suspension of interacting, deformable particles in a Newtonian liquid, presents a difficult obstacle to the complete theoretical treatment of its shear stress-shear rate behavior. Recent work at the M.I.T. Blood Rheology Laboratory (33,98) has shown that a rheological model developed by Casson (24) is useful as an empirical method of correlating shear stress-shear rate data for blood in the low shear rate range. In the low shear rate region, it is proposed that the red cells in blood aggregate to form flexible, rod-like aggregates called rouleaux. The rouleaux have a length which is a function of the shear rate; their length decreases as the shear rate increases. Since blood normally contains a high concentration of red cells (40 to 50 percent), there is considerable interaction between the particles and the rouleaux. This type of suspension behavior agrees well with the mathematical model suggested by Casson.

Casson's model suspension consists of solid particles suspended in a Newtonian liquid. The particles are mutually attractive, so that at low shear rates the individual particles aggregate. The length of the aggregates varies inversely with the shear rate.

The original formulation of this model was for dilute suspensions and related the axial ratio of the particles to a cohesive force between the particles and to the shear rate. The result of this model is an expression relating the shear stress and shear rate for the suspension as follows:

$$\tau^{1/2} = s\dot{\gamma}^{1/2} + \tau_y{}^{1/2} \qquad (11)$$

where

τ = shear stress, dynes/cm^2

τ_y = yield shear stress, dynes/cm^2

$\dot{\gamma}$ = shear rate, inverse seconds (sec^{-1})

s = a constant

The coefficient s is directly related to the suspending medium viscosity and inversely related to the volume fraction of liquid in the suspension.

The important empirical result of Equation (11) is that it predicts a straight line when shear stress-shear rate data are plotted on square root coordinates. The intercept of the line with the shear stress axis is $(\tau_y)^{1/2}$, the square root of the yield shear stress, and s is the slope of the straight line. Any material under stress will flow to relieve the stress if given sufficient time. Thus, the concept of a yield stress involves a time consideration

in its definition, and $\tau_y^{1/2}$ is usually determined by extrapolation from a finite shear rate.

It has been previously shown that for any fluid, Newtonian or non-Newtonian, plots of $\dot{Q}/D^3$ versus $\Delta PD/L$ should coincide for any combination of experimental variables if the following assumptions are valid:

1) $\tau = f(\dot{\gamma}$ only)

2) steady, incompressible, laminar flow

3) no slip at the tube wall

4) no end effects

Considering the above theoretical basis, pressure drop-flow rate data can be correlated as plots of quantities proportional to Q/D^3 and $\Delta PD/L$. The actual groups used are:

$$\tau_w = \frac{\Delta PD}{4L} \quad \text{and} \quad \bar{U} = \frac{4Q}{\pi D^3} \tag{12}$$

The quantity τ_w is the wall shear stress for steady flow, and $\bar{U}$ is the average flow velocity expressed in tube diameters per unit time. τ_w is expressed in dynes/cm^2, and $\bar{U}$ has the same dimensions as shear rate and is expressed as sec^{-1}. For a Newtonian fluid, Equation (6) gives

$$\tau_w = 8\mu\bar{U} \tag{13}$$

It can be seen that $\bar{U}$ is one-eighth the wall shear rate for a Newtonian fluid; and furthermore, $\bar{U}$ provides a convenient measure of flow rate since it can be estimated directly by microscopic observation of the experimental fiber. That is, if the red cells are seen to be flowing at an average speed of one tube diameter per second, then $\bar{U} = 1 \text{ sec}^{-1}$.

Both types of plots, $\tau^{1/2}$ versus $\dot{\gamma}^{1/2}$ and τ_w versus $\bar{U}$, are commonly used to correlate blood flow data. It is also common practice to plot $\tau^{1/2}$ versus $\bar{U}^{1/2}$. Once again, over a limited $\bar{U}$ range, a straight line results (6).

Investigations at the M.I.T. Blood Rheology Laboratory

Until recently, little more was known about the rheological behavior of blood than that Poiseuille's law did not hold and that 'apparent viscosity' varied with tube diameter and flow rate. Within the last few years, workers at the Massachusetts Institute of Technology have obtained reliable shear stress-shear rate data for human blood (6,7,33,35,57,93,95,96,97,98,99,100). Using a sensitive Couette viscometer operating on a magnetic torque principle, and a capillary viscometer free from surface artifacts, a variety of red cell suspensions were studied. Some of the important results of these investigations are summarized below:

1) Shear rate-shear stress relations were found as a function of hematocrit and temperature.

2) It was found that blood exhibits a definite, measurable yield shear stress which depends on hematocrit and fibrinogen concentration but is essentially independent of temperature.

3) Red cells suspended in plasma are rheologically identical to whole blood, indicating the unimportance of white cells and platelets for experimental measurements.

4) The rheological model proposed by Casson (24) was found to correlate the data at low shear rates both in Couette and capillary flow.

5) Whole blood is "pseudo Newtonian" in the sense that at high shear rate the slope of a shear stress-shear rate plot is constant, and the extrapolated slope passes through the origin.

6) Selective additions of proteins to red cell-saline suspensions indicated that fibrinogen is responsible for cellular aggregation and thus the yield shear stress. Partially defibrinated blood showed a greatly reduced yield stress, and red cells suspended in isotonic saline showed

no yield value.

7) It was confirmed that plasma, serum, and in fact, any aqueous solutions of plasma proteins in the range of physiological concentrations are Newtonian both in Couette and capillary flow.

8) Wall effects are significant in a Couette viscometer, especially at low shear rates, and rough-walled cylinders are necessary in order to obtain accurate data. No axial migration is observed in a capillary viscometer.

Benis found that deviations in the $\tau_w - \bar{U}$ curves occurred below values of $\bar{U}$ equal to about 1 sec^{-1} when tubes smaller than 500 microns in diameter were used. He found that for a given $\bar{U}$ (below 1 sec^{-1}), the shear stress increased as the tube diameter decreased. He suggested that this phenomenon was the result of red cell aggregation and also of the tendency of the red cells to adhere to the surface of the glass tubing at $\bar{U}$'s below 1 sec^{-1}. Benis deduced from the increase in shear stress as the tube diameter decreases that the yield stress may be a function of tube diameter. It was later found that the anomolous

results found by Benis were due to sedimentation (93). Therefore, it is impossible to determine the yield stress (except in tubes with diameters below about 16 microns where three-dimensional sedimentation networks are not present) by extrapolating capillary tube data to zero $\bar{U}$. It was concluded that results obtained below $\bar{U}$ equal to about 1 sec^{-1} are not reliable.

9) The shear stress-shear rate relation for blood is identical whether determined in a concentric cylinder viscometer or a capillary viscometer, and the extrapolated value of the yield shear stress is also the same for both instruments. Plasma also has a unique shear stress-shear rate relation (Newtonian) whether determined in a Couette or a capillary viscometer. Charm (27,30) insists that blood is not pseudo Newtonian and that both blood and plasma behave differently in different viscometers. However, he finds that plasma is non-Newtonian and has a yield stress. His differences are probably due to experimental artifacts or calibration errors. Charm uses a cone and plate viscometer and makes no attempt to eliminate the free

surface artifact which has caused considerable experimental error in the past (138).

10) It was found that the rheological behavior of blood is not affected by the addition of anti-coagulants.

11) The moderate addition of high molecular weight (above 40,000) dextran to red cell suspensions increases the apparent viscosity when compared to isotonic saline controls. The moderate addition of dextran to a red cell suspension always increases the yield stress.

As would be expected, a higher concentration of particles (higher hematocrit) increases both the shear stress at a given shear rate and the yield stress value of the suspension. The relationship between the yield shear stress and hematocrit has been investigated by Cokelet and others (15,33), and an empirical equation has been found to correlate data for blood with hematocrits below about 50 percent.

$$\tau_y = a(H - H_c)^3 \qquad H \geq H_c$$
$$\tau_y = 0 \qquad H < H_c \tag{14}$$

where a is a constant, and H_c is the critical hematocrit below which

the red cell-plasma suspension cannot have a yield stress. When the hematocrit is below H_c, there are not enough particles present in a given volume of suspension to build up the three-dimensional structure needed to give stationary blood a yield shear stress.

Another experimental variable that has an important effect on the rheological properties of blood is the temperature. The yield shear stress is independent of temperature, but at finite rates of shear, lowering the temperature increases the measured shear stress. The change in shear stress at finite rates of shear is due to suspending media viscosity changes over small temperature changes.

It should be emphasized that the above results were determined using capillary tubes larger than about 130 microns in diameter. Although a number of investigators have made measurements in small tubes, there are presently no reliable experimental data relating the pressure drop-flow rate behavior of human blood flowing through capillary tubes less than 130 microns in diameter (16,76,110).

Results Concerning the Average Hematocrit Inside a Capillary Tube

It is possible that the flow properties of blood should become truly a function of the tube diameter at some small tube diameter, say 20 to 60 microns, due to the particulate nature of blood, but an apparent failure of the continuum model in a tube as large as 220 microns does not seem reasonable. Since the diameter of the red

cell is about 8 microns, the ratio of tube diameter to particle diameter is about 25 for a 220-micron tube. Instead, there is considerable evidence that another mechanism is responsible for the decrease in shear stress at constant $\bar{U}$ for tubes less than 300 microns (44,75).

When a suspension of solid particles in a liquid flows through a circular tube, the average concentration (volume fraction of suspended particles) inside the tube is less than the feed reservoir concentration. It is easily shown that this phenomenon can occur only if radial migration of the solid particles is present (131) since the exit mixing-cup H is the same as the feed reservoir H. Radial migration of the particles is caused by a mechanical interference with the tube wall in such a way that a particle cannot have its center closer to the tube wall than its radius. This causes a partial void of particles near the wall, whereas in the bulk of the suspension the particles can pack as closely as desired. The other cause of radial migration is hydrodynamic and is due to the rotation the particles acquire because of the velocity gradient across the tube. Radial migration occurs in suspensions of neutrally bouyant, non-neutrally buoyant, spherical and non-spherical, rigid and non-rigid particles. It occurs in Newtonian as well as non-Newtonian suspending fluid.

Concentration changes that occur when a suspension of rigid particles flows through a tube have been investigated by several authors (91,129). In all cases it was found that the concentration in the tube was less than the reservoir concentration, indicating migration toward the tube axis. The most complete investigation of dilute suspensions was done by Sutera (129). He found that the concentration reduction in the tube increased with increasing Reynolds Number (up to about 60, then became independent of Re) and decreasing tube-to-particle diameter ratio. The reduction was found to be independent of feed reservoir concentration in the range 5 to 25%. No literature appears to date on concentrated (25 to 65%) suspensions.

There is little doubt that a layer of unknown thickness, which contains mostly plasma, is present when blood flows through a capillary tube. However, the causes (mechanical or hydrodynamic) and the thickness are still uncertain. There is considerable evidence that the plasma layer at the wall is due to mechanical interference between the red cell and the tube wall, and not due to hydrodynamic forces acting on the red cell. The magnitude of the pure plasma layer has been found to be approximately 1 to 2 microns in thickness (8,56,104), which is of the predicted mechanical interference magnitude (132) and the thickness of the layer is not a function of flow rate (133), whereas the magnitude of the hydro-

dynamic force should increase as the flow rate increases, predicting an increase in the thickness of the plasma layer as the flow rate increases.

Regardless of the cause(s) or the magnitude(s), the concentration of red cells flowing through a capillary tube is not uniform throughout a cross-section of the tube, but is smaller near the wall (104). This fact has been used by several authors (91, 129,131) to demonstrate that the "average" hematocrit inside the capillary tube is less than the feed reservoir hematocrit, when blood flows through the tube at steady state. The "average" hematocrit inside the tube would be obtained by instantaneously stopping the flow and measuring the total volume of red cells trapped in the tube and dividing by the total volume of the tube.

This phenomenon seems at first a bit hard to believe, and one asks "If the hematocrit inside the tube is less than the reservoir hematocrit, then where did the red cells go?" To add to the confusion, it has been shown that the hematocrit of the blood leaving the capillary tube is the same as that in the feed reservoir (as required by steady state conditions). The claim is, then, that the blood in the tube has a hematocrit less than the feed reservoir, but the blood flowing out of the tube has the same hematocrit as the feed reservoir. This apparent paradox is easily proven possible mathematically, but a mathematical proof is not intuitively satisfying.

Theoretical Results

A non-rigorous, qualitative proof that is somewhat more appealing than an integral proof goes as follows. Consider a feed reservoir with hematocrit H_f, a capillary tube with hematocrit H_t, and a discharge stream with hematocrit H_d, as shown in Figure 7.

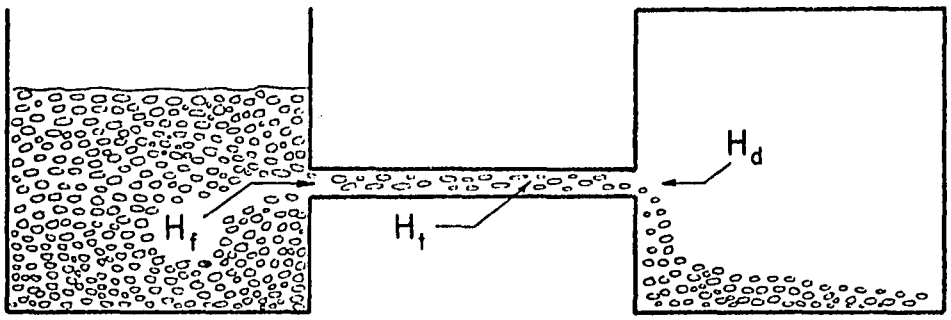

Figure 7. Capillary Viscometer with Hematocrits H_f, H_t, and H_d.

When operation is such that steady conditions in the tube have been achieved, what goes in must come out and $H_f = H_d$ or there would be an accumulation or depletion of red cells in the capillary tube. To show that $H_t \leq H_d = H_f$, it is necessary to consider a way to measure the hematocrit inside the capillary tube. One way would be to stop the flow, remove the tube and centrifuge the tube and its contents, and then take the ratio of the red cell pack length divided by the tube length as the "average" tube hematocrit. (Experimentally, this is a poor choice of methods due to the fact that the

long tubes used in a capillary viscometer cannot be centrifuged, in the presently available equipment, at a sufficiently high speed to insure complete packing of the red cells). Another way to measure the hematocrit inside the tube, at least conceptually, is to consider packing all the red cells in the center of the tube (H = 1.0), leaving only plasma in the annulus. This is shown in Figure 8.

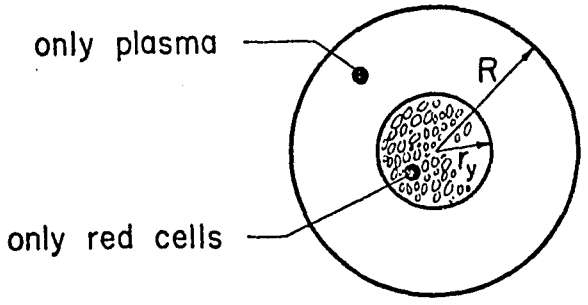

Figure 8. Annulus of Pure Plasma Surrounding Red Cell Pack.

In this geometry, the hematocrit is:

$$H_t = \frac{\pi r_y^2 L}{\pi R^2 L} = r_y^2/R^2 \qquad (15)$$

where r_y is the radius of the red cell pack and R is the tube radius.

The hematocrit of the blood being discharged from the tube, H_d, is the ratio of the flow rate of red cells divided by the total flow rate. Now consider the fact that there is a plasma layer at the tube wall. In order to dramatize this layer, assume that the layer is very thick and that the red cells migrate all the way to the center of the tube and pack tightly. This situation represents the maximum thickness that the plasma layer can have, and this particular concentration distribution of red cells is shown in Figures 8 and 9. Figure 9 also shows the approximate velocity profile.

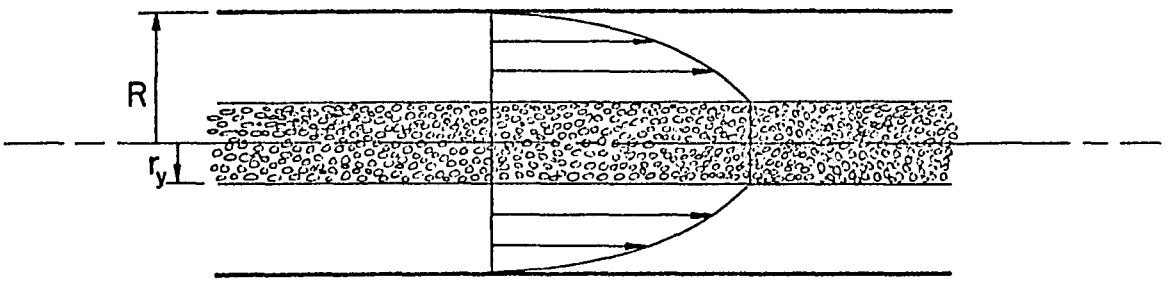

Figure 9. Concentration Distribution and Velocity Profile.

The velocity profile would be blunt in the center of the tube due to the solid core of red cells, and parabolic outside the red cell pack due to the presence of pure plasma. The hematocrit flowing out of the tube is:

$$H_d = \frac{Q_{\text{red cells}}}{Q_{\text{total}}} = \frac{(U)_{\text{red cells}} \quad (\text{Area})_{\text{red cells}}}{(U)_{\text{total}} \quad (\text{Area})_{\text{total}}} \qquad (16)$$

Since the area of the red cell pack divided by the total area is:

$$\frac{(\text{Area})_{\text{red cells}}}{(\text{Area})_{\text{total}}} = \frac{\pi r_y^2}{\pi R^2} = r_y^2/R^2 \qquad (17)$$

and since $(U)_{\text{red cells}}$ is larger than $(U)_{\text{total}}$, $H_d \geq \frac{r_y^2}{R^2} = H_t$. That is, the ratio of the areas is the same as the tube hematocrit, H_t, from Equations (15) and (17), and the average red cell velocity is larger than the average fluid velocity; therefore, from Equation (16), $H_d \geq H_t$. Since the feed reservoir hematocrit is equal to the discharge hematocrit, $H_f = H_d$, then $H_t \leq H_f$.

Of course, the red cells do not accumulate compactly in the center of the capillary tube, and an even more simplified reason for the reduction of the hematocrit inside the tube is: Since the fluid velocity is smaller near the wall than it is near the axis, the red cells have a larger average velocity than the plasma (due to the void of red cells near the wall); the 'mixing cup' concentration of red cells will be larger than the concentration inside the tube.

An important point is that the thickness of the plasma layer may not be a function of the tube diameter, down to some small value

of the tube diameter, say 40 microns. Thus, a 150-micron tube could have approximately the same plasma layer thickness as a 1000-micron tube. As the diameter of the tube increases, the effect of this layer loses its importance with respect to causing a measurable decrease in the hematocrit inside the tube. At a nominal diameter of 300 microns, the hematocrit inside the tube is essentially identical with the feed reservoir hematocrit. All tubes of a diameter of 300 microns and larger thus have approximately the same tube hematocrit as the feed reservoir hematocrit.

As the tube diameter decreases below 300 microns, the constant thickness layer of plasma becomes a larger percentage of the total flow cross-section and the hematocrit inside the tube continues to decrease relative to the feed reservoir hematocrit.

Although the thickness of the plasma layer is about the same for all size tubes, it does depend on the feed reservoir hematocrit. As the feed reservoir hematocrit increases above 30 percent, the thickness of the plasma layer decreases for tubes less than 130 microns (56).

As pointed out previously, both mechanical and hydrodynamic effects may be present causing radial migration of the particles, resulting in a decrease in the average concentration inside the tube. Thus, the concentration reduction is a direct measure of the amount of radial migration present. The mechanical effect is only

a function of the particle size and is independent of flow rate and reservoir concentration. The hydrodynamic force is dependent on the particle size (to the third power), the flow rate, and on the feed reservoir concentration. As the reservoir concentration increases, the ability of the particles to migrate decreases due to interaction between particles. From the above considerations it should be expected that as the flow rate increases, the reduction in concentration should increase. In other words, at low Reynolds Number, entrance phenomena become important. In fact, the magnitude of the hydrodynamic force determines at what position down the tube the uniform entering concentration of the feed reservoir is converted to the steady state concentration distribution (how fast the particles migrate to an equilibrium position). Also, as D/2d decreases (the particle size becomes larger for a given tube), the concentration reduction should increase since the hydrodynamic force becomes larger (αd^3) and also because the mechanical effect becomes larger (more fluid and fewer particles at the wall). As the concentration increases, the hydrodynamic effect should become smaller and as the tube becomes filled with the maximum number of particles it can hold, the hydrodynamic effect should disappear completely, leaving the residual concentration reduction due only to the mechanical effect.

Although a number of complicated reasons have been given to account for the fact that at a constant $\bar{U}$ the shear stress decreases as the tube diameter decreases, below 300 microns, the reason is simply that the measured hematocrit in the feed reservoir does not correspond to the actual hematocrit inside the capillary tube.

It has been known for quite some time that, at constant $\bar{U}$, the shear stress increases as the hematocrit increases. Thus, if the actual hematocrit inside the capillary tube is used instead of the feed reservoir hematocrit, the τ_w - $\bar{U}$ relationship for blood may be consistent and blood may not fail to satisfy the requirements of the continuum model.

Measurement of the Actual Hematocrit Inside the Capillary Tube

In order to investigate the above statements, it was necessary to determine the actual hematocrit inside the capillary tube, and then compare the τ_w - $\bar{U}$ relationship obtained with a similar one from an 811-micron tube with the same hematocrit found inside the small tube, not the feed reservoir hematocrit for the small tube. For tubes with inside diameters larger than about 300 microns, the hematocrit inside the tube is essentially the same as in the feed reservoir.

As mentioned earlier, attempts have been made to determine the actual hematocrit inside the tube by stopping the flow and then centrifuging the tube and its contents in order to determine the ratio of the red cell pack length to the tube length (44,75). The apparatus used in these attempts probably did not have a constant feed reservoir hematocrit, and had inadequate mixing in the feed reservoir, so it is difficult to interpret the results found in these experiments. The apparatus of Fåhraeus had sufficient mixing to insure that sedimentation would not be present, but rouleaux formation was present. The apparatus of Davis had no mixing at all, and it is quite possible that sedimentation seriously affected his results. Both these investigators determined the tube hematocrit by centrifuging the experimental fiber being tested.

The hematocrit of the blood inside the 29-micron diameter capillary tube was measured by passing blood with a known reservoir hematocrit through the tube until steady state was reached, then stopping the flow, removing the tube from the capillary viscometer, and breaking the tube into four sections, each about 2.5 inches long. Then, about 0.25 inches of sealing clay was forced into one end of each capillary tube and the end carefully flame sealed. The tubes were then centrifuged at 5500 g for 10 minutes, and the ratio of the red cell pack length to the total length of the blood column was taken as the tube hematocrit. It was found that

ten minutes was a sufficient length of time to insure complete packing of the red cells into the bottom of the tube. No correction was made for trapped plasma in the red cell pack, since the magnitude of this error is at most 1% (28). The tube was inspected under the microscope both before and after flame sealing in order to determine if the heat had affected the blood in the tube. It was found that flame sealing did not affect the blood (this was also demonstrated by comparison with tubes that were not flame sealed--though as a rule, flame sealing was required in order to prevent the escape of red cells from the tube at high, 5500 g, centrifugal speeds). The hematocrit of the four sections usually agreed within about two percent of the average value.

A technique found to be much more accurate in measuring the tube hematocrit (for the 59-micron and larger diameter tubes) was as follows:

1) Set up the capillary viscometer as usual.
2) Measure the feed reservoir hematocrit (H_f) using a capillary tube with an ID of 1100 microns.
3) At a given flow rate, determine when steady state has been reached. (Constant pressure drop and/or visual observation through the microscope).
4) Allow an additional 10 tube volumes of blood to flow through the tube, then stop the flow, and

remove the tube from the capillary viscometer (discharge reservoir end first).

5) Carefully remove all the blood from both ends of the capillary tube.

6) Using another capillary viscometer, pump all of the blood out of the tube, using 10 tube volumes of isotonic saline, into a spectrometer cuvette containing a measured amount of a cyanide solution. The dilution ratio is the same as for the calibration curve (1000 to 1). It was found that the isotonic saline used to pump the blood out of the tube does not affect the value of the spectrometer reading. It was also observed microscopically that 2 or 3 tube volumes of isotonic saline was sufficient to remove all the blood from the capillary tube.

7) Mix the contents of the cuvette and read the percent transmittance with the spectrometer. The spectrometer wavelength was 425 millimicrons. It was found that a 1% error in the measured percent transmittance caused a 1% error in the value of hematocrit measured. Typically, it was possible to repeat the above steps and determine

additional values of percent transmittance to within ± 0.2 percent.

8) Repeat at different flow rates, reservoir hematocrits, and for different tube diameters.

The method used is known as the cyanmethemoglobin method, and has been used for years clinically (101). The reagent used to break the red cell membrane (called lysing) was obtained from Hycel, Inc. The experimental procedure is very sensitive to hemolysis since total hemoglobin is measured, and a slight amount of hemolysis can affect the hematocrit of the blood a moderate amount without affecting the total hemoglobin concentration.

A Coleman Model 6A spectrometer was used to determine the concentration of red cell contents as well as to prepare a calibration curve. The calibration curve of percent transmittance vs. blood hematocrit was made by mixing a known quantity of blood (with a known hematocrit) with a known quantity of lysing solution as follows:

1) Withdraw exactly 0.04 mls of blood from the well mixed feed reservoir of the capillary viscometer into a calibrated Sahli type pipette with a precision of ± 1% and an ID of 800 microns.
2) Mix the 0.04 mls of blood with 40 mls of drabkins solution prepared by mixing one vial of drabkins

powder with 4 liters of distilled water.

3) Measure the percent transmittance with the spectrometer and also measure the feed reservoir hematocrit.

4) Repeat at different feed reservoir hematocrits.

The same dilution ratio (1000 to 1) was used when working with the volume of blood contained in the experimental capillary tube.

The possible reasons for the hematocrit to be lower in the tube than in the feed reservoir are 1) mechanical interference between the red cell membrane and the tube wall, 2) hydrodynamic forces acting on the red cells causing them to migrate to the center of the tube, and 3) mechanical interference at the tube entrance, restricting the red cells from entering the tube.

In order to test reason 3, it was necessary to measure the hematocrit of the blood flowing out of the tube and compare this hematocrit with the feed reservoir hematocrit. If physical blocking was present at the tube entrance, the discharge hematocrit (H_d) would not be the same as the feed reservoir hematocrit, but instead lower. The exit hematocrit was measured by carefully sealing a microhematocrit tube (using vacuum grease) against the discharge end of the 59- and 99-micron ID capillary tubes, and then pumping blood from the feed reservoir through the tubes and into the microhematocrit tube. Both the discharge and feed hematocrits were then

determined by centrifuging microhematocrit tubes. Exit hematocrits were measured with complete mixing in the feed reservoir and also during the steady state sedimentation period using no stirring in the feed reservoir. The ratio of exit hematocrit to feed hematocrit varied between 0.99 and 1.01, and this is shown in Figure 10. The stirring rate had no effect on this ratio and thus, rouleaux formation in the feed reservoir is not important in determining the hematocrit of the blood that enters the capillary tube (indicating that Fåhraeus' apparatus did not have an experimental artifact). The results agree with those found by Sutera (130) using flat and conical openings and suspensions of rigid spheres. He found that the discharge concentration was equal to the feed concentration to within 3% for both the conical and the flat entrance sections.

Figure 11 shows the relative hematocrit, defined as the ratio of the tube hematocrit to the reservoir hematocrit, as a function of reservoir hematocrit for the experimental tubes used (221, 153.5, 128, 99, 75, 59, and 29 micron ID). All data points were measured at least three times. Again, data taken during the steady state sedimentation period in the feed reservoir with no stirring agree with the data taken when the blood in the feed reservoir was adequately mixed. Also shown in Figure 11 are the data taken for red cells suspended in isotonic saline.

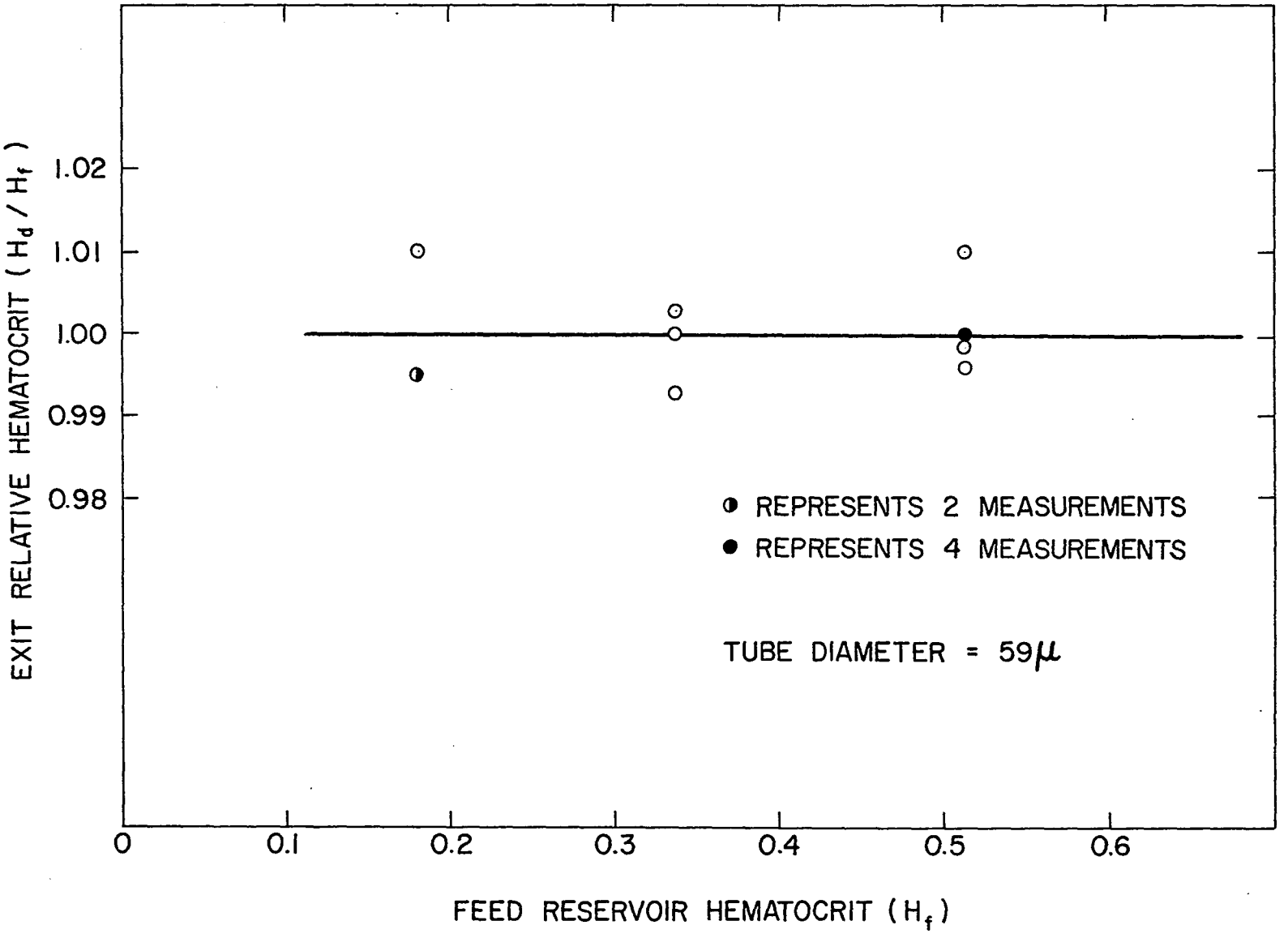

Figure 10. Exit Relative Hematocrit vs. Feed Reservoir Hematocrit.

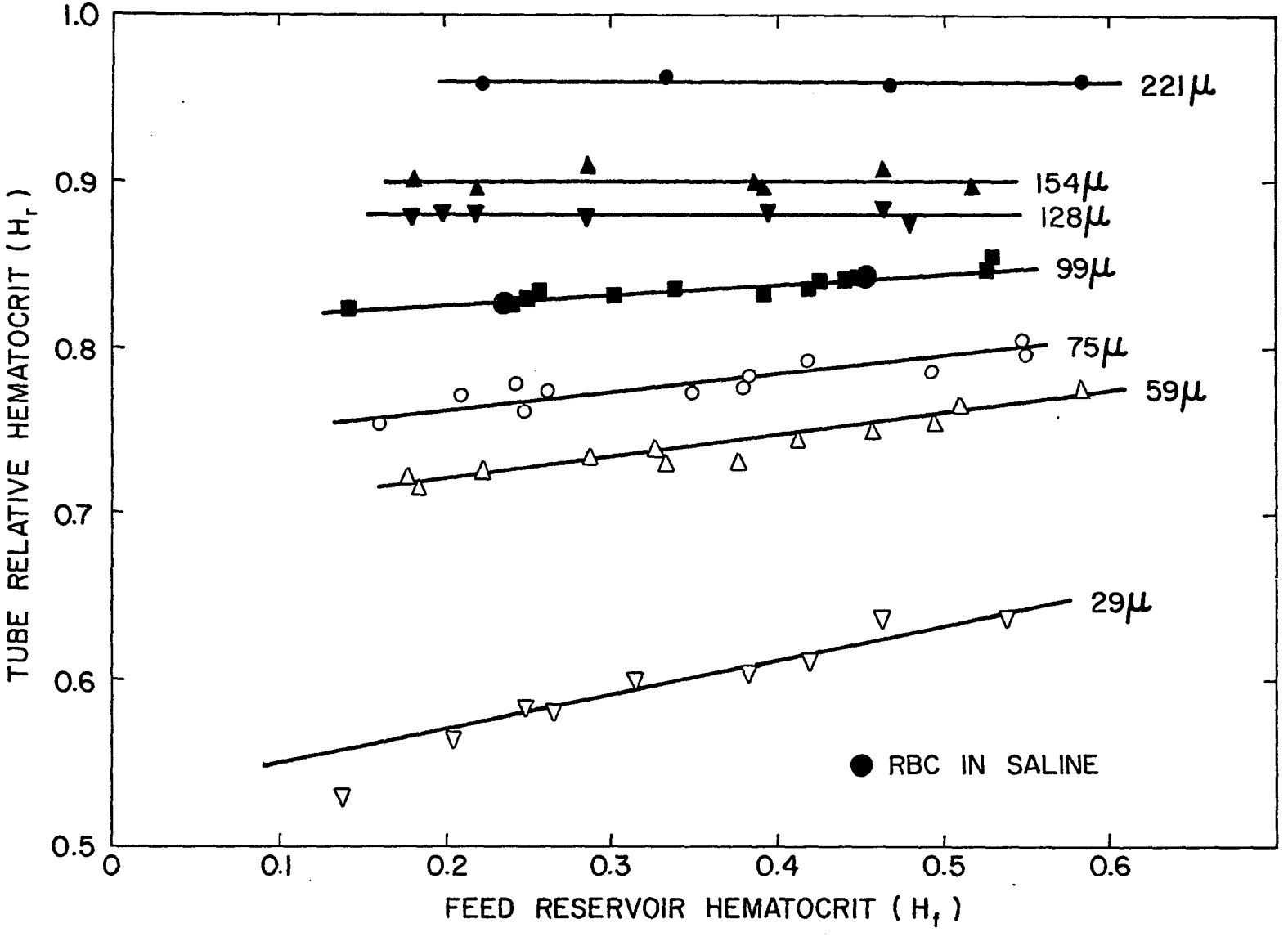

Figure 11. Tube Hematocrit vs. Feed Hematocrit for Tubes Larger Than 29 Microns ID.

It was found that the relative hematocrit is not a function of the reservoir hematocrit for tubes with inside diameters of 128 microns ID and larger. As the tube diameter decreases below 128 microns, the value of H_r becomes a function of the feed reservoir hematocrit, with a positive slope. Also, the slope of the line increases linearly as the tube diameter decreases, while the intercept decreases linearly with the logarithm of the tube diameter. The solid lines shown in Figure 11 were determined by a least squares fit. The slopes of the lines were replotted as $d(H_r)/d(H_f)$ vs. tube diameter, and a straight line was drawn through the data points. This is shown in Figure 12, and this line was used in determining Equation (18). The inside diameters of the capillary tubes were first calculated as usual from Equation (8) using the measured value of ΔP and obtaining Q from Equation (10). Figure 13 shows the relative hematocrit as a function of feed reservoir hematocrit for tubes with 23, 15.3, and 8.7 microns ID. It is to be noted that the above mentioned capillary tubes are thin-walled tubes as opposed to the 29-micron and larger tubes. The outside diameter of the 23-micron tubes was about 35 microns, and direct measurements of H_r by centrifuging the experimental capillary tubes was impossible. The value of the tube hematocrit was determined by counting the number of red cells in a given length of the capillary tube. For each size capillary tube, a length of about 10 tube

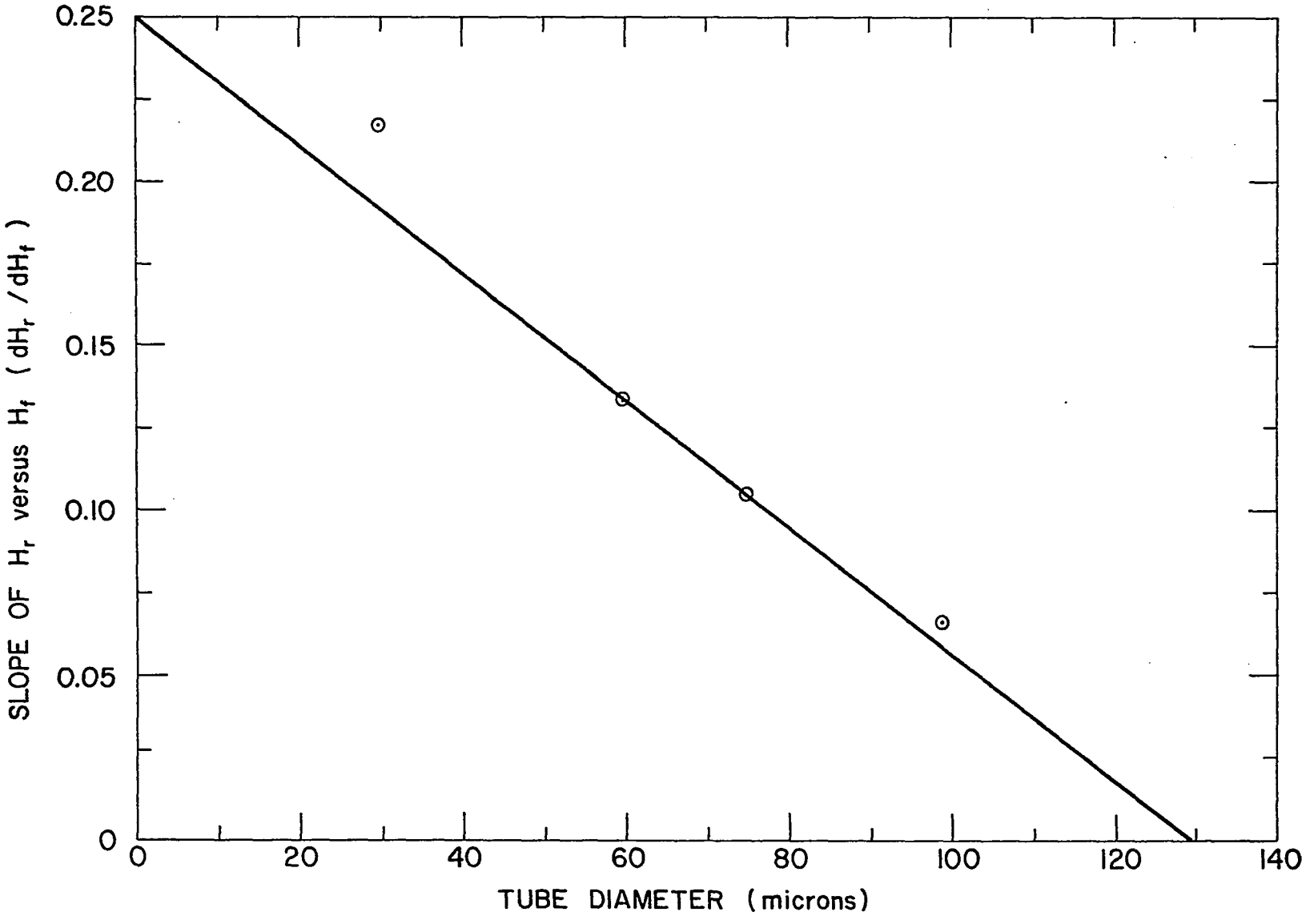

Figure 12. Slope of H_r vs. H_f as a Function of Tube Diameter.

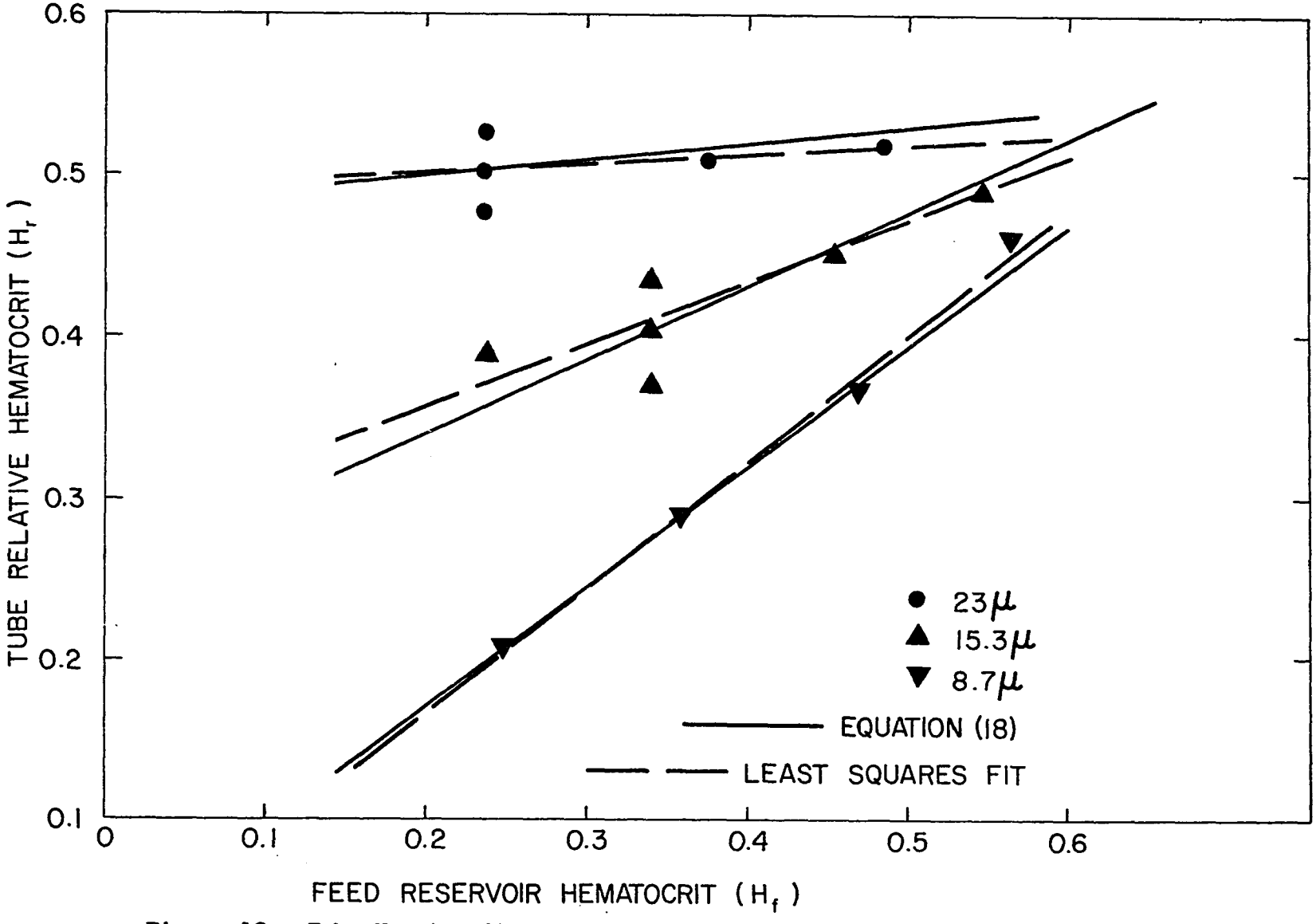

Figure 13. Tube Hematocrit vs. Feed Hematocrit for Tubes Less Than 29 Microns ID.

diameters was used. The average volume of 107.5 cubic microns was used for the red cell volume (23). Thus, H_t equals the volume of the red cells divided by the volume of the test section. This method was found to be very crude, and if blood with the same reservoir hematocrit was measured repeatedly, by stopping the flow and counting the number of red cells in the control volume, then starting up the flow, then stopping the flow and recounting the number of red cells, the tube hematocrit could vary by $\pm$ 10 percent. Also, the red cell volume itself varies by up to 17 percent (23). However, the variation in red cell volume is random and for the average volume used probably represents the average volume of the red cells counted. The average of all readings for a given feed reservoir hematocrit was used as the tube hematocrit. Also shown in Figure 13 is a least squares fit of the data points.

Davis (75) found that H_r is not a function of flow rate between Reynolds Numbers (based on apparent blood viscosity) of 0.15 and 30. This indicates an insufficient radial force, and radial migration of the red cells toward the tube axis due to hydrodynamic force is probably not present. It is probable that mechanical, not hydrodynamic forces cause the decrease of the hematocrit inside the tube. Data were taken at different $\bar{U}$'s between 1 and 200 for a reservoir hematocrit of 0.340. It was found that H_r is not a function of flow rate in the range investigated.

The investigation of unsteady flow was restricted to either accelerating or decelerating flow (pulsating or oscillating flows were not investigated). It was found that if the capillary tube was removed from the viscometer while the flow was decelerating, the H_r value was usually larger (by up to 10%) than for steady flow. Accelerating flow usually caused the H_r value to be slightly lower (between 2 and 5%) than for steady flow.

It has been found that below $\bar{U} = 1$, sedimentation occurs in capillary flow and it is suspected that Davis' data were affected by either sedimentation or unsteady flow conditions.

In order to investigate the mechanism that causes the average tube hematocrit to be less than the feed reservoir hematocrit, suspensions of red cells in plasma-dextran and hardened red cells in plasma were investigated in a 29-micron tube.

For the measurements with red cells suspended in a plasma-dextran solution, a 3% dextran by weight unfiltered plasma solution was prepared. The osmotic pressure of the original plasma was 297 mOm, and the osmotic pressure of the dextran solution was 306.5 mOm. The plasma was initially opaque after the addition of the sugar, but eventually got fairly clear. Because the osmotic pressure of the sugar mixture was higher than pure plasma, 0.8 mls of water was added to 25 mls of the solution in order to bring the osmotic pressure back down to about 295 mOm. The viscosity of the

3% by weight dextran solution was 2.98 times higher than the original plasma. The sugar was Dextran 250 with a molecular weight based on light scattering of approximately 250,000. Dextran, a polyglucose, is produced by microbiological polymerization of glucose, usually by the bacteria Leuconostoc Mesenteroides. The dextran used here was obtained from Pharmacia Inc.

Red cells were added to the plasma-dextran solution until the hematocrit reached 0.517. After steady state was reached, with $\overline{U} = 47$, the flow was stopped and the tube was removed from the viscometer. The tube was broken into four sections and critosealed and flame sealed. The tube was then centrifuged for 30 minutes and the tube hematocrit was measured to be 0.318. This gives an H_r of 0.614; the predicted H_r is 0.634. Then another 29-micron tube was put into the viscometer and the feed hematocrit changed to 0.403. After steady flow was reached, the tube was removed, sealed, and centrifuged. The tube hematocrit was 0.252. This gives H_r = 0.625. The predicted H_r is 0.610. It was suggested (113) that migration is a function of the viscosity of the suspending media; therefore, adding sugar should do something to H_r because of the plasma viscosity change.

Hardened red cells suspended in plasma were also investigated in order to determine if flexibility contributed to the reduction of hematocrit inside the capillary tube. Hardened red cells

were prepared by the 2% Acetaldehyde method (73). It has been shown (29) that hardened red cells do not pack tightly; in fact, 0.60 is the maximum concentration that can be obtained using hardened red cells. Although H_r is independent of this packing problem, the values of H_f measured were multiplied by 0.60 to obtain the true feed reservoir hematocrits.

The hardened red cells were washed twice in plasma and then suspended in plasma and placed in the feed reservoir. The initial feed hematocrit was measured to be 0.440. This gives a corrected value of 0.264. The hardened cells flowed through the tube very easily and showed no plugging tendency for about one hour, but then the tube started to plug up. Apparently the axial hematocrit fluctuations are temporary plugging conditions, and occur in a suspension of hardened red cells to the same degree as in normal whole blood with the buffy coat removed. The tube was removed and the measured tube hematocrit was 0.274 (corrected to 0.164). This gives an H_r of 0.623. The predicted value is 0.582. It was noticed that the cells did not pack as tightly in the capillary tube when centrifuged as did normal red cells. The feed reservoir hematocrit was changed to 0.298 (corrected to 0.179), and the tube hematocrit was found to be 0.170. This gives H_r equal to 0.57. The predicted value is 0.566.

It appears that the reduction in hematocrit occurs for red

cells in plasma, red cells in saline, red cells in dextran-plasma, and for hardened red cells in plasma. Within experimental error, the reduction is the same for all these suspensions. This is shown in Figure 14. The mechanism responsible for the reduced hematocrit is probably simple wall exclusion of the red cells as discussed by Vand. Hydrodynamic migration does not seem to be present, suspending fluid viscosity is not important, and flexibility is not important.

Blood samples from six different people were used during the course of the experimentation. Although the calibration curves were slightly different for each blood sample, the value of H_r for a given set of variables is independent of the blood sample and agrees with the saline control.

Figure 15 shows the relative hematocrit as a function of tube diameter for a reservoir hematocrit of 0.405. The data of Fahraeus, who used a single feed reservoir hematocrit of 0.405, are also shown. The data of Davis, for red cells suspended in isotonic saline, with a feed reservoir hematocrit of 0.40 are also included.

Figure 16 shows that the data taken in the 23 and 8.7-micron tubes do not agree very well with larger tube results. Error bands are included to emphasize that measuring H_r by counting red cells is a very crude method of determining red cell volume. The 15.3- and 23-micron tubes seem to fall below the continued curve from larger tubes. This could be due to the fact that it was very

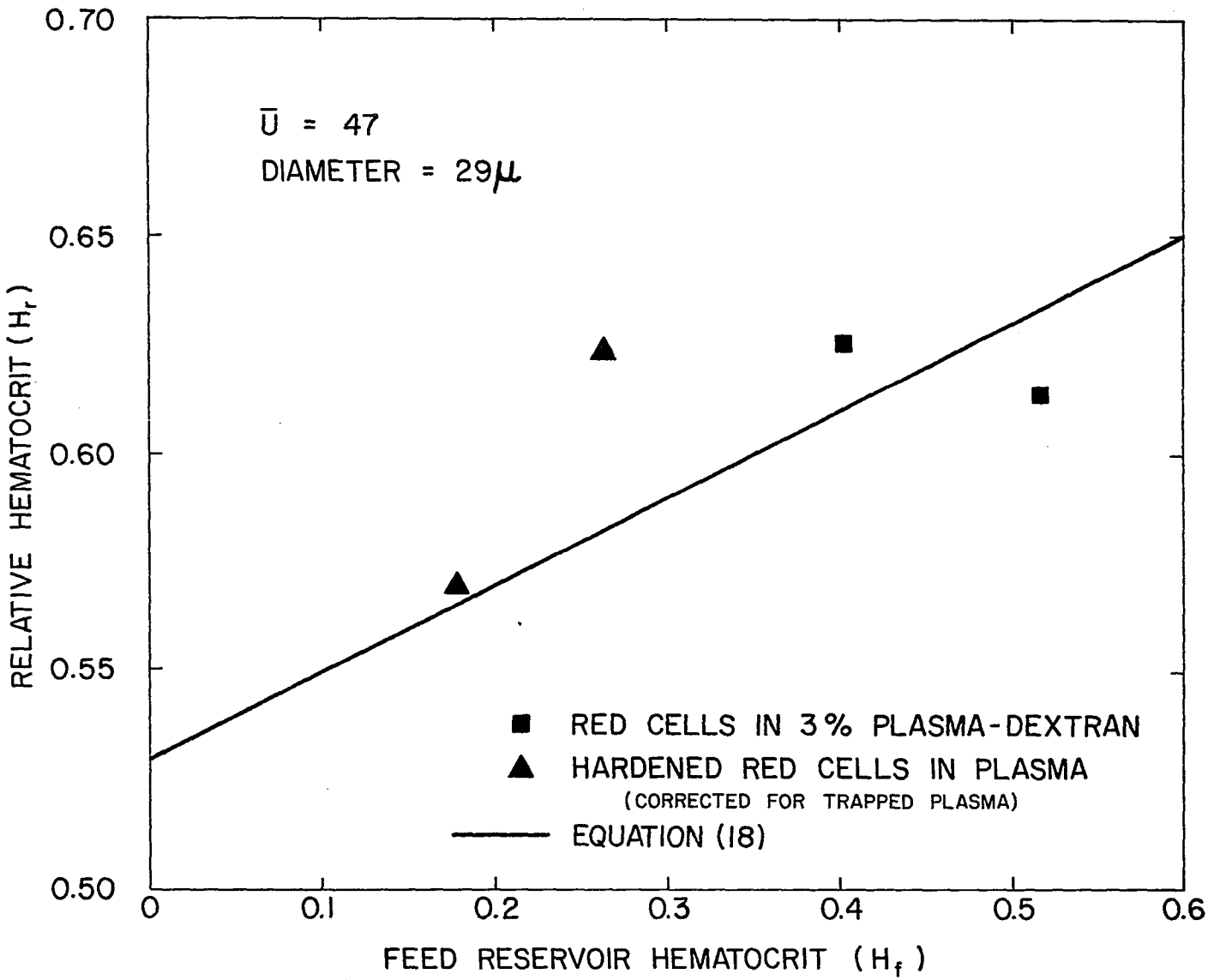

Figure 14. Tube Hematocrit vs. Feed Hematocrit for Modified Suspensions Flowing Through a 29-Micron Tube.

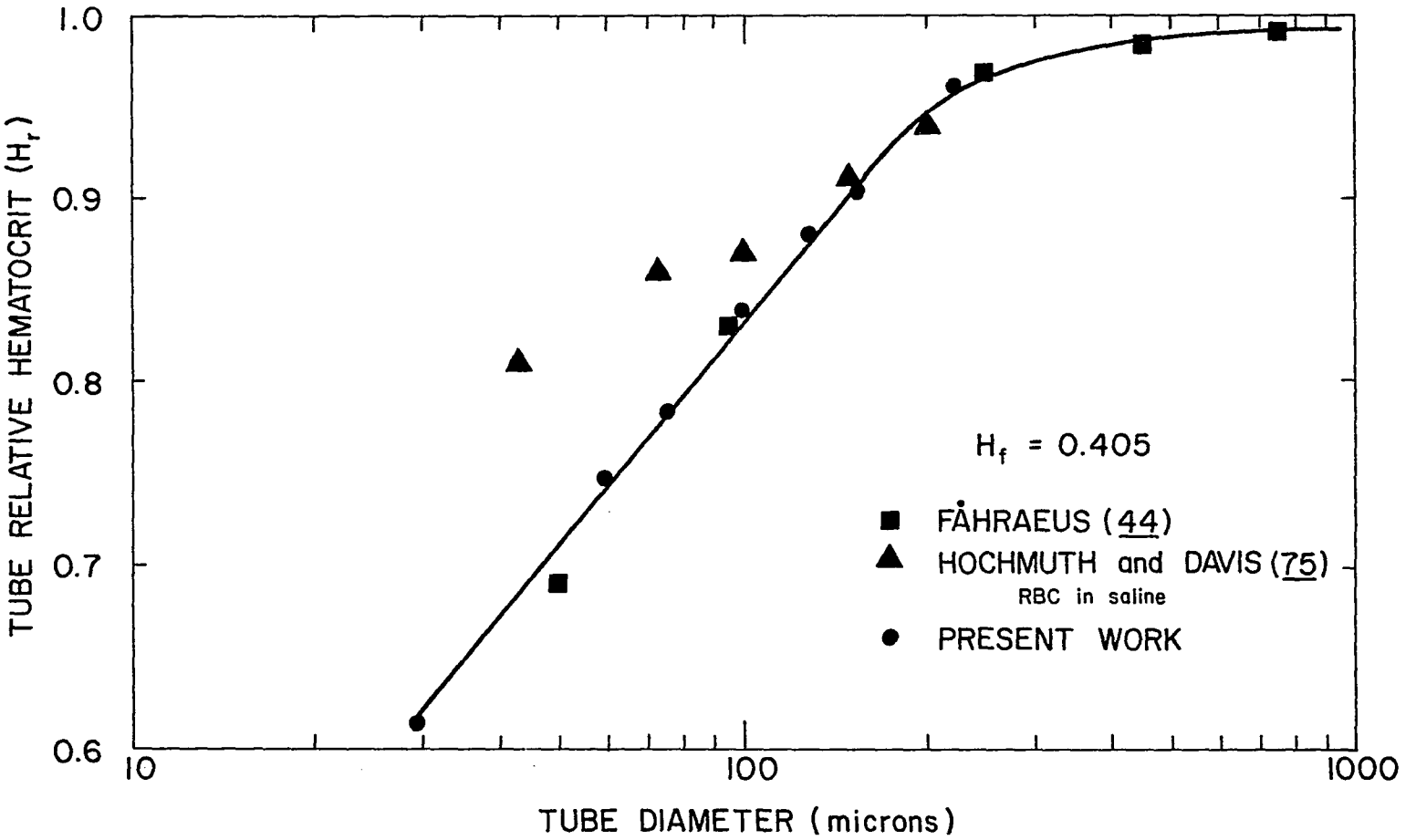

Figure 15. Semi-Log Plot of Tube Hematocrit vs. Tube Diameter for H_f = 0.405.

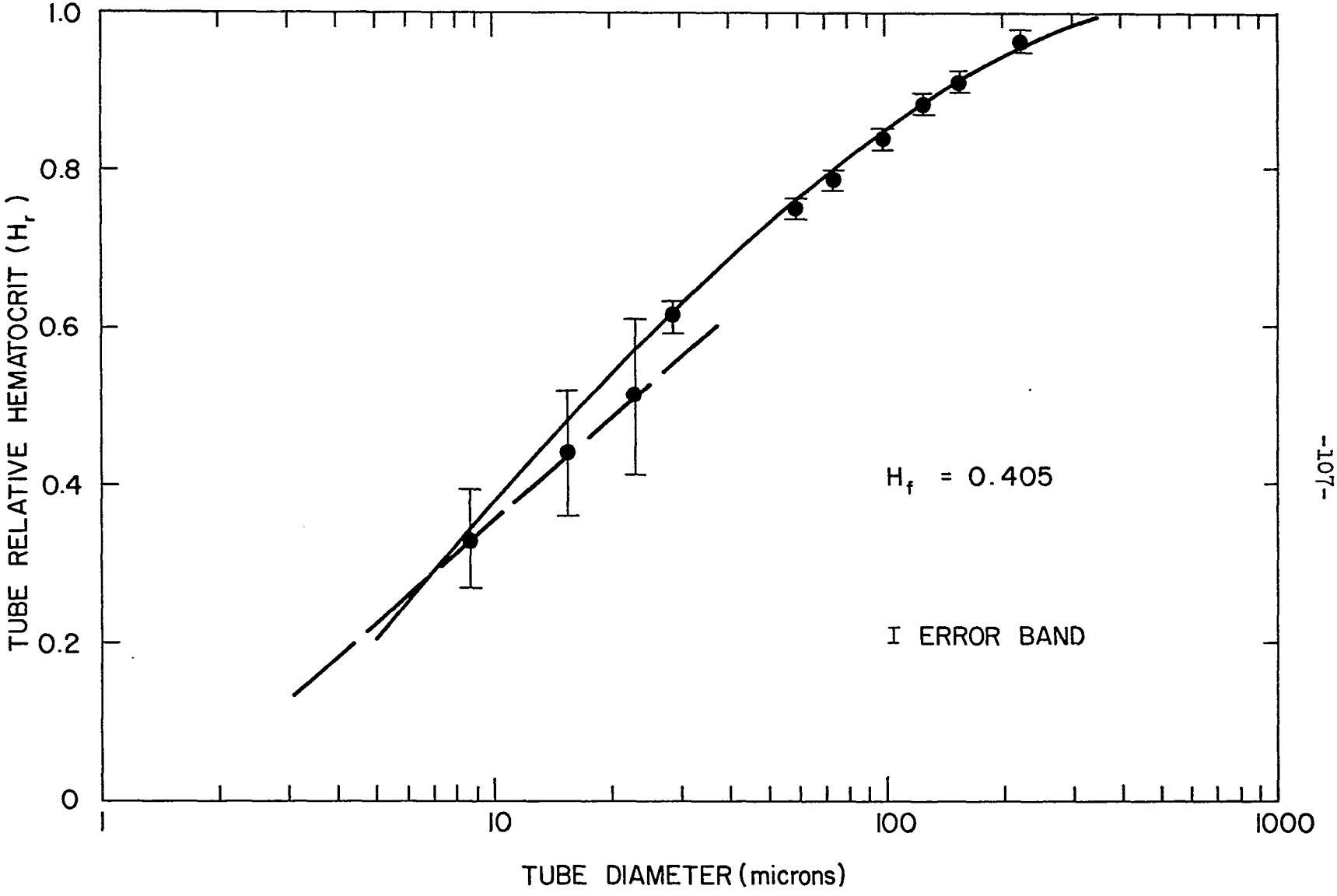

Figure 16. Semi-Log Plot of Tube Hematocrit vs. Tube Diameter for All Experimental Tubes.

difficult to count all the red cells in the test section of the 23-micron tube. It is possible that some cells present in the test section were hidden from view and not counted. If these cells had been counted, H_r would have increased. For the 15.3-micron tube, it was not nearly as difficult to be sure that all the cells in the test volume were counted, and this is reflected in H_r being only slightly below the suspected value. For the 8.7-micron tube, all cells could be counted.

The experimental curves in Figures 11 and 13 can be approximated by the following equations:

$$
\begin{aligned}
H_r &= -0.024+0.1754\ \ln D+(-0.046D+1.15)(H_f-0.45) && 8 < D \leq 25 \\
H_r &= -0.019+0.1899\ \ln D+(0.25-0.00195D)(H_f-0.45) && 25 < D \leq 60 \\
H_r &= 0.1171+0.1562\ \ln D+(0.25-0.00195D)(H_f-0.45) && 60 < D \leq 125 \\
H_r &= 0.1171 + 0.1562\ \ln D && 125 < D \leq 280 \\
H_r &= 1.0 && 280 < D
\end{aligned}
\qquad (18)
$$

The hematocrit in the core of the tube was calculated from Equation (13) and from:

$$H_{core} = r_y^2/(R-\delta)^2 \qquad (19)$$

where δ is the plasma layer thickness. Combining these equations gives:

$$H_{core} = H_t R^2/(R-\delta)^2 \qquad (20)$$

Since $H_t = H_r H_f$, the final equation becomes:

$$H_{core} = H_r H_f R^2/(R-\delta)^2 \qquad (21)$$

The core hematocrit was first calculated for a 285-micron ID tube (where H_r first becomes approximately equal to 1.0) assuming a plasma layer thickness of 4 microns. A plasma thickness of 4 microns was chosen because a thickness of one red cell radius (4 microns) is generally thought to be the correct plasma layer thickness for cells traveling through a tube with their axes parallel to the centerline. A value of 1 or 2 microns could have also been chosen (for cells passing through the tube with their axes perpendicular to the centerline). Using a different value of the plasma layer thickness produces results qualitatively analogous to those presented below.

It was found that $H_c = 1.03\ H_f$. Using this relation, and rearranging Equation (21), the plasma layer thickness was calculated for the experimental tubes used. The equation is:

$$\delta = R\left[1 - (H_r H_f/H_{core})^{1/2}\right] \qquad (22)$$

For the 99, 75, 59, and 29-micron tubes, the plasma layer thickness depends on H_f since H_r is a function of H_f for these tubes. The values calculated are shown in Table V.

TABLE V. CALCULATED VALUES OF THE PLASMA LAYER THICKNESS FOR DIFFERENT TUBES.

Tube Diameter (microns)	H_f	δ (microns)
221	0.2	3.8
221	0.5	3.8
153.5	0.2	4.9
153.5	0.5	4.9
128	0.2	5.0
128	0.5	5.0
99	0.2	5.3
99	0.5	4.9
75	0.2	5.2
75	0.5	4.5
59	0.2	4.8
59	0.5	4.1
29	0.2	3.7
29	0.5	3.2

These values for the plasma layer thickness are all within reasonable limits. Perhaps the plasma layer thickness should continue to

increase as the tube diameter decreases, but perhaps a different flow pattern (or a different degree of deformability of the red cell membrane) exists for each size tube.

Benis (6) has presented the integral equations describing the mixing cup and the tube hematocrit. In these equations the hematocrit is assumed to vary with radial position. It was not possible to deduce the radial hematocrit profile from these integral equations even when experimental data were used in conjunction with the integral equations.

Because it was found that the tube hematocrit (or relative hematocrit) varies with tube diameter, it was considered desirable to present the shear stress-shear rate relations separately, depending on the tube diameter. Results are presented for tubes larger than 300 microns and less than 300 microns. Because of the suspension properties of blood, results for tubes less than 300 microns are presented in two groups--larger than 29 microns, and smaller than 29 microns.

Results Obtained Using a Capillary Viscometer and Tubes Larger Than 300 Microns

Experimental Results

Pressure drop-flow rate data were taken for a normal blood sample at various hematocrits ranging from 0.123 to 0.593 using an

811.5-micron tube. As with water, the rotation of the stirring bar did not affect the pressure drop-flow rate relations when blood was the experimental fluid. The τ_w - $\bar{U}$ correlation obtained from the experimental measurements is shown in Figure 17. It can be seen that as the hematocrit decreases, the log-log relationship between τ_w and $\bar{U}$ becomes linear. At a hematocrit of 0.123, the line is straight but the slope is not equal to one, and therefore, blood is still not Newtonian even at this low hematocrit. At hematocrits above about 0.30, the curve becomes non-linear and at H = 0.593 the curvature is very noticeable.

The experimental data were plotted on a semi-log graph as τ_w vs. H at constant $\bar{U}$ and it was observed that the data points can be approximated by a straight line. This plot is shown in Figure 18, and the equations for the straight lines are discussed in the next paragraph. It should be noted that the data points do not lie exactly on a straight line but a linear approximation seems reasonable. The solid lines on Figure 15 were determined by a least squares fit, and the data points in Figure 16 were taken from these solid lines. Thus, some uncertainty exists in the actual placement of the points in Figure 16. It does appear that the points for H less than about 0.30 fall above the line for $\bar{U}$ greater than 2.0 and below for $\bar{U}$ less than 2.0, whereas the data points for H larger than 0.30 lie below the line for $\bar{U}$ greater than 4.0 and above for

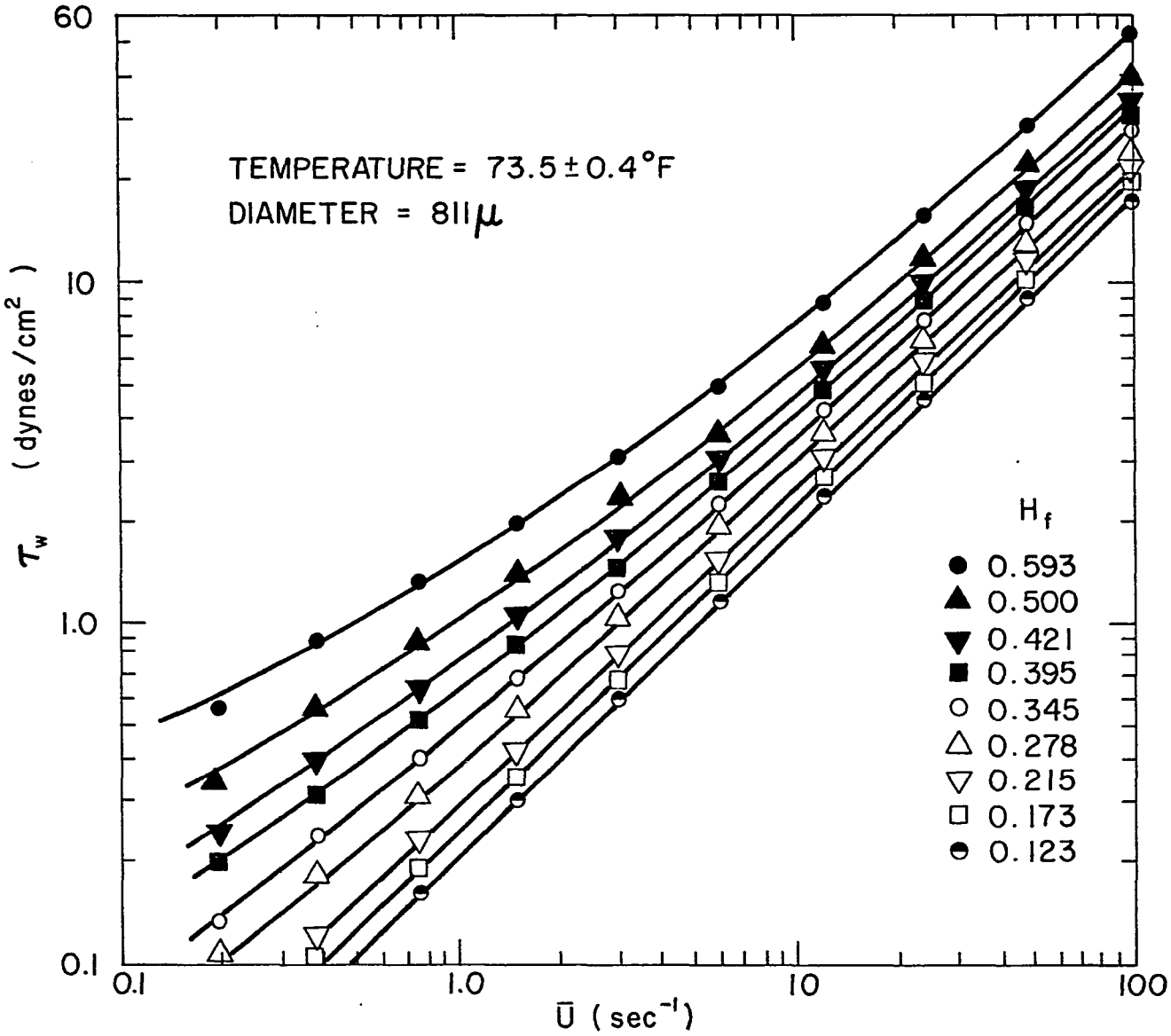

Figure 17. τ_w - $\bar{U}$ Plot for Red Cells in Plasma, 811-Micron Tube.

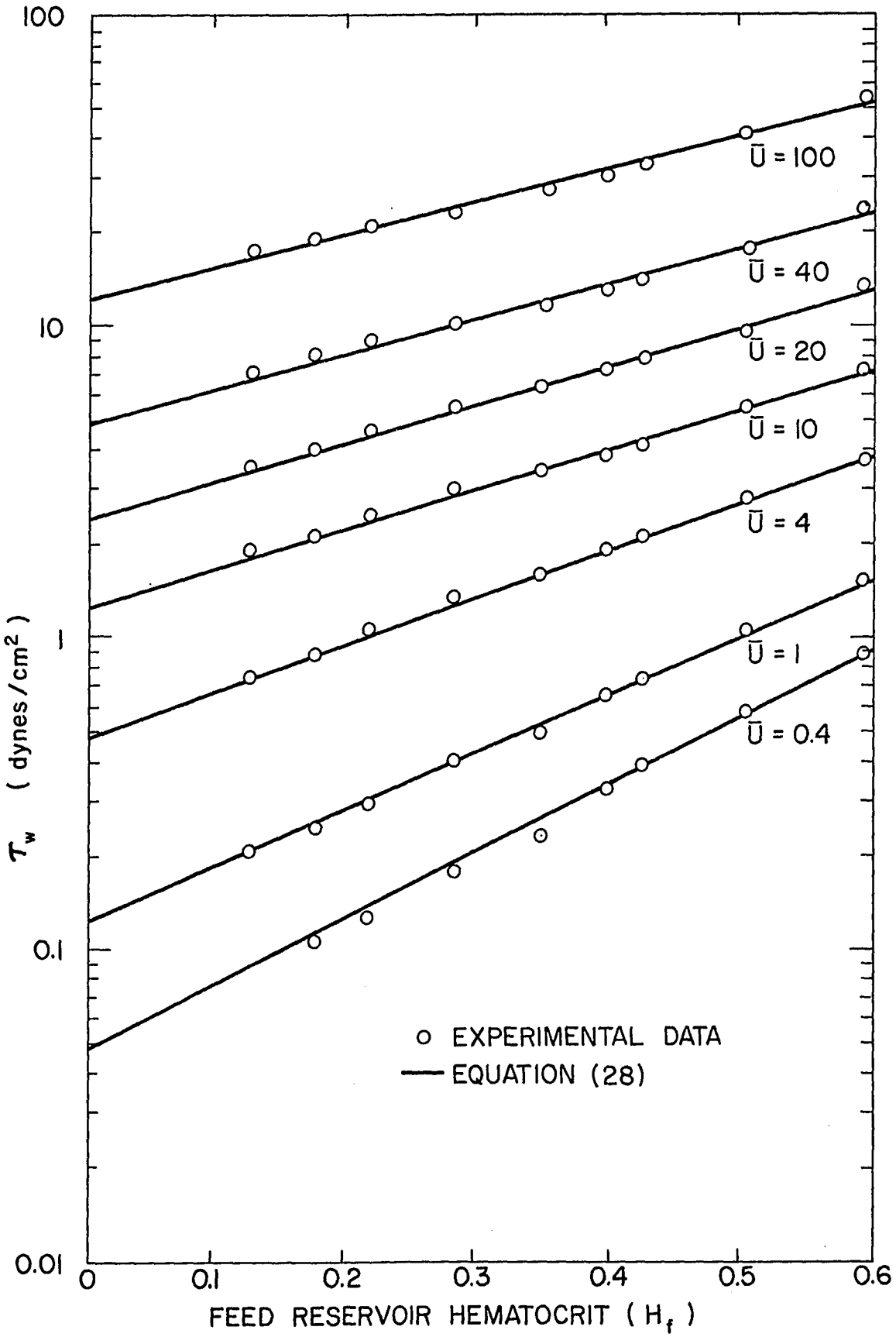

Figure 18. Semi-Log Plot of τ_w - H at Constant $\bar{U}$, 811-Micron Tube.

$\bar{U}$ less than 4.0. Thus, ln τ_w is perhaps not truly a linear function of H at constant $\bar{U}$.

It was found that Reynolds Numbers based on apparent blood viscosity were less than 10^{-2}; kinetic energy corrections were negligible. Also, the ratio of tube length to tube diameter was at least 300 and typically above 1000. End effects were also negligible.

As previously mentioned, a linear relationship between ln τ_w and H at constant $\bar{U}$ describes the experimental data with reasonable accuracy. The relationship is:

$$\ln \tau_w = \alpha H + \beta \tag{23}$$

where α and β are positive. Equation (23) produces the relationship

$$\tau_w = Ae^{BH} \tag{24}$$

In the limit as H goes to zero, pure plasma is flowing through the tube, and the Newtonian (Poiseuille) equation should prevail for plasma; and from Equation (13):

$$A = 8\mu_p \bar{U} \tag{25}$$

Therefore,

$$\tau_w = 8\mu_p \bar{U} e^{BH} \tag{26}$$

where μ_p is the plasma viscosity at the experimental temperature.

It was observed that as $\bar{U}$ increases, the slope, B, decreases. Therefore, B was evaluated as a function of $\bar{U}$. It was found that:

$$B = 4.2/\bar{U}^{C} \tag{27}$$

where C is almost constant. If B were constant, independent of $\bar{U}$, Equation (26) would predict Newtonian behavior for blood. B depends on $\bar{U}$ because blood is not Newtonian. Combining Equations (26) and (27) gives:

$$\tau_w = 8\mu_p \bar{U} \exp(4.2xH/\bar{U}^{C}) \tag{28}$$

The values of C, which best describe the data of Figure 18, are given in the following table.

TABLE VI. VALUES OF C, THE EXPONENT IN EQUATIONS (27) AND (28).

$0.4 \leq \bar{U} < 1.0$	C = 0.16
$1.0 \leq \bar{U} < 3.0$	C = 0.14
$3.0 \leq \bar{U} < 17.0$	C = 0.15
$17.0 \leq \bar{U} < 30.0$	C = 0.14
$30.0 \leq \bar{U} < 50.0$	C = 0.13
$50.0 \leq \bar{U} < 100.0$	C = 0.12

where $0.10 < H < 0.60$.

Since it was known that as H approached zero, Equation (13) would hold, the intercepts of the lines shown in Figure 18 were determined from the known plasma viscosity at the experimental temperature. The τ_w - $\bar{U}$ relationship for pure plasma at 73.5 and 98.6°F is shown in Figure 19.

The solid lines shown in Figure 18 were generated from Equation (28) using the values of C shown in Table VI. Equation (28) and the values of C from Table VI were then used to reproduce the original data and this is shown in Figure 20. The data of Benis (6) and Meiselman (93) were then predicted from Equation (28) and the results are shown in Figure 21.

The accuracy of Equation (28) could be increased as much as desired by including more significant figures in the values of C and by reducing the range of $\bar{U}$ over which that particular value of C applies. If a computer is available to perform the calculations, it would be advisable perhaps to use more significant figures and smaller $\bar{U}$ intervals. The reason for leaving the calculation as simple as possible is to facilitate rapid numerical answers for engineering design purposes. The values chosen for C give curves that, in most cases, approximate the data as well as the least squares fit. The values of C given in Table VI provide excellent correlation of experimental data at hematocrits between 0.35 and 0.45, and $\bar{U}$ between 50 and 100, the most commonly required data

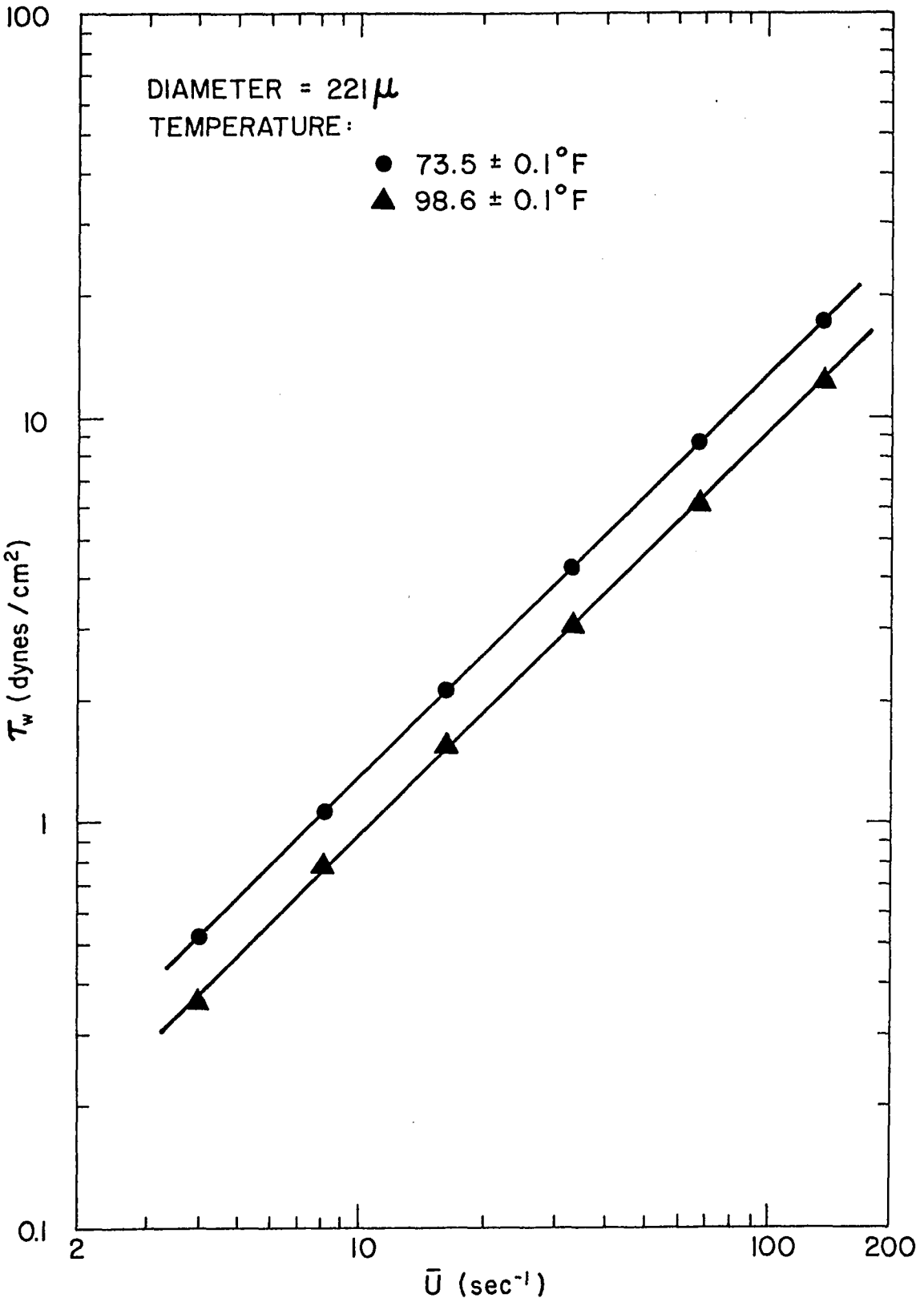

Figure 19. τ_w - $\bar{U}$ Plot for Plasma at 98.6 and 73.5°F

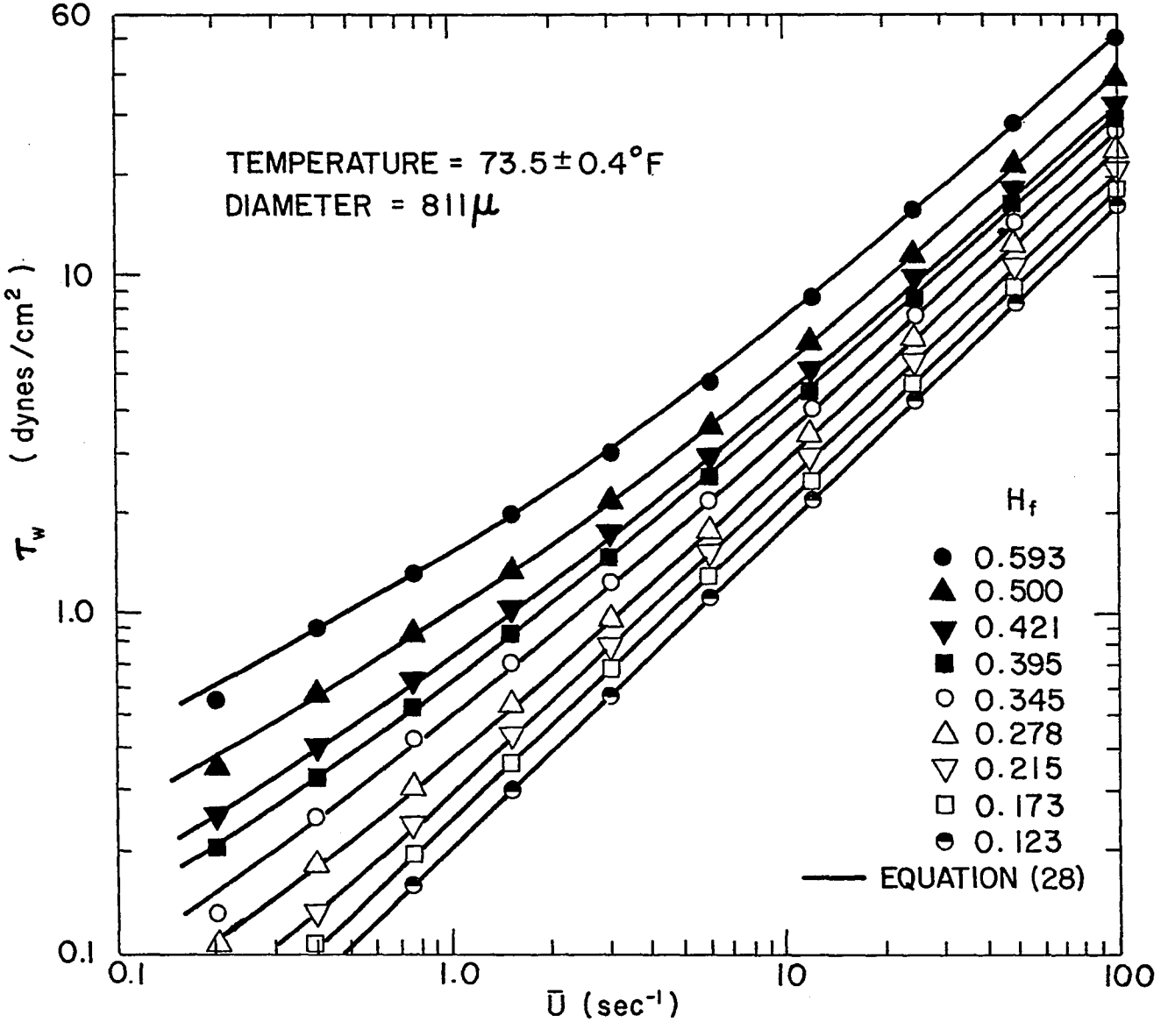

Figure 20. τ_w - $\bar{U}$ Data Predicted from Equation (28).

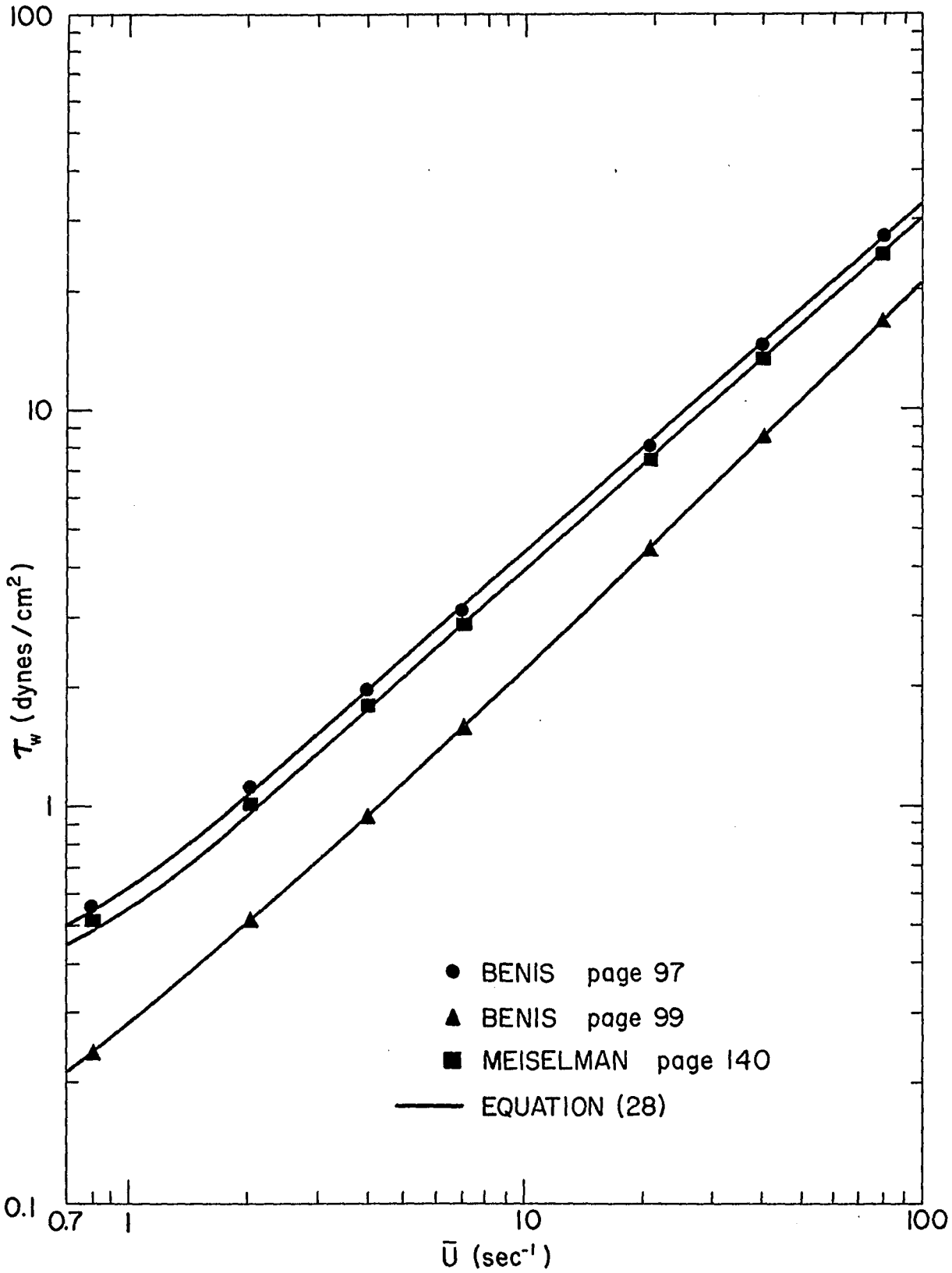

Figure 21. τ_w - $\bar{U}$ Data of Benis and Meiselman Predicted by Equation (28).

for the flow of whole human blood. For actual flow through the living circulation, it has been found (for the hamster cheek pouch) that values of $\bar{U}$ are typically of the order of 50 to 100 sec^{-1} (6). Also, C is constant over this range of $\bar{U}$. For $\bar{U}$ between 50 and 100, Equation (26) becomes:

$$\tau_w = 8\mu_p \bar{U} e^{4.2xH/\bar{U}^{0.12}} \qquad (29)$$

Thus, it is seen that once the temperature and hematocrit are fixed, a τ_w - $\bar{U}$ plot can be prepared in a minimum of time. The plasma viscosity as a function of temperature can be found from (93).

It is also important that Equations (28) and (29) not be applied outside the limits set in Table VI. For example, as H approaches 1.0, the shear stress at the wall should become very large, at least larger than predicted by the exponential in Equation (28). Also, as $\bar{U}$ approaches zero, C must also approach zero in such a way as to prevent τ_w from becoming infinite, and using a value of C from Table VI can produce a large error. At $\bar{U}$ below about 1.0, sedimentation occurs in the capillary viscometer and seriously affects the accuracy of the data.

It is also possible to express the τ_w - $\bar{U}$ correlation as:

$$\tau_w = 8\mu_p \bar{U}^{G} \exp(EH) \qquad (30)$$

where E is independent of $\bar{U}$ and G is a number less than 1.0. This scheme was found to be inferior to the one utilized in Equation (26). The reason is that G is a function of $\bar{U}$, as is B in Equation (26), but G depends much more strongly on $\bar{U}$, and also on H, than does B. It is also known that blood can only be represented as a power law fluid, as in Equation (30), over a very small shear rate range. Therefore, using Equation (28) and the values of C found from Table VI is considered the best method of predicting $\tau_w - \bar{U}$ data for blood. Equation (24) has also been found useful for correlating the data from experiments using dog blood (94).

It is hoped that Equation (28) will find considerable usefulness in the design and control of blood flow equipment such as the artificial kidney and in addition be of some use in the treatment of certain blood diseases. For example, in Waldenstrom's macroglobulinaemia the viscosity of the blood plasma increases dramatically due to the synthesis of anomalous proteins. In order to reduce the overall viscosity of the blood, the hematocrit is reduced by the body in an attempt to reduce the work required of the heart in circulating the blood through the body. As the hematocrit is decreased, the flow of blood through the circulatory system must increase in order to supply sufficient nourishment to all parts of the body. Lowering the hematocrit reduces the viscosity of the blood, but it increases the required pumping rate of the heart.

There is an optimum hematocrit at which the work done by the heart is a minimum. It is expected that Equation (28) will be able to play a role in determining this optimum hematocrit in place of the present trial and error experiments performed on the patient afflicted with this ultimately fatal disease (119).

Theoretical Equations Where the Continuum Model Applies

An attempt was made to compare the experimental data with a number of 'standard' flow models such as the Bingham plastic, power law fluid, power law fluid with a yield stress, and the Casson model. Benis (6) has already used the Casson model to correlate his data, but he used experimental constants in the Casson model which he obtained from his data. Also, Benis found that the Casson model correlated his data satisfactorily only below $\bar{U}$ equal to about 10. It is intended that any theoretical model found successful for correlating blood flow data should not require experimental constants taken from the same data that the theory is expected to correlate. It would be better to make assumptions about the flow properties of blood and then develop a theory which could be used to test these assumptions. If experimental constants are needed, then the empirical equation developed in the last section might as well be used from the beginning.

The various models chosen as possible candidates for describing the flow of blood (Bingham plastic, power law fluid, and power law fluid with a yield stress) were solved for the shear rate and then substituted into Equation (6). The results of integration are:

Bingham plastic:

$$\tau_w = 2\mu_p \bar{U} \left[1/4 - 1/3 \left\{\frac{\tau_y}{\tau_w}\right\} + 1/12 \left\{\frac{\tau_y}{\tau_w}\right\}^4 \right]^{-1} \tag{31}$$

Power law fluid:

$$\tau_w = K(6\bar{U} + 2\bar{U}/n)^n \tag{32}$$

Power law fluid with a yield stress:

$$\tau_w = K(2\bar{U})^n \left[\frac{n}{n+1} \left[1 - \frac{\tau_y}{\tau_w} \right]^{\frac{n+1}{n}} \left\{ 1 - \frac{2n}{2n+1} \left[1 - \frac{\tau_y}{\tau_w} - \frac{n}{3n+1} \left(1 - \frac{\tau_y}{\tau_w} \right)^2 \right] \right\} \right]^{-n} \tag{33}$$

Also, the Casson model equation is:

$$\tau_w = 2\bar{U}s^2 \left[1/4 + 1/3 \left\{\frac{\tau_y}{\tau_w}\right\} - 4/7 \left\{\frac{\tau_y}{\tau_w}\right\}^{1/2} - 1/84 \left\{\frac{\tau_y}{\tau_w}\right\}^4 \right]^{-1} \tag{34}$$

In their present form, neither the Bingham plastic nor the power law fluid with a yield stress models can be solved explicitly for τ_w in terms of τ_y and $\bar{U}$. The first step toward making the equations more manageable was to substitute Equation (14), $\tau_y = a(H-H_c)^3$, for the yield stress, into the above equations. This requires experimental data in order to calculate a and H_c in Equation (14). Even then, the equations still cannot be solved explicitly for τ_w. When values of τ_w were put into the equations, and the equations solved for $\bar{U}$, the results were quite a bit different from the experimental data.

A second approximation was to substitute $H^{1/2}$ for $\frac{\tau_y}{\tau_w}$. This approximation is based on the idea that if all the red cells migrated to the center of the tube (which they probably do not), then the velocity profile would be blunt in the center (out to the edge of the red cell pack) and parabolic in the pure plasma region (from the edge of the red cell pack to the wall of the tube). This is the same velocity profile as exhibited by a Bingham plastic (143). For a Bingham plastic, $\frac{\tau_y}{\tau_w} = \frac{r_y}{R}$, where r_y is the radius at which the blunt profile turns into a parabolic profile. It was already shown that the hematocrit inside the tube can be approximated by $\frac{\pi r_y^2 L}{\pi R^2 L}$, where L is the length of the tube and r_y is the outer edge of the red cell pack. Thus, $\frac{r_y}{R} = H^{1/2} = \frac{\tau_y}{\tau_w}$.

Therefore, the approximation

$$\frac{\tau_y}{\tau_w} = H^{1/2} \tag{35}$$

was used in the Bingham plastic model and the result is shown in Figure 22. This approximation is supposed to work best at high $\bar{U}$ when it is most likely that the red cells could migrate to the center of the tube. It is seen in Figure 22 that the model works best at low $\bar{U}$ and gets increasingly worse as $\bar{U}$ increases. Therefore, either the model or the assumption, Equation (35), is inappropriate for describing the flow properties of blood.

The next step was to evaluate n, the exponent, and K, the viscosity constant, in the power law models. K was set equal to the plasma viscosity and n was evaluated as a function of hematocrit. K is actually a dimensional constant with the dimensions depending on the value of n. Substituting the plasma viscosity for K was simply in keeping with the analogy. Regardless of what value was chosen for K, the power law fluid model failed for all reasonable values of n, and in fact decreased when it should have increased. It was therefore discarded. The power law fluid with a yield stress model, a complex expression to say the least, is shown in Figure 23. In this model, n is not a constant (at constant hematocrit), but changes as $\bar{U}$ changes. Here, again, the plasma viscosity

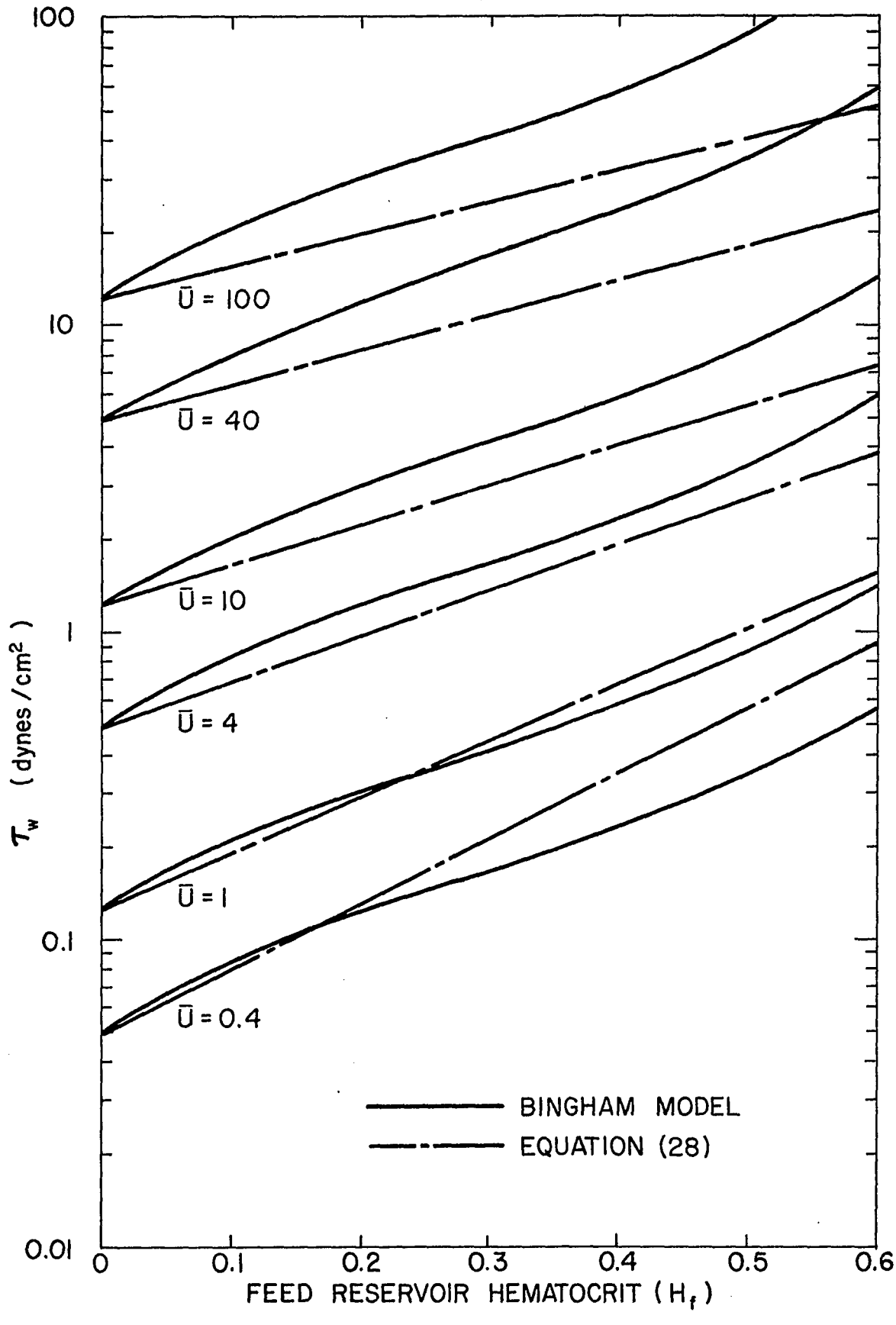

Figure 22. Ln τ_w - H_f at Constant $\bar{U}$ for the Bingham Model.

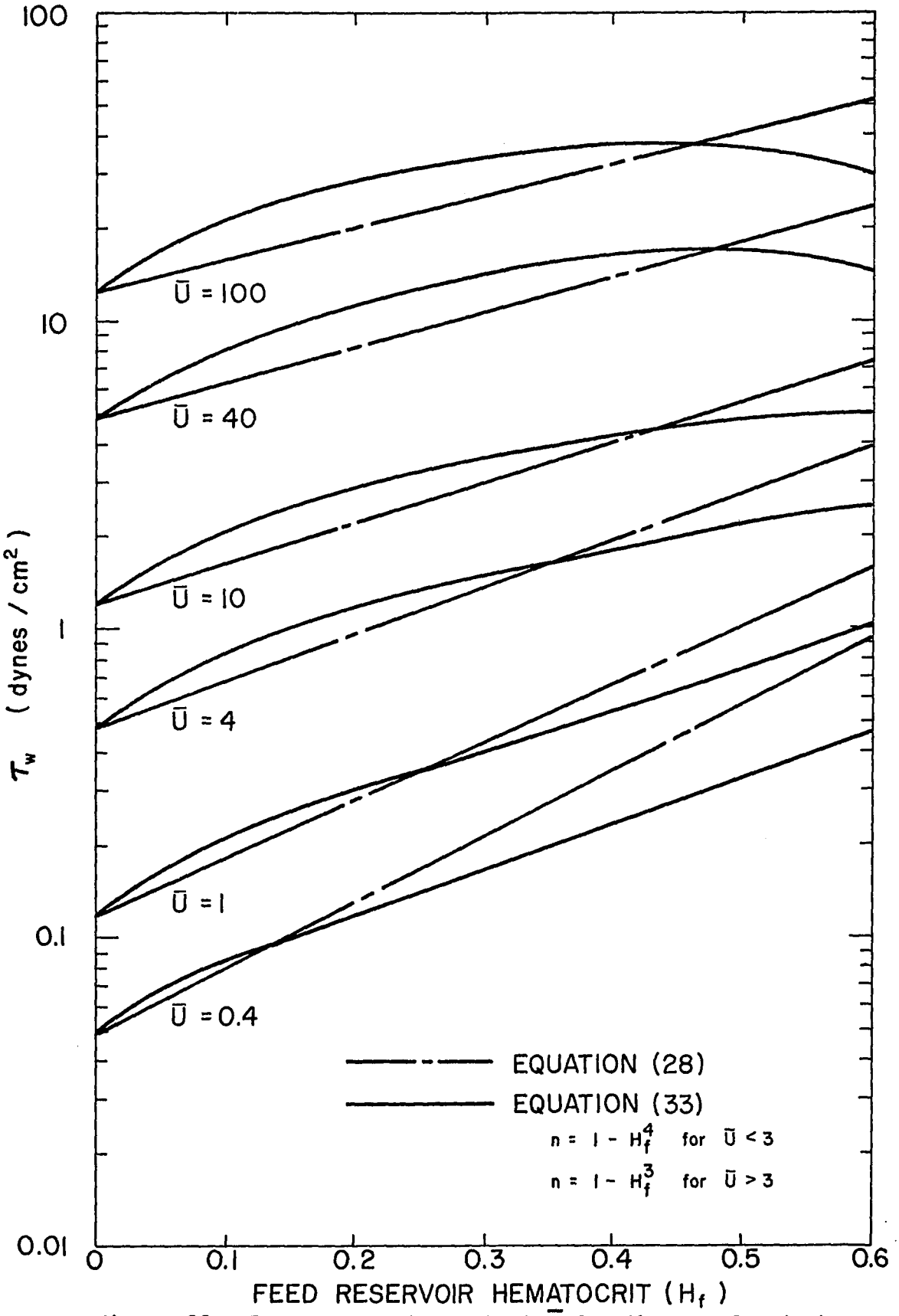

Figure 23. Ln τ_w - H_f at Constant $\bar{U}$ for the Pseudo-Bingham Model.

was used for K. When other values of K were used, the agreement with experimental data was not improved. This simply reflects the fact that blood is not a power law fluid except over a very limited shear rate (or $\bar{U}$) range.

In summary, all attempts to correlate blood flow data with existing basic flow models proved entirely unsatisfactory even when considerable latitude was taken in evaluating the unknown terms in the equations. We are thus left with only the empirical equation of the last section and the hope of developing a new theory on which to base an acceptable blood flow model.

An attempt was made to develop a simplified theory in the hope that the theory would be able to correlate the experimental data with reasonable accuracy, or at least guide future efforts aimed at a better understanding of the flow properties of blood.

In the development of any new theory, it is first necessary to make a number of simplifying assumptions and then either justify the assumptions or improve them. The necessary assumptions that allow a theory to be developed are 1) the total force measured at the capillary tube wall is equal to the Newtonian force caused by the plasma, plus the force due to the presence of the suspended particles, 2) the combined force of the particles is assumed to be equal to the force of an individual particle times the number of particles present in the suspension, 3) the only force that the particles add to

the total force is the Stokes' law drag. The Stokes' law was chosen because of the low Reynolds Number. The forces that could be present include a) the Stokes' drag, b) the radial force tending to migrate the particles across streamlines, c) the force due to angular acceleration of the particles migrating across the streamlines, and d) the force caused by the normal acceleration of the particles.

Force 'c' is neglected by assuming that the particles that do migrate across the streamlines acquire a very small change in angular velocity. Force 'd', the force due to particle boundary acceleration, is neglected by assuming that the red cell does not deform during flow (after an initial deformation). Force 'a', the Stokes' law drag, is given by:

$$F_t = 6\pi\mu_p dV_a \tag{36}$$

Force 'b', the radial migration force, is given by the Rubinow-Keller theory (115) and is equal to:

$$F_r = \pi d^3 \rho\ \Omega \times V_a \tag{37}$$

In the Rubinow-Keller theory, which was derived for a rotating-translating sphere in an infinite fluid, Ω is the angular velocity of the particle and V_a is the axial slip velocity. This is the same as V_a in the Stokes' law force, Equation (36). It is the <u>average</u>

fluid velocity minus the particle velocity. For a particle moving through an infinite fluid at rest, V_a is just the negative of the particle velocity.

Jeffrey (82) found that Ω, the angular velocity, is given by:

$$\Omega = 2V_m r/R^2 \tag{38}$$

where V_m is the centerline velocity, R is the tube radius, and r is a radial position. Goldsmith and Mason (58) verified the above equation to within 1% for $r/R < 0.04$. The average angular velocity is given by:

$$\langle\Omega\rangle = \int \Omega da \Big/ \int dA = 4V_m/3R \tag{39}$$

The calculation of V_a, the axial slip velocity, presents considerable difficulty. The fluid velocity is less than the particle velocity on the wall side of the particle but larger on the axis side of the particle. The particle velocity can be measured directly, but since the fluid velocity is different at various points surrounding the particle, the <u>average</u> fluid velocity is difficult to calculate. Note that the velocity gradient across the sphere causes the rotation. It is convenient to assume that the axial slip velocity is given by:

$$V_a = V(r) - 1/2 \left[V(r+d) + V(r-d)\right] \tag{40}$$

where the velocity gradient is assumed to be parabolic and equal to:

$$V(r) = V_m \left[1 - (r/R)^2 \right] \tag{41}$$

It can be seen that in Equation (40), V_a is defined as the fluid velocity at the center of the sphere minus the average of the fluid velocities at the outer and inner edges of the particle. With these definitions, Equation (40) becomes:

$$V_a = +V_m d^2/R^2 \tag{42}$$

Note that Equation (42) is independent of radial position, and all the particles have the same axial slip velocity. This relationship was essentially verified by Goldsmith and Mason (58,59). Combining Equations (36) and (42) gives, for the translational force exerted by a single particle:

$$F_t = 6\pi \mu_p d^3 V_m/R^2 \tag{43}$$

Combining Equations (37), (39), and (42) gives the radial force exerted by a single particle:

$$F_r = 4\pi d^5 \rho V_m^2/3R^3 \tag{44}$$

For a parabolic flow field:

$$V_m = 2(U) = 2\left\{\frac{4Q}{\pi D^2}\right\} = 2D\bar{U} = 4R\bar{U} \tag{45}$$

Dividing Equation (44) by Equation (43) and using Equation (45), the ratio of the radial force to the translational force is:

$$\frac{F_r}{F_t} = 8d^2 \rho \bar{U}/9\mu_p \tag{46}$$

The presence of d^2 in the numerator of Equation (46) suggests that the radial force can be neglected compared to the translational force. Thus, the total force exerted by the suspension on the capillary tube wall is given by Equation (43), and using Equation (45):

$$F_{total} = 24\pi \mu_p d^3 \bar{U} n_t R + F_{Newtonian} \tag{47}$$

where n_t is the number of particles and $F_{Newtonian}$ is the Newtonian force of the liquid portion of the suspension. From the definition of the shear stress at the wall, $F_{Newtonian} = 2\pi RL \tau_w$, where τ_w is the shear stress at the wall. Thus, equation (47) becomes, using Equation (13):

$$F_{total} = 24\pi \mu_p d^3 \bar{U} n_t/R + 16\pi RL\mu_p \bar{U} \tag{48}$$

where μ_p is again the plasma viscosity. n_t, the number of particles in the suspension, is related to the hematocrit as follows:

$$H = n_t(\text{volume of a red cell})/\text{total volume} \tag{49}$$

In order to calculate the volume of a red cell, the average thick-

ness of the red cell is taken to be d/3 (see Figure 1). Thus, Equation (49) becomes:

$$H = \frac{\pi n_t d^2 (d/3)}{\pi R^2 L} = n_t d^3/3R^2L \tag{50}$$

Therefore, n_t is equal to:

$$n_t = 3R^2LH/d^3 \tag{51}$$

Equation (48) becomes:

$$F_{total} = \frac{24\pi\ \mu_p d^3 \bar{U}}{R} (3R^2LH/d^3) + 16\pi RL\mu_p \bar{U}$$

or:

$$F_{total} = 16\pi RL\mu_p \bar{U}(1 + 4.5H) \tag{52}$$

Finally, using the fact that $F_{total} = 2\pi RL\ \tau_w$, Equation (52) becomes:

$$\tau_w = 8\mu_p \bar{U}(1 + 4.5H) \tag{53}$$

Note that Equation (53) predicts Newtonian behavior for blood, once H is fixed.

Since the derivation of Equation (53) assumes that all the particles act as individuals, it is expected that this equation should work best for red cells in saline or at high $\bar{U}$, where formations of rouleaux and three-dimensional networks of rouleaux are absent.

Equation (53) is plotted in Figure 24 for $\bar{U} = 100$.

In order to improve the previous derivation, it is necessary to improve the assumptions that were made at the start, and take into account the facts that at low $\bar{U}$, all the particles do not act as individuals, but group together into rouleaux of varying length, and that these rouleaux interact with each other (see Figure 3); and also that the deformation of the red cells increases with $\bar{U}$.

There is a constraint on the minimum number of rouleaux possible. Consider a section of capillary tubing of length L, and assume that the rouleaux are parallel to the tube axis and that all the rouleaux in this section of tubing have enough particles such that the length of every rouleaux is also L. Then the hematocrit in this section of tubing is:

$$H = \frac{\pi d^2 L}{\pi R^2 L} \quad n_o = d^2 n_o / R^2 \qquad (54)$$

where n_o is the number of rouleaux present. It now becomes necessary to use experimental data concerning the number and length of the rouleaux as a function of $\bar{U}$ and hematocrit (31,60,118). An equation describing the force on a rouleaux would then have to be derived. Such an equation would be similar to an equation describing the force on a finite cylinder. The total force exerted by the fluid would be equal to the sum of the Newtonian force of the plasma plus the force of each rouleaux times the number of rouleaux in the tube.

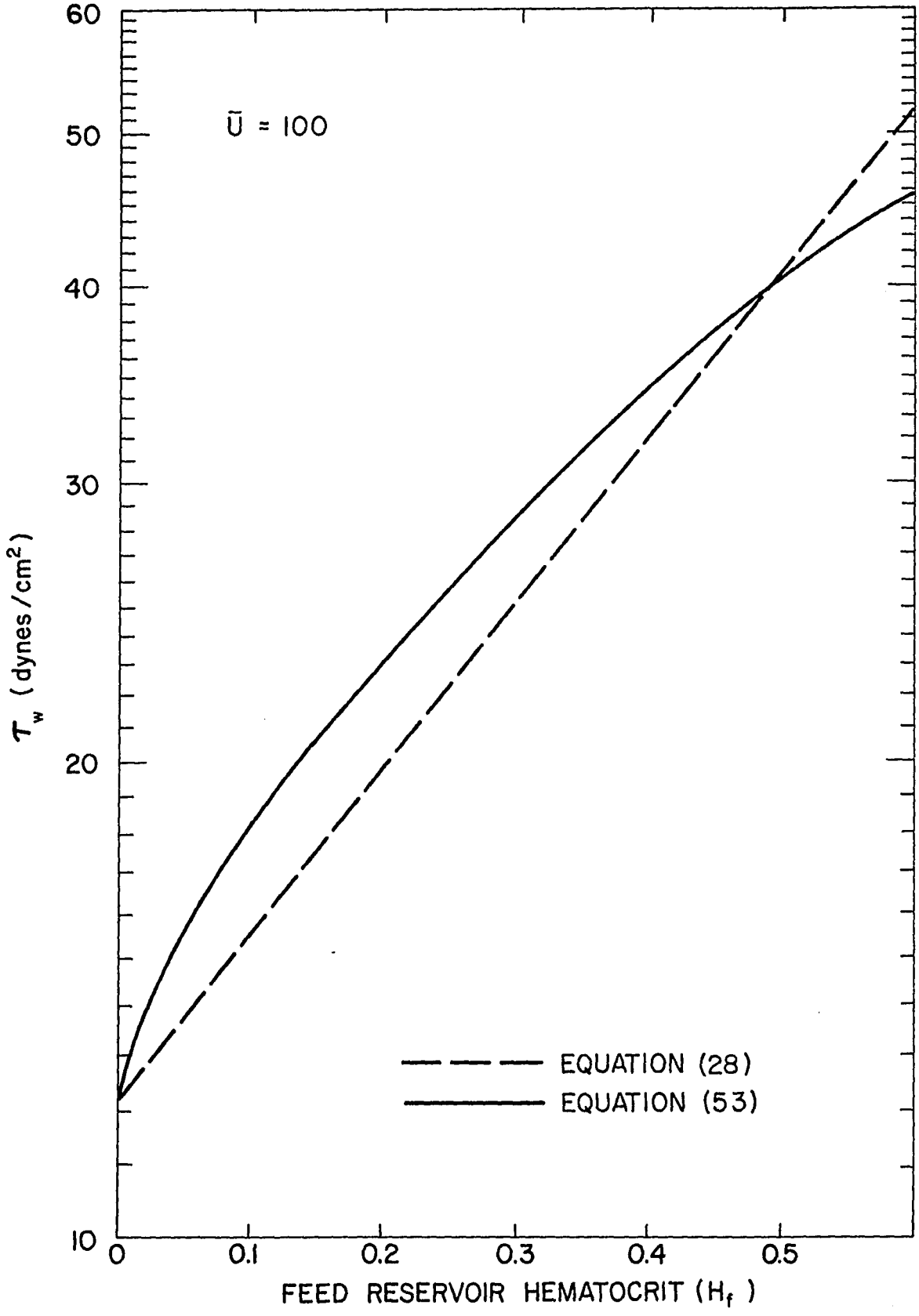

Figure 24. Ln τ_w - H_f at $\bar{U}$ = 100 for Stokes Law Model.

Two-body and three-body interactions would have to be taken into consideration. Deformation of the red cells is probably also important.

Results Obtained Using a Capillary Viscometer and Tubes Smaller Than 300 Microns I.D.

Experimental Results

Pressure drop-flow rate data were taken using normal human blood at constant reservoir hematocrits ranging from 0.151 to 0.559 for a number of different tube diameters ranging from 29 to 221 microns. The τ_w - $\bar{U}$ correlations obtained from the experimental data are shown in Figures 25 through 31 for the 221, 153.5, 128, 99, 75, 59, and 29-micron tubes, respectively. It can be seen from close inspection of the curves for different tubes that have approximately the same feed reservoir hematocrit that as the tube diameter decreases, the shear stress decreases for a given $\bar{U}$. This behavior is known as the Fåhraeus-Lindqvist effect, and is considered by some workers to be the result of the failure of continuum fluid mechanics to describe the flow properties for a particulate suspension as the ratio of tube diameter to particle diameter decreases to below about 15. It has been established that for tubes larger than about 300 microns, the flow properties of normal human blood are independent of tube diameter (45). The lines shown in Figures 25

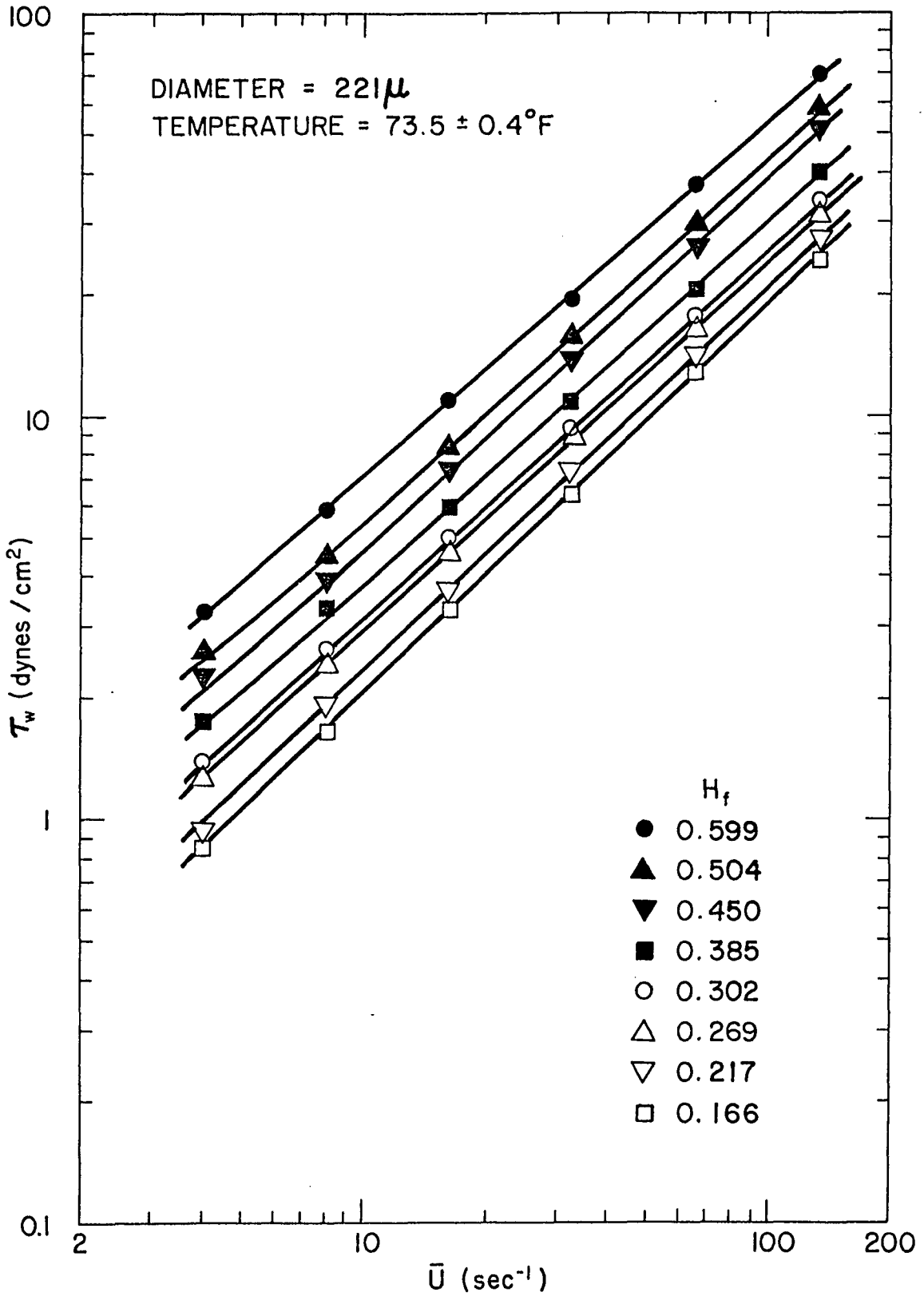

Figure 25. τ_w - $\bar{U}$ Plot for Red Cells in Plasma, 221-Micron Tube

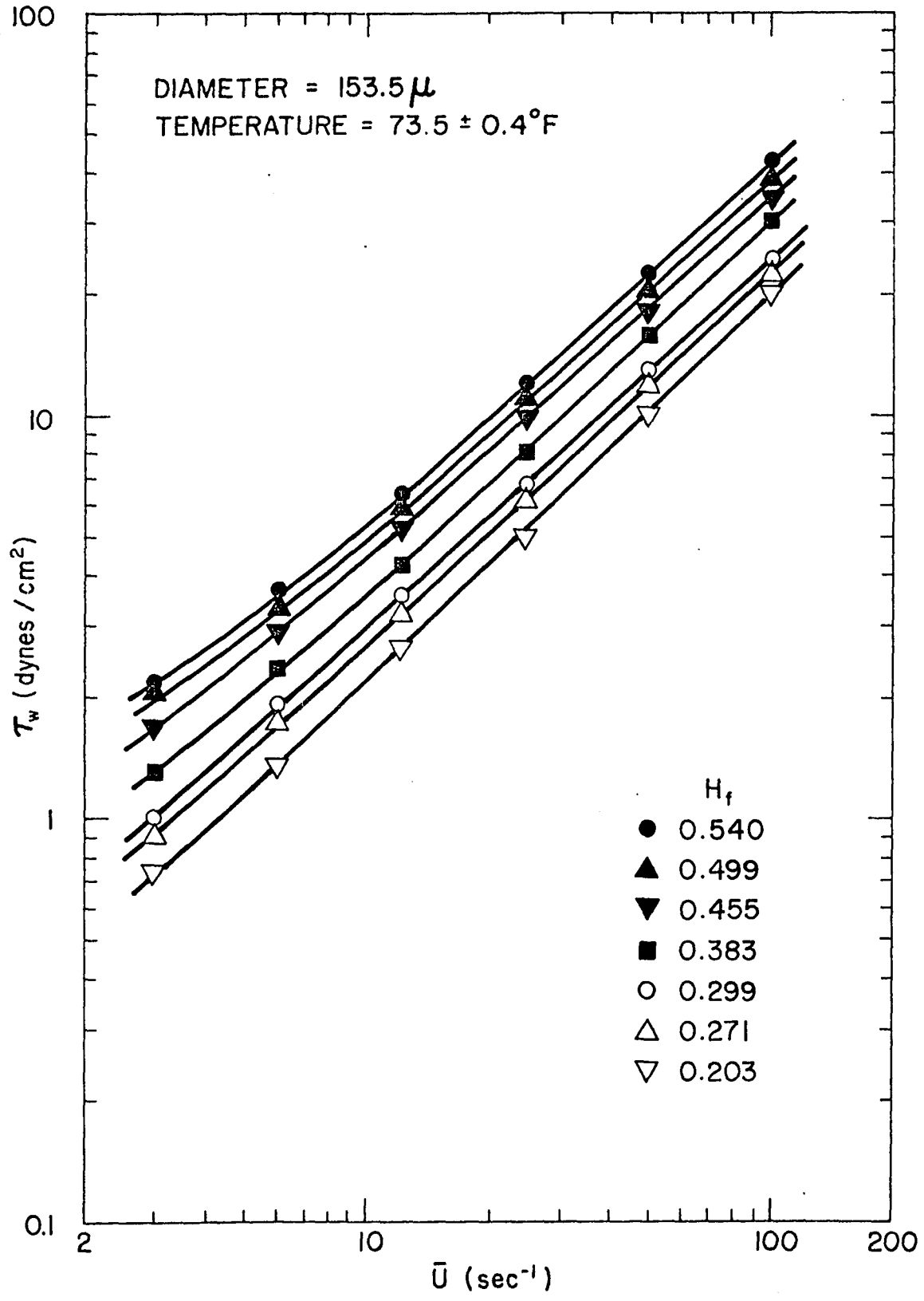

Figure 26. τ_w - $\bar{U}$ Plot for Red Cells in Plasma, 153.5-Micron Tube

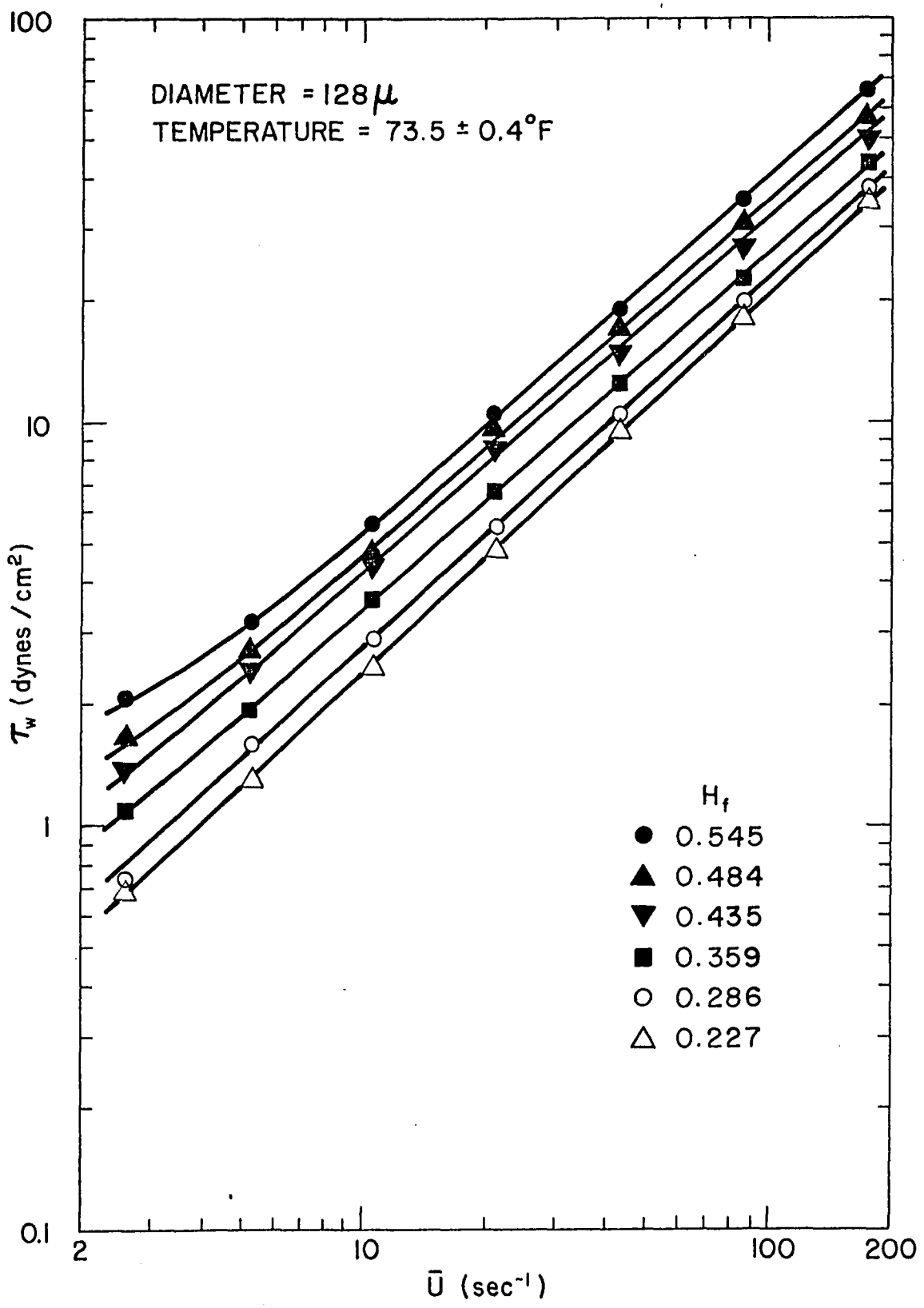

Figure 27. τ_w - $\bar{U}$ Plot for Red Cells in Plasma, 128-Micron Tube

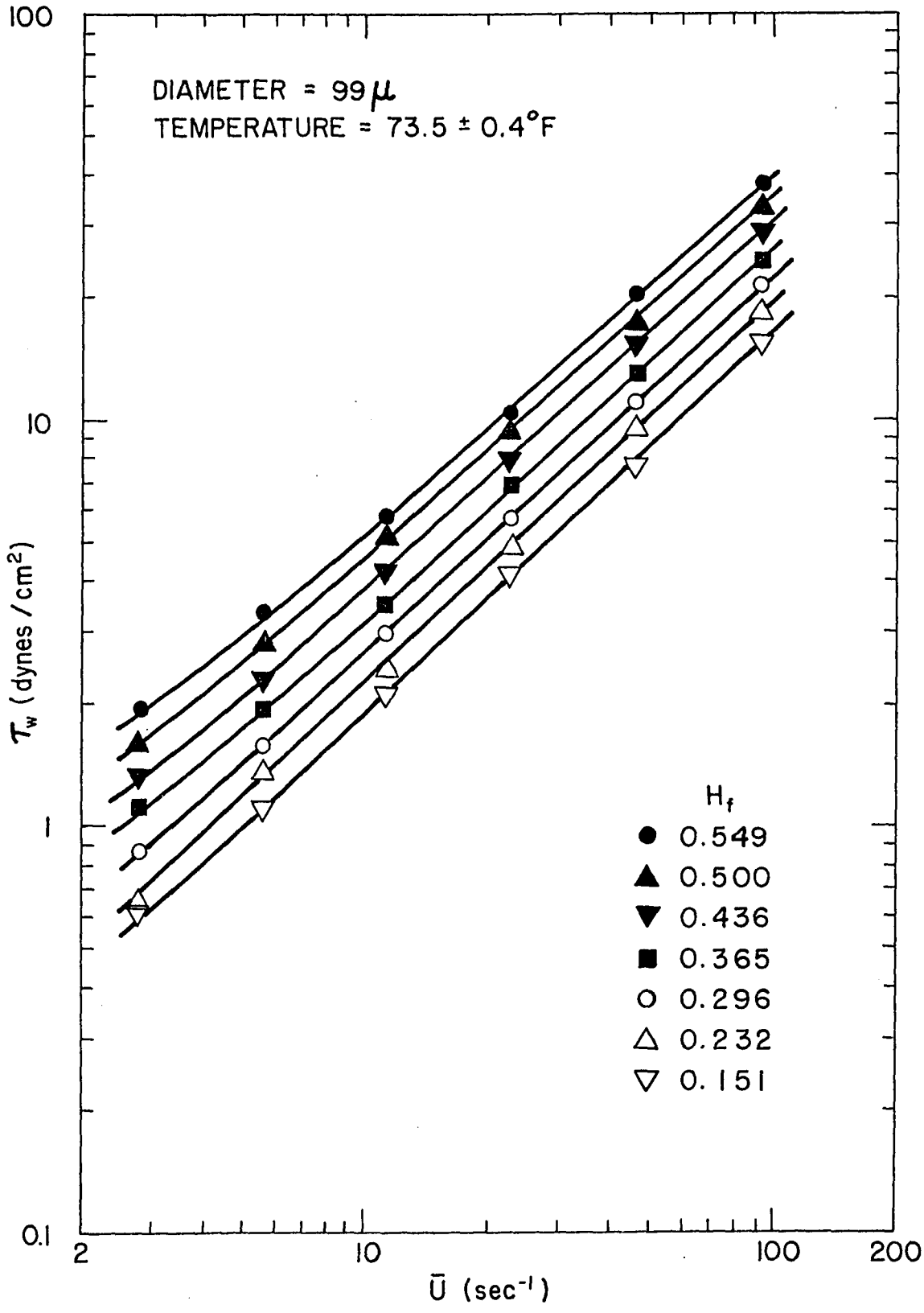

Figure 28. τ_w - $\bar{U}$ Plot for Red Cells in Plasma, 99-Micron Tube

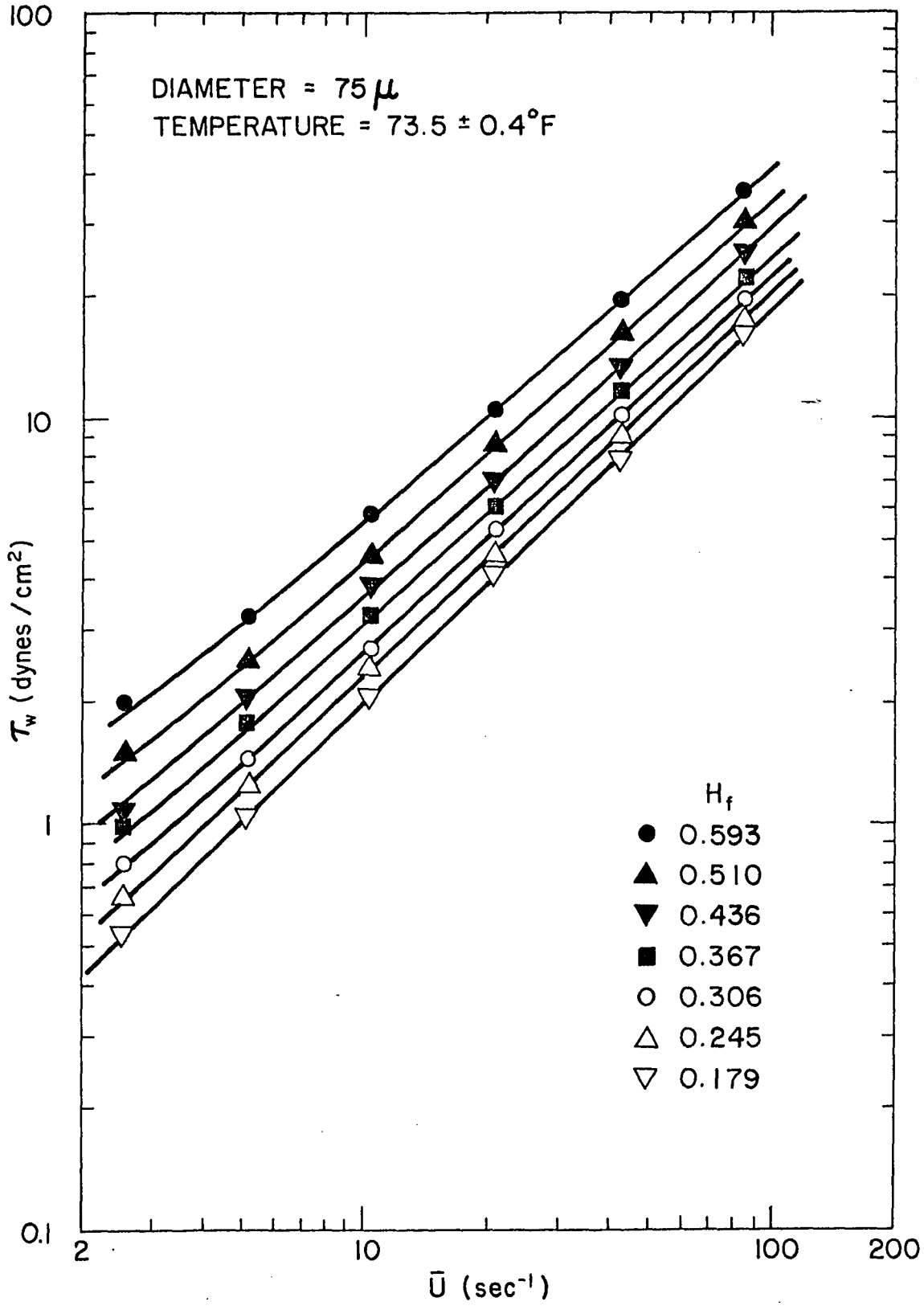

Figure 29. τ_w - $\bar{U}$ Plot for Red Cells in Plasma, 75-Micron Tube

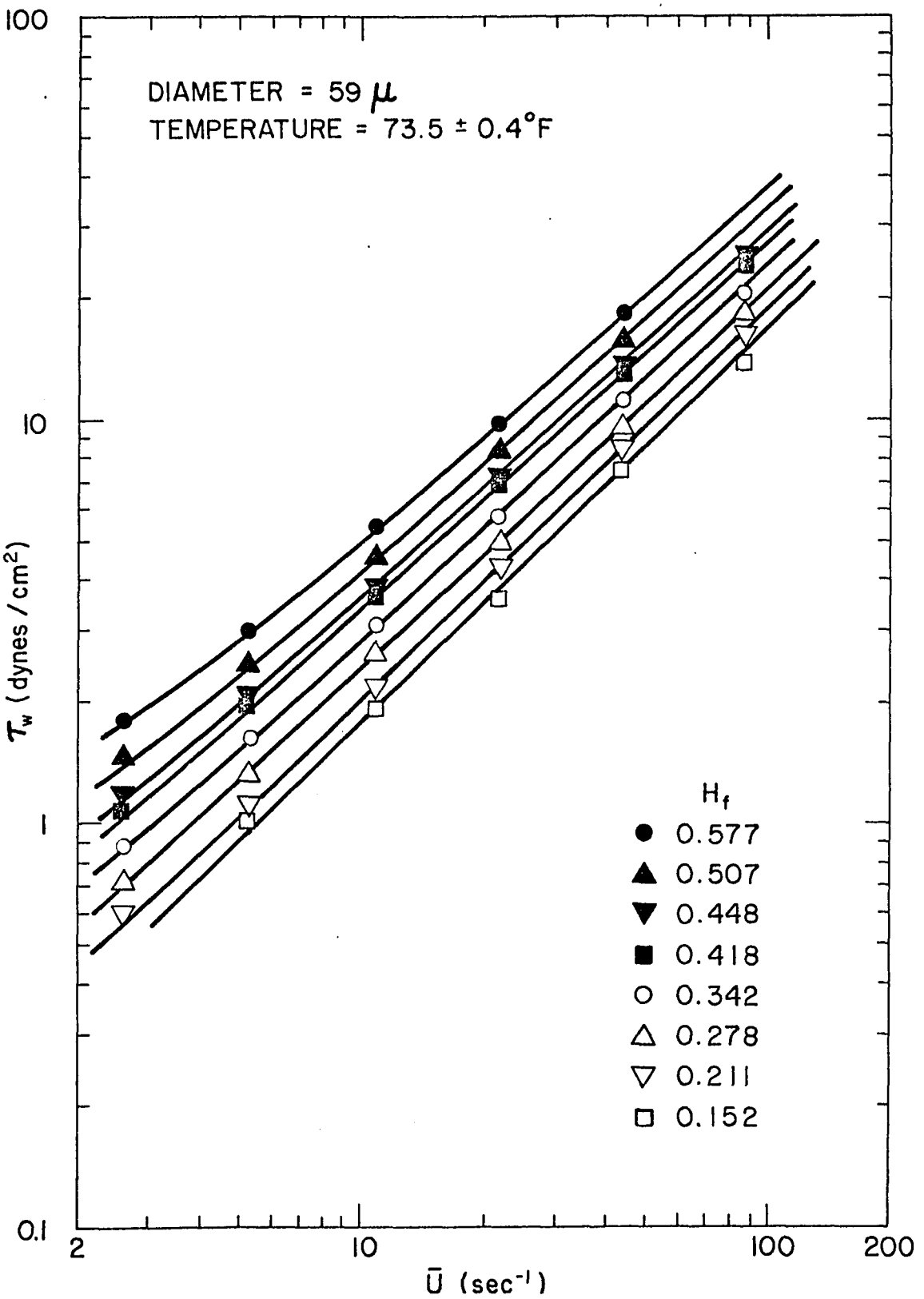

Figure 30. τ_w - $\bar{U}$ Plot for Red Cells in Plasma, 59-Micron Tube

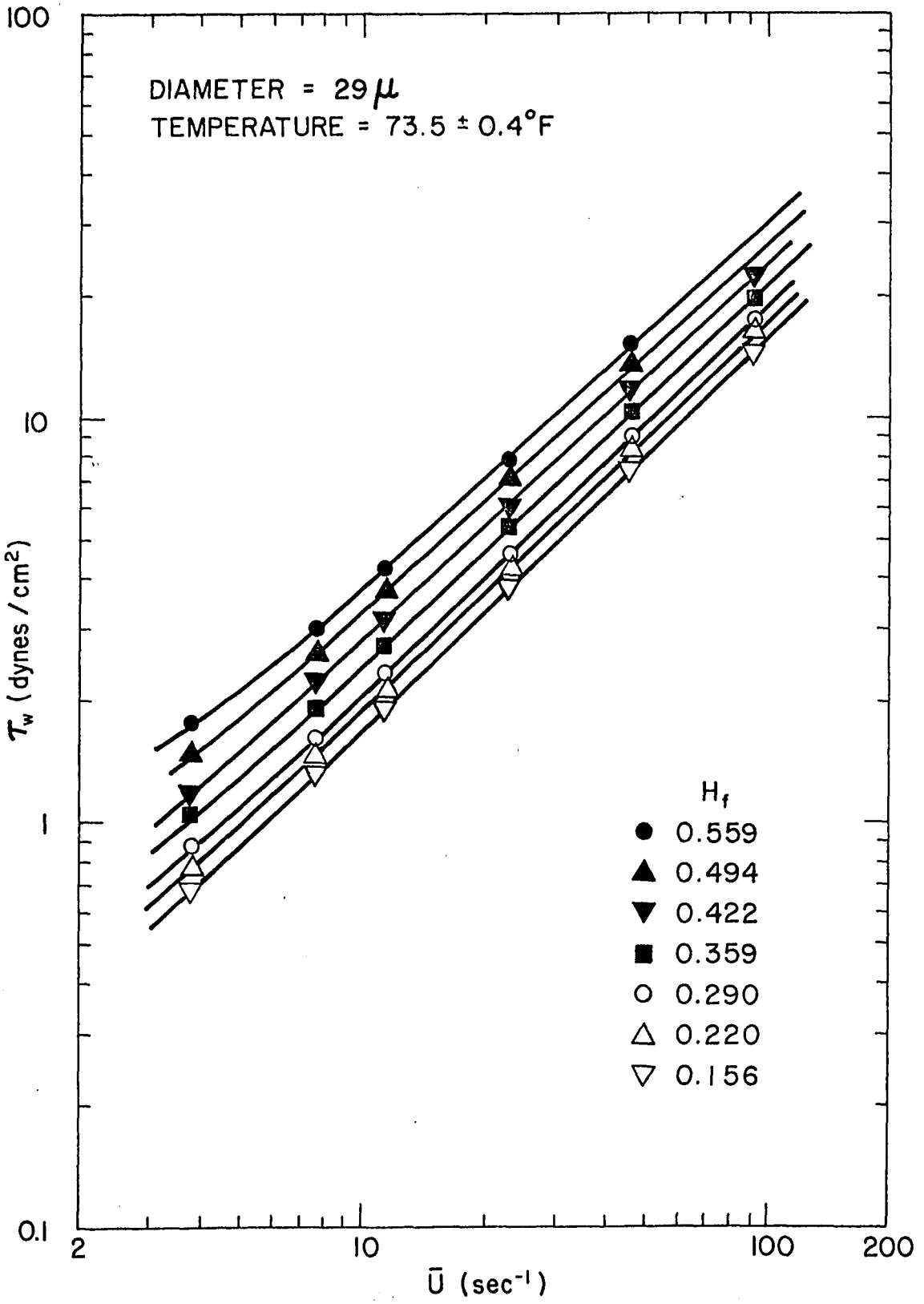

Figure 31. τ_w - $\bar{U}$ Plot for Red Cells in Plasma, 29-Micron Tube

through 31 were determined by a least squares fit. These lines were then used to determine ln τ_w versus H_f at $\bar{U}$'s of 10, 40, and 100. This is shown in Figure 32. The solid lines in Figure 32 were computed from the H_r versus H_f data of Figure 11. Figure 33, shown below, demonstrates how the lines were computed from the H_r versus H_f data.

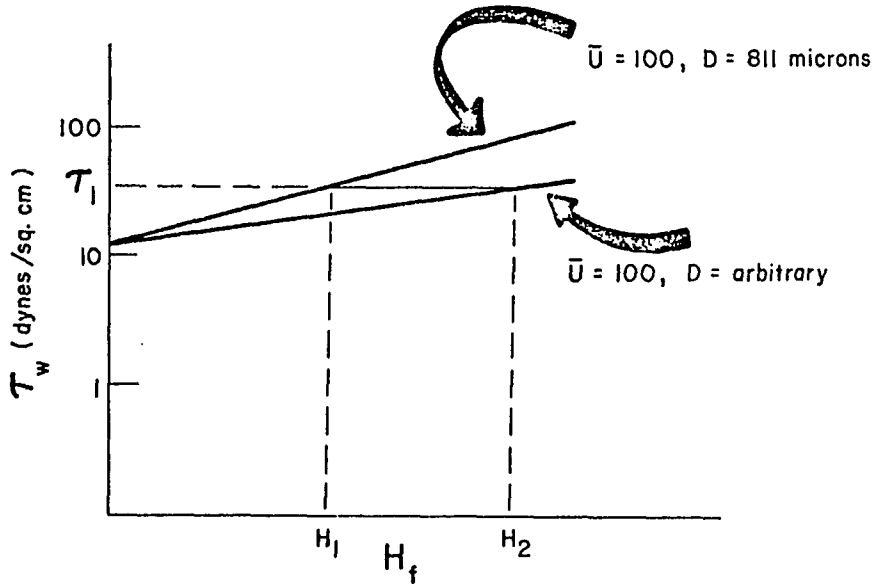

Figure 33. Ln τ_w vs. H_f at Constant $\bar{U}$.

For a given small tube, the feed reservoir is measured to be H_2. From a plot of τ_w vs. $\bar{U}$ at a hematocrit of H_2, the shear stress is found to be τ_1 at a $\bar{U}$ of 100. If the continuum model still holds, the proper hematocrit that should give a shear stress of τ_1 is H_1 (from Figure 18). H_1 is assumed to be the hematocrit inside the tube,

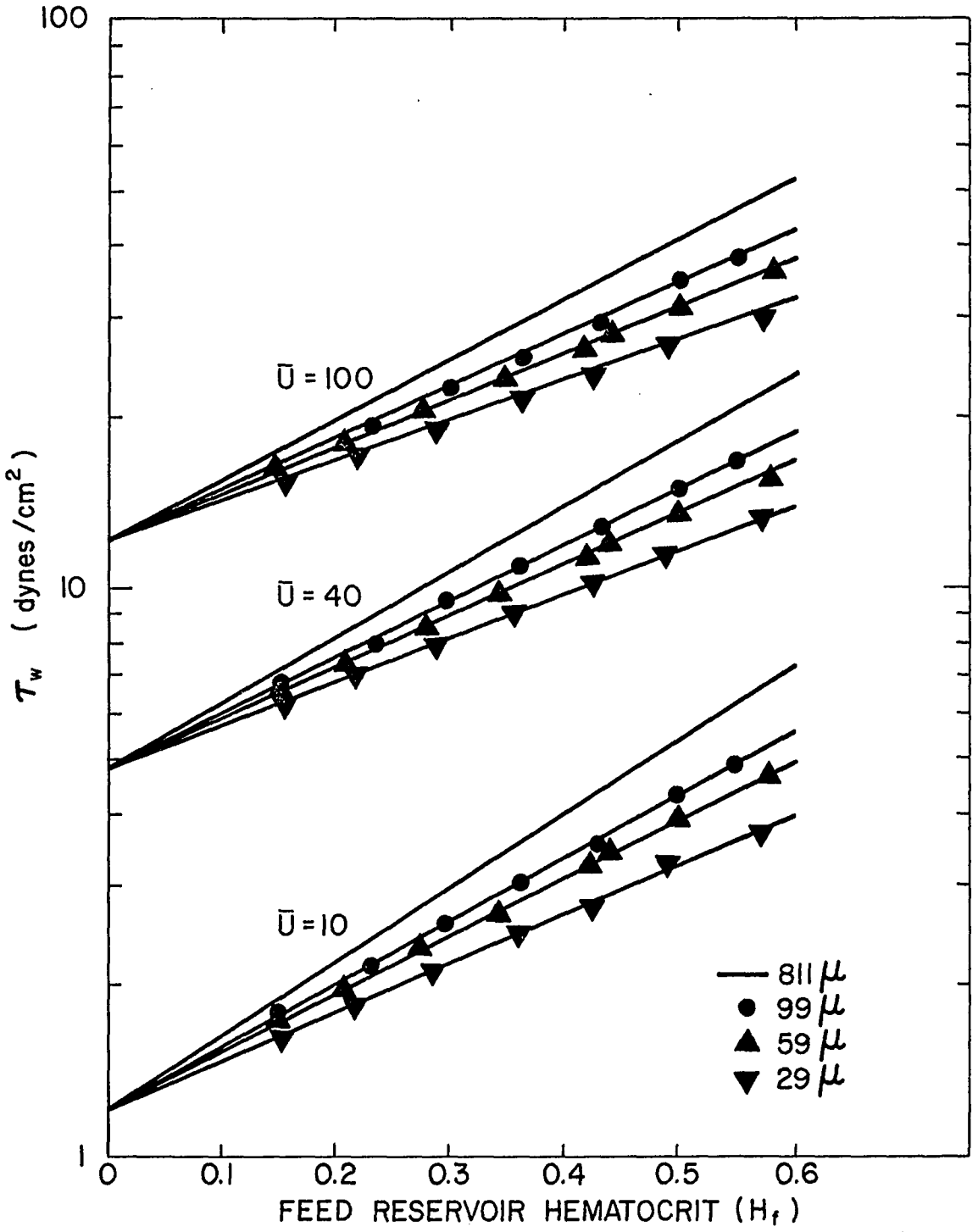

Figure 32. Ln τ_w - H_f at Constant $\bar{U}$, Predicted Data.

therefore $H_r = H_1/H_2$. In this way, the solid lines for tubes of 99, 59, and 29 microns ID are shown in Figure 32. The agreement between the theoretical lines based on a continuous fluid agree quite well with the experimental measurements. By changing the procedure slightly, H_r can be calculated for each experimental tube by using Figure 18. For $\bar{U}$'s of 10, 40, and 100, the shear stress at a given reservoir hematocrit is used to find a corresponding tube hematocrit from Figure 18. In this way, H_r as a function of H_f can be found for all reservoir hematocrits used with a given tube. The results of this procedure are shown in Figure 34. The error bands on the calculated points represent the various values calculated between $\bar{U}$'s of 10, 40, and 100. The solid lines are from Equation (18).

The method used to obtain Figures 32 and 34 is correct in principle but does not provide a quantitative picture of how accurately the data can be predicted by using the continuum model and the tube hematocrit instead of the reservoir hematocrit. In order to do this, Equation (28) and the values of C found in Table VI were combined with Equation (18), which gives H_r as a function of H_f for a given diameter tube. The predicted lines and the original data are shown in Figures 35 through 41 for the tubes from 221 down to 29 microns in diameter.

Within reasonable accuracy, (7% maximum and typically 0.5%), an equation has been found that enables the prediction of $\tau_w - \bar{U}$

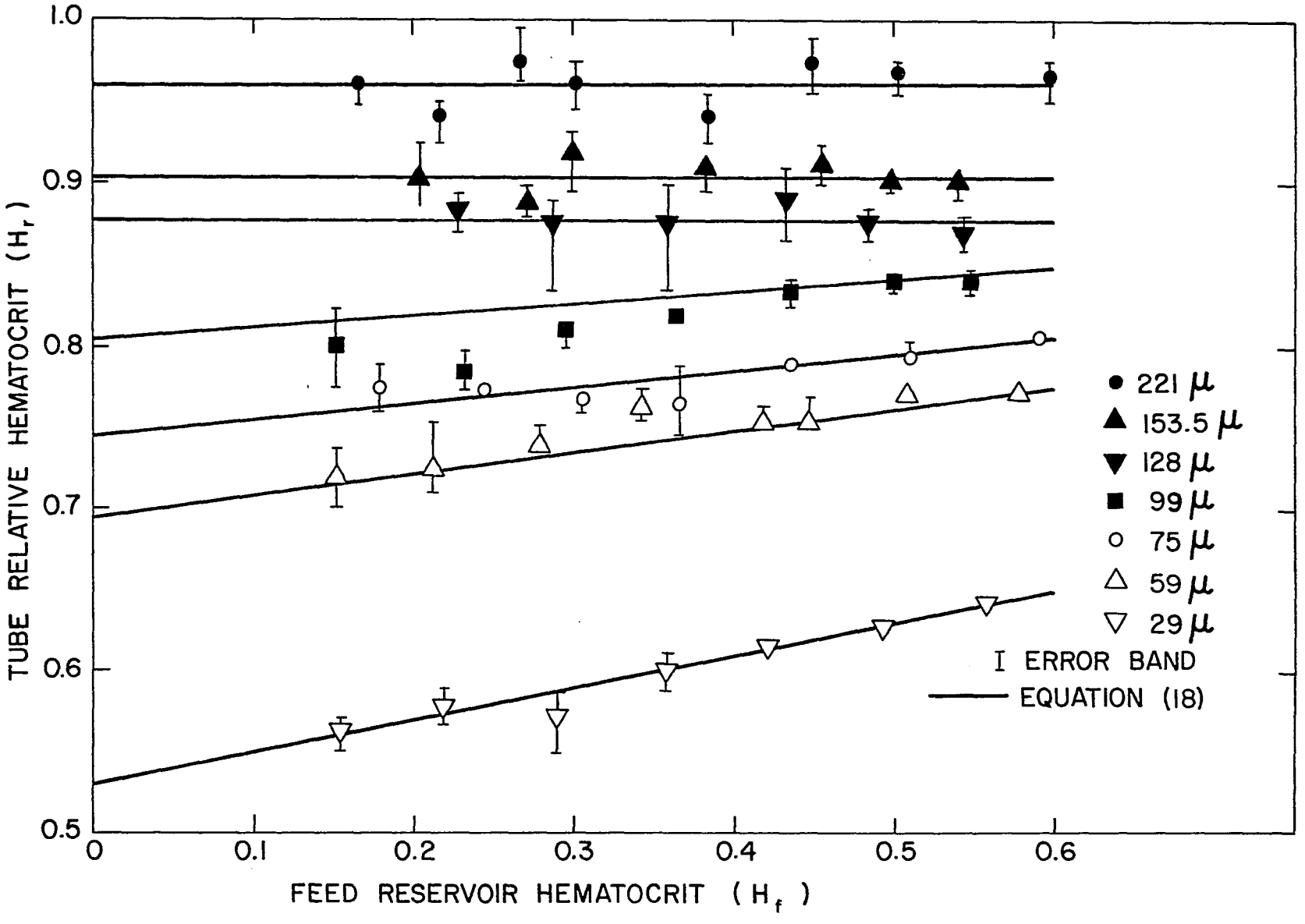

Figure 34. Relative Hematocrit vs. Feed Hematocrit, Predicted Data.

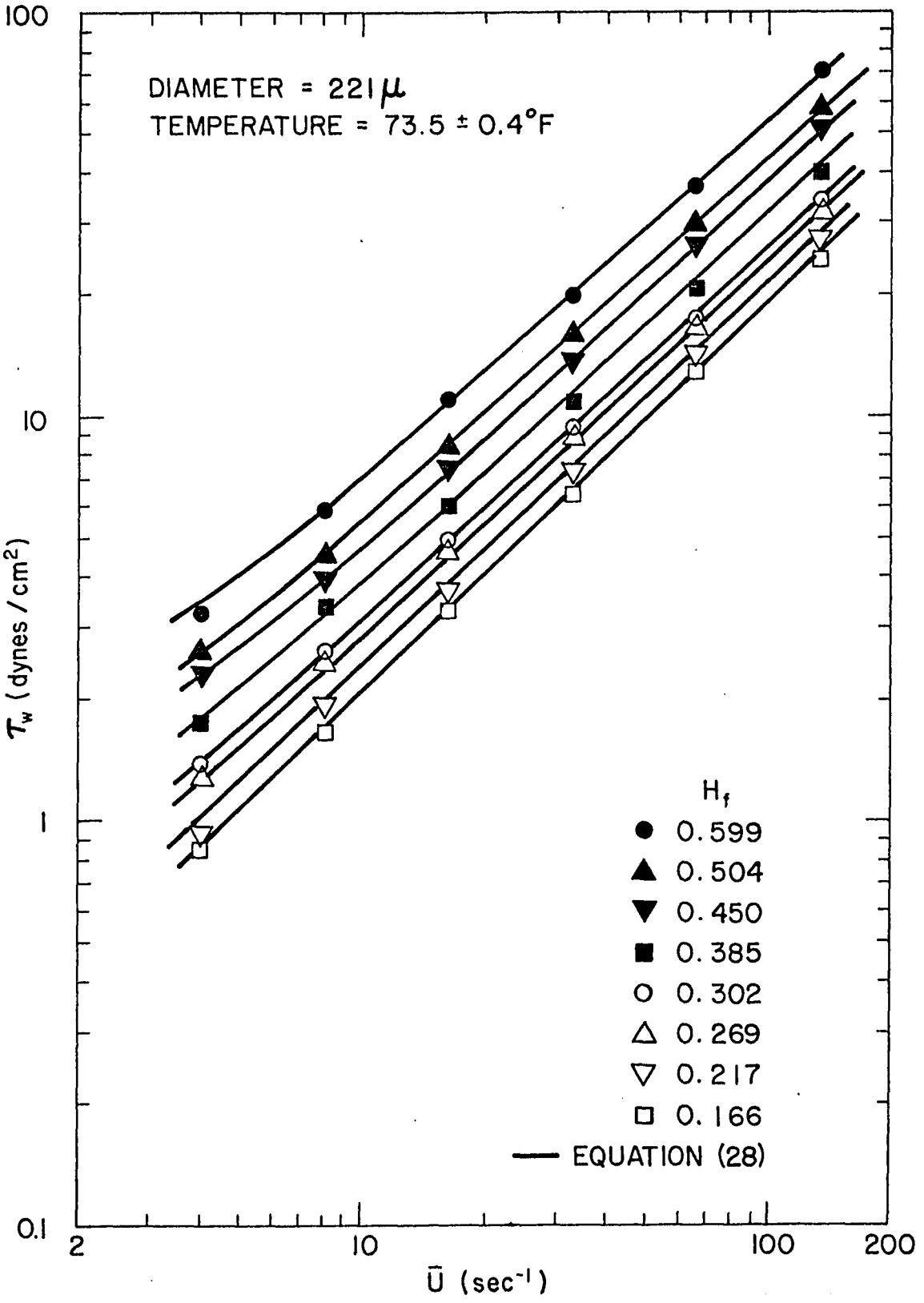

Figure 35. Predicted τ_w - $\bar{U}$ Plot for Red Cells in Plasma, 221-Micron Tube

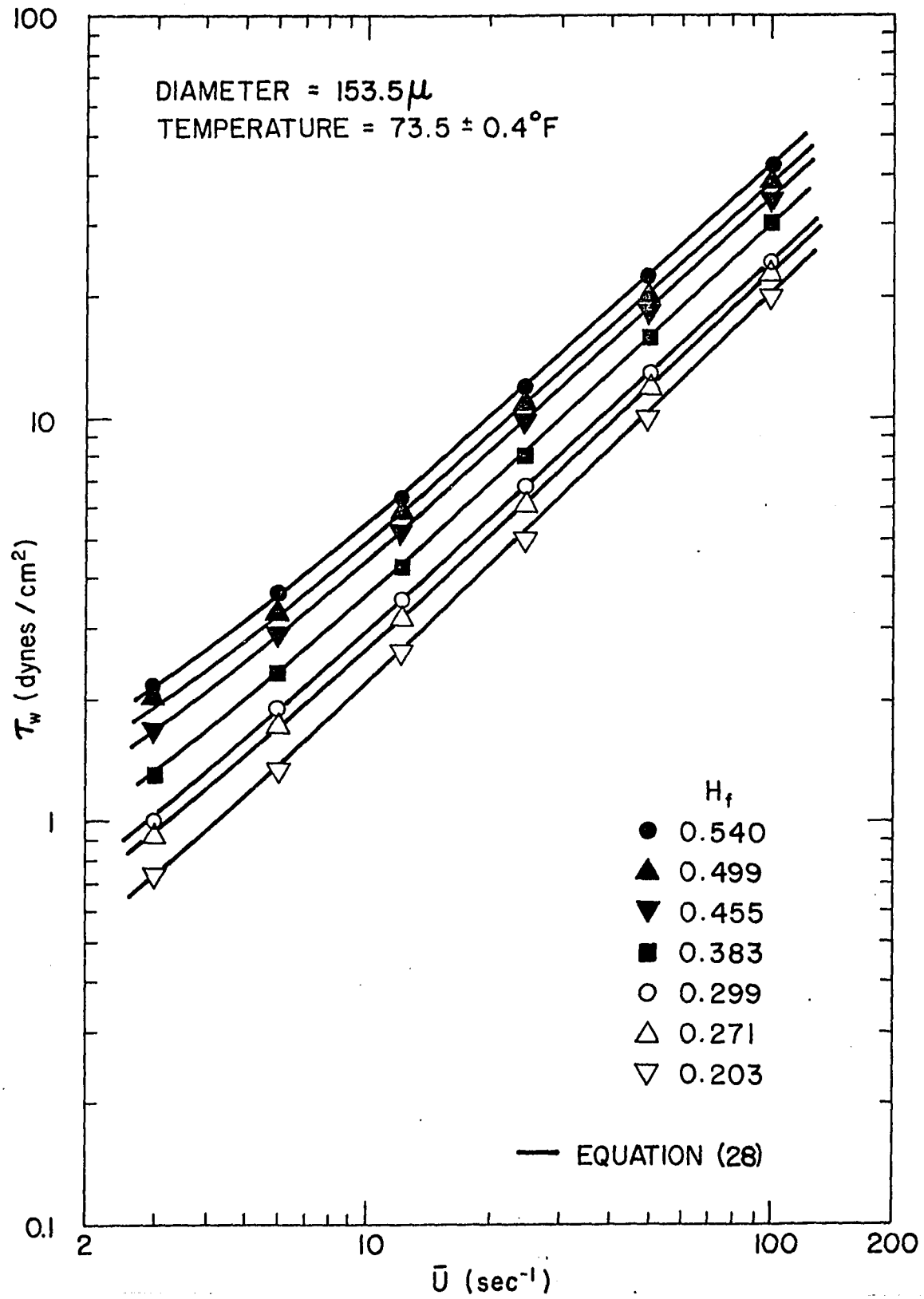

Figure 36. Predicted τ_w - $\bar{U}$ Plot for Red Cells in Plasma, 153.5-Micron Tube

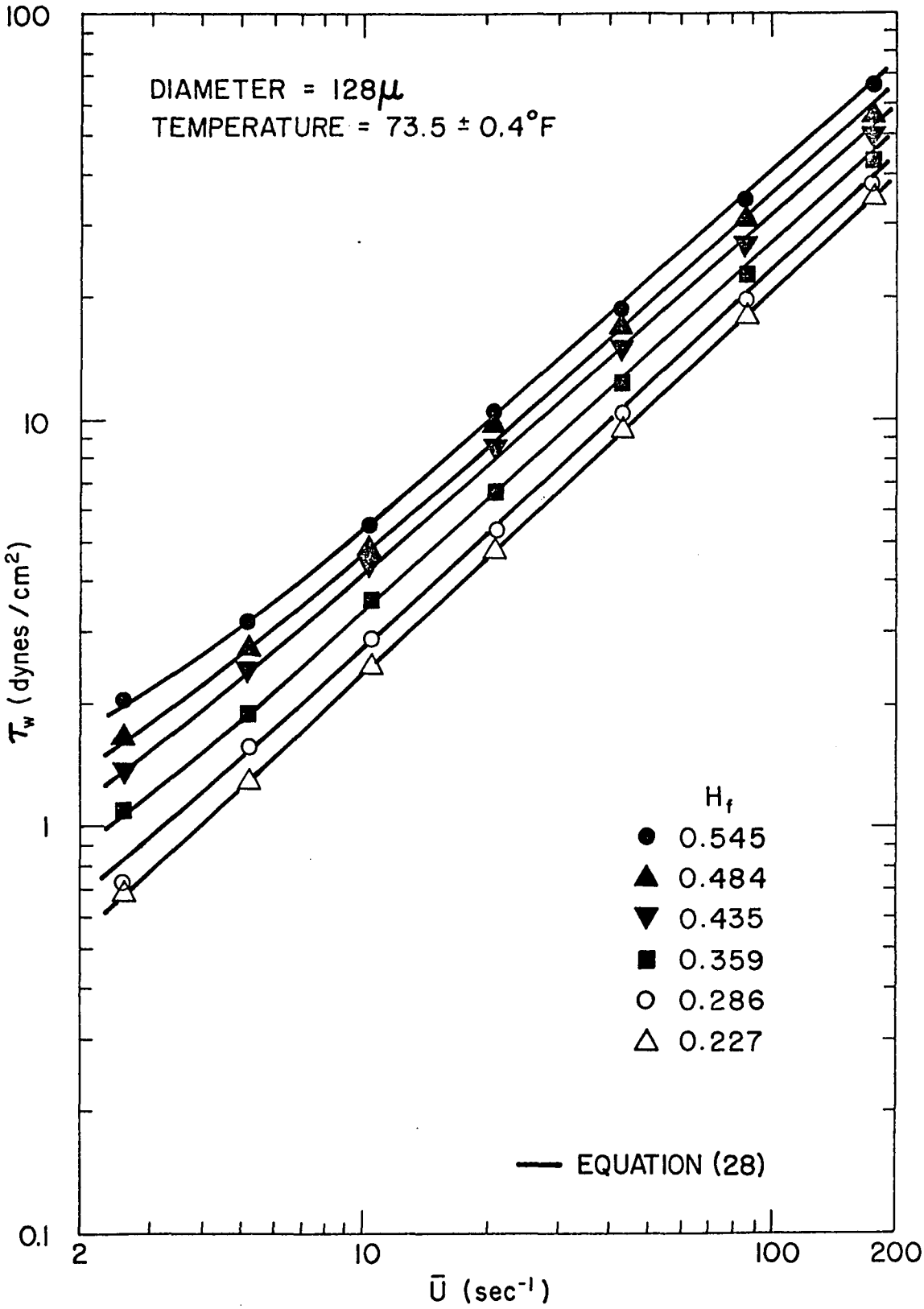

Figure 37. Predicted τ_w - $\bar{U}$ Plot for Red Cells in Plasma, 128-Micron Tube

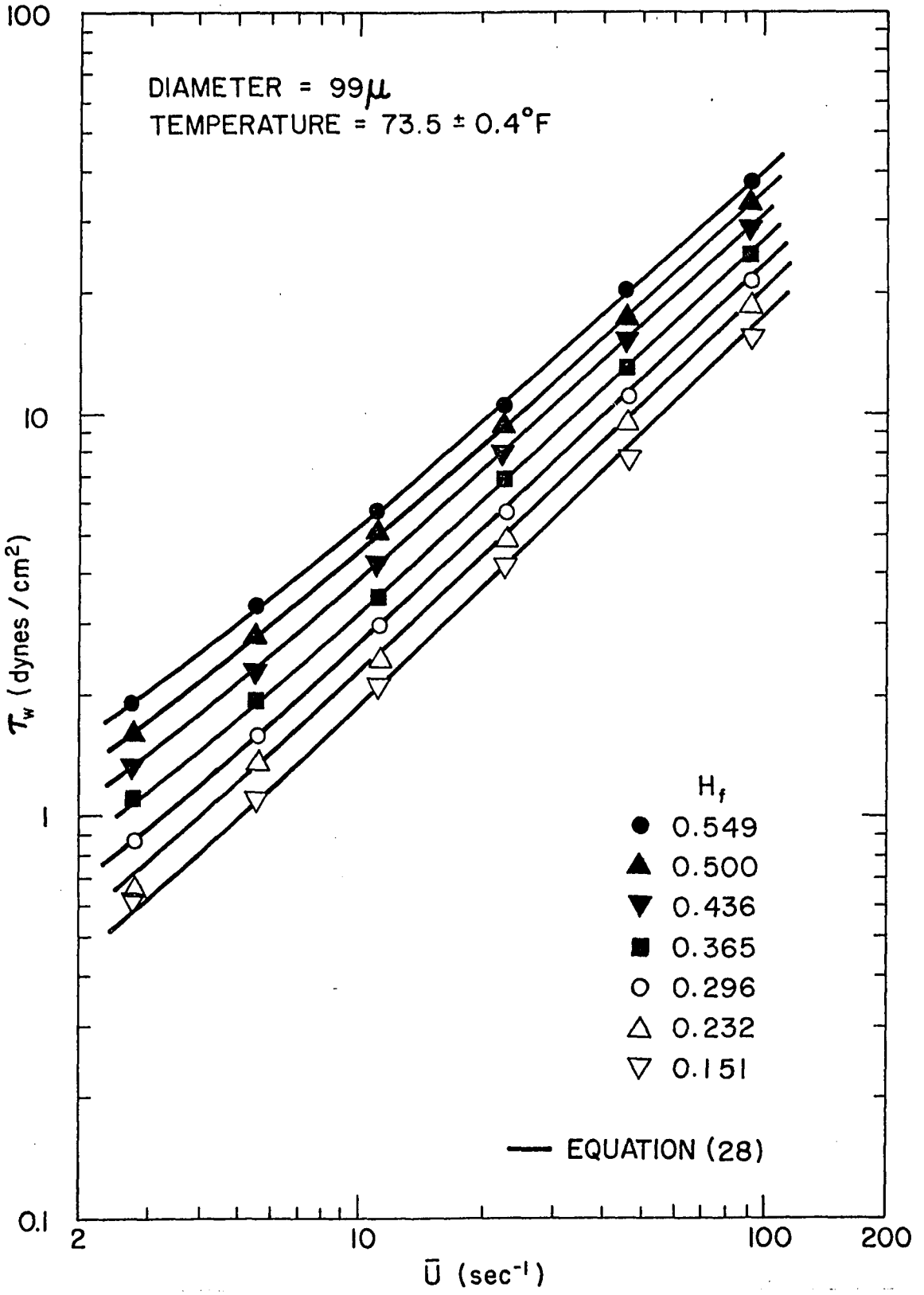

Figure 38. Predicted τ_w - $\bar{U}$ Plot for Red Cells in Plasma, 99-Micron Tube

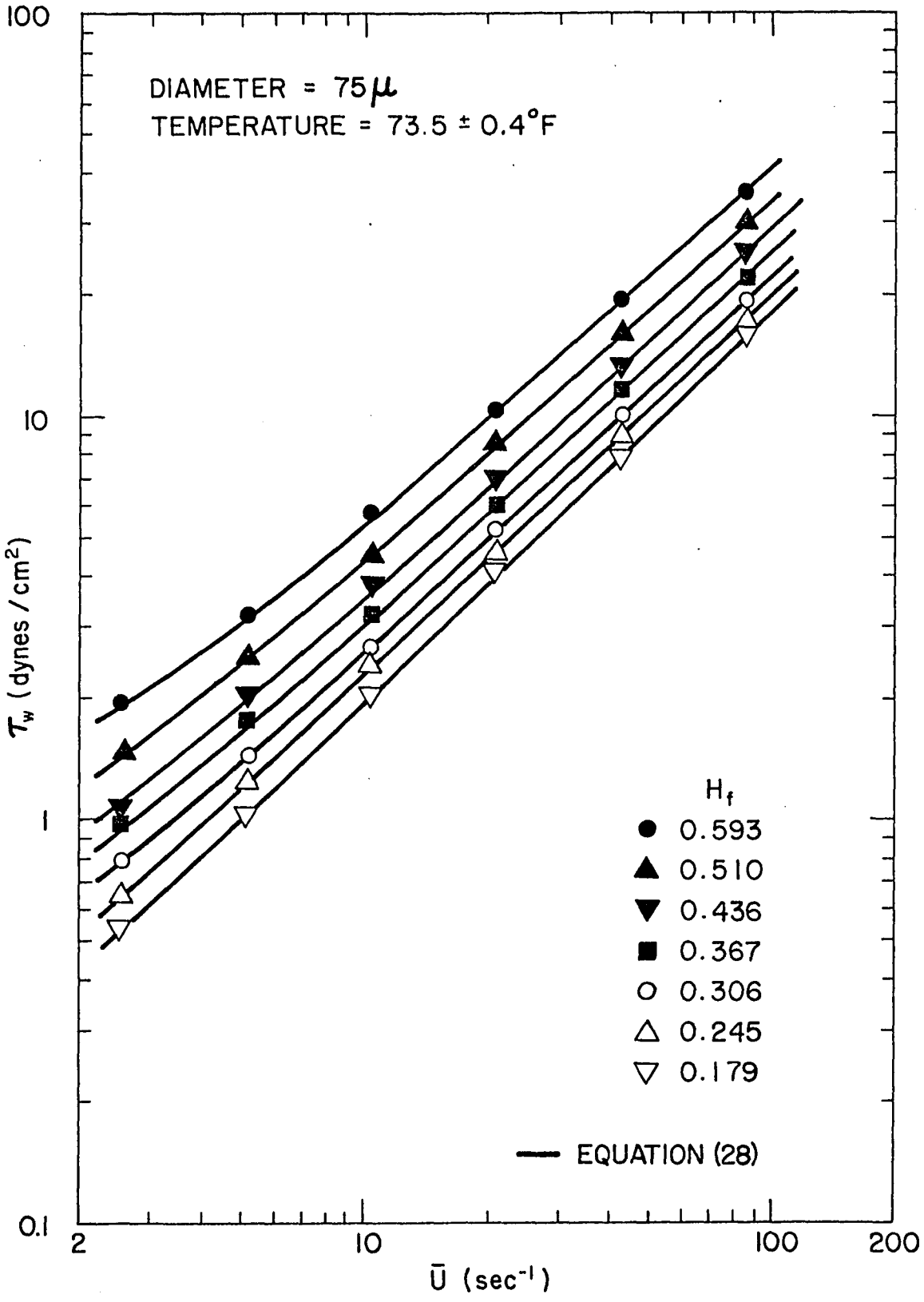

Figure 39. Predicted τ_w - $\bar{U}$ Plot for Red Cells in Plasma, 75-Micron Tube

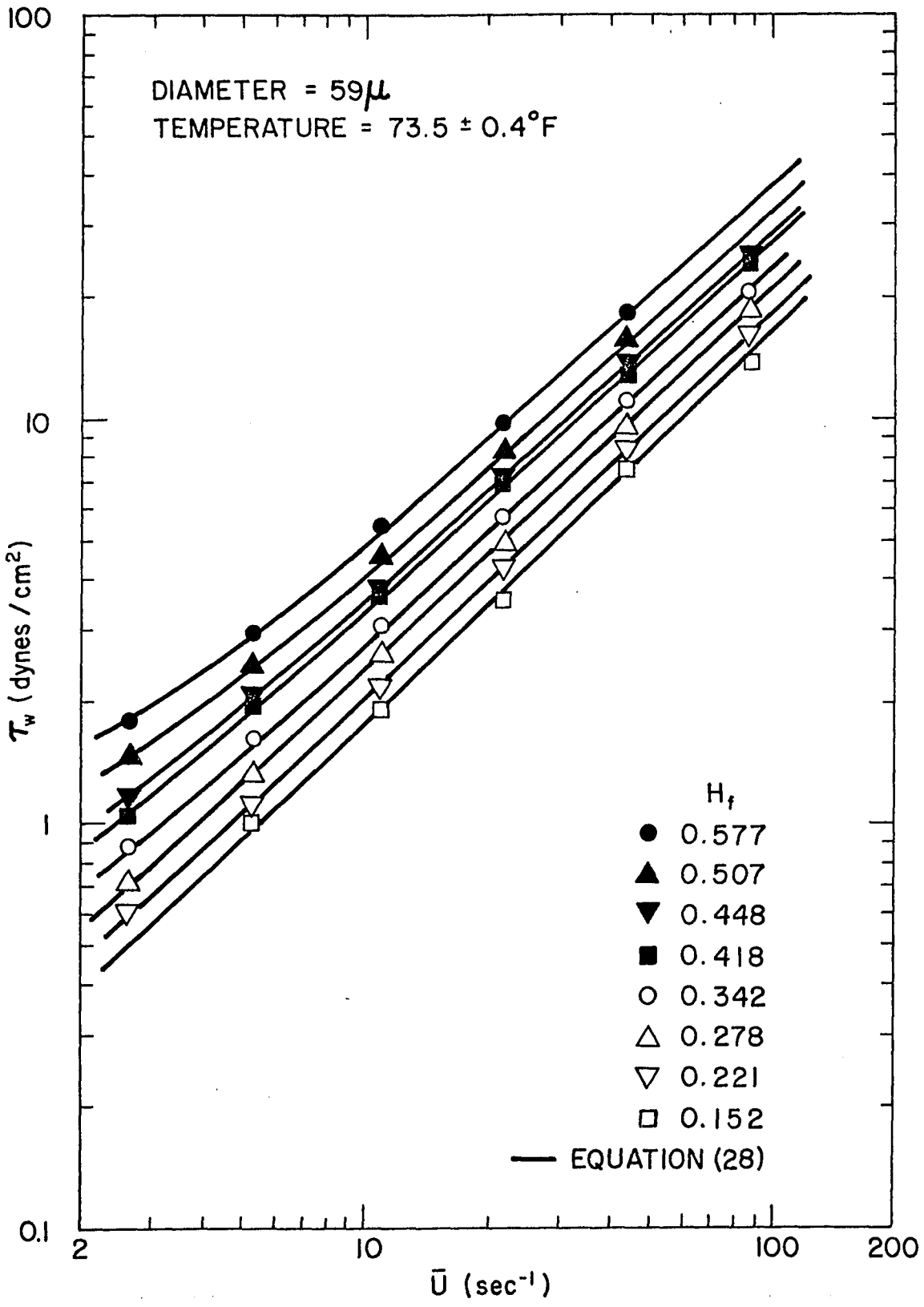

Figure 40. Predicted τ_w - $\bar{U}$ Plot for Red Cells in Plasma, 59-Micron Tube

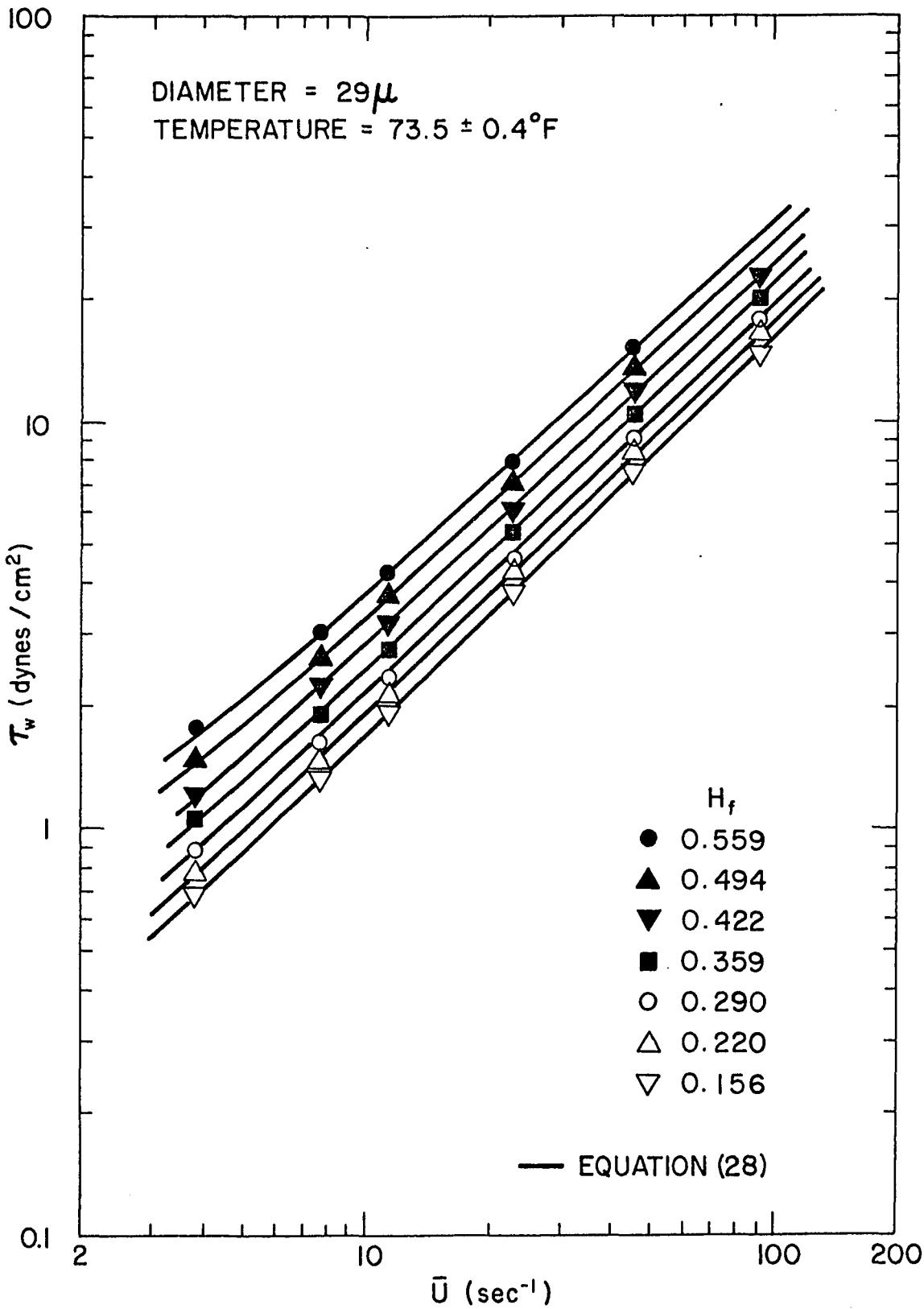

Figure 41. Predicted τ_w - $\bar{U}$ Plot for Red Cells in Plasma, 29-Micron Tube

curves for hematocrits between 0.15 and 0.60, and all tube diameters down to 29 microns, once the temperature and feed reservoir hematocrit of the blood sample are fixed.

The interesting point is that the derivation of the equation of motion assumes that there are continuous values of the fluid properties. A substance such as blood, which contains solid particles suspended in a Newtonian fluid does not satisfy the requirements of a continuous fluid. As the diameter of the experimental capillary tube decreases, the ratio of the red cell diameter to the tube diameter increases, and eventually blood can no longer be considered as a continuous fluid. When this happens, the equation of motion may not be valid since the key assumption used in the derivation of the equation of motion is no longer valid. However, the rheological properties of blood are still predictable in a 29-micron tube where the traditional criterion of continuum model applicability has failed.

The Flow of Blood Through a 29-Micron ID Tube

The only experimental tube that produced any unusual results was the 29-micron ID tube. The hematocrit of the blood flowing through this size capillary tube was not always constant, although most of the time the hematocrit of the blood flowing through the tube appeared constant when the flow was observed through a microscope

(150x). However, at times the hematocrit of the blood in the tube seemed to decrease sharply and even reach zero for a short time. Then, following a reduction in hematocrit, the hematocrit appeared to be much higher than the average for a short time. The length of these non-average hematocrit sections was usually only about 100 to 1000 microns, but sometimes they were as long as 1 cm. The length of the increased hematocrit section was usually about the same length as the preceding reduced hematocrit section. A section of increased hematocrit was seldom observed without a preceding reduction in hematocrit, but occasionally the hematocrit would appear to increase above the average for a length of about 500 microns, then drop back to the average. Apparently the length of each capillary section used to determine the average hematocrit inside the capillary tube was long enough to eliminate errors associated with the observed axial hematocrit variations. This fluctuation of local hematocrit was noticed during the pressure drop-flow rate experiments as well as during the experimental measurements of the tube hematocrit. Once again, the length of the capillary tube was sufficient to eliminate a fluctuating pressure drop as the hematocrit fluctuated across a given point in the tube.

The cause of the axial hematocrit fluctuations is not known, but they are suspected to be the result of either platelet or red cell aggregation at the tube entrance. Therefore, possible methods of

platelet removal were investigated. Whole blood filtered through a 14-micron filter was placed in the feed reservoir. No hemolysis was produced by filtering, but the 14-micron filters were a pink color after use. Flow was started through a 29-micron tube, but no axial hematocrit variation was observed for 1.5 hours. Then the flow slowed down to about 0.1 the original velocity for about 15 minutes, at which time the flow accelerated, but the axial hematocrit variation was present. Apparently, filtering the blood through the 14-micron filter did not remove the problem. Also, the free flow for over an hour indicated that the problem takes time to develop.

The blood was removed from the feed reservoir and it was found that red scum was on the portion of the capillary tube that extended into the reservoir. When the red scum was washed with isotonic saline, it turned into white scum. Although the tube was covered with scum, the entrance did not appear to have any scum on it. A tube that had been coated with Siliclad, a silicone compound which renders the coated surface non-wettable by water, was placed in the viscometer. The blood again flowed smoothly for about 1.5 hours, then partially plugged up. Apparently, Siliclad doesn't help and since the first tube removed most of the platelets and white cells, the problem must be the result of red cell problems <u>inside</u> the tube.

Reversing the flow for a short distance did not remove the problem; therefore the difficulty is probably not at the entrance.

It was noticed that centrifuging does not remove all the platelets and white cells. Although most of them collect in the buffy coat during centrifugation, white streaks observed in the red cell pack indicate that some white cells and platelets remained in the blood that was placed in the viscometer feed reservoir.

In order to see if a density difference could be produced that would favor the removal of white cells and platelets, blood was centrifuged at 39° and 77°F. For the blood centrifuged at 77°F, the buffy coat was crumbly and came off as many small sections. Quite a few red cells were lost in removing the buffy coat. For the blood centrifuged at 39°F, the buffy coat came off as a continuous film with no loss of red cells. When pouring the remaining red cells into other tubes, white streaks were noticed in both the 39° and 77° samples. However, the 77°F tube had about 1.5 times as much white stuff left in the red cell pack as the 39°F tube. These red cells were then centrifuged for 10 more minutes. After centrifuging, a few white specks were observed in the 77°F tube and nothing was seen in the 39°F tube. When pouring the contents out of the centrifuge tubes, a small number of white lines were seen in the 77°F tube but nothing was seen in the 39°F tube. It is suspected that the white lines are platelets and white cells.

A large tube of blood (39°F) was centrifuged for 10 minutes and the buffy coat and plasma removed. Glass wool was placed in the tube and left in contact with the blood for 5 minutes in order to remove platelets and white cells. When the red cells were poured out of the centrifuge tube, white streaks were still visible. Apparently, glass wool is not effective in the removal of platelets and/or white cells.

A suspension of red cells in isotonic saline was prepared from whole blood with the plasma and buffy coat removed. The hematocrit of the sample was about 10%. After centrifuging the red cell-saline suspension, a small white film was on the surface. This was removed. As the red cells were poured out of the tube, white streaks were seen throughout the red cells, but most of the white stuff settled to the bottom. Washing the red cells in saline, removing the top film and then taking only the upper 70% of the red cells and then re-washing two or three times might get out all the white stuff.

It has been suggested that the most effective way to remove platelets is to centrifuge whole blood, throw away 25% of the red cells with the buffy coat, then re-centrifuge and throw away the upper 25% of the remaining red cells, then repeat once more. (121).

When the blood flow was observed under the microscope, the same four regions of flow found by Benis were seen in this study. Benis observed tubes with diameters between about 200 to 800 microns. Even in tubes with inside diameters equal to 29 microns, the same flow patterns were observed except for the fluctuations previously mentioned. This may account for the fact that the flow properties of blood are still predictable in a 29-micron ID tube even though the continuum assumption probably does not hold. The flow patterns previously reported by Benis are summarized here.

1) For flows above $\bar{U}$ equal to about 25 sec^{-1}, only individual cells are observed--no rouleaux. As the flow decreases to a $\bar{U}$ of about 5 sec^{-1}, the individual red cells can be seen rolling along the wall. For a 29-micron tube, no adhesion to the tube wall was noted.
2) As the flow rate decreases even more, say to $\bar{U}$ equal to about 1 sec^{-1}, the red cells start to aggregate. This was observed also in the 29-micron tube.
3) As the flow continues to decrease, the aggregates become very large and plug flow occurs.
4) Eventually, the flow stops completely, and a yield pressure exists.

With the exception of the observed fluctuating hematocrit, the flow regimes observed in this study correspond to those found by Benis (6).

The volume of isotonic saline contained in the capillary viscometer system was large enough so that slight thermal changes caused large volume changes, sometimes as large as the flow rate of blood through the capillary tube. The thermal expansion of H_2O at 20°C is 0.207×10^{-3} per °C. The volume of liquid in the system is about 50 mls. Therefore, the volume will change about 0.01 mls for a temperature change of 1°C, or about 0.0001 mls for a temperature change of 0.01°C. A typical flow rate was about 0.00001 ml/min. For this reason, the temperature had to be controlled to within $\pm$ 0.01°F or better during the measurement of an experimental point. Between experimental points, the temperature changed as much as $\pm$ 0.1°F.

For this tube, the data points coincide with the predicted continuous fluid lines within a maximum error of $\pm$ 4% and typically the agreement is within $\pm$ 0.5%. The calculated maximum error in the shear stress for a given $\bar{U}$ is $\pm$ 3%, and the calculated maximum error in $\bar{U}$ is $\pm$ 2%.

In order to dramatize the effect the reduction of hematocrit inside the tube has on the flow properties of blood, Figure 42 shows a $\tau_w - \bar{U}$ plot for $H_f = 0.422$ using the 29-micron and 811-micron

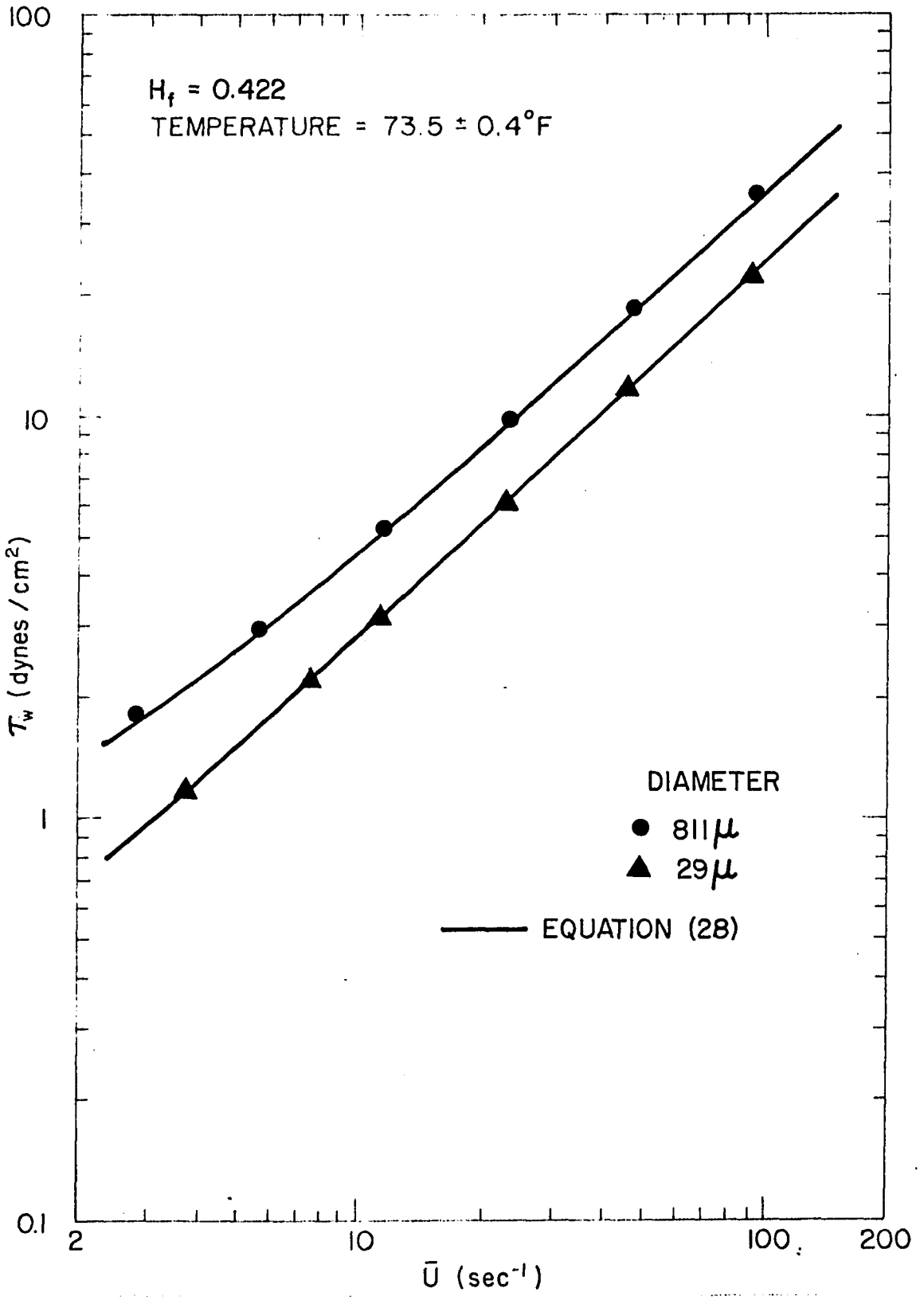

Figure 42. τ_w - $\bar{U}$ Plot Comparing Blood Flow Through a 29-Micron Tube with Flow Through an 811-Micron Tube

tubes. Clearly, if the feed hematocrit is used for the 29-micron tube (curve for the 811-micron tube), an error of 50% can be obtained.

Blood Flow Data Taken at 98.6°F.

In order to determine whether Equation (28) could predict blood flow data taken at 98.6°F by simply using the viscosity of plasma at 98.6°F instead of the viscosity at 73.5°F, data were taken in a 221-micron tube at 98.6°F. The results are shown in Figure 43 and the prediction made by Equation (28) is shown in Figure 44. It can be seen that the actual shear stress for a given $\bar{U}$ is lower than predicted. This may mean that the decrease in viscosity of the red cell contents must be taken into account in order to accurately predict the correct shear stress-shear rate relationship (31). Other factors that may contribute to the decrease in predicted viscosity are considered by Brooks et al (22).

Data were then taken for blood that had been heated to 111°F for 20 minutes, then cooled to 98.6°F. The results are shown in Figure 45 and the predicted results are shown in Figure 46. Figure 47 shows the results plotted as ln τ_w vs H at $\bar{U}$'s of 10, 40, and 100.

For the blood with 72% hematocrit, there was a scum on top of the blood that grew larger with time. The scum got caught on a

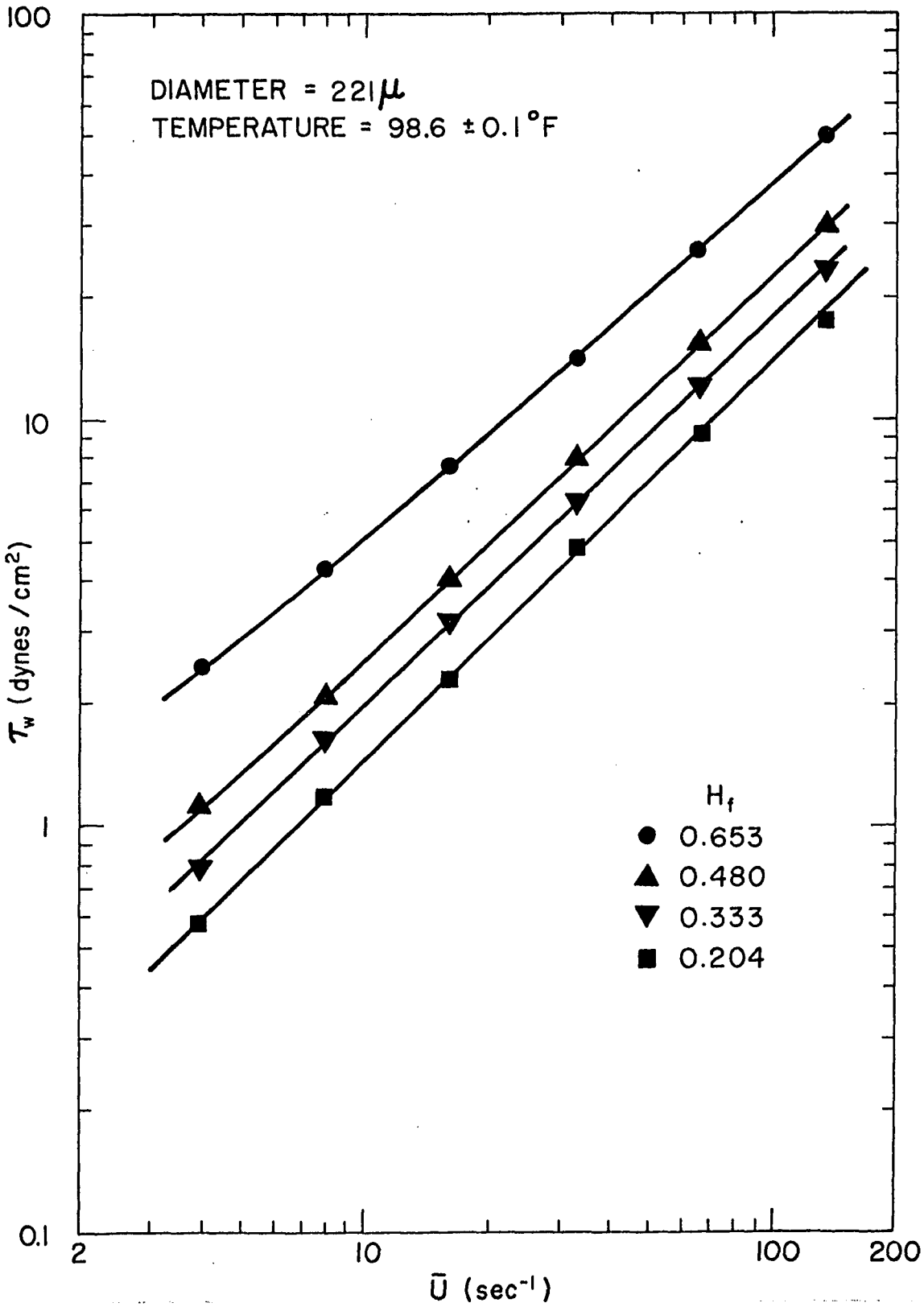

Figure 43. τ_w - $\bar{U}$ Plot for Red Cells in Plasma, 221-Micron Tube. Temperature = 98.6°F

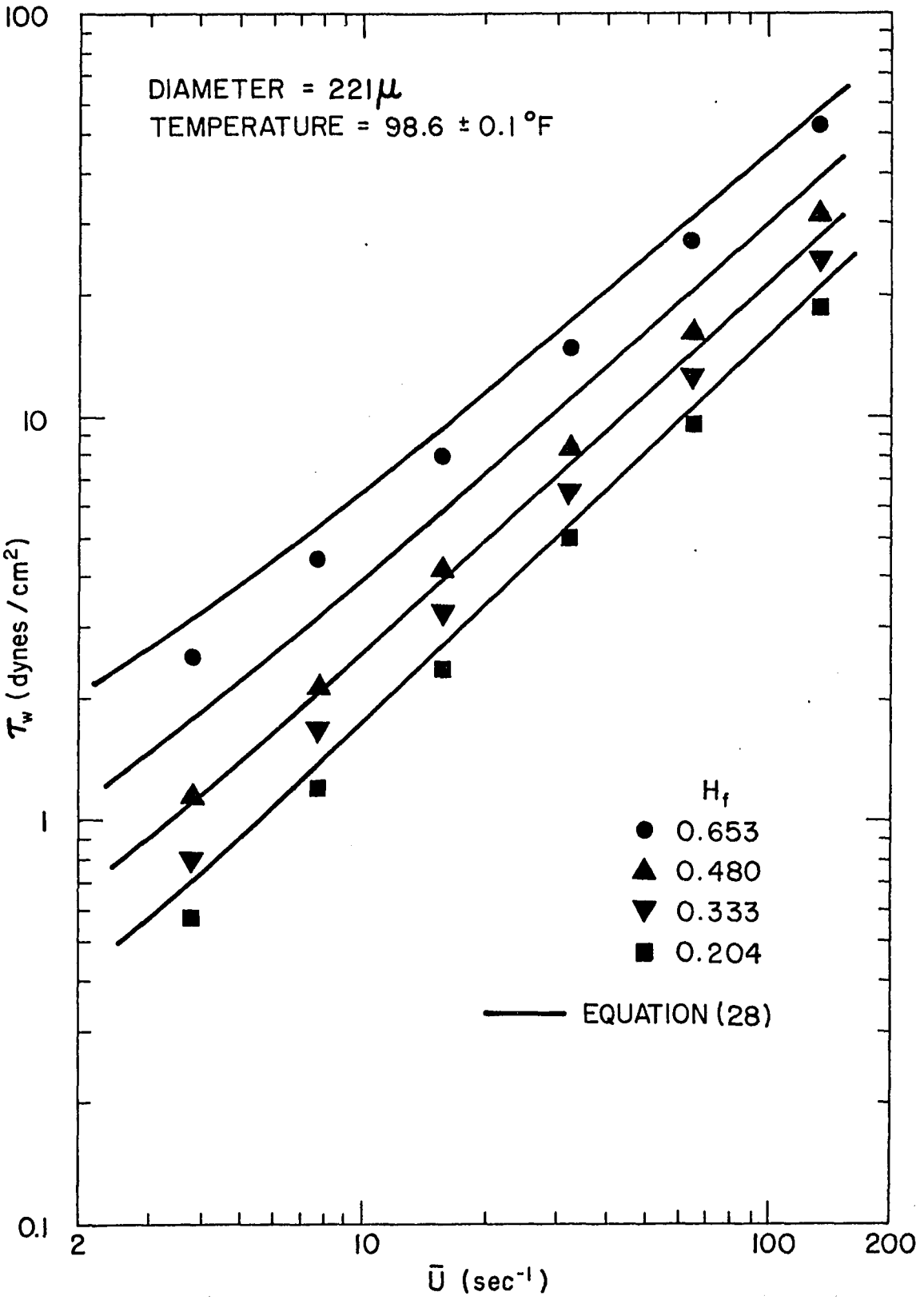

Figure 44. Predicted τ_w - $\bar{U}$ Plot for Red Cells in Plasma, 221-Micron Tube. Temperature = 98.6°F

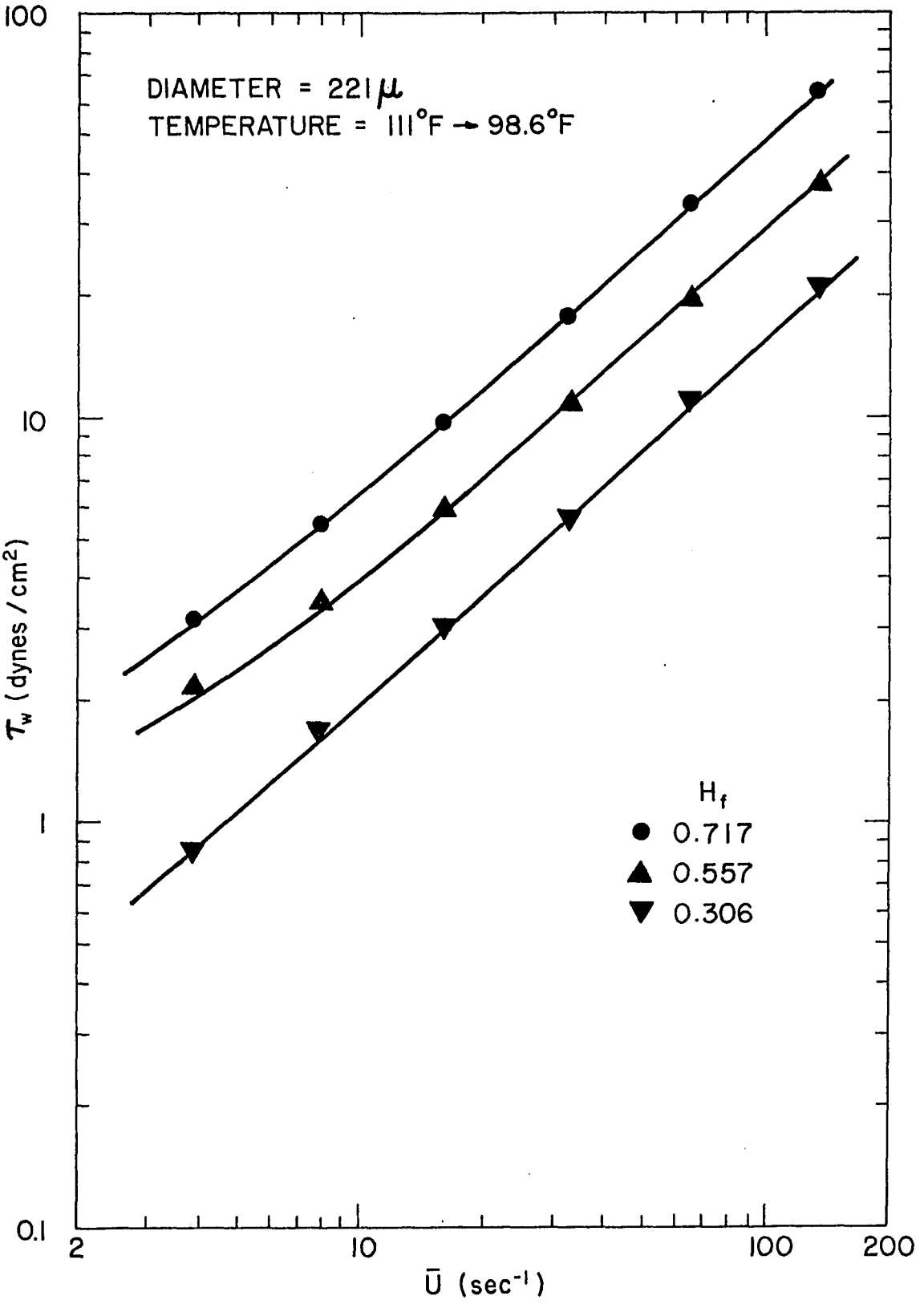

Figure 45. τ_w - $\bar{U}$ Plot for Red Cells in Denatured Plasma, 221-Micron Tube. Temperature = 98.6°F

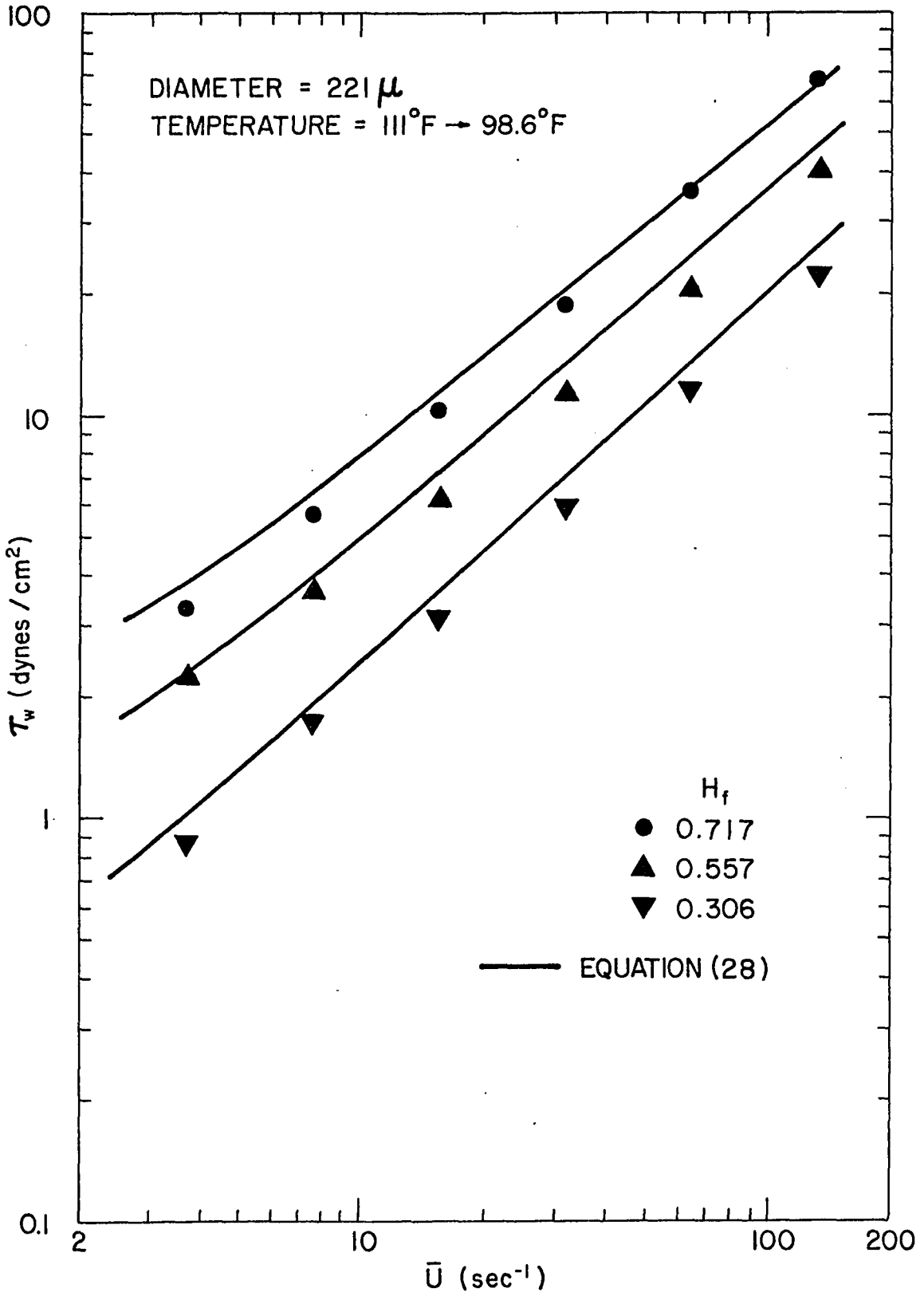

Figure 46. Predicted τ_w - $\bar{U}$ Plot for Red Cells in Denatured Plasma, 221-Micron Tube. T = 98.6°F

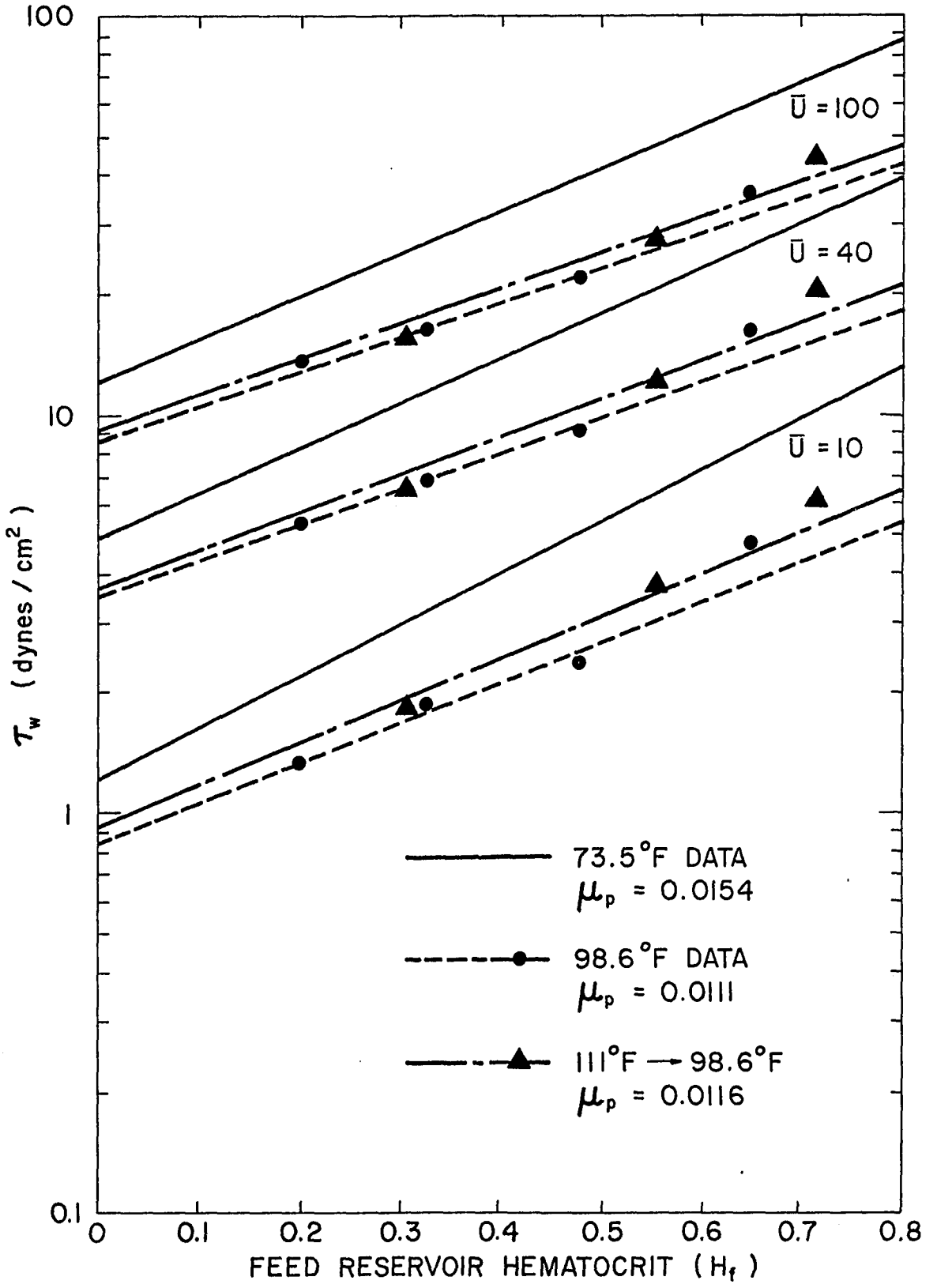

Figure 47. Ln τ_w - H_f at Constant $\bar{U}$, Normal and Denatured Plasma.

microhematocrit tube. It was like the scum on the top of an old paint can. Perhaps inside the body (where the scum must remain in the blood) the scum can cause a blockage. The final size of the scum was about 0.1 cc for 30 cc of blood. After the scum was removed, a hard film developed (about 0.1 cc) that would not stick to a microhematocrit tube. The hard film was about the size of a dime and about as thick as a thumbnail (about 0.03 inches). It was very wrinkled on top. If the scum and this film had to go through the blood vessels, it appears that it would cause a fatal problem. No scum developed for the 56% hematocrit. Clearly, pathological blood (along with flexibility and elasticity studies) is an important area of future investigation.

It was found that the heating process causes no hemolysis of the blood, but the blood is much more susceptible to hemolysis; the stirring bar caused some hemolysis after only one hour. When normal blood is tested at 98.6°F, the amount of hemolysis is larger than at 73.5°F but much smaller than for the abnormal blood.

Results Obtained Using a Capillary Viscometer and Tubes Smaller Than 29 Microns I.D.

Experimental Blood Flow Results

Shear stress-shear rate data were taken for the 8.7, 15.3, and 23-micron ID tubes and the data are shown in Figures 48, 49, and 50. Least squares lines are also shown. It is interesting to

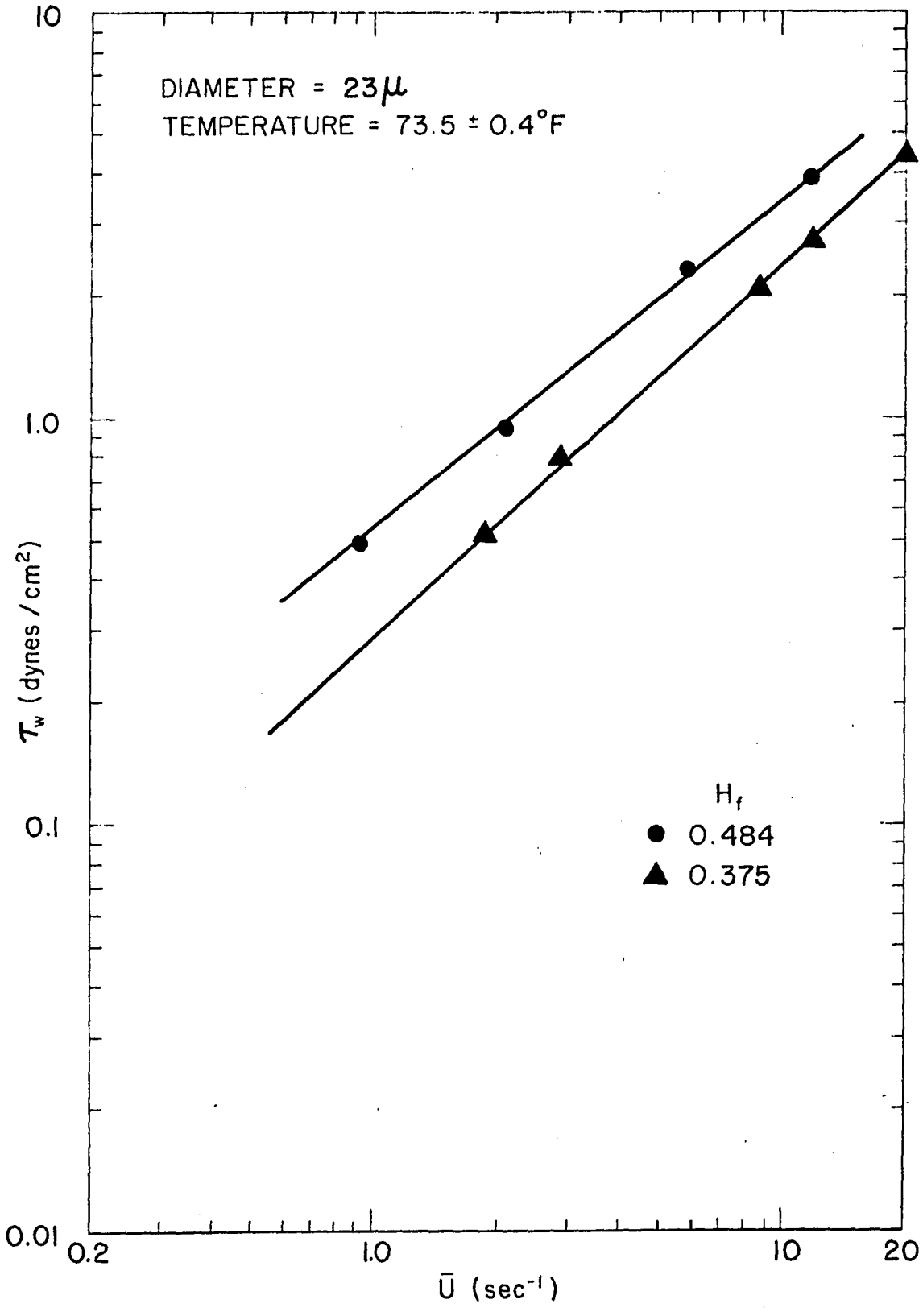

Figure 48. τ_w - $\bar{U}$ Plot for Red Cells in Plasma, 23-Micron Tube

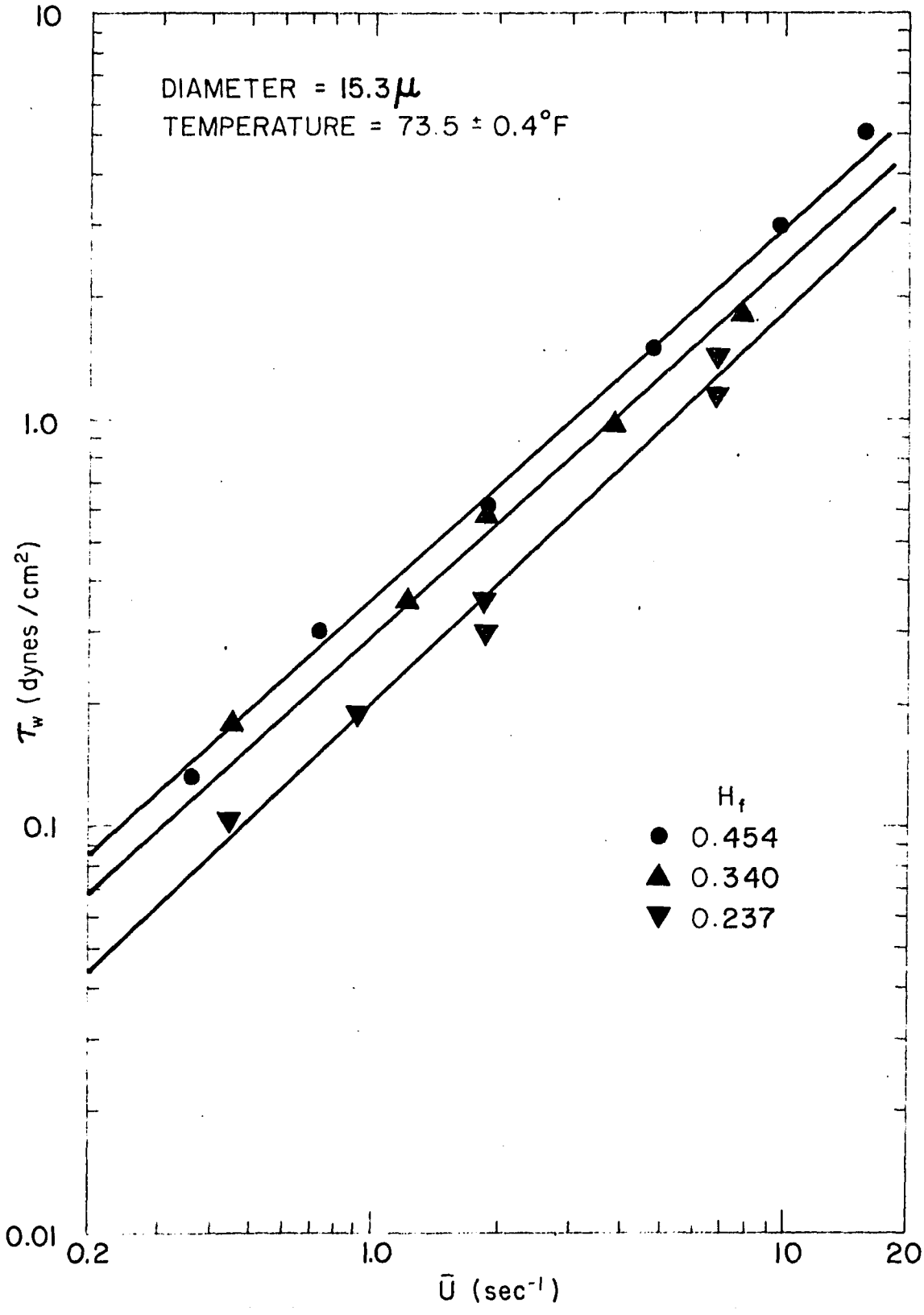

Figure 49. τ_w - $\bar{U}$ Plot for Red Cells in Plasma, 15.3-Micron Tube

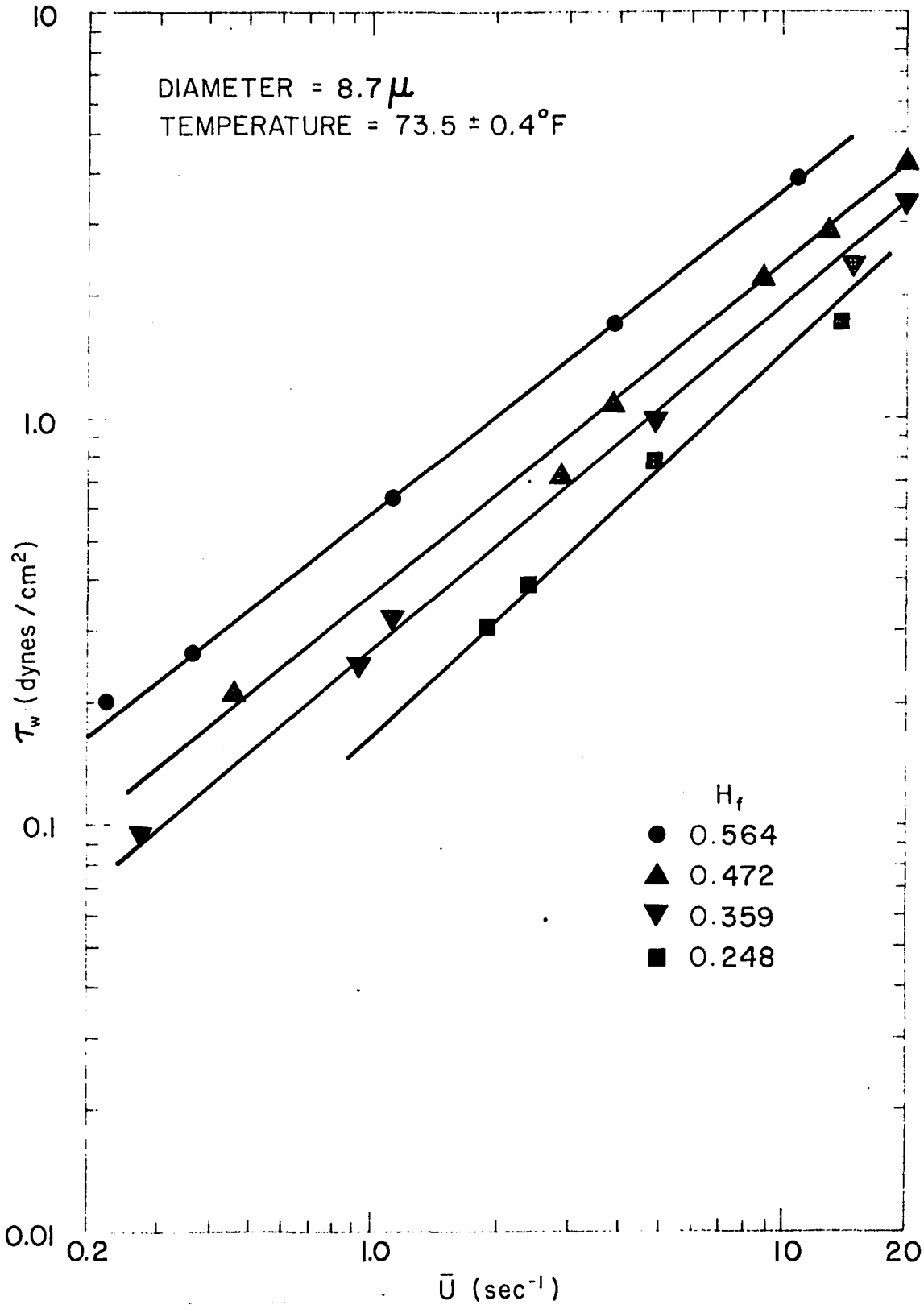

Figure 50. τ_w - $\bar{U}$ Plot for Red Cells in Plasma, 8.7-Micron Tube

note that all tubes (23, 15.3, and 8.7-micron tubes) plug at almost exactly 1.5 hours. The shear stress-shear rate relation predicted by Equation (28) for these tubes is shown in Figures 51, 52, and 53. When the measured value of the tube hematocrit is used to predict the fluid properties of blood flowing through the tubes, a number of important results are found.

The pressure decay method is not very sensitive to random temperature fluctuations since a smooth curve can be drawn through a jerky one. However, the error involved in drawing the slope at a given pressure drop was very large. For this reason, the average flow velocity through a given diameter capillary tube was determined by timing the red cell motion for a distance of about 20 tube diameters. Thus, $\bar{U}$ was measured directly (for a given pressure drop) by measuring red cell velocity. In tubes larger than about 8 microns, $\bar{U}$ is not the same as the red cell velocity. Still, $\bar{U}$ values reported are considered accurate to within $\pm$ 5%. However, $\bar{U}$ was estimated as the velocity of red cells near the center of the tube.

It can be seen in Figures 51, 52, and 53 that in almost all cases the measured shear stress is larger (for a given $\bar{U}$) than predicted by Equation (28). More specifically, the experimental shear stress for the 8.7-micron tube is considerably larger, while the shear stress is only slightly larger for the 15.3-micron tube. The

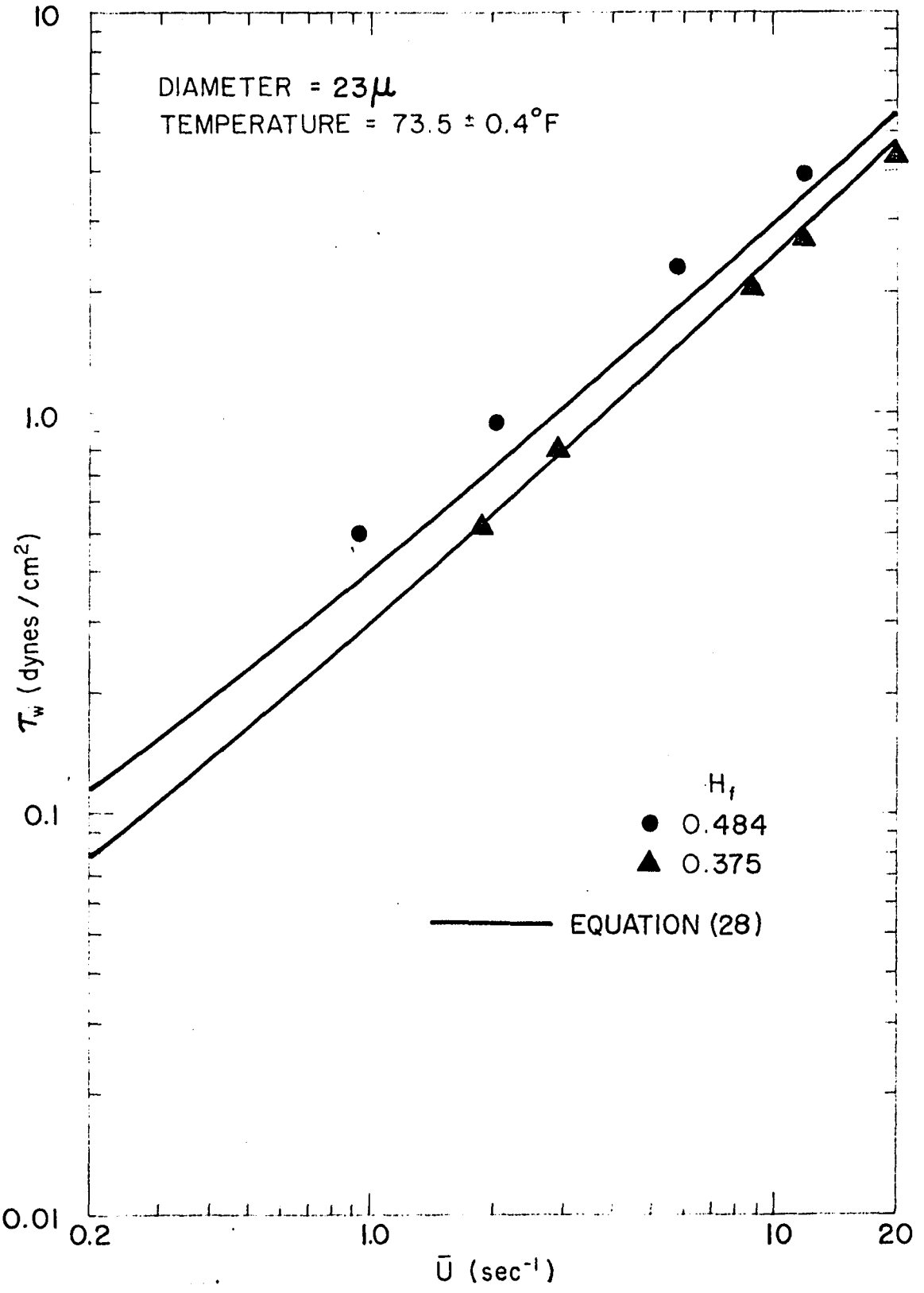

Figure 51. Predicted τ_w - $\bar{U}$ Plot for Red Cells in Plasma, 23-Micron Tube

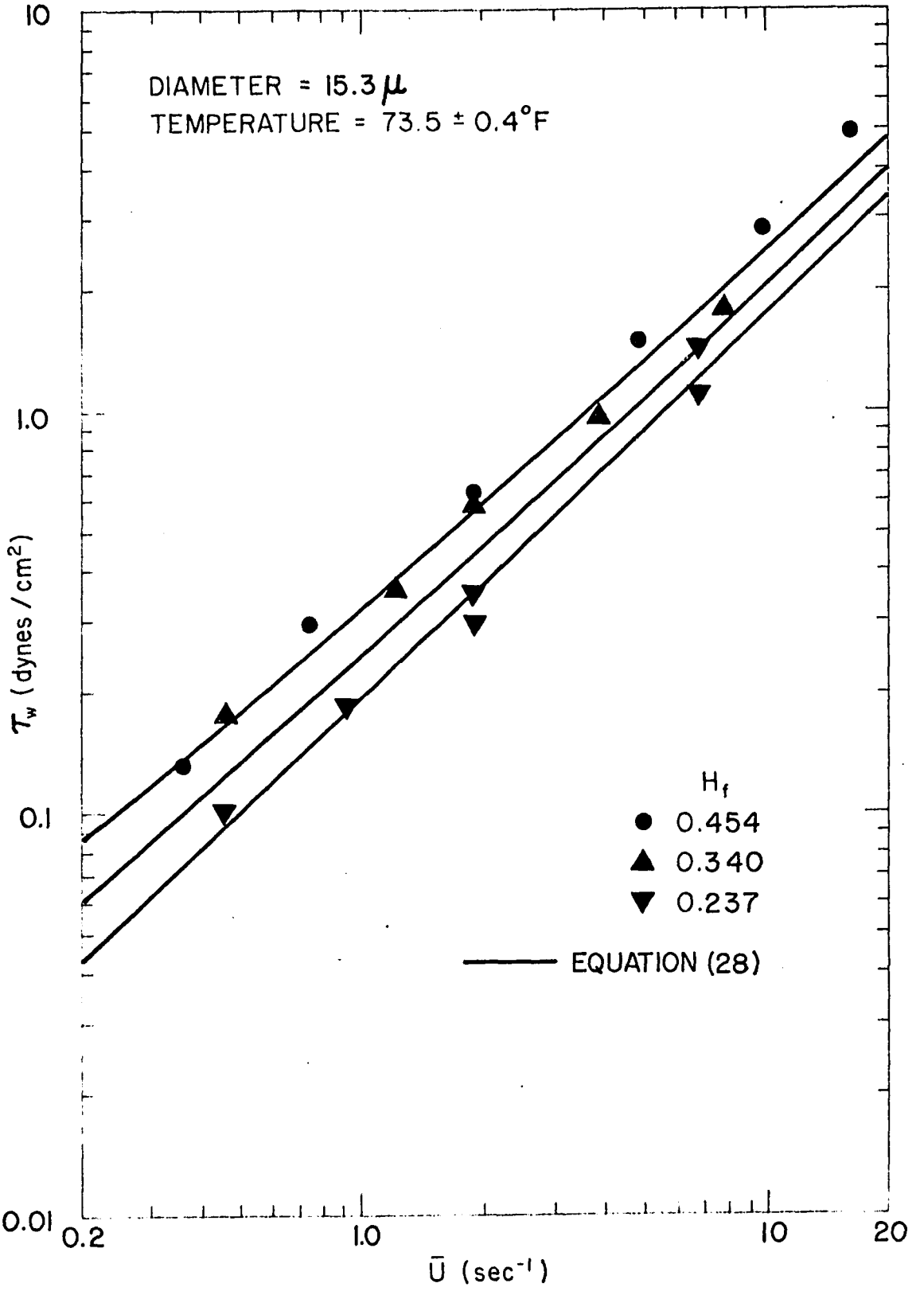

Figure 52. Predicted $\tau_w = \bar{U}$ Plot for Red Cells in Plasma, 15.3-Micron Tube

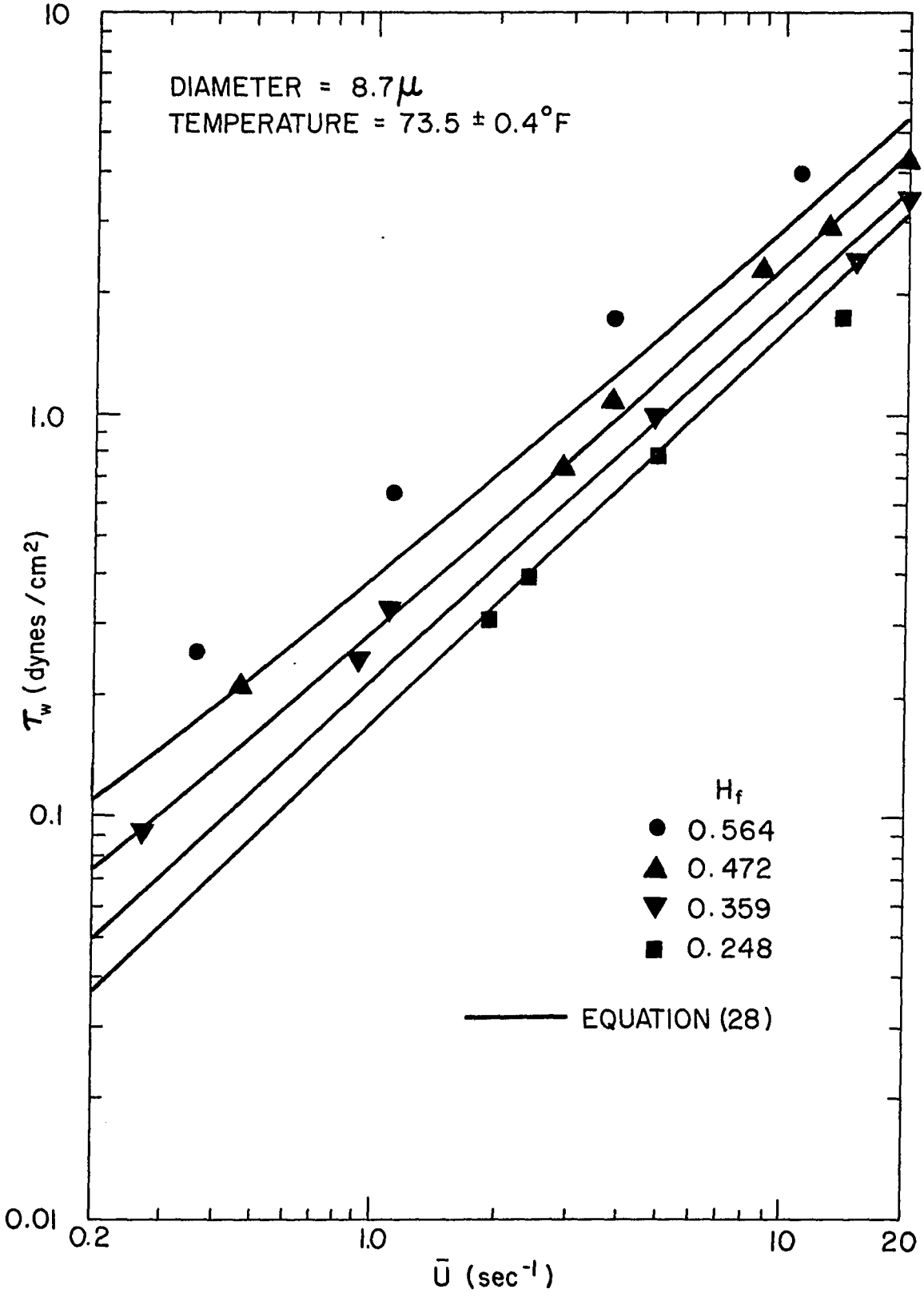

Figure 53. Predicted τ_w - $\bar{U}$ Plot for Red Cells in Plasma.

large deviation in the 8.7-micron tube may be a measure of the energy required to deform the red cells or it may be the energy required to break up the rouleaux at the tube entrance, or both. The smallest discrepancy (for the 15.3-micron tube) may be the result of Whitmore's predicted minimum viscosity in a 16-micron tube.

Under the light microscope, the red cells appear as clear objects, and only the outline of the cell is visible. The flow behavior for the 23-micron tube appeared to be much like that found in the larger tubes. There was no special orientation of cells or of rouleaux.

For the 15.3-micron tube, careful attention was given to the fact that the red cell velocity is perhaps not an accurate measure of $\overline{U}$. Observation did reveal that the velocity profile was essentially flat in the sense that red cells that seemed to be adjacent to the tube wall had the same velocities as red cells in the center of the tube. It was very difficult to observe the red cells when the velocity was larger than about 10 tube diameters per second. At velocities where the individual red cells were still discernable, the red cells were only barely deformed. Rouleaux (2 and 3 cells) formed up to $\overline{U} = 7$.

For the 8.7-micron tube, it was noticed that only about one out of thirty groups of cells is a single cell. Most groups had 3 to 15 red cells but some had as many as 50 cells. It was difficult

to get an overall picture of exactly what the distribution of red cells was since only a length of about 200 microns was visible. At least ten times this length is required in order to speculate on red cell grouping. It does appear that perhaps an entrance affect is responsible for the large spaces (500 microns at times) between groups of red cells. For H_f larger than 0.36, the red cells became much more evenly spaced. Even though there was some clearance between the red cell and the tube wall, the red cells were very bullet-shaped. Single red cells would tumble as they moved down the tube.

It was impossible to tell for sure if a large red cell was at the head of each group and a small red cell at the tail, as in Whitmore's model. However, due to the resolution of the light microscope it is entirely possible that an undetected size difference could occur.

It was observed that when plugging started to occur, the new plug could be removed by reversing the flow. About 10 minutes would elapse before another removable plug would start to form.

Another interesting observation for the 8.7-micron tube was that at low $\bar{U}$ many red cells adhered to the tube wall. These cells could be removed by increasing $\bar{U}$ above about 50, but the cells again stuck to the tube wall when a low $\bar{U}$ was once again used.

An even more unusual and surprising result (and contrary to all results reported in the literature) is that when the flow was stopped, the red cell did not lose its parabolic shape but remained deformed. Even when the flow was reversed, the cells started to reverse their direction still deformed as though flowing in the opposite direction. An entrance effect may allow the cells to enter the tube in only one way, and the red cells may be such that they can only deform in one way.

In order to investigate some of the other unusual properties of blood that occur in tubes below about 20 microns, the data were replotted at $\tau_w^{1/2}$ vs. $\bar{U}^{1/2}$ (a modified Casson plot). By combining Equations (7) and (11), the following equation is obtained:

$$\tau_w^{1/2} = \tau_y^{1/2} + s\left[2(3+N)\right]^{1/2} \bar{U}^{1/2} \qquad (55)$$

For a small shear rate range, N is constant and linear behavior is predicted when $\tau_w^{1/2}$ is plotted as a function of $\bar{U}^{1/2}$. Such a plot is shown in Figures 54, 55, and 56. It should be noted that the Casson Equation is valid only at very low $\bar{U}$'s; at low $\bar{U}$, blood is highly non-Newtonian (see Figure 18) and N is <u>not</u> near one. Therefore, to approximate Equation (55) by:

$$\tau_w^{1/2} = \tau_y^{1/2} + s(8\bar{U})^{1/2} \qquad (56)$$

is not a valid use of the Casson model. Figures 54, 55, and 56 start

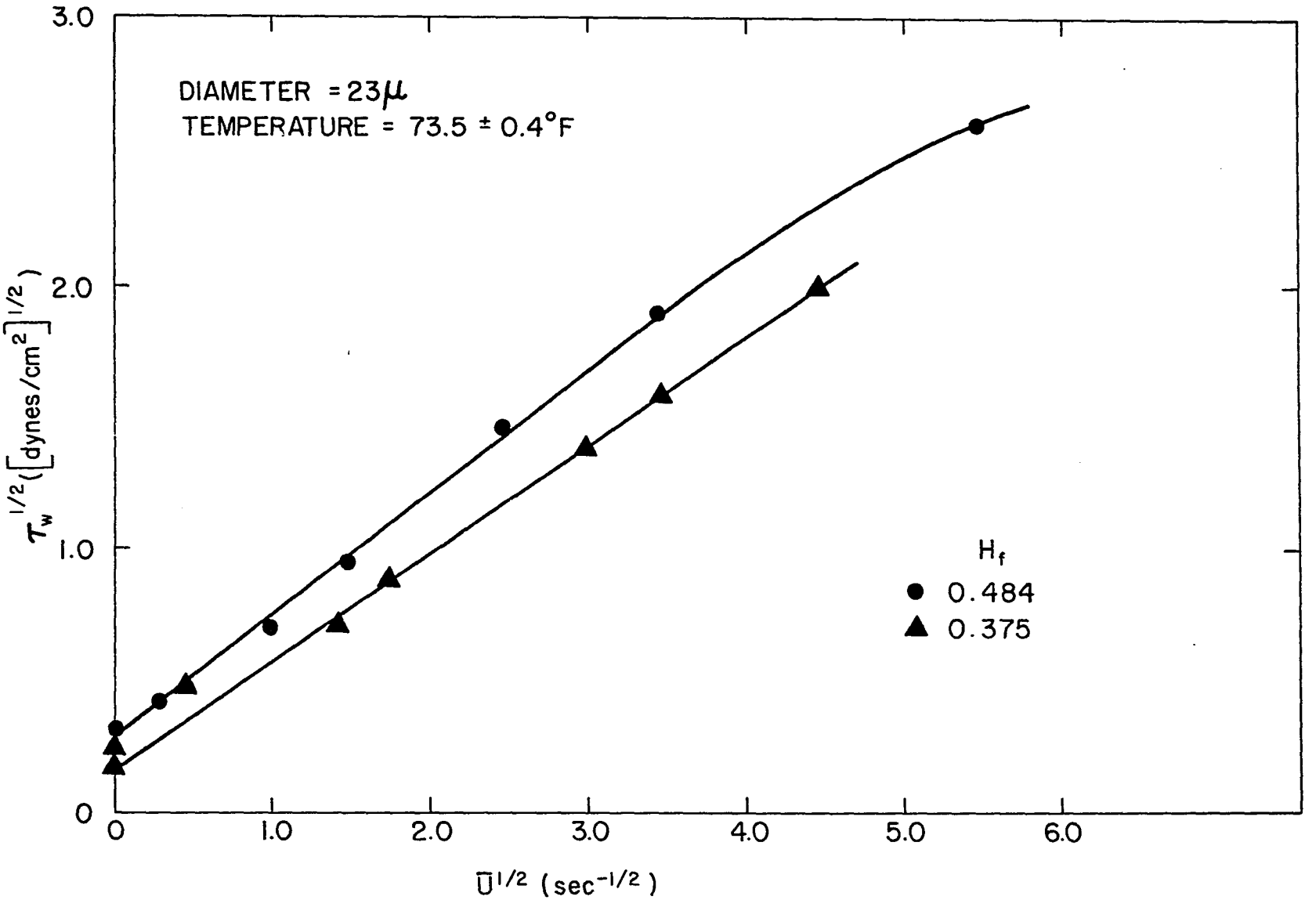

Figure 54. $\tau_w^{1/2}$ - $\bar{U}^{1/2}$ Plot (Casson Plot) for Red Cells in Plasma.

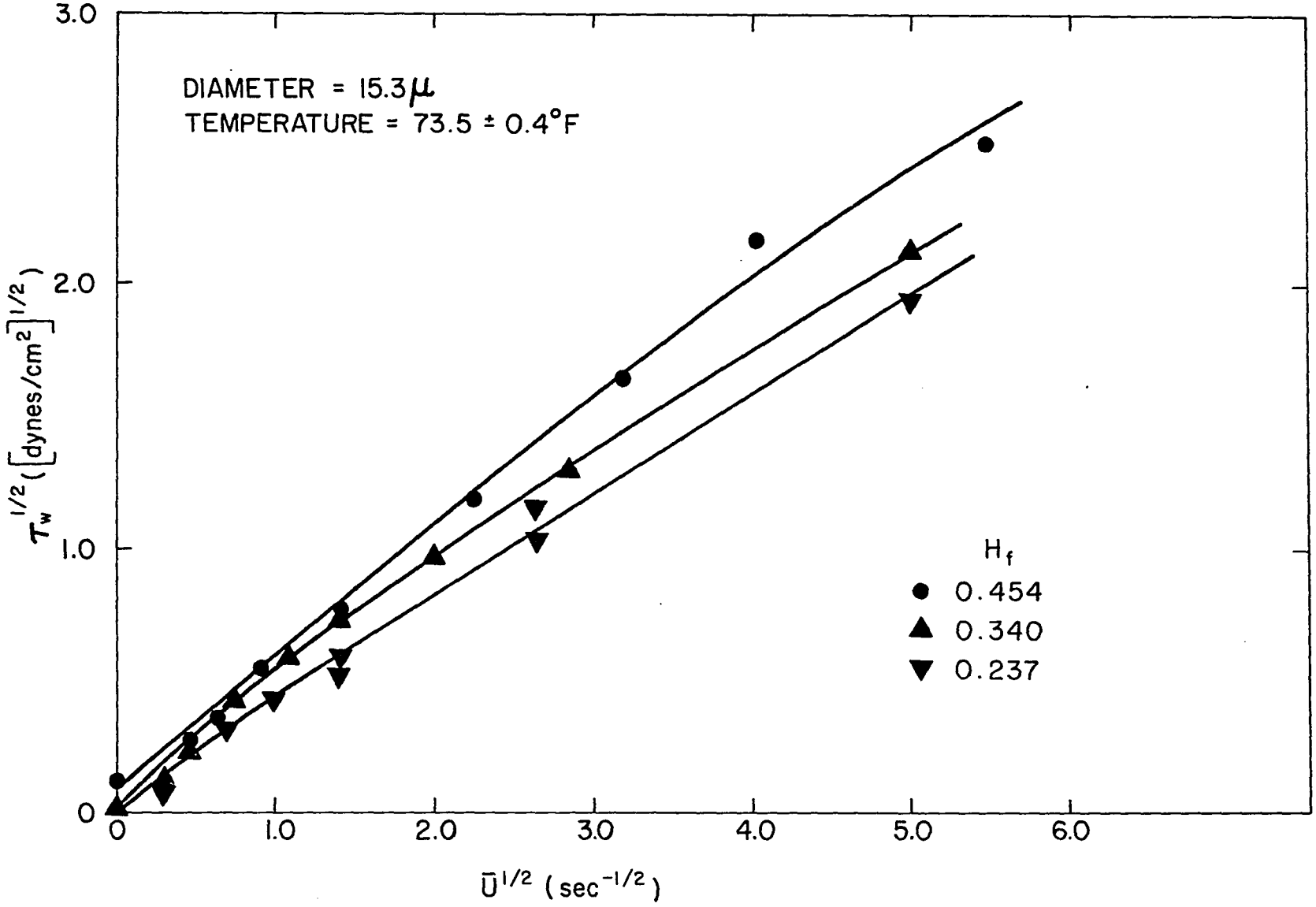

Figure 55. $\tau_w^{1/2}$ - $\bar{U}^{1/2}$ Plot (Casson Plot) for Red Cells in Plasma.

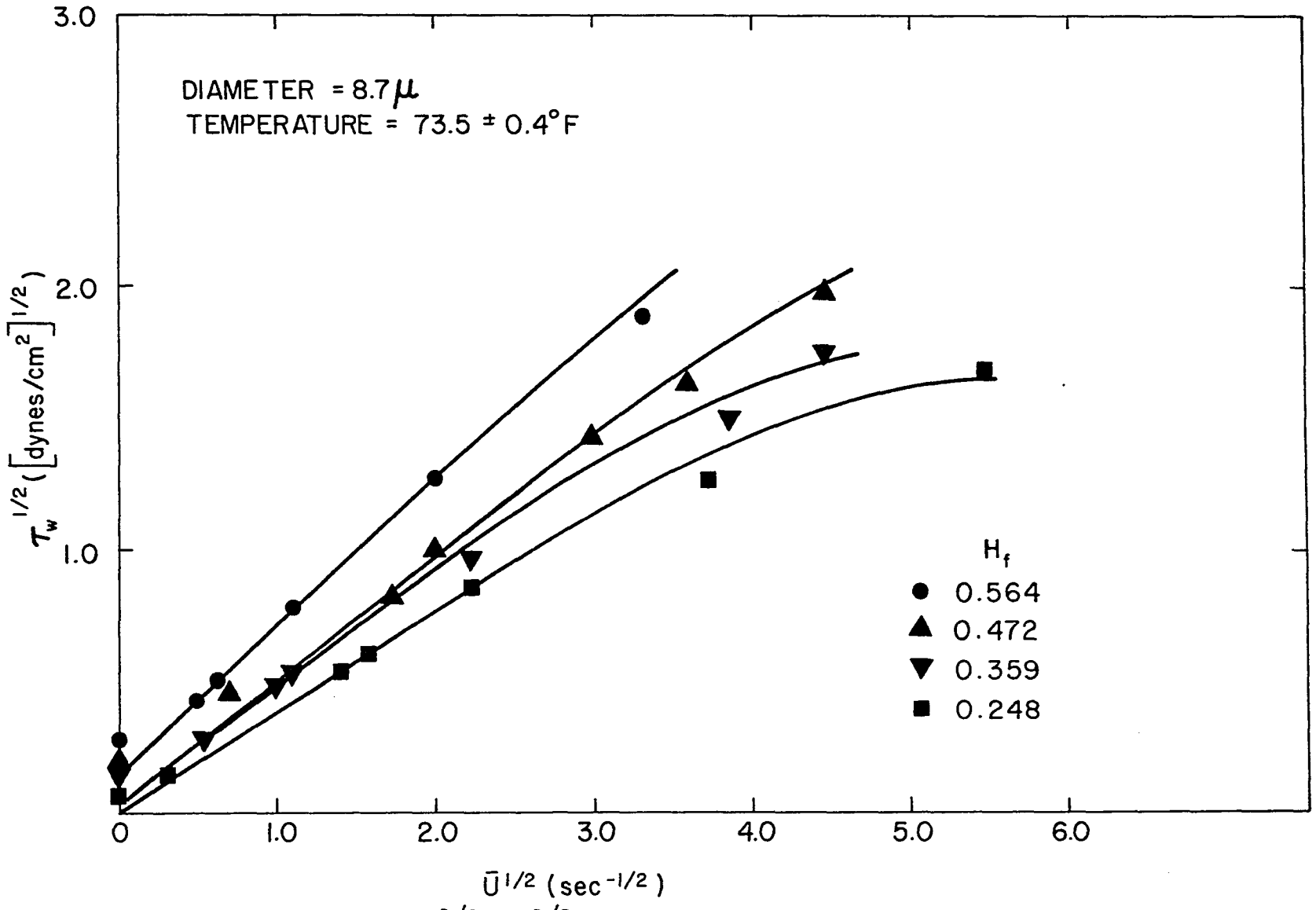

Figure 56. $\tau_w^{1/2}$ - $\bar{U}^{1/2}$ Plot (Casson Plot) for Red Cells in Plasma.

to show curvature above $\bar{U} \simeq 4$. The yield stresses shown in the figures were determined by moving a red cell (8.7-micron tube) or a small group of red cells (15.3- and 23-micron tubes) back and forth and recording the pressure required to initiate the motion. It can be seen that the 23-micron tube exhibits a yield stress that corresponds with the extrapolation of points taken at finite shear rates.

In a 15.3-micron tube, it is impossible for three-dimensional red cell networks, and rouleaux with their axes not parallel to the centerline, to form. Therefore, it might be suspected that the yield stress found in blood and attributed to the aggregation of red cells into mechanical networks at low shear rates may not be found in a tube between 9 and about 16 microns in diameter. Figure 55, for the 15.3-micron tube, seems to substantiate such a claim since no yield stress was measured for feed reservoir hematocrits of 0.237 and 0.340. For a feed reservoir hematocrit of 0.454, a yield stress was measured, but the extrapolated curve using the points measured at small finite shear rates passes through the origin. The effect of sedimentation on shear stress-shear rate measurements found at low shear rate in larger tubes may disappear in tubes with diameters smaller than, say, 16 microns due to the fact that sedimentation is not possible in such a small tube.

In order to check the qualitative finding of Lighthill's lubrication theory, it was found desirable to plot the excess shear stress as a function of $\bar{U}^{1/2}$. Since the excess shear stress (defined as the measured shear stress minus the Newtonian shear stress) is a direct measure of the excess pressure (for a given tube), and $\bar{U}^{1/2}$ is a direct measure of the square root of the red cell velocity, a linear relation is predicted by the lubrication theory. Such a plot is shown in Figure 57 and it is clear that a linear relation is not found, except possibly at $H_f = 0.359$. It is possible that an 8.7-micron tube is too large for the lubrication theory to apply; the extreme deformation of the red cell observed indicates that considerable hydrodynamic force is exerted on the red cell membrane, most of which occurs in the close proximity of the tube wall.

The Continuum Model

When analyzing the measured blood flow data (pressure drop and flow rate) in terms of rheological groups found mathematically to predict a unique relationship (at constant temperature and hematocrit), it is assumed that blood is a continuous fluid. In fact, when deviations from this unique relation are observed, the claim is usually made that the continuum model has failed. The purpose of this work has been, in part, to investigate the properties of blood in light of the fact that the supposedly unique relationship is not unique but depends on the diameter of the experimental tube

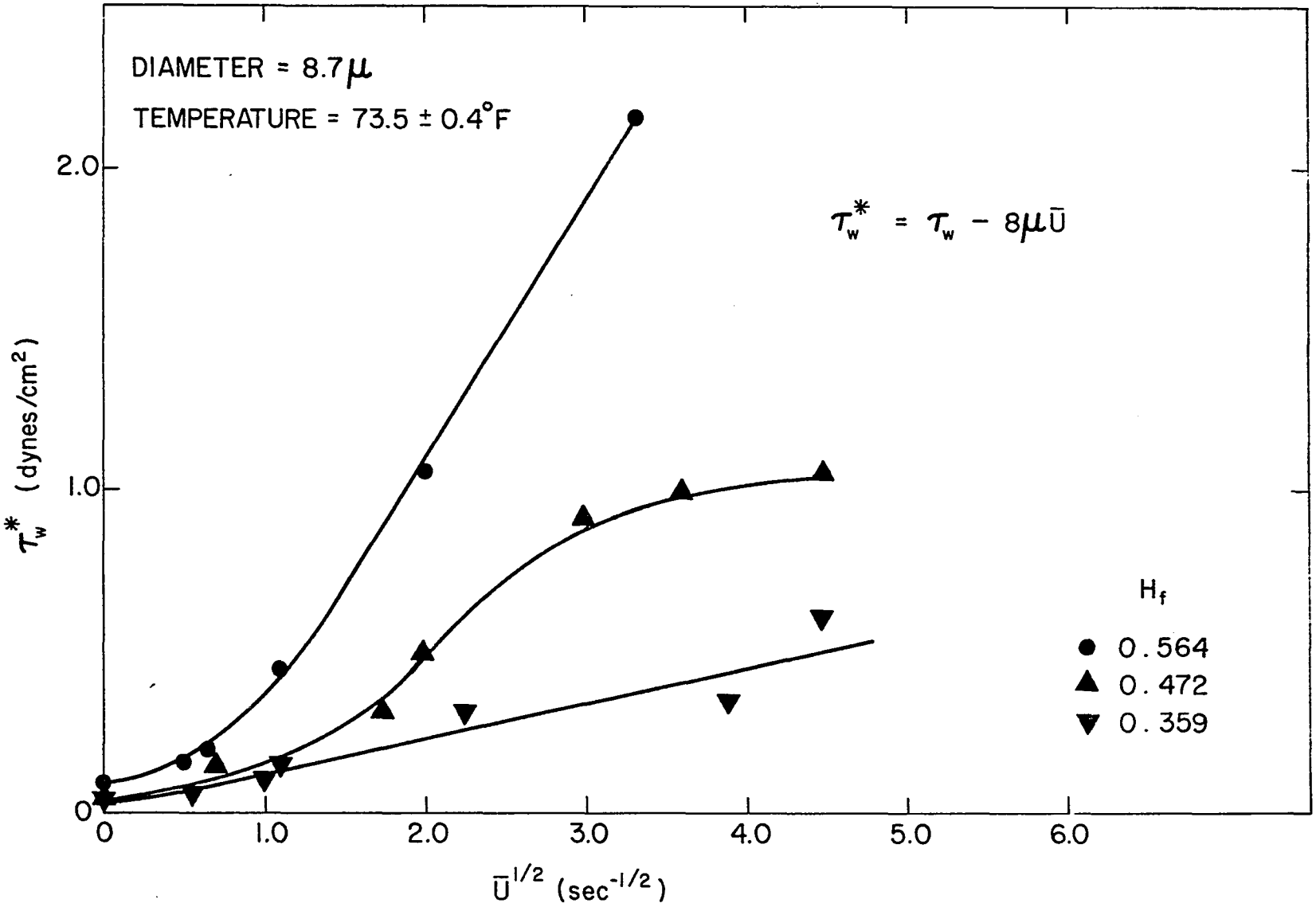

Figure 57. τ_w^* - $\bar{U}^{1/2}$ Plot for Red Cells in Plasma, 8.7-Micron Tube.

as the tube diameter decreases below about 300 microns. For a tube as small as 29 microns, the rheological properties of blood were predicted from a knowledge of the average hematocrit inside the capillary tube. For the 23, 15.3, and 8.7-micron tubes, the data are not as accurately predicted as for the 29-micron and larger tubes. However, the discrepancy between predicted and measured values does not necessarily imply that the continuum model has failed. The usual criteria used for establishing the limits of applicability of the continuum model is the ratio of the smallest dimension of the flow channel to the particle diameter. If this ratio is above about 10, the continuum model is said to apply. For blood, this means that blood should not be treated as a continuous fluid any time the experimental capillary tube used is less than about 100 microns. However, it has been shown (Figure 41) that the rheological properties of blood are still predictable in a 29-micron tube, where the usual criteria for continuum mechanics is apparently violated. Clearly, choosing appropriate criteria for determining the limits of applicability of the continuum model is not a simple matter. Changes in the red cell shape, aggregation, and many other physically occurring processes may be important in characterizing the prediction of blood flow properties. It may also be true that a single measurement ratio, as mentioned above, may not be sufficient with respect to the application of continuous integration; it may be

necessary to consider that in a long tube, the axial average of the properties may give the correct prediction even though considerable fluctuation of properties may be occurring in the axial and radial direction.

Figure 42 gives an indication of the magnitude of the difference in measured properties (at constant hematocrit) for an 811-micron tube and a 29-micron tube. It was shown that this discrepancy was due simply to the use of the incorrect hematocrit parameter. It may very well be that the inclusion of red cell deformation as an important parameter in characterizing blood flow properties will uniquely determine the shear stress-shear rate relationship for blood in tubes of all sizes (31).

CONCLUSIONS

1. It was shown mathematically and measured experimentally that the "average" hematocrit of the blood flowing through a capillary tube is lower than the feed reservoir hematocrit.

2. The discharge stream hematocrit was measured to be equal to the feed reservoir hematocrit.

3. It was found that in tubes less than 300 microns but larger than 100 microns, the relative hematocrit (tube hematocrit divided by the feed reservoir hematocrit) is independent of the feed reservoir hematocrit and the flow rate.

4. In tubes less than 100 microns ID, the relative hematocrit depends on the feed reservoir hematocrit, and the slope of the relative hematocrit vs. the feed reservoir hematocrit increases linearly with a decrease in tube diameter.

5. In tubes less than 300 microns, the relative hematocrit has a linear dependence on the logarithm of the tube diameter.

6. The hematocrit found inside the 10- and 16-micron capillary tubes was consistent with results found in larger tubes.

7. Within experimental error, the same reduction in hematocrit was found for red cells suspended in isotonic saline and in 3% by weight dextran-plasma. Hardened red cells in plasma also showed the same reduction in hematocrit.

8. A mathematical analysis indicates that the reduction in the hematocrit inside the capillary tube is consistent with a hypothetical 3 to 5 micron plasma layer gap at the tube wall.

9. An experimental equation was developed that allows the prediction of the shear stress-shear rate relationship in the vicinity of 73.5°F, once the temperature, hematocrit, and tube diameter have been fixed.

10. The shear stress of blood exhibits an exponential dependence on the tube hematocrit. Also, the slope of a $\ln \tau_w - H_f$ plot increases as $\bar{U}$ decreases.

11. It was confirmed that plasma is Newtonian at 73.5 and 98.6°F.

12. It was found that the existing fluid models do not describe the flow properties of blood over a very wide range of shear rate.

13. The Einstein equation using the Stokes Law drag, was redeveloped for blood. It was found that this equation does not describe the shear stress-shear rate relation for blood except at a hematocrit of 0.5.

14. It was found that theoretical equations that take rouleaux formation into account (such as a finite cylinder equation) have not been exploited. Such equations would need presently non-existent data on the length of rouleaux as a function of shear rate.

15. The hematocrit inside the capillary tube was found to be the correct hematocrit parameter for predicting the shear stress-shear rate relationship--not the feed reservoir hematocrit.

16. The shear stress-shear rate relationship is predictable by the developed equation (using the tube hematocrit) for all tubes down to and including the 29-micron tube. This indicates that the integrated equation of motion is still applicable even though the continuous fluid assumption has probably failed.

17. Thermal expansion is a serious problem in capillary viscometers using tubes less than about 40 microns.

18. Blood flow at 98.6°F shows less shear stress than is predicted by a plasma viscosity change from 73.5 to 98.6°F. (Blood viscosity is lower than predicted). This is due to changes in red cell properties.

19. Red blood cells suspended in denatured plasma (plasma heated to 111°F for 20 minutes, then cooled to 98.6°F) shows only a slight

increase in shear stress for a given shear rate (slight increase in viscosity), but a sludgy film forms in the blood.

20. Tube plugging was a problem in 8.7, 15.3, 23- and 29-micron tubes. The source of the problem is still not known, but carefully removing the white cells and platelets reduces the problem. The tubes could sometimes be unplugged by reversing the flow.

21. The pressure decay method used by Benis was found to be satisfactory (due to the slow change of pressure in small tubes) in 10-micron tubes.

22. Blood does not exhibit a yield stress in a 15-micron tube since rouleaux formation is restricted. The rouleaux that did form had their axes parallel to the tube axis. With this orientation, a mechanical network did not form.

23. The theory of Lighthill does not apply to the flow of blood through an 8.7-micron tube.

RECOMMENDATIONS FOR FURTHER WORK

1. Experimental data should be taken on the length of rouleaux (number of red cell per rouleaux) as a function of hematocrit and shear rate. Such data are necessary for the development of a theoretical equation describing blood flow.

2. Better thermal insulation and temperature control should be developed for capillary viscometer systems. Temperature control of $\pm$ 0.002°F is required in tubes as small as 10 microns.

3. The brief entry made into the field of abnormal blood flow demonstrated that much work can and should be done in attempting to compare abnormal blood flow to the results obtained with normal blood. It is easy to then determine whether changes in the red cell or the plasma have occurred (for example, by suspending red cells from the abnormal blood in normal plasma).

4. It is recommended that an investigation be started in order to determine why small tubes plug up and why an axial hematocrit variation is observed. Methods to eliminate the plugging problem can then be developed. It is possible that plugging and the axial hematocrit variations are caused by the same agents. Axial hematocrit fluctuations are observed in flow through the living circulation. The fluctuations observed in the 8.7-micron tube may be

due to entrance conditions.

5. It is recommended that motion picture studies be made of flow through 8 to 16-micron tubes in conjunction with pressure drop measurements. In this way, more accurate (and permanent) records can be made of the $\tau_w - \bar{U}$ relationship. Also, cell deformation can be more accurately observed.

6. It is recommended that the observed red cell deformation in an 8.7-micron tube be studied carefully to see if the observed deformation is real or only an artifact.

7. An investigation relating the measured red blood cell velocity and the true flow rate should be undertaken.

8. It is recommended that small tubes (10 microns) of different length be used to determine if the measured yield stress is due to red cell membrane-capillary tube wall friction (tube length dependent) or to rouleaux breakup at the tube entrance (tube length independent).

APPENDIX A

The use of a capillary viscometer to study the pressure drop-flow rate behavior of blood is essential to the complete understanding of blood rheology. The construction of capillary viscometers requires the use of two reservoirs, one or both of which contain blood. The higher pressure blood reservoir must be constantly stirred in order to prevent sedimentation and to maintain a uniform suspension of red cells. Stirring can be accomplished by either an up-and-down motion of a magnetic stirring bar or by centrifugal stirring. It is possible that centrifugal stirring requires a high rotational speed to accomplish adequate mixing. At the same time, high centrifugal speeds create a vortex flow and continuously produce a fresh blood-air interface, which is undesirable. The existence of a radial concentration distribution of red cells is also possible due to centrifugal force.

The radial concentration distribution of red cells at different heights in a healthy human blood sample contained in a beaker and stirred by a magnetic stirring bar rotating on the bottom of the container was investigated. The results were used to determine if centrifugal stirring can be used to agitate blood (and attain complete mixing) in the higher pressure blood reservoir of a capillary viscometer.

The apparatus used to obtain information on the vortex flow of healthy human blood is shown in Figure A-1. The apparatus consisted of a 100-ml beaker, a 3/8" x 1" teflon-coated Alnico magnet used as the stirring bar, a Thomas magnetic stirring motor and equipment required to measure a given radial position. The apparatus was coated with Siliclad, a silicone compound, and baked at 100°C for ten minutes. Also included in the apparatus required were hematocrit measuring capillary tubes, Critoseal (a putty used to seal one end of a capillary tube), and a high speed centrifuge. The equipment used to accurately measure a given radial position is shown in Figure A-2.

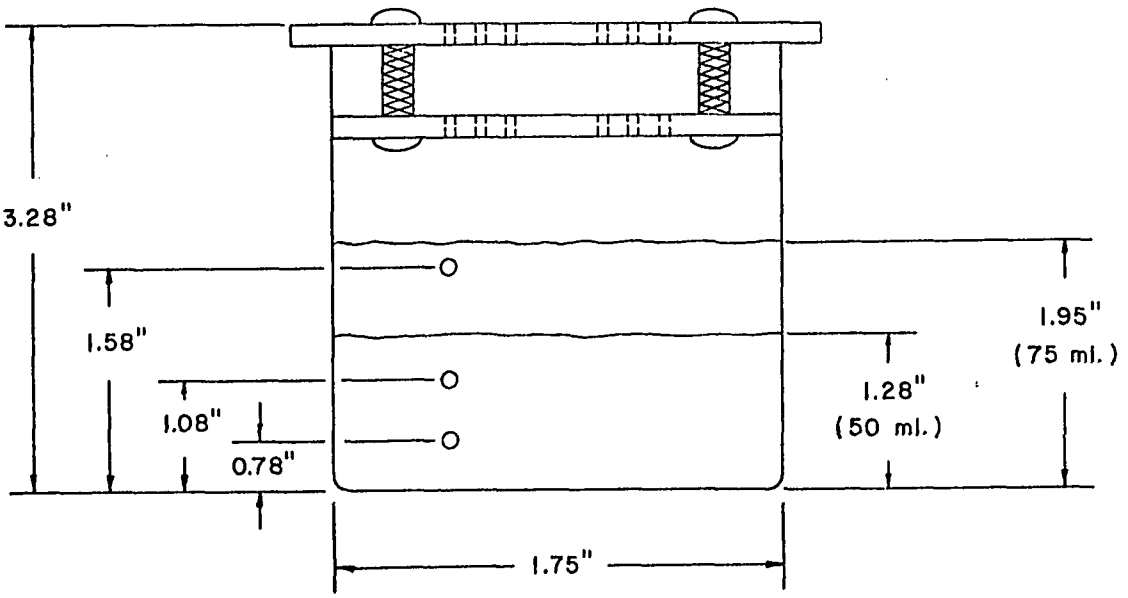

Figure A-1. Apparatus Used to Study the Vortex Flow of Blood.

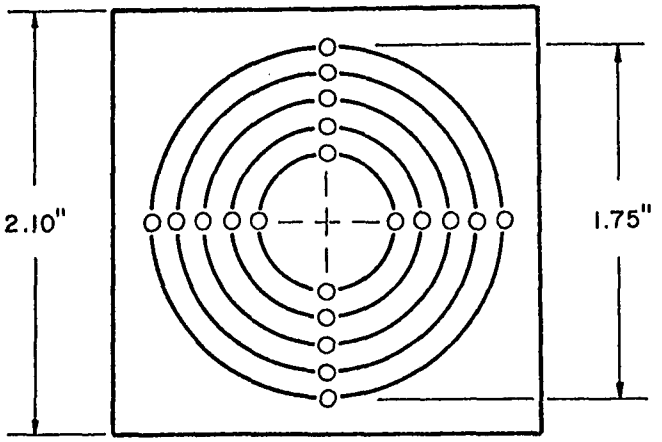

Figure A-2. Equipment Used to Measure a Given Radial Position.

The apparatus was filled with 75 mls of ACD (an anti-coagulant) treated human blood at 25°C. The blood was used within 20 hours after donation. The stirring bar was allowed to rotate at a given rpm for 10 minutes to reach steady state. Partially settled blood was found to be completely remixed within 10 minutes at 100 rpm. Samples were then withdrawn (two samples minimum at each location) at all radial positions and all angular positions by inserting a capillary tube into the blood at a given position and height, allowing the blood to flow into the capillary tube, then withdrawing the capillary tube and sealing one end with Critoseal. The samples were then centrifuged at 5500 g for over three minutes to allow complete packing of the red cells.

Three different heights were used to check the region near the bottom where secondary flow and stirring bar interference are important, the middle region, and the region near the free surface. The heights measured from the bottom were 0.78, 1.08, and 1.58 inches. The height of the blood in the 75-ml sample was 1.95 inches.

A total of 260 hematocrit measurements were recorded. An additional 75 measurements were taken to check suspected erroneous values. Blood samples were taken at fourteen equally spaced (1/16") radial positions in order to determine the radial concentration distribution. At the completion of the experiment, a 20-ml plasma sample from the experimental blood was collected by centrifuging a 50-ml sample of whole blood, and stored at -10°C to be used for further examination. A 20-ml plasma sample obtained from unused blood kept at 4°C was also stored at -10°C. A slight pink coloration was noted in both plasma samples indicating that some of the red cells were destroyed (hemolysis). Since both samples had the same pink coloration, it is not suspected that the stirring bar caused the red cells to be destroyed.

At least five bulk hematocrit measurements were taken at the beginning and end of the experiment. The bulk hematocrit samples were taken from blood that had been mixed completely with a stirring rod, and from blood in the original container mixed by shaking. At the completion of a set of measurements at a given stirrer rotational speed, the rpm was changed, ten minutes were allowed to reach

steady state, and the above procedure repeated. Rotational speeds of 100, 250, and 650 rpm were investigated. The rotational speed was determined using a strobelight with water as the experimental liquid. After completing tests at the three different rpm's, approximately 25 mls of blood were removed from the apparatus until 50 mls remained. A complete set of measurements were recorded at 100 rpm at a height of 1.08" above the bottom of the container. The height of the blood in the 50-ml sample was 1.28".

A sedimentation test showed that the blood used in this experiment had a very low sedimentation rate. Normal blood settles at about 9 to 11 millimeters per hour at 25°C. The blood used in this experiment settled at about 2.0 millimeters per hour at 25°C. It is not known if or how this variable affects the radial concentration distribution.

With the exception of suspected erroneous readings, all samples had a hematocrit (volume fraction of red cells) of between 0.38 and 0.41. Measurements taken at a given radius, height, and rpm also had a range between 0.38 and 0.41. It must be concluded that the experimental uncertainty in the hematocrit measurement accounts for the hematocrit variations between 0.38 and 0.41. The error in the measured hematocrit can be caused by 1) plasma leakage through the Critoseal (a sealing compound used to seal one end of the capillary tube after the tube is filled with a blood sample),

causing a high hematocrit reading, 2) leakage of red cells through the Critoseal causing a low hematocrit reading (a red coloration was occasionally observed in the white Critoseal), 3) both plasma and red cell leakage causing an undetermined error, and 4) the error associated with measuring the red cell length and the plasma column length. The measurement error is probably the most significant error. This error is largest in the shortest total sample length. The combination of these four sources of error account for a total error of $\pm$ 1.5 hematocrit percent. The average sample for a given location was usually very close to 38.5 hematocrit percent. It has been shown that for the diameter capillary tubes used in this experiment, (1.1 mm), the hematocrit in the capillary tube is equal to the hematocrit at the point where the measurement is made. It is not known whether or not the insertion of the capillary tube affects the value of the hematocrit measured by the tube.

It was observed that the average hematocrit in the 50-ml sample at 100 rpm and the middle height was about 0.7 hematocrit percent lower than the average reading with 75 mls of blood and the same operating conditions. This could be due to the destruction of the red cells previously noted. Other than this one exception, it was found that the hematocrit is independent of radial or angular position, height of the measured blood sample, and the rpm of the stirring bar. The bulk hematocrit dropped from 0.398 to 0.393

units over a four-hour period. This again could be due to hemolysis. The average bulk hematocrit was determined from at least five measurements and it is suspected that the drop could also be due to the uncertainty in the measured hematocrits since both sets of measurements had overlapping values.

During one run at 100 rpm, the stirring bar was intentionally displaced to one side by moving the beaker. Measurements were taken at the middle height. No change in hematocrit was observed. The radial measurements were made directly above the stirring bar. The stirring bar was then displaced to the opposite side of the beaker and measurements were again taken. Within experimental error, all measurements were the same. Therefore, it is concluded that the hematocrit is completely independent of the use of a centrifugal stirring bar to agitate the blood.

It was found that 100 rpm was sufficient to completely mix partially settled blood. This was the minimum speed possible with the magnetic stirring motor used. The extremely slow sedimentation rate observed could influence the minimum rpm required to completely mix partially settled blood.

At 100 rpm, the vortex shape of the free surface was less than 1/16" below the motionless position at the centerline. At 250 rpm, the free surface was about 1/8" below the motionless position at the centerline, and about 0.8" below the motionless position at 650 rpm.

APPENDIX B

Details of Experimental Fibers

Fiber	D, Microns	Length, cm.	Material
L-1	811 ± 1	30.48 ± 0.02	Machined Glass
L-2	221 ± 0.5	20.84 ± 0.02	Machined Glass
L-3	153.3 ± 0.4	38.69 ± 0.02	Machined Glass
L-4	128 ± 0.3	22.50 ± 0.02	Machined Glass
M-1	99 ± 0.2	30.60 ± 0.02	Machined Glass
M-2	75 ± 0.2	25.83 ± 0.02	Machined Glass
M-3	59 ± 0.1	30.60 ± 0.02	Machined Glass
S-1	29 ± 0.1	30.53 ± 0.02	Soft Glass
S-2	23 ± 0.2	27.38 ± 0.02	Styron 666
S-3	15.3 ± 0.2	26.82 ± 0.02	Styron 666
S-4	8.7 ± 0.2	27.66 ± 0.02	Soft Glass

BIBLIOGRAPHY

1. Abramson, H.A. et al., "Electrophoresis of Proteins", Reinhold Pub. Co., N.Y. (1942).

2. Albert, S.N., "Blood Volume", Anesth., 24, 231 (1963).

3. Aroesty, J., and J.F. Gross, "Convection and Diffusion in the Microcirculation", Microvascular Research, 2, 247 (1970).

4. Bayliss, L.E., "Rheology of Blood and Lymph", in "Deformation and Flow in Biological Systems", A. Frey-Wyssling, ed. North Amst. Pub. Co., Amsterdam (1952).

5. Bayliss, L.E., "A Quantitative Study of the Hemodynamics in the Living Microvascular System", Am. J. Anatomy, 110, 125 (1962).

6. Benis, A.M., "The Flow of Human Blood Through Models of the Microcirculation", Sc.D. Thesis, M.I.T., Cambridge, Mass. (1964).

7. Benis, A.M., E.W. Merrill et al., "The Flow of Human Blood Through Hollow Fibers", J. Appl. Physiol., 20, (1965).

8. Bennett, L., "Red Cell Slip at a Wall in Vitro", Science, 155, 1554 (1967).

9. Bingham, E.C., and R. Thompson, "The Correction in Viscometry When Using Capillary Tubes Which Have Trumpet-Shaped Openings", J. Rheol., 1, 418 (1930).

10. Bishop, C., "The Red Blood Cell", Academic Press, N.Y. (1965).

11. Blair, E., "Clinical Hypothermia", McGraw-Hill, N.Y. (1964).

12. Bloch, E.H., "A Quantitative Study of the Hemodynamics in the Living Microvascular System", Am. J. Anatomy, 110, No. 2, 125 (1962).

13. Bloor, M.I.G., "The Flow of Blood in the Capillaries", Phys. Med. Biol., 13, 443 (1968).

14. Bohlin, T., "On the Drag on a Rigid Sphere Moving in a Viscous Liquid Inside a Cylindrical Tube", Transactions of the Royal Institute of Technology, Stockholm, No. 155 (1960).

15. Bolger, J.C., "Rheology of Kaolin Suspensions", Sc.D. Thesis, M.I.T., Cambridge, Mass. (1960).

16. Braasch, D., and W. Jennet, "Erythrocyte Flexibility, Hemoconcentration and Blood Flow Resistance in Glass Capillaries with Diameters Between 6 and 50 Microns", 5th European Conference on Microcirculation (H. Harlers, ed.), 109 (1969).

17. Branemark, P.I., and J. Lindstrom, "Shape of Circulating Blood Corpuscles", Biorheology, 1, 139 (1963).

18. Brenner, H., "The Stokes Resistance of an Arbitrary Particle --II", Chemical Engineering Science, Vol. 19, 599 (1964).

19. Brenner, H., "Rheology of Two-Phase Systems", Annual Review of Fluid Mechanics, 2, 137 (1970).

20. Brewer, D.B., "Renal Clearances of Dextrans of Varying Molecular Weights", Proc. R. Soc. Med., 44, 561 (1951).

21. Brillouin, M., "Jean Leonard Marie Poiseuille", J. Rheol., 1, 345 (1930).

22. Brooks, D.E., Goodwin, J.W., and G.V.F. Seaman, "Interactions Among Erythrocytes Under Shear", J. of Applied Physiology, 28, 172 (1970).

23. Canham, P.B., and A.C. Burton, "Distribution of Size and Shape in Populations of Normal Human Red Cells", Circulation Research, 22, 405 (1968).

24. Casson, N., "Rheology of Disperse Systems", C.C. Mill, ed., Chapt. 5, Pergamon Press, N.Y. (1959).

25. Chandrasekhar, S., "Hydrodynamic and Hydromagnetic Stability", Oxford Press, London (1961).

26. Chen, T.C., and R. Skalak, "Spheroidal Particle Flow in a Cylindrical Tube." Tech. Rep. No. 2, Project NR 062-393, Dept. of Civil Engn. and Engn. Mech., Columbia University. (1968).

27. Charm, S.E., G.S. Kurland, and M. Schwartz, "Absence of Transition in Viscosity of Human Blood Between Shear Rates of 20 and 100 sec^{-1}." J. of Applied Physiology, 26, 389 (1964).

28. Chien, S. et al., "Plasma Trapping in Hematocrit Determination." Proc. Soc. Exp. Biol. Med., 119, 1155 (1965).

29. Chien, S., R.J. Dellenback, S. Usami, G. Seaman, and M. Gregersen, " Centrifugal Packing of Suspensions of Erythrocytes Hardened with Acetaldehyde." Proc. Soc. Exptl. Biol. Med., 127, 982 (1968).

30. Charm, S.E., and G.S. Kurland, "Discrepancy in Measuring Blood in Couette, Cone and Plate, and Capillary Tube Viscometers." J. of Applied Physiology, 25, 786 (1968).

31. Chien, S., "Shear Dependence of Effective Cell Volume as a Determinant of Blood Viscosity." Science, 168, 927 (1970).

32. Cohn, E.J., et al., "The Characteristics of the Protein Fractions of Human Plasma." J. Clin. Invest., 23, 417 (1944).

33. Cokelet, G.R., "The Rheology of Human Blood." Sc.D. Thesis, M.I.T., Cambridge, Mass. (1963).

34. Cokelet, G.R., "Comments on the Fahraeus-Lindqvist Effect." Biorheology, 4, 123 (1967).

35. Cokelet, G.R., E.W. Merrill, et al., "The Rheology of Human Blood--Measurements Near and at Zero Shear Rate." Trans. Soc. Rheol., 7, 303 (1963).

36. Cokelet, G.R., and H. Meiselman, "Rheological Comparison of Hemoglobin Solutions and Erythrocyte Suspension." Science, 162, 275 (1968).

37. Copley, A.L., et al., "Viscosity Studies and Anomalous Flow Properties of Human Blood Systems with Heparin and Other Anticoagulants." J. Gen. Physiol., 26, 49 (1942).

38. Copley, A.L., "Rheological Problems in Biology." Proc. Inter. Rheol. Conf. (1948), pp. 1-54. North Holland Publ. Co., Amsterdam (1949).

39. Davson, H., "Textbook of General Physiology", 2nd ed., Chapts. 7 & 8. Little, Brown; Boston, Mass. (1960).

40. Dintenfass, L., "Viscosity of Blood at High Haematocrits Measured in Microcapillary (Parallel-Plate) Viscometer at r= 3-30 Microns." Proc. Intern. Conf. Haemorheol., 1, 197 (1966).

41. Dryden, H.L., F.D. Murnaghan, and H. Bateman, Hydrodynamics, Bulletin No. 84 of the National Research Council, pg. 103. National Academy of Sciences (1932).

42. Erk, S., "On the Deviations of the Pressure Drop in a Capillary From the Poiseuille Law." J. Rheol., 2, 205 (1931).

43. Fahraeus, R., "The Suspension Stability of Blood." Acta. Med. Scand., 55, 1 (1921).

44. Fahraeus, R., "The Suspension Stability of Blood." Physiol. Rev., 9, 241 (1929).

45. Fahraeus, R., and T. Lindqvist, "The Viscosity of Blood in Narrow Capillary Tubes." Am. J. Physiol., 96, 562 (1931).

46. Fahraeus, R., "The Influence of the Rouleaux Formation of the Erythrocytes on the Rheology of the Blood." Acta. Med. Scand., 161, 151 (1958).

47. Faxen, H., "Die Bewegung einer starren Kugel längs der Achse eines mit zäher Flussigkeit gefüllten Rohres." Arkiv fur Matematik, Astronomi och Fysik, Vol. 17, No. 27, pp. 1-28 (1922).

48. Fitz-Gerald, J.M., "Mechanics of Red Cell Motion in Very Narrow Capillaries." Proc. Roy. Soc. London, Series B, 174, 193 (1969).

49. Fitz-Gerald, J.M., "Implications of a Theory of Erythrocyte Motion in Narrow Capillaries." J. Applied Physiol., 27, 912 (1969).

50. Fulton, G.P., and B.R. Lutz, "The Use of the Hamster Cheek Pouch and Cinephotomicrography for Research on the Microcirculation and Tumor Growth, and for Teaching Purposes." Boston Medical Quart., 8, 1: 13-19 (1957).

51. Fulton, G.P., and J.J. Berman, Proc. 6th Annual Symp. on Blood. Wayne University. Throm. Diath. Haem., 1, 559 (1957).

52. Fulton, G.P., and B.R. Lutz, "Kinemicrography of Living Blood Vessels." Med. and Biol. Illustration, 7, pp. 26-31 (1957).

53. Fulton, G.P., "Blood Flow in the Small Vessels." Motion picture produced in the Dept. of Biology, Boston University, Boston, Mass.

54. Fung, Y.C., "Blood Flow in the Capillary Bed." J. Biomechanics, 2, 353 (1969).

55. Gabe, I.T., and L. Zatz, "Studies of Plasma Viscosity Under Conditions of Oscillatory Flow." Biorheology, 5, 86 (1968).

56. Gaehtgens, P., H.J. Meiselman, and H. Wayland, "Velocity Profiles of Human Blood at Normal and Reduced Hematocrit in Glass Tubes Up to 130 Microns Diameter." Microvascular Research, 2, 13 (1970).

57. Gilinson, P.J., Jr., C.R. Dauwalter, and E.W. Merrill, "A Rotational Viscometer Using an A.C. Torque to Balance Loop and Air Bearing." Trans. Soc. Rheol., 7, 319 (1963).

58. Goldsmith, H.L., and S.G. Mason, "Axial Migration of Particles in Poiseuille Flow." Nature, 190, 1095 (1962).

59. Goldsmith, H.L., and S.G. Mason, "The Flow of Suspensions Through Tubes, I. Single Spheres, Rods and Discs." J. Colloid Sci., 17, 448 (1962).

60. Goldstone, J., H. Schmid-Schonbein, and R. Wells, "The Rheology of Red Blood Cell Aggregates." Microvascular Research, 2, 273 (1970).

61. Gregersen, M.I., C.A. Bryant, W.E. Hammerle, S. Usami, and S. Chien, "Flow Characteristics of Human Erythrocytes Through Polycarbonate Sieves." Science, 157, 825 (1967).

62. Guest, G.M., "Osmometric Behavior of Normal and Abnormal Human Erythrocytes." Blood, 3, 541 (1948).

63. Guyton, A.C., "Textbook of Medical Physiology," 1st ed., pp. 346, W.B. Saunders, Philadelphia, Pa. (1961).

64. Haberman, W.L., and R.M. Sayre, "Motion of Rigid and Fluid Spheres in Stationary and Moving Liquids Inside Cylindrical Tubes." David Taylor Model Basin Report No. 1143 (1958).

65. Hall, C.E., and H.S. Slayter, "The Fibrinogen Molecule: Its Size, Shape, and Mode of Polymerization." J. Biophys. and Biochem. Cytology, 5, 11 (1959).

66. Hansen, T.A., "Osmotic Pressure Effect of the Red Cells--Possible Physiological Significance." Nature, 190, 504 (1961).

67. Happel, J., and B.J. Byrne, "Motion of a Sphere and Fluid in a Cylindrical Tube." Industrial and Engineering Chem., 46, No. 6, 1181 (1954).

68. Happel, J., and H. Brenner, "Low Reynolds Number Hydrodynamics." Prentice-Hall, Inc., Englewood Cliffs, N.J. (1965).

69. Hardwicke, J., et al., "Effect of Dextran of Various Molecular Sizes on Erythrocyte Sedimentation Rate." Nature, 166, 988 (1950).

70. Hardwicke, J., "The Use of Dextran to Study Erythrocyte Sedimentation." Proc. R. Soc. Med., 44, 559 (1951).

71. Hardwicke, J., and J.R. Squire, "The Basis of the Sedimentation Rate." Clin. Sci., 11, 333 (1952).

72. Haynes, R.H., "Rheological Properties of Blood", in "Blood Vessels and Lymphatics." D.I. Abramson, ed., Academic Press, N.Y. (1962).

73. Heard, D.H., and G.V.F. Seaman, "The Action of Lower Aldehydes on the Human Erythrocyte." Biochem. Biophys. Acta, 53, pp. 366-374. (1961).

74. Herschel, W.H., "On the Rate of Shear in Capillary Tubes." J. Rheol., 1, 505 (1930).

75. Hochmuth, R.M., and D.O. Davis, "Changes in Hematocrit for Blood Flow in Narrow Tubes." Presented at the International Conf. on Microcirculation, Gothenburg, Sweden. (1968).

76. Hochmuth, R.M., R.N. Marple, and S.P. Sutera, "Capillary Blood Flow: I. Erythrocyte Deformation in Glass Capillaries." Microvascular Research, in Press (1970).

77. Hodgeman, C.D., et al., "Handbook of Chemistry and Physics", 38th ed., pg. 2030, Chemical Rubber Pub. Co., Cleveland, Ohio. (1956).

78. Hubbard, D., and G. L. Lucas, "Ionic Charges of Glass Surfaces and Other Materials and Their Possible Role in the Coagulation of Blood." J. App. Physiol., 15, 265 (1960).

79. Intaglietta, M., R.F. Pawula, and W. R. Tompkins, "Pressure Measurements in the Mammalian Microvasculature." Microvascular Research, 2, 212 (1970).

80. Isenberg, I., "A Note on the Flow of Blood in Capillary Tubes." Bull. of Math. Biophysics, 15, 149 (1953).

81. Joly, M., "Dispositif Pour La Viscosimètre Précise de Systèmes Contenant des Protéines." Biorheol., 1, 15 (1962).

82. Jeffrey, G.B., "The motion of Ellipsoidal Particles Immersed in a Viscous Fluid." Proc. Roy. Soc., A102, 161 (1922).

83. Karnis, A., H. Goldsmith, and S. Mason, "The Kinetics of Flowing Dispersions." J. of Colloid and Inter. Sci., 22, 531 (1966).

84. Krieger, I.M., and S.H. Maron, "Direct Determination of the Flow Curves of Non-Newtonian Fluids." J. App. Physics, 23, 147 (1952).

85. Kynch, G.J., "The Slow Motion of Two or More Spheres Through a Viscous Fluid." J. Fluid Mech., 5, 193 (1959).

86. Ladenburg, R., "Uber den Einfluss von Wanden auf die Bewegung einer Kugel in einer reibenden Flussigkeit." Annalen der Physik, Vol. 23, 4th Series, pp. 447 (1907).

87. Lee, R.E., "Anatomical and Physiological Aspects of the Capillary Bed in the Bulbar Conjunctiva of Man in Health and Disease." Angiology, 6, 369 (1955).

88. Lee, J.S., and Y.C. Fung, "Modeling Experiments of a Single Red Blood Cell Moving in a Capillary Blood Vessel." Microvascular Research, 1, 221 (1969).

89. Lighthill, M.J., "Pressure-Forcing of Tightly Fitting Pellets Along Fluid-Filled Elastic Tubes." J. Fluid Mech., 34, 113 (1968).

90. Maude, A.D., and R. L. Whitmore, "Theory of the Flow of Blood in Narrow Tubes." J. Appl. Physiol., 12, 105 (1952).

91. Maude, A.D., and R. Whitmore, "The Wall Effect and Viscometry of Suspensions." British Journal of Applied Physics, 7, 98 (1956).

92. McDonald, D.A., "Blood Flow in Arteries." Arnold Ltd., London. (1960).

93. Meiselman, H.J., "Some Physical and Rheological Properties of Human Blood." Sc.D. Thesis, M.I.T., Cambridge, Mass. (1965).

94. Meiselman, H.J., Personal Communication. (1969).

95. Merrill, E.W., et al., "Blood Rheology--Effect of Fibrinogen Deduced by Addition." Sub. to Circ. Resh. (1965).

96. Merrill, E.W., et al., "Non-Newtonian Rheology of Human Blood --Effect of Fibrinogen Deduced by Subtraction." Circ. Resh., 13, 48 (1963).

97. Merrill, E.W., et al., "Rheology of Blood and Flow in the Microcirculation." J. Appl. Physiol., 18, 255 (1963).

98. Merrill, E.W., et al., "Rheology of Human Blood Near and at Zero Flow." Biophys. J., 3, 199 (1963).

99. Merrill, E.W., C.S. Cheng., and G.A. Pelletier, "Yield Stress of Normal Human Blood as a Function of Endogenous Fibrinogen." J. of Appl. Physiol., 26, 1 (1969).

100. Merrill, E.W., and G. Pelletier, "Viscosity of Human Blood: Transition from Newtonian to Non-Newtonian." J. of Appl. Physiol., 23, 178 (1967).

101. Natelson, S., "Microtechniques of Clinical Chemistry," 2nd ed., Thomas. Springfield, Ill. Pg. 229 (1961).

102. Page, L.B., and P.J. Culver, "A Syllabus of Laboratory Examinations in Clinical Diagnosis." Harvard Press, Cambridge, Mass. (1960).

103. Pappenheimer, J.R., "Role of the Red Blood Corpuscles in the Regulation of Renal Blood Flow and Glomerular Filtration Rate." The Physiologist, 3, 20 (1958).

104. Phibbs, R.H., "Hemorheology," A.L. Copley, ed. Pg. 620. Pergamon Press, N.Y. (1968).

105. Poiseuille, J.L.M., "Recherches Experimentales Sur le Mouvement des Liquides dans les Tubes de Tres-Petits Diametres." Annales de Chimmie et de Physiol. VII, 50 (1843).

106. Ponder, E., "Tonicity-Volume Relations in Partially Hemolyzed Hypotonic Systems." J. Gen. Physiol., 33, 177 (1949).

107. Prandtl, L., and O.G. Tietjens, "Applied Hydro- and Aeromechanics," pg. 21, Dover, N.Y. (1934).

108. Prankerd, J.A.J., "The Red Cell." Oxford, Blackwell Scientific Publications. (1961).

109. Prothero, J., and A.C. Burton, "The Physics of Blood Flow in Capillaries. I. The Nature of the Motion." Biophysical Journal, 1, 565 (1961).

110. Prothero, J., and A.C. Burton, "The Physics of Blood Flow in Capillaries: I. The Nature of the Motion." Biophysical J., 1, 565 (1961).

111. Prothero, J., and A.C. Burton, "The Physics of Blood Flow in Capillaries. II. The Capillary Resistance to Flow." Biophysical J., 2, 199 (1962).

112. Reiner, M., "Slippage in a Non-Newtonian Liquid." J. Rheol., 2, 337 (1931).

113. Rosenblum, W.I., Personal Communication. Univ. of Virginia Medical School, Richmond, Va. (1970).

114. Rourke, M.D., and Ernstene, "A Method for Correcting the Erythrocyte Sedimentation Rate for Variations in the Cell Volume Percentage of Blood." J. Clin. Invest., 8, 545 (1930).

115. Rubinow, S.I., and J.B. Keller, "The Transverse Force on a Spinning Sphere Moving in a Viscous Fluid." J. Fluid Mech., 11, 447 (1961).

116. Saffman, P.G., "On the Motion of Small Spheroidal Particles in a Viscous Liquid." J. Fluid Mech., 1, 540 (1956).

117. Scatchard, G., et al., "Chemical, Clinical, and Immunological Studies on the Products of Human Plasma Fractionation." J. Clin. Invest., 23, 458 (1944).

118. Schmid-Schonbein, H., P. Gaehtgens, and H. Hirsch, "On the Shear Rate Dependence of Red Cell Aggregation in Vitro." J. Clin. Invest., 47, 1447 (1968).

119. Schwab, P.J., and J.L. Fahey, "Treatment of Waldenstroms Macroglobulinemia by Plasmapheresis." The New England Journal of Medicine, 263, 574 (1960).

120. Scott-Blair, G.W., "An Equation for the Flow of Blood, Plasma, and Serum Through Glass Capillaries." Nature, 183, 613 (1959).

121. Seaman, Geoffry, Personal Communication. (1970).

122. Segre, G., and A. Silberberg, "Radial Particle Displacements in Poiseuille Flow of Suspensions." Nature, 189, 209 (1961).

123. Segre, G., and A. Silberberg, "Behavior of Macroscopic Rigid Sphere in Poiseuille Flow." J. Fluid Mech., 14, 136 (1962).

124. Skalak, R., and P.I. Branemark, "Deformation of Red Blood Cells in Capillaries." Science, 164, 717 (1969).

125. Skalak, R., "Mechanics of the Microcirculation." Symposium on Biomechanics, LaJolla, Calif. Ed. by Y.C. Fung. In press (1970).

126. Stimson, M., and G.B. Jeffery, "Proceedings of the Royal Soc. of London, 111, Series A., pg. 110 (1926).

127. Stone, S.B., "The Kinetic Energy Correction in Fluid Flow." J. Rheol., 1, 240 (1930).

128. Sutera, S.P., and R. M. Hochmuth, "Large Scale Modeling of Blood Flow in the Capillaries." Report No. 1, Brown University School of Engineering. (1966).

129. Sutera, S.P., and V. Seshadri, "Concentration Changes of Suspensions of Rigid Spheres Flowing Through Tubes." Report No. 2, Brown University School of Engineering. (1967).

130. Sutera, S.P., Personal Communication, Brown Univ., Maryland. (1968).

131. Thomas, H.W., "The Wall Effect in Capillary Instruments: An Improved Analysis Suitable for Application to Blood and Other Particulate Suspensions." Biorheology, 1, 41 (1962).

132. Vand, V., "Viscosity of Solutions and Suspensions." J. of Phys. and Colloid Chemistry, 52, 277 (1948).

133. Vand, V., "Viscosity of Solutions and Suspensions, II." J. Phys. Coll. Chem., 52, 300 (1948).

134. Vejlens, G., Acta, Path. Microbiol. Scand., 33 97 (1938).

135. Wakiya, S., "A Spherical Obstacle in the Flow of a Viscous Fluid Through a Tube." J. of the Phys. Soc. of Japan, 8, No. 2, 254 (1953).

136. Wang, H., and R. Skalak, "Viscous Flow in a Cylindrical Tube Containing a Line of Spherical Particles." Columbia University, N.Y. (1967).

137. Wayland, H., "Blood Rheology and Its Relation to Microcirculatory Flow." Presented at the U.S.-Japan Cooperative Seminar on Biophysics and Bioengineering of the Peripheral Circulation, Nagoya, Japan. Pg. 21. (1967). Gastroenterology, 52, 342 (1967).

138. Wells, R.E., and E.W. Merrill, "Shear Rate Dependence of the Viscosity of Whole Blood and Plasma." Science, 133, 763 (1961).

139. Wells, R. E., "Rheology of Blood in the Microvasculature." N.E.J. of Med., 270, 832 (1964).

140. Whitmore, R.L., "Hemorheology and Hemodynamics." Biorheology, 1, 201 (1963).

141. Wiederhielm, C.A., J.W. Woodbury, S. Kirk, and R. F. Rushmer. "Pulsatile Pressures in the Microcirculation of Frog's Mesentery." Amer. J. Physiol., 207, 173 (1964).

142. Whitmore, R.L., "A Theory of Blood Flow in Small Vessels." J. Appl. Physiol., 22, 767 (1967).

143. Wilkinson, W.L., "Non-Newtonian Fluids." Pergamon Press, N.Y. (1960).

144. Zweifach, B.W., "Functional Behavior of the Microcirculation." Pg. 15-17. C.W. Thomas, Springfield, Ill. (1961).

145. Zweifach, B.W., "Pathophysiology of the Blood Vascular Barrier." Angiology, 13, 345 (1962).

PROPOSITION I

It is proposed that the quiet interval between eruptions of Old Faithful Geyser can be predicted with greater accuracy than the method now employed by the rangers at Yellowstone National Park.

A mathematical model of an eruption cycle is based on the assumption that the flow rate of water into Old Faithful's reservoir is constant.

THE PREDICTION OF OLD FAITHFUL'S NEXT ERUPTION

Old Faithful is by far the most famous geyser in the world. It is located in the Upper Geyser Basin in the valley of the Firehole River, which flows through the southwest-central part of Yellowstone National Park, Wyoming. Although the discovery and naming of the geyser are credited to the Washburn-Langford-Doane expedition of 1870, the geyser was well known to James Bridger and other mountain men for many years before 1870 (3). Since its discovery in 1870, the tourist travel to Yellowstone National Park has grown from a few saddle parties to many million motor transported visitors each season. To many people, Old Faithful has become the symbol of national parks. Other large geysers have gone dormant; new ones have evolved, and the predictability of most has varied. Old Faithful, consistent in its pattern, has not changed in any measurable way since its discovery. For this reason, Old Faithful has always been singled out as Yellowstone's major attraction. The magnificence and power of an eruption of Old Faithful thrills even the most sophisticated observer.

The many misconceptions as well as the interesting facts of this geyser have necessitated many research papers as well as a few books devoted to the description of Old Faithful. While reading some of the papers or sections of some of the books describing the

prediction of the eruption interval, two interesting facts stand alone.

The first fact is that the average time between eruptions is extremely constant (3). This high degree of regularity arises because Old Faithful is an isolated, self-contained unit. Secondly, the prediction of the quiet interval between eruptions is very inaccurate in spite of a large number of available parameters. Presently, the quiet interval is predicted from the length of the previous eruption. (4).

The prediction of the next eruption of Old Faithful is made by the Ranger-Naturalist located inside the Old Faithful Visitor Center, and is reported with a plus and minus five minute interval. The sign stating the predicted time might read: "Old Faithful Geyser may erupt between 11:30 and 11:40". These predictions are frequently in error and the observers are constantly pestering the Park personnel with statements such as, "Well, it was late that time;" or "It played before it was due", depending on whether it was over or under the predicted interval.

The predicted interval is estimated from the duration of the last eruption as follows:

eruption length	quiet interval
1.5 to 2.0 min	40 min
3.0 to 4.5 min	68 to 70 min
4.5 to 5.0 min	85 min

For eruptions between 2.0 and 3.0 minutes, the ranger predicts a quiet interval between 40 and 68 minutes, based on experience (5).

Observation and statistical studies indicate that a short quiet interval is usually followed by a long quiet interval; an over-average interval is not necessarily followed by an under-average one. Usually, long and short quiet intervals alternate but sometimes long intervals predominate by a ratio of two or three to one. Old Faithful ejects steam throughout the quiet interval, but after a short eruption the steam just comes out at a slow rate, while for a long eruption steam puffs of considerable force follow the end of the eruption for about one minute; then the passive steam begins.

As mentioned earlier, these predictions are frequently in error by a considerable amount and even when observation space is not a problem, at least 50% of the people that watch an eruption arrive 30 minutes before the predicted time of the eruption, and at least 90% arrive about 15 minutes before the predicted time. This indicates that the observers place very little faith in the rangers' predictions. This skepticism on the part of the observers was noted on a very cold and windy day even though a warm lodge was only a few feet away (but out of range of a good view of the eruption of Old Faithful). It is obvious that an improved method of

predicting the quiet interval of Old Faithful is needed, and this need is clearly recognized by the employees of Yellowstone National Park (2).

As mentioned previously, the average eruption interval is quite constant. Peale (6) found, from 97 observations made in 1878, that the average interval was 65.1 minutes. Seventy years later the average interval calculated from 11,048 eruptions was 65.12 minutes.

Based on the fact that over a period of 100 years the average quiet interval has been constant (about 65 minutes), and also it is constant for as few as 10 eruptions, it appears that the flow of water into the geyser reservoir during the quiet interval is relatively constant, and it has been reported (1) that over a long period, the average volume of water ejected per eruption is also constant. The assumption used to improve the prediction of the next eruption is that either the volume of water or the amount of heat that flows into the reservoir is constant for a short interval, even for each individual eruption.

During the quiet interval, exactly as much water flows into the reservoir as flowed out during the preceding eruption. Therefore, it is necessary to determine the volume of water ejected per eruption, i.e., $\int_0^T Q(t)dt$ where $Q(t)$ is the volumetric flow rate of

water and steam out of the geyser during the eruption, which lasts for a time T. This assumption is illustrated in Figure 1 and in Equation (1).

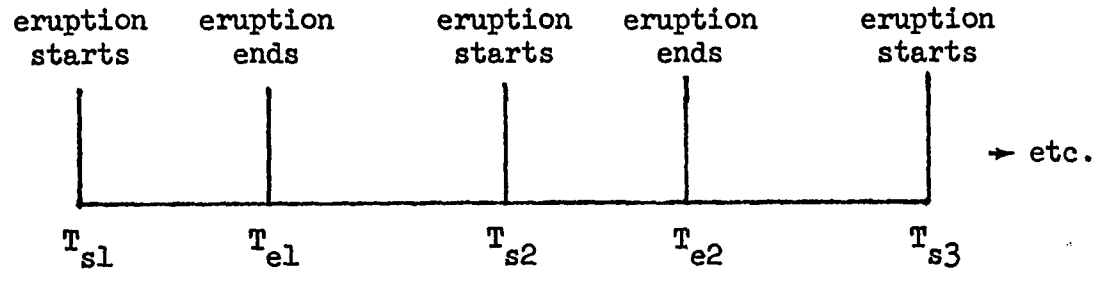

Figure 1. Old Faithful's Eruption Schedule.

$$\int_{T_{s1}}^{T_{e1}} Q(t)dt = C_1(T_{s2} - T_{e1})$$

$$\int_{T_{s2}}^{T_{e2}} Q(t)dt = C_1(T_{s3} - T_{e2}) \qquad \text{etc.} \qquad (1)$$

Since $Q(t) = V(t)A$, where $V(t)$ is the velocity of the geyser jet and A is the area of the vent, a pitot tube placed at the base of the geyser cone could be used to measure the velocity of the jet by operating a pressure transducer. The pressure transducer signal could be relayed to the Visitor Center by either an underground cable

or by a radio signal. Since this method of measuring velocity would alter the natural formation of Old Faithful, such an idea is not acceptable to the Old Faithful rangers.

An alternate way to approximate the flow rate from the exit jet is to measure the height of the geyser jet as a function of time, since $V(t) \propto h^{1/2}(t)$ where h is the height of the water column. Since $Q(t) = V(t)A$,

$$\int_0^T Q(t)\,dt = A\int_0^T V(t)dt \tag{2}$$

and

$$V(t) \simeq \left[2gh(t)\right]^{1/2} \tag{3}$$

therefore:

$$\int_{T_{s1}}^{T_{e1}} Q(t)dt = (2g)^{1/2}A \int_{T_{s1}}^{T_{e1}} h^{1/2}(t)dt = C_1(T_{s2} - T_{e1}) \tag{4}$$

if

$$C_2 = C_1/(2g)^{1/2}A \tag{5}$$

then

$$\int_{T_{s1}}^{T_{e1}} h^{1/2}(t)dt = C_2(T_{s2} - T_{e1}) \tag{6}$$

A number of eruptions are measured and from the data, C_2 is deter-

mined. Then, from Equation (6) the time of the next eruption can be determined:

$$T_{s2} = \frac{1}{C_2} \int_{T_{s1}}^{T_{e1}} h^{1/2}(t)dt + T_{e1} \qquad (7)$$

Note that C_1 has dimension of ft^3/sec and C_2 has dimensions of $ft^{1/2}$.

Since the installation of a pitot tube for test purposes was not permitted, it was found necessary to measure the height of Old Faithful's water column as a function of time in order to determine the accuracy of the assumption and therefore, whether an improved method for predicting the next eruption could be found. It would be much preferred to measure the velocity of the outlet jet directly since the height of the eruption is affected by the weather. When the air is still, cool, and humid, large condensing clouds of steam spread out and hover about the water column masking the true height. Above the column, these clouds ascend vertically for several hundred feet. The impression of such an eruption would vary greatly from an eruption seen when the air was warm and dry, resulting in little condensation of steam. Or, if a strong wind is blowing, as much as 50 feet is sheared off the top of the water column.

The actual height to which Old Faithful plays presents as much variation as the length of water play. Unless there is an exact correlation between the height of an eruption and the length of that eruption, it does not seem likely that eruption length alone should be sufficient for predicting the next eruption.

The heights of a number of eruptions were measured by triangulation and motion pictures. The pictures were analyzed frame by frame and the height of the water column was determined by the reading of a Philadelphia rod (a calibrated measuring stick placed between the geyser and the camera). The error in measuring the height is $\pm$ 3% and is the result of an error in measuring the baseline, the error in reading the height of the geyser as located on the Philadelphia rod, and the error in measuring the distance between the camera and the Philadelphia rod. The baseline was 265 $\pm$ 5 feet, and the distance between the Philadelphia rod and the camera was 11.2 feet. A typical eruption is shown in Figure 2 and the heavy solid lines represent the mathematical approximation used to simplify the calculation (and the number of measurements needed to predict the next eruption).

A mathematical equation was found to fit each simplified portion of Figure 2, as follows:

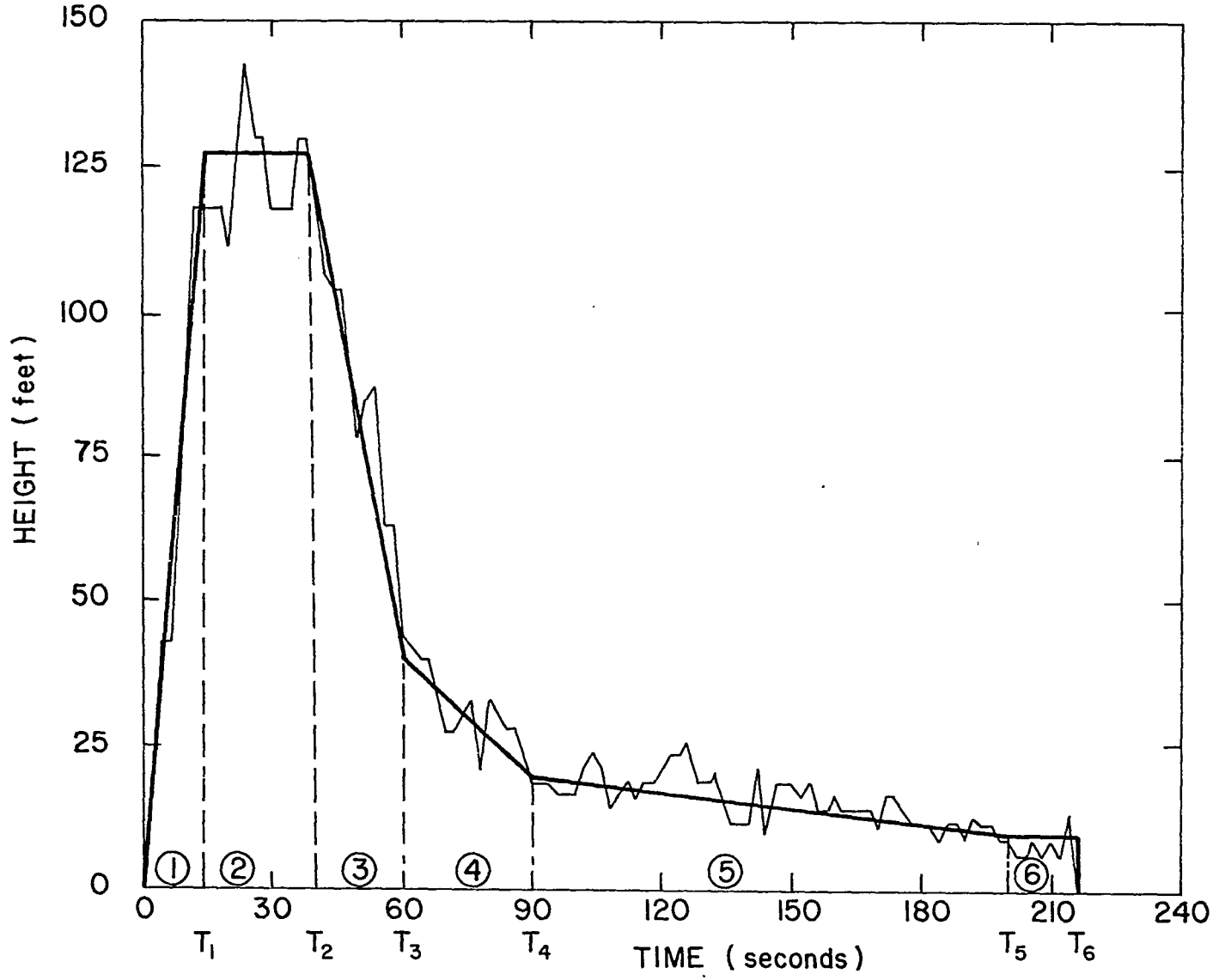

Figure 2. A Typical Eruption of Old Faithful Geyser.

1. $$h(t) = \frac{H_1}{T_1}\, t \qquad (8)$$

2. $$h(t) = H_1 \qquad (9)$$

3. $$h(t) = \left\{\frac{(H_1 - 40)(t - T_3)}{T_2 - T_3} + 40\right\} \qquad (10)$$

4. $$h(t) = \left\{\frac{(40-20)(t-T_4)}{T_3 - T_4} + 20\right\} \qquad (11)$$

5. $$h(t) = \left\{\frac{(20-10)(t-T_5)}{T_4 - T_5} + 10\right\} \qquad (12)$$

6. $$h(t) = 10 \qquad (13)$$

The square root of the expression was integrated between the times for that portion of the eruption. The results are:

1. $$\frac{2}{3}\left[\frac{H_1}{T_1}\right]^{1/2} T_1^{3/2} \qquad (14)$$

2. $$H_1^{1/2}\,(T_2 - T_1) \qquad (15)$$

3. $$\frac{2}{3}\left[\frac{T_2 - T_3}{H_1 - 40}\right]\left[40^{3/2} - H_1^{3/2}\right] \qquad (16)$$

4. $$\frac{2}{3}\left[\frac{T_3-T_4}{40-20}\right]\left[20^{3/2} - 40^{3/2}\right] \qquad (17)$$

5. $$\frac{2}{3}\left[\frac{T_4-T_5}{20-10}\right]\left[10^{3/2} - 20^{3/2}\right] \qquad (18)$$

6. $$10^{1/2}(T_6-T_5) \qquad (19)$$

Using Equations (14) through (19) and the measured quiet interval, the constant C_2 in Equation (6) was determined for each eruption and the following quiet interval. Then, using the average of the calculated constants, the eruptions were predicted. The actual time of an eruption, along with the prediction made by the Old Faithful ranger and the prediction from this method are shown in Table I.

TABLE I. PREDICTED AND ACTUAL ERUPTION TIME OF OLD FAITHFUL.

Actual Eruption Time	Ranger's Prediction	Proposed Method
12:58:08	12:55 - 1:05	12:58:07
1:16:45	1:01 - 1:11	1:15:21
1:49:15	1:45 - 1:55	1:49:19
1:56:00	1:58 - 2:08	1:55:57
3:03:07	3:00 - 3:10	3:03:16
3:11:22	3:05 - 3:15	3:10:24
4:22:27	4:00 - 4:10	4:04:22
5:29:10	5:33 - 5:43	5:34:43
6:40:00	--- ---	6:40:12

The eruption that started at 4:22:27 presents a problem both for the rangers and for the proposed method. Sometimes, following several splashes, one occurs which suggests that the eruption is starting. But for some reason, the large splash may fail to trigger the eruption. When this happens the eruption may be delayed for as long as 20 minutes and usually about 5 minutes. Such was the case with the eruption that finally started at 4:22:27. The first surge that appeared to be the start of the eruption occurred at 4:13:12.

It was not checked, but it is possible that the heavy splash that appears to be the initiation of the eruption but fails to trigger the eruption could be treated as an eruption and the real eruption predicted from the volume of water ejected by the heavy surges.

It can be seen that the suggested method represents only a slight improvement over the method used by the rangers at Old Faithful's location (they use the length of the eruption only). However, by measuring the velocity of the geyser jet in place of the approximate method of measuring the geyser height, it is suggested that the method of predicting the next eruption of Old Faithful could be improved significantly.

Even if it is not possible to increase the accuracy of predicting the next eruption to the extent of justifying the expense of installing the necessary equipment, several other advantages could be obtained by installing monitoring equipment. First, when it is cloudy

and rainy (for example, during the early spring), it is impossible to determine when the eruption of Old Faithful starts and when it stops. In such cases, it is impossible to predict the next eruption at all. Also, in winter it is difficult to observe an eruption due to fog and a generally overcast sky. By measuring the length of an eruption and the following quiet interval by means of a pitot tube, eruptions could be monitored both day and night, summer and winter.

REFERENCES

1. Allen, E.T., and A.L. Day. "Hot Springs of Yellowstone National Park." Carnegie Institution of Washington Publ. No. 466, 184 (1935).

2. Anderson, J.K., Personal Communication. Superintendent, National Park Service, Yellowstone National Park, Wyoming. 82190 (1969).

3. Fix, P.F. "Regularity of Old Faithful Geyser, Yellowstone National Park, Wyoming." Am. J. of Science, 247, 246 (1949).

4. Marler, G.D. "The Story of Old Faithful." Yellowstone Library and Museum Assn. (1969).

5. Marler, G.D., Personal Communication. Ranger, National Park Service, Yellowstone National Park, Wyoming. (1969).

6. Peale, A.C. "Thermal Springs (Of Yellowstone National Park): Old Faithful Geyser." U.S. Geol. and Geog. Survey of the Territories, 12, 220 (1883).

PROPOSITION II

It is proposed to show that a paper presented by Gerrard, which asserts that the velocity profile of a fluid flowing through a tube can be uniquely determined by measuring the thrust and the corresponding flow rate, is incorrectly formulated. An example is discussed that demonstrates the non-uniqueness of the velocity profile at a fixed ratio of thrust to flow rate.

VELOCITY PROFILES IN TUBE FLOW

The knowledge of the exact velocity profile of a fluid flowing through a tube is recognized as being of extreme importance. Experimental techniques are important tools in determining the velocity profile for a large number of cases, but these techniques have many restrictions. A number of fluid rheology models have been developed and many real fluids obey these models with a great degree of accuracy. From these models the velocity profile can be predicted. The velocity profile determination is of course important for a number of reasons such as the prediction of radial profiles of certain variables (e.g., temperature) from a knowledge of the velocity profile and the mixing cup temperature. In order to predict heat and mass transfer in flowing systems, it is also necessary to determine the velocity distribution in the fluid.

The most common experimental methods for determining the velocity profile are the traversing pitot tube, the hot wire bubble generator, doppler methods, streak pictures and dye tracing techniques. All of these techniques have limitations such as dimensional restrictions on the system, Reynolds number range, transparancy of the liquid, etc. Also, most of the experimental efforts have been confined to the turbulent flow regime. Of particular interest is non-isothermal, laminar flow and very little has been done on such systems. Even simple Newtonian liquids lose their parabolic velocity profile in non-isothermal flow conditions.

From the above discussion, it appears that a simplified method for indirectly determining the velocity profile would be an important development in fluid mechanics. The radial distribution of many important properties could then be determined by simply measuring the mixing cup property. This explains the enthusiasm with which a paper, presented at the eighth annual meeting of the Society of Rheology (and subsequently published in the Transactions of the Society of Rheology), was received. The synopsis of the paper, presented by Gerrard (1), reads:

> "The terminal velocity profile of a liquid flowing in a capillary (tube) can be determined quite accurately from a simultaneous measurement of the mass flux (throughput) and momentum flux (thrust). The flow may be of almost any type, i.e., laminar, transitional, turbulent, most shear-sensitive, and most non-isothermal cases. The assumptions embodied appear to be quite logical and exclude very few types of flow systems."

Although it would be an extremely valuable contribution to fluid mechanics if the method were correct, it is proposed to show that the proof used by Gerrard does not permit the conclusion that the velocity profile is uniquely determined by measuring the flow rate and the corresponding thrust. An example is presented to disprove the claim.

Gerrard's proof is based on the assumption that both du/dr and d^2u/dr^2 are less than zero for all values of the tube radius. The assumption could have been stated <u>less than or equal to zero</u>, since for most fluids du/dr is zero at $r=0$ and for many fluids (e.g., power law fluids), $d^2u/dr^2 = 0$ at $r=0$.

The thrust exerted by a fluid leaving a capillary tube is:

$$T = \int_0^R 2\pi\rho(r)U^2(r)\ r\ dr \qquad (1)$$

and the flow rate is:

$$Q = \int_0^R 2\pi\rho(r)U(r)\ r\ dr \qquad (2)$$

For both Equations (1) and (2), an infinite number of velocity profiles exist that satisfy either equation separately. For the non-isothermal case, the density varies across the tube radius and this would complicate the calculation of U(r). In the following discussion, the density is assumed constant.

The argument used by Gerrard is that the ratio of thrust to flow rate produces a unique determination of the velocity profile:

$$T/Q = \int_0^R 2\pi U^2(r)\ r\ dr \Big/ \int_0^R 2\pi U(r)\ r\ dr \qquad (3)$$

The proof of this argument goes as follows. Assume a velocity distribution, U(r), which produces a thrust T and a flow rate Q. Now suppose that there exists another velocity distribution, U*(r), which

produces a thrust T* and a flow rate Q*, not equal to T and Q. However, the ratios are the same:

$$T/Q = K = T^*/Q^* \tag{4}$$

From Equation (4), it is seen that:

$$T^*/T = Q^*/Q = M \qquad M \neq 1 \tag{5}$$

or

$$T^* - MT = 0 \tag{6}$$

and

$$Q^* - MQ = 0 \tag{7}$$

Then from Equations (1) and (6):

$$\int_0^R r[U^{*2}(r) - MU^2(r)]\, dr = 0 \tag{8}$$

and from Equations (2) and (7):

$$\int_0^R r[U^*(r) - MU(r)]\, dr = 0 \qquad (9)$$

Equation (8) gives:

$$\int_0^R r[U^*(r) + \sqrt{M}U(r)][U^*(r) - \sqrt{M}U(r)]\, dr = 0 \qquad (10)$$

From Equation (10), two possible solutions exist: (a) $U^*(r) = \sqrt{M}U(r)$ and (b) the integrand takes on values for which the integrand is positive for part of the integration range and negative for the remaining part--the requirement is that the positive portion exactly balances the negative portion so that the net value of the integral is equal to zero.

The analogous possibilities of solutions to Equation (9) are: (c) $U^*(r) = MU(r)$ and (d) the same argument as used in (b) only the integrand is $U^* - MU$ instead of $U^{*2} - MU^2$.

The discussion of these possibilities is straight forward: (a) and (c) can only hold simultaneously if $M = 1$, which is not allowed. By using the argument that $(U^* - MU)$ is less than $(U^* - \sqrt{M}U)$, since Equation (5) can be defined so that M is larger than one, it is shown that Equations (9) and (10) cannot both hold at the same time. Gerrard then states that the above arguments "prove" that $U^*(r)$ must

be equal to U(r) and the velocity profile is unique.

Figure 1 (similar to Gerrard's Figure 1) shows either $r(U^* - MU)$ or $r(U^{*2} - MU^2)$ plotted as a function of tube radius. The graph shows a portion that is positive and a portion that is negative. Gerrard's argument is that for U and U* that give a zero integral for $r(U^* - MU)$, the integral will not be zero when $r(U^{*2} - MU^2)$ is the integrand. No proof of this statement is given although an explanation is attempted. The explanation is that, since $(U^* - \sqrt{MU})$ is larger than $(U^* - MU)$, all the $r(U^{*2} - MU^2)$ ordinate values will be larger than the $(U^* - MU)$ ordinate values. However, Gerrard misinterprets the term $(U^* + \sqrt{MU})$. He claims that this term increases across the area. This is backwards; $(U^* + \sqrt{MU})$ decreases across the area.

Consider a graph similar to Gerrard's Figure 1 with the tube wall portion positive, and the centerline portion negative. Now when $(U^* - MU)$ is negative, $(U^{*2} - MU^2)$ will be more negative very near the axis; $(U^* + \sqrt{MU})$ can be assumed larger than 1. As the integration proceeds from right to left, the term $(U^* + \sqrt{MU})$ continues to decrease in a non-linear way. It is impossible to evaluate the overall effect in the form of a proof; an example is needed.

Gerrard considered a power law fluid and that model will be used here as one possible rheological model. Gerrard divided the fluid velocity by the average velocity in order to make the velocity dimensionless. This is a poor choice since all fluid models will therefore have the same dimensionless flow rate and this is not

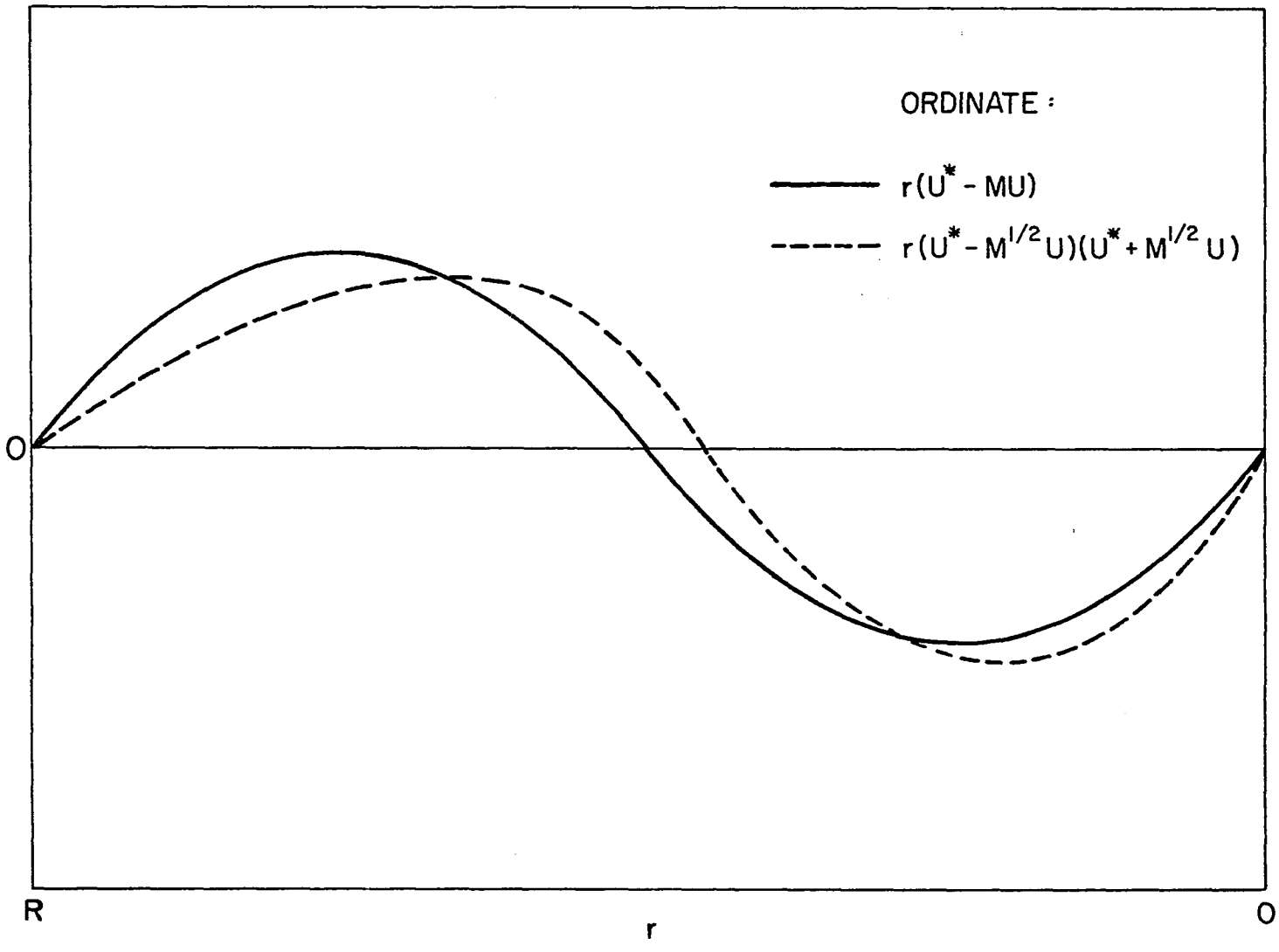

Figure 1. Graphical Integration of U^*-MU or $U^{*2}-MU^2$.

required. A better way is to divide by the centerline velocity.

Along with the power law model, the Bingham plastic model will be used. In the Bingham plastic model, both du/dr and d^2u/dr^2 are zero for small r and for this reason it was assumed that both du/dr and d^2u/dr^2 were equal to or less than zero as opposed to Gerrard's statement that du/dr and d^2u/dr^2 be less than zero. Careful inspection of the argument that he used clearly allows both du/dr and d^2u/dr^2 to be equal to zero.

For the power law fluid model:

$$U(r)/U_m = 1 - (r/R)^{\frac{n+1}{n}} \tag{11}$$

and for the Bingham plastic fluid model:

$$U(r)/U_m = \frac{1 - (r/R) - 2\tau_y/\tau_w(1 - r/R)}{(1 - r_y/R)^2} \qquad r \geq r_y \tag{12}$$

$$U(r)/U_m = 1 \qquad r \leq r_y \tag{13}$$

Putting these velocity expressions into Equation (3) gives:

$$T/Q = \frac{n+1}{2n+1} (U_m)_{PL} \tag{14}$$

for the power law model, and:

$$T/Q = \frac{2 - (28/5)X + 4X^2 + 2X^4 - 4X^5 + (8/3)X^6}{3 - 10X + 11X^2 - 4X^3 + X^4 - 2X^5 + X^6} (U_m)_{BP} \qquad (15)$$

$$X = \tau_y/\tau_w$$

for the Bingham plastic. Equation (14) is shown in Figure 2 and Equation (15) is shown in Figure 3. It can be seen from these two Figures that, if $(U_m)_{BP} = (U_m)_{PL}$, it is possible for these two different model fluids to have the same ratio of thrust to flow rate. The question is--how much difference is there between the two velocity profiles at a fixed T/Q if the centerline velocities are choosen to be equal? (If the centerline velocities are not the same, then Gerrard's claim cannot be satisfied. Therefore, in this argument, the centerline velocities for the two different fluids are set equal). Figure 4 shows the two dimensionless profiles for $T/(QU_m)$ equal to 0.85. The error shown in Figure 4 (29% at r/R = 0.90) is sufficient to discount Gerrard's uniqueness claim.

It has been shown that the method proposed by Gerrard for uniquely determining the velocity profile of most flow systems by measuring the thrust and corresponding flow rate is in fact not unique and in spite of the great need for such a method, Gerrard's method does not satisfy the need.

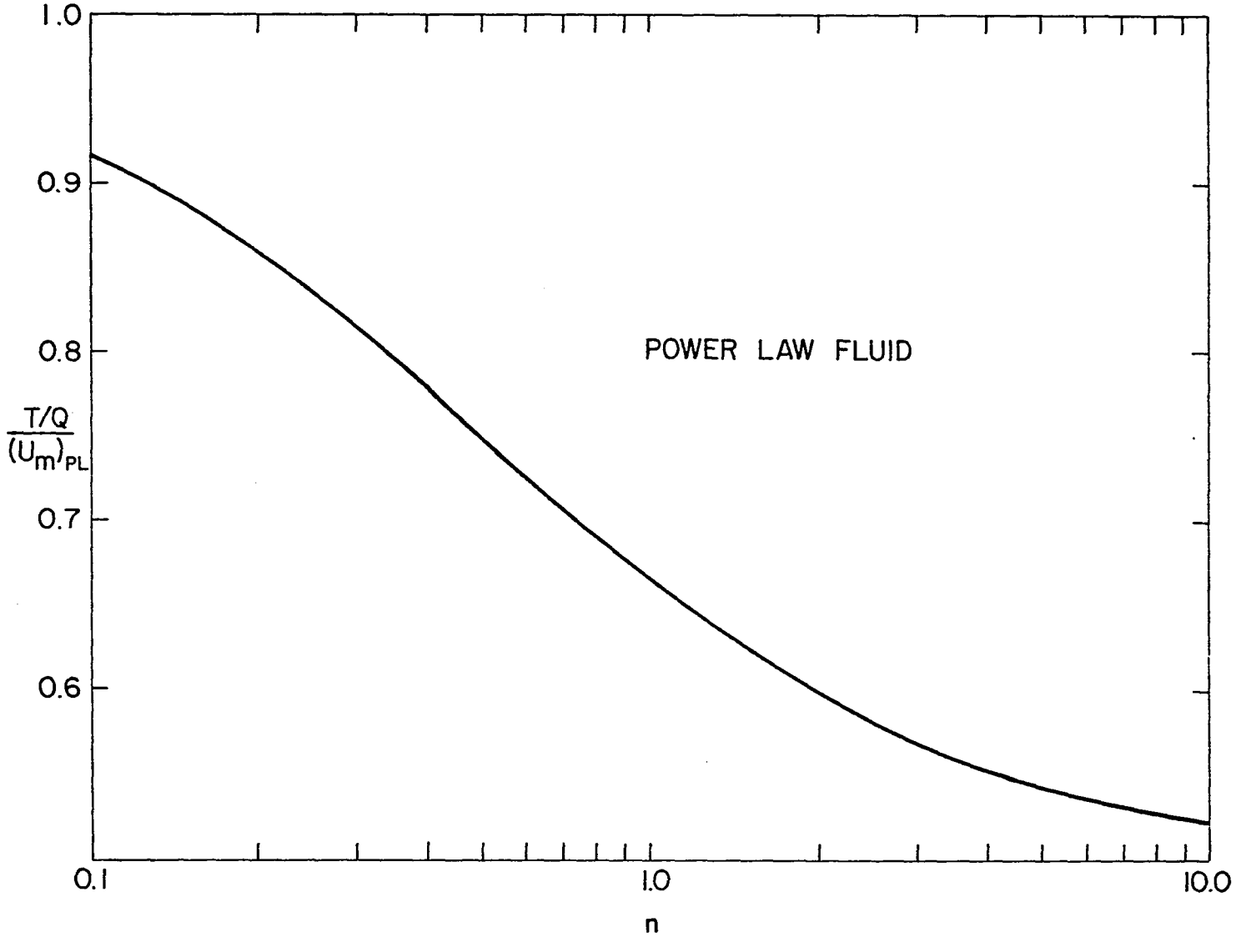

Figure 2. Ratio of Momentum Flux to Mass Flux as a Function of the Power Law Exponent.

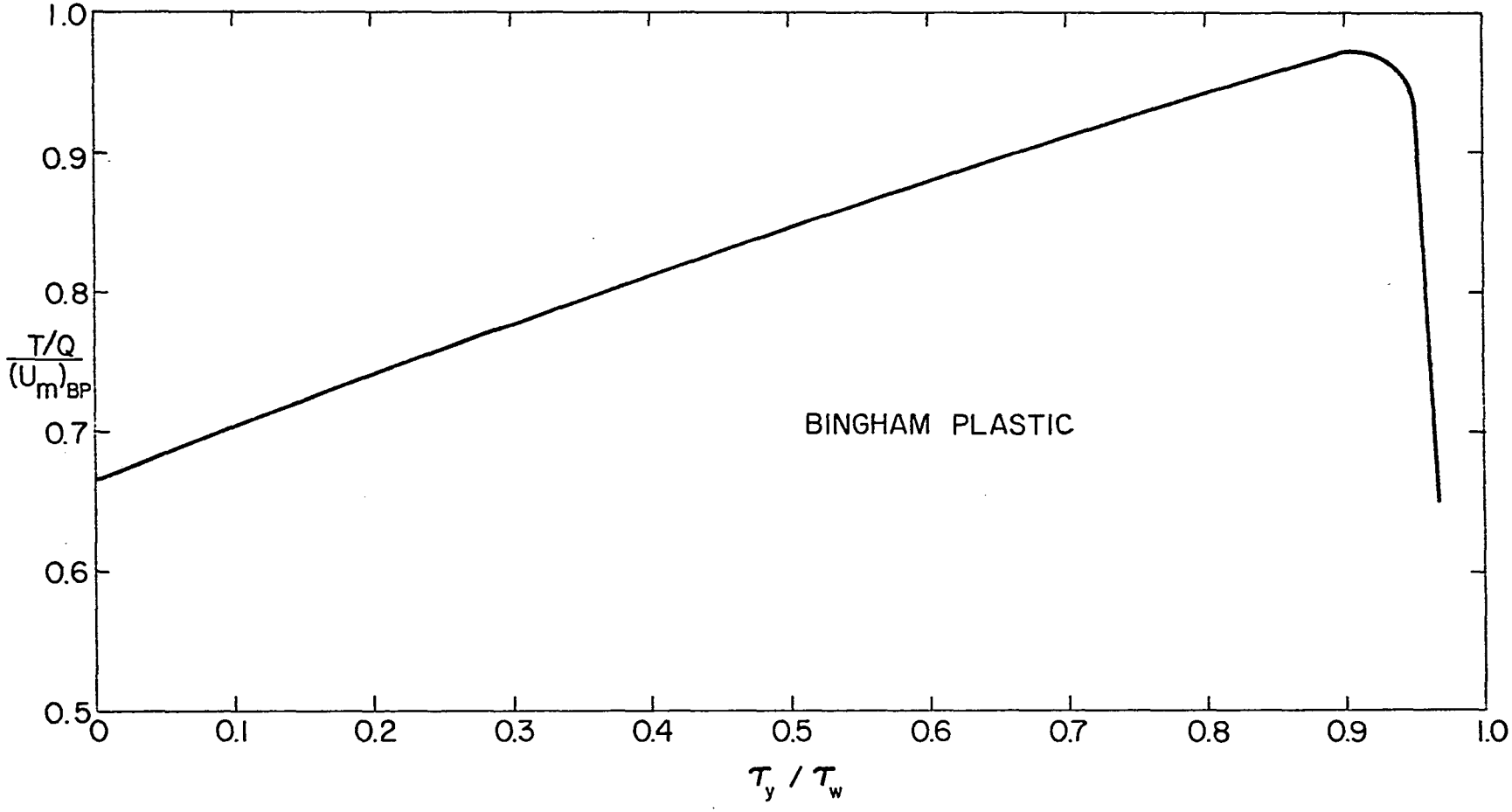

Figure 3. Ratio of Momentum Flux to Mass Flux as a Function of τ_y/τ_w.

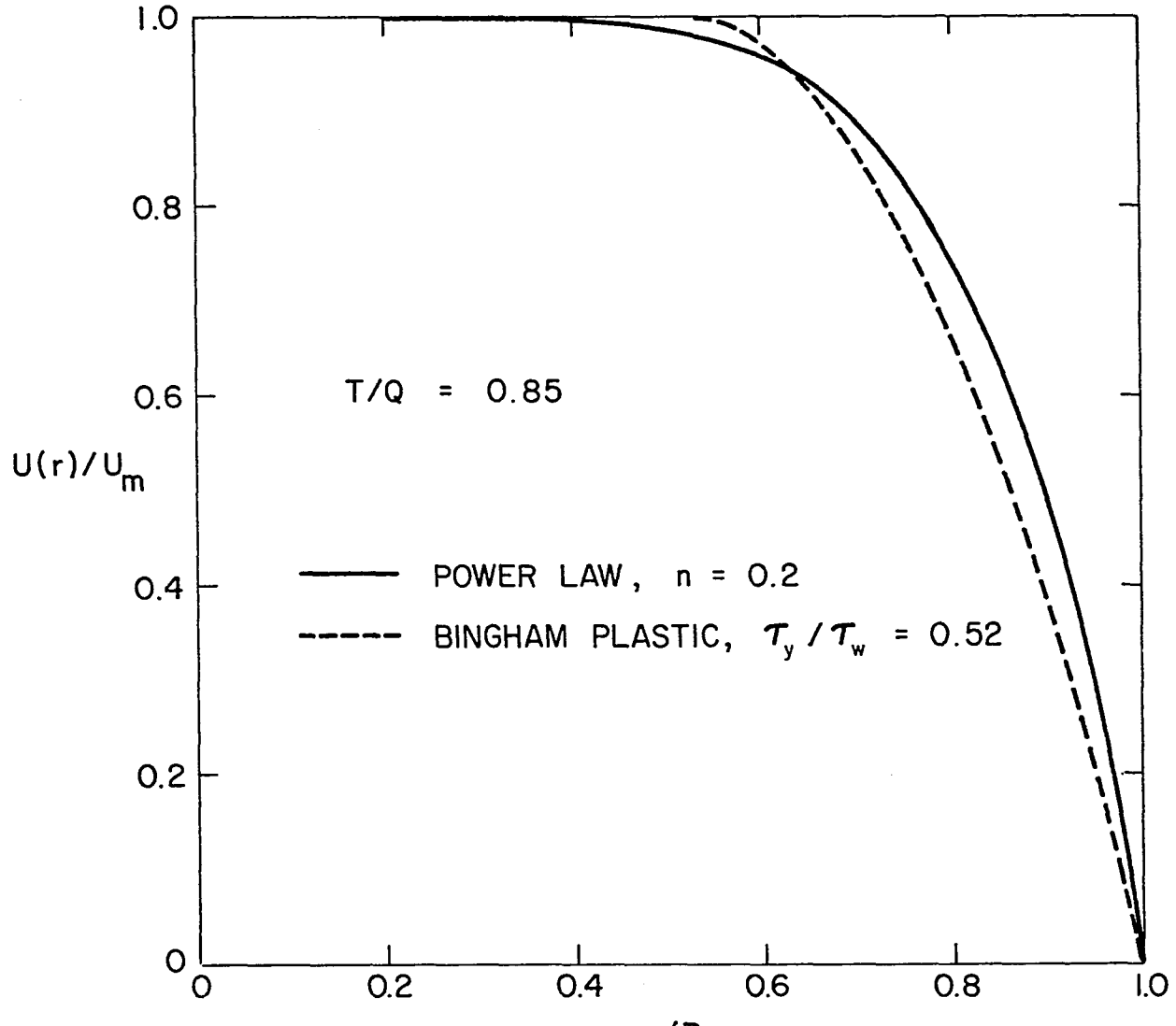

Figure 4. Dimensionless Velocity Profiles for the Power Law Fluid and the Bingham Plastic.

REFERENCES

1. Gerrard, J.E., "Velocity Profiles in Tube Flow.", Trans. Soc. Rheol., 8, 137 (1964).

PROPOSITION III

It is proposed to show, using the information available on Old Faithful Geyser, that the eruptive mechanism put forth by Reinhart does not apply to Old Faithful, but that a mechanism put forth by Geis can explain how Old Faithful Geyser erupts.

INTRODUCTION

Since the early 1800's, a number of theories have been presented in order to explain the mechanism by which geysers erupt. Any acceptable theory must explain the initiation, duration of water play, the eventual termination of the eruption, and the quiet period between eruptions. A complete discussion of the theories is given by Allen and Day (1), Barth (2), and Golovina and Malov (11). All of the theories presented to date fall into two general classes.

The earliest theories, called the "steam chamber theory" for future reference, assume that an underground reservoir is connected to the geyser tube. This reservoir is continually filling with water, and eventually overflows into an evacuated, high temperature cavity and boils; the steam that forms displaces the water-steam mixture up through the geyser tube and out the vent, resulting in the spectacular display witnessed by an observer.

The second class of theories, called the "critical column theory", which was originated and developed by Bunsen (1), again supposes that a large reservoir full of water is connected to the geyser tube. Because free circulation is at a minimum in the long, narrow geyser tube, the water temperature increases from the top downwards to the bottom of the geyser tube. The heating process continues until the water is near the boiling point at the corres-

ponding total pressure (atmospheric pressure plus the hydrostatic head). The water in the column is unstable because low temperature, high density water is situated above higher temperature, lower density water. The limited free circulation does allow some hot water to attain a low enough total pressure so that either steam or dissolved gases evolve and the water above this level is displaced out of the geyser tube, lowering the hydrostatic pressure on the remaining water. At this time the remaining water is above its boiling point (due to the reduction in total pressure) and flash boiling occurs throughout the column and the water-steam mixture is expelled through the geyser vent into the air.

Because no two geysers are alike with respect to physical construction, supply of water and heat, etc., it is expected that either class of mechanism may completely explain the behavior of a single geyser, but more likely for the majority of geysers, neither mechanism can, by itself, explain the behavior. In the majority of geysers, the water in the column is not very close to the boiling point for the total pressure at that location, but at some depth the temperature is above the atmospheric boiling point. In these cases, the column of water would have to be displaced a large distance before flash boiling could occur. Thus, most geysers probably erupt by means of steam formation in a steam chamber, and when enough steam is generated to lift the column to above the boiling point, the water

in the column flash boils. When the water in the reservoir is exhausted (either through the geyser tube or through the inlet channels), the eruption ceases and a brief period of steam evolution occurs. In the majority of geysers described in the literature, the eruption begins very slowly, followed by a short period of intense water activity where the height of the water jet is at a maximum. The height of the water jet then drops considerably and the remainder of the eruption is at a much lower height; a period of steam activity follows the termination of the eruption. The brief expulsion of water usually observed a few seconds before the eruption could indicate the initial generation of steam.

It is interesting that, even in light of much more complete records of geyser performance and information concerning other factors that might yield an indication of a true mechanism, such as the response of the geyser to fluctuations of barometric pressure, rainfall, etc. (an excellent discussion of these factors is given by Allen and Day (1), and by White (17)), no new theories have been advanced since the middle 1800's. In fact, the only systematic effort to obtain data that would allow a new theory to be developed was done by White (17). In spite of this lack of quantitative information (such efforts are seriously hampered by the fact that most geysers are either within National Parks and therefore restricted to superficial observation, or are inaccessible), a mechanism was put

forth by Rinehart (16) to explain the eruption cycle of Old Faithful, unquestionably the most famous of all geysers.

Old Faithful has a bimodally distributed eruption cycle with modes at 50 and 72 minutes. The long interval between eruptions occurs about twice as often as the short interval (16).

A short time after Rinehart presented his mechanism, Geis (9,10) presented a different mechanism to explain the bimodal behavior of Old Faithful. Rinehart's theory falls into the "critical column" class, while Geis' theory falls into the "steam chamber" class. Both theories can explain the bimodal eruption interval as well as the seismic data taken by Rinehart. Very little additional information seems to be available to test either theory.

It is proposed to show, using the available data, that Rinehart's mechanism does not apply to Old Faithful, while Geis' mechanism, modified slightly, is better able to explain the internal structure of Old Faithful.

DISCUSSION

Realizing that Rinehart's mechanism falls into the "critical column" class, as first proposed by Bunsen, and that Geis' model falls into the "steam chamber" class, it would be best to examine both classes in more detail.

The general description of the internal construction of a geyser belonging to the "critical column" class is shown in Figure 1.

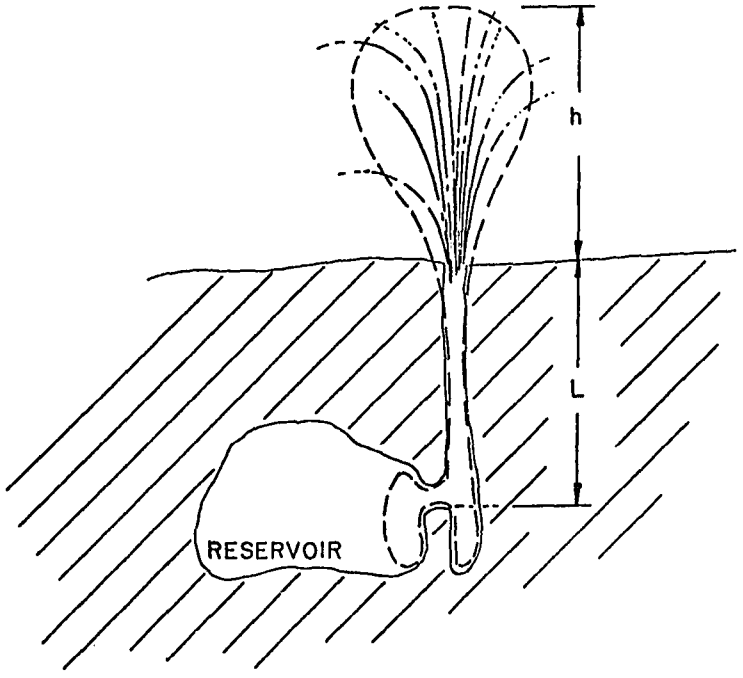

Figure 1. Bunsen's Modified Geyser Model: "Critical Column".

The water in the geyser tube is assumed to be near the boiling point corresponding to the total pressure. If the column is assumed to be adiabatic, the open form of the First Law of Thermodynamics:

$$dE_s = \delta q - \delta w + \sum_i (H_i + PE_i + KE_i)dm_i - \sum_o (H_o + PE_o + KE_o)dm_o \qquad (1)$$

reduces to:

$$(H_i + PE_i - H_o - PE_o) = 0 \qquad (2)$$

after the additional assumptions of steady state and no accumulation of water in the system (the system is shown enclosed by the dotted lines) are made. Equation (2) reduces to:

$$L + h = (H_i - H_o)/g \qquad (3)$$

Assuming that the enthalpy of the inlet stream (H_i) is the same as the enthalpy of the water at depth L, and that the enthalpy of the outlet stream corresponds to the conditions at the surface, the height of the water jet can be calculated from experimental data concerning the depth of the geyser tube (L), the temperature at the bottom of the geyser tube and the quality of the jet.

In order to demonstrate that Equation (3) is accurate in spite of a number of assumptions and at the same time demonstrate that the "critical column" mechanism does completely describe the behavior of

certain geysers, a man-made geyser known to have no steam chamber was thoroughly investigated by White (17), and his data concerning the November 20, 1945 eruption will be used as an example.

In the man-made geyser studied by White, the geyser tube is approximately 35 feet long, and the temperature in the reservoir immediately prior to the eruption was 114°C (237°F). The surface boiling point was 95.5°C (204°F). In the reservoir some flash boiling will occur, but in the first approximation it can be shown that the flash boiling is isenthalpic. For this reason, the enthalpy (thermodynamic properties of water were taken from (12)) of the inlet stream was taken as the enthalpy of saturated liquid at 237°F (203.28 BTU/lb). Actually, the liquid is not saturated, but the effect of pressure on the enthalpy for water is negligible (when the liquid enters the system it is saturated).

In order to calculate the amounts of liquid water and steam that leave the system, further approximations must be made. The liquid flow rate during the bursting stage was measured (110 gal/min) but the steam flow rate is unknown. The steam flow rate is assumed to be equal to the total flow rate minus the liquid flow rate. The total flow rate, during the bursting stage, was determined from the equation:

$$Q = (V)A \qquad (4)$$

where (V) is the velocity of the exit stream (assumed to be equal to $(2gh)^{1/2}$, neglecting wind resistance which is valid for the center of the water jet), and A is the area of the vent (the tube was a six-inch diameter steel pipe). The volumetric flow rates are then converted to mass flow rates using the densities of liquid water (allowance was made for the cooling of the water when measured by White) and the density of steam at 204°F.

By fixing the vent temperature, the pressure and the enthalpy (the enthalpy at the vent can be determined by an equation analogous to Equation (3)), the quality of the exit jet is automatically determined if the liquid and vapor are in equilibrium (perhaps a poor assumption). Thus, the height of the water jet could be determined independently of the liquid and total flow rates. A comparison of both methods for Old Faithful shows fair agreement; the predicted heights of the jet differ by about 30 per cent.

The total mass flow rate of steam also contains a contribution due to the vaporization of liquid water that left the vent superheated. White states that the water was superheated much above the surface boiling point. The mass of steam from this source was considered equal to:

$$(\text{mass of liquid}) \times C_{p(\text{liquid})} \times (\text{degree of super heat}) / \Delta H_{vap} \qquad (5)$$

The heat of vaporization was taken at the temperature of the superheated jet (surface boiling point plus degree of superheat). From the mass of liquid and the mass of vapor, the enthalpy of the outlet stream is then calculated. The specific enthalpies are taken at 204°F (172.02 BTU/lb for liquid and 1147.40 BTU/lb for vapor).

Calculation gave the following results:

TABLE I. WATER JET HEIGHT FOR THE GEYSER STUDIED BY WHITE (17).

Degree of Superheat (°F)	Height of Jet (feet)
0	94.8
2	83.6
3	78.3
4	73.0
5	68.0

White states that the maximum eruption height was 60 to 75 feet. Thus, the above derivation of Equation (3) is justified.

Similar calculations on Old Faithful, to be discussed later, where the degree of superheat has been measured and found to be 5°F (13), are shown in Table II. Old Faithful's water jet is 130 to 150 feet high (13). For this height, the depth of the geyser tube is less than 40 feet.

TABLE II. HEIGHT OF OLD FAITHFUL'S WATER JET.

Depth of Geyser Well (ft)	Height of Jet (ft)
25	46.9
50	254.0
75	667.0
100	1290.0
150	3067.0
200	4436.0
300	7231.0
400	9244.0

Since the water source must have some means for supplying water to the reservoir, the first thought is that as the column erupts, the pressure inside the reservoir increases considerably and much of the water is lost by reversing the flow through the channels supplying the reservoir. Perhaps the entire difference between the height (or volume) predicted by Equation (3) and the actual height (volume) can be accounted for by assuming that the excess water escapes from the reservoir through the channels that supply water during the quiet interval. This is incorrect; the water lost through the supply channels due to the high internal pressure during an eruption can shorten the duration of the eruption, but the loss of water does not affect the height of the eruption. In fact, for a "critical column" geyser,

the pressure in the reservoir is lower during an eruption than during the quiet period, and water continues to flow into the reservoir during the eruption.

Realizing that, from the above, only those geysers very near the surface can be "critical column" geysers, it is interesting to note that the Waimangu Geyser of New Zealand, which presumably had a long geyser tube and perhaps did operate on the "critical column" mechanism, erupted to a height of over 1600 feet and finally blew itself up (5)!

The water jet heights predicted from Equation (3) involve the subtraction of two large numbers which yield a small value. Thus, the accuracy of all answers is only within $\pm$ 30 feet.

The "steam chamber" theory requires a cavity devoid of liquid water (the cavity contains steam); the steam may not be in equilibrium with the liquid water. Eventually, liquid water overflows into the cavity, flash boils, and drives the contents out of the liquid reservoir. In the "steam chamber" theory, the pressure at the bottom of the tube increases and this increase in pressure causes the liquid in the tube to remain liquid until very near the surface. In the "critical column" theory, the pressure at the bottom of the geyser tube is lowered, allowing flash boiling to occur throughout the tube as well as in the reservoir.

OLD FAITHFUL

Old Faithful's geyser tube has been explored and found to be at least 75 feet deep (13). This represents only the straight portion so the tube may be much longer. The ground temperature near Old Faithful has been measured by Fenner (6), and these measurements were used to determine the water temperature in Old Faithful as a function of depth. The water temperature was chosen equal to the ground temperature. If the water was hotter than the ground, the values shown in Table II would be even higher, and it is improbable that the water could be cooler than the ground (if the water was cooler, and then cooled down during the eruption, the ground temperature would eventually drop). Also, the data taken by Fenner was obtained a few hundred yards from Old Faithful's vent, and the temperature in the immediate vicinity of a geyser would probably be higher than at a distance removed from the geyser. Thus, the water is probably hotter than the values chosen and Table II shows the lower limit for the height of the water jet.

In order to calculate the height of Old Faithful's water jet, the temperature of the water as a function of depth, the area of the vent and the maximum flow rate are needed. The vent is elliptic and has major axes of 23 and 60 inches (13). The maximum flow rate was determined by considering measured average and maximum flow rates for

other geysers. The geyser studied by White had the same ratio of maximum to average height and also the same ratio of duration of maximum height to total water play as Old Faithful (15). White found that the maximum flow rate was about three times the average flow rate. For Old Faithful, this predicts a maximum flow rate of about 7,500 gal/min. The temperature of the water was taken from Fenner for depths greater than 100 feet and extrapolated down to 25 feet using the difference between the water temperature and the boiling point found by White. The temperatures used were 215, 230, 246, 262, 292, 309, 336, and 352°F for the depths of 25, 50, 75, 100, 150, 200, 300, and 400 feet, respectively.

Old Faithful has a cone of geyserite which extends about 10 feet above ground level. Therefore, the depths reported in Table II are relative to the top of this cone. From Equation (3), Old Faithful's reservoir is less than 30 feet below the ground.

The following facts are necessary to appreciate both Rinehart's and Geis' models (13):

1. A short duration of water play is followed by a short interval between eruptions.
2. A long duration of water play is followed by a long interval between eruptions.
3. Eruptions last from 1.5 to 5 minutes.

4. A long duration of water play produces a higher water jet.
5. A short duration of water play produces a lower water jet.
6. Two successive long duration eruptions occur frequently.
7. Two successive short duration eruptions almost never occur.

RINEHART'S MODEL

Rinehart was somewhat careless when he presented his mechanism (14), since, as shown in Figure 2, it is unworkable. With a slight modification, his mechanism can explain the bimodal distribution of eruption interval lengths, the above facts, and his seismic data.

Rinehart postulates that a short duration of water play would empty only one reservoir, and a long duration of water play would empty both. Thus, during a short water play, Reservoir A would empty while Reservoir B was not yet at the critical eruption temperature. But, then as Reservoir A refilled, Reservoir B would be nearing the critical eruption temperature, and both reservoirs would shortly discharge. After both reservoirs emptied, a longer time would be required to reach the critical temperature for another eruption. Thus, all the above facts are explained.

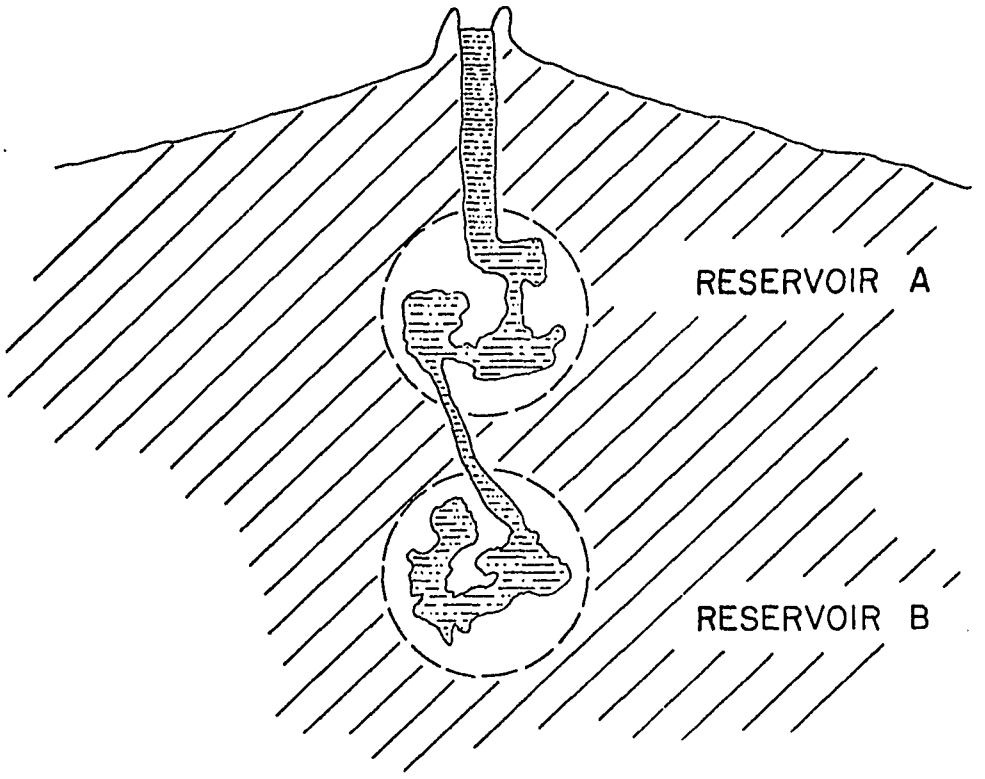

Figure 2. Rinehart's Proposed Mechanism (14,15).

However, Rinehart overlooked the fact that any time that Reservoir A erupted, the reduction of the height of the water column would allow Reservoir B to discharge (Reservoir B must always be hotter than Reservoir A). This difficulty can be eliminated by revising Rinehart's model as shown in Figure 3.

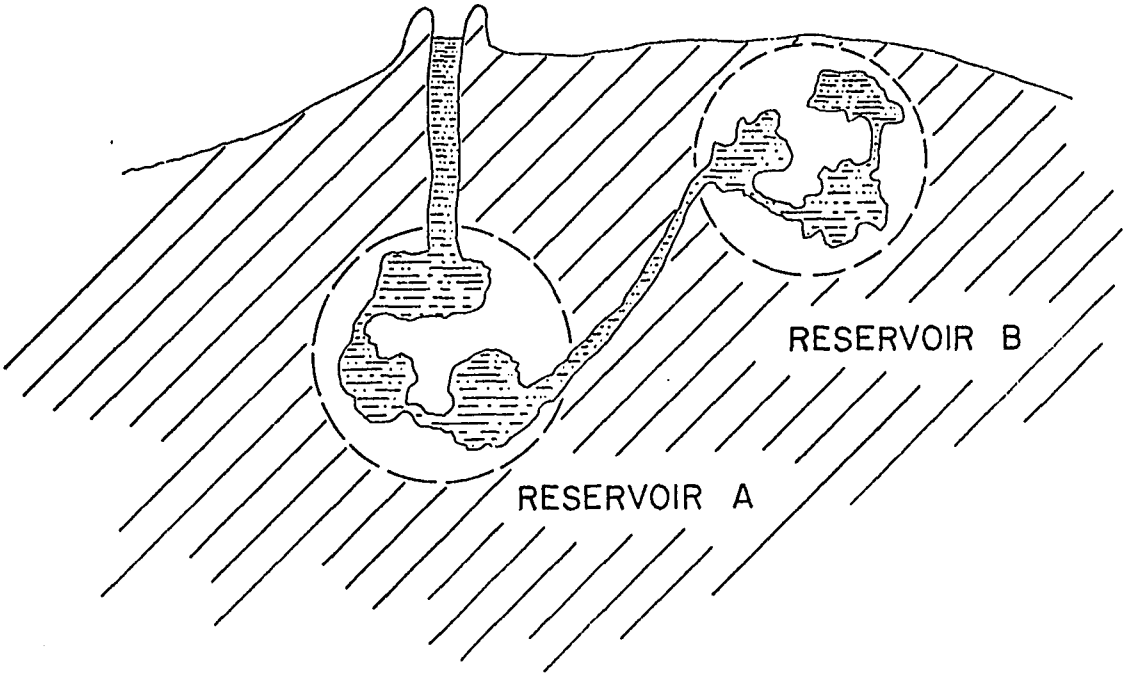

Figure 3. Rinehart's Mechanism Slightly Modified.

Now, simply discharging Reservoir A would not require that Reservoir B be discharged. The reservoirs are supposed, by Rinehart, to be very restricted. Thus, in Figure 3, some water could flow from Reservoir B into Reservoir A (the water in Reservoir B, being cooler than the water in Reservoir A, may terminate the eruption before Reservoir A was completely empty), but this is unimportant to the operation of the modified mechanism. Rinehart comments that a warm cone of geyserite lies about 60 to 70 meters from the vent of Old Faithful. He suggests that possibly the reservoir serving that now

extinct geyser could have broken through to Old Faithful's own reservoir or vent. By allowing the geyser tube to be short enough (less than 30 feet, according to Equation (3)), Rinehart's mechanism seems workable. However, Rinehart's modified model does not satisfy Facts 4 and 5.

If Reservoir B was situated above Reservoir A, as shown in Figure 3, and Reservoir A was only 30 feet below the ground, it is more than likely that Reservoir B would have been discovered by Rinehart himself, who made seismic recordings at different locations around Old Faithful's geyser vent but found no difference in the readings taken at different locations. It is highly improbable that Reservoir B is symmetric with respect to the geyser tube (which is straight to a depth of 75 feet), and at the same time located above Reservoir A. Also, Rinehart reports that his seismic readings were 'not near surface'.

Moreover, the amount of dissolved salts deposited by Old Faithful indicates that the temperature of the water supplying the reservoirs must be at least 401°F, requiring the water to come from a depth of at least 600 feet (8). It is possible that as the water rises from 600 feet, the salts that separate out as the water is cooled are carried along as a suspension, and then deposited inside the reservoir and subsequently blown out the geyser tube during an eruption, but 600 feet (minimum due to the twisting path) is unlikely. It is highly

unlikely that Rinehart's theory applies to Old Faithful since the reservoirs would have to be so close to the surface that they would have been discovered.

GEIS' MODEL

An attempt to justify Geis' theory requires 1) showing that the mechanism satisfies the previously stated facts, 2) experimental evidence is consistent with Geis' model, and 3) that such a mechanism can work in the first place (a severe criticism was presented by Fournier (7) which will be discussed at the appropriate time).

Geis was also careless about the presentation of his model, which is shown in Figure 4.

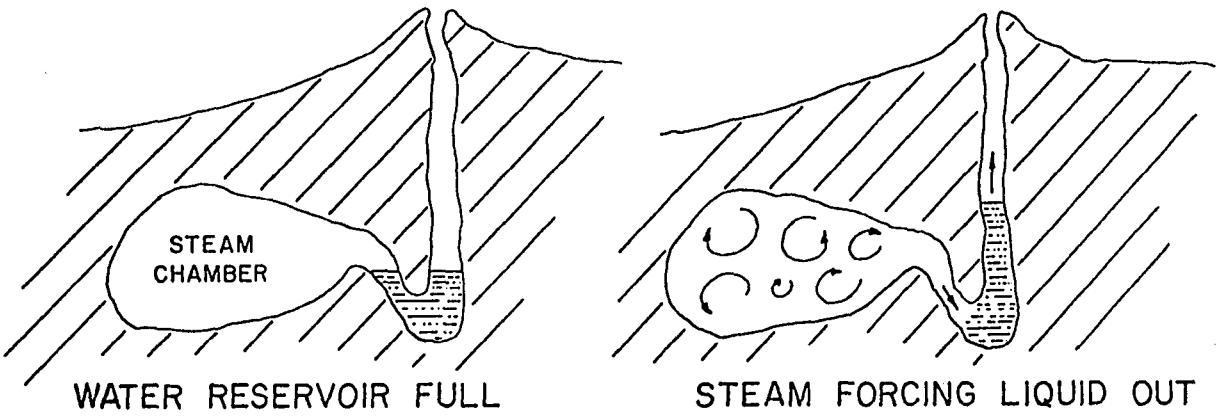

Figure 4. Geis' Proposed Model.

As presented, Geis' model does not conform to certain facts (not yet stated) concerning the behavior of Old Faithful. Some additional facts concerning the performance of Old Faithful are (13):

1. After an eruption, the water level rises gradually to within a few feet from the top of the geyser tube.
2. The average interval between eruptions is extremely constant and equal to 65.1 minutes.
3. The volume of each eruption is between 10,000 and 12,000 gallons.
4. When the interval between eruptions is long, there are more preliminary splashes than when the interval is short.

An additional fact concerning geysers similar to Old Faithful is:

5. It is not true that there is a regular increase in the temperature of the geyser system from the end of one eruption to the beginning of another eruption. Many geysers level off in temperature and show no subsequent increase in temperature (4).

Rinehart's theory requires an increase in temperature up to the succeeding eruption.

Fact 2 above implies that the flow rate into the geyser system (over a long period of time) is constant. Fact 1 is not met by Geis' formulation of his model. The model should have had the geyser tube

full of water (the pressure in the steam chamber is not at atmospheric pressure, but at a pressure equal to the hydrostatic pressure of the water in the geyser tube plus atmospheric pressure). Perhaps another modification might be made such that Geis' model now resembles:

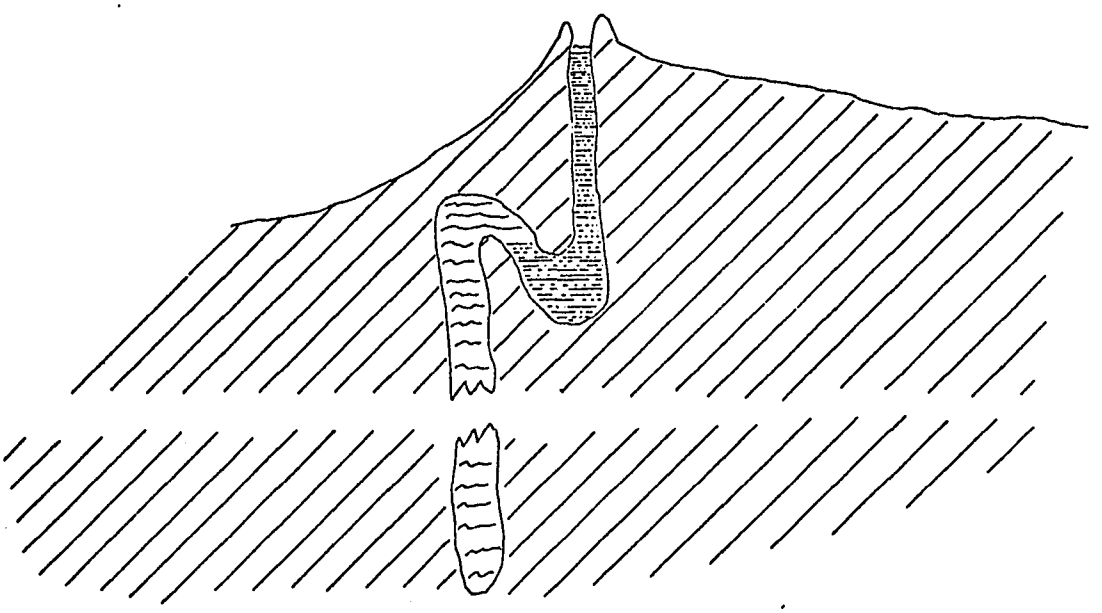

Figure 5. Modified Model of Geis.

Geis' explanation of the model is that the reservoir fills with water, then some of the water spills over into the steam chamber and flash boils, producing an eruption. Usually a sufficient quantity of water spills into the steam chamber to completely evacuate the reservoir, but on occasion only a small amount of water spills into

the steam chamber and the reservoir is not completely emptied; it thus takes a shorter time for the reservoir to refill and another eruption to take place. When a large quantity of water spills into the steam chamber, the internal pressure is larger, producing a higher water jet. Thus, all the facts are again verified as well as the additional facts.

If, during an eruption, the high internal pressure prevents any steam from forming in the geyser column (except near the surface), the pressure as a function of depth can be determined (3). The Reynolds Number during an eruption is about 10^8 and the pressure is approximately 1 lb/in^2 per foot of depth plus atmospheric pressure. Thus, if the column is 100 feet long, the pressure at the bottom of the geyser tube during an eruption would be 111 lb/in^2. The temperature of the ground at this depth is 262°F (if Fenner's data applies) but the boiling point of water is 336°F at this depth. The main objection to Geis' model is that it is physically unrealistic to assume that the ground is hot enough to boil any water that overflows into the steam chamber (at 200 feet, 386°F is the boiling point, but the temperature is only 310°F).

Thus, the steam chamber would have to be much hotter than the surrounding ground. Therefore, it is improbable that the steam chamber is at the same level as the water reservoir. A better explanation is that the steam chamber extends downward a few hundred

feet. This chamber might consist of cracks, fissures, and small voids in the rock structure but it is shown as a cylinder in Figure 5. By hypothesis, this chamber extends down far enough to boil a sufficient quantity of water to expel some or all of the contents of the water reservoir.

Marler (13) has demonstrated that Old Faithful did not build its underground structure, but instead inherited it from a hot spring. The hot spring could have had a much longer tube; the lower portion of the tube now being the steam chamber.

In the upper section of the geyser column, the pressure would eventually become low enough so that flash boiling could occur. However, flash boiling is not instantaneous and the liquid column is rising at almost 100 feet/sec. Thus, it is possible that even if boiling did start to occur at a depth of about 50 feet (it would if the geyser tube was about 200 feet long), it would only take 0.5 second for that water to be expelled. Some liquid would flash to steam, adding to the geyser height, but most of the water would boil in the trumpet-shaped opening of Old Faithful or else outside the geyser tube and thus expand against the atmosphere instead of adding to the geyser jet height.

The amount of liquid water that flash boils in this 0.5 seconds can be approximated by considering the start of the geyser eruption. For Old Faithful, the jet rises (approximately linearly) from zero to

140 feet in about 14 seconds, or 10 ft/sec. For White's geyser, the jet rises from zero to 65 feet in 30 seconds, or about 2 ft/sec. If the initial surge of the geyser jet is due to the formation of steam, then the maximum volume of steam produced in 0.5 seconds is less than 45 ft^3, or, approximately 2 lbs of liquid vaporizes in the upper 50 feet of Old Faithful's geyser tube. This expansion would only add approximately 15 feet to the height of the water jet. The suggestion is that the temperature at the bottom of the trumpet-shaped exit is only a few degrees lower than at the bottom of the geyser tube. As soon as the jet enters the exit section, the absence of confining walls allows very rapid flash boiling and the temperature of the jet drops to 204°F by the time the jet leaves the exit section. Visual observation of the horizontal expansion directly above the exit section indicates that flash boiling in the exit section is almost instantaneous.

As shown earlier (Table I), increasing the degree of superheat decreases the height of the water jet. This is because liquid that vaporizes outside the geyser tube (either above the vent or in the exit section) does not contribute its energy toward lifting the water, but instead uses its energy to expand against the atmosphere.

In 1969, Fournier (7) published a paper strongly criticizing Geis' model. Fournier starts off by saying that Geis' model resembles Bunsen's model. This is clearly incorrect; Rinehart's model is

similar to Bunsen's model. He then presents a heat transfer calculation demonstrating that only 25 percent of the steam required to displace the water in the reservoir could be generated after 30 seconds of flash boiling. However, Old Faithful erupts for 2 to 4 minutes. Also, if the radius of the steam chamber was doubled (Fournier arbitrarily chooses a cavity of 46,000 liters), all the steam required could be generated in 30 seconds. The real point is that the temperature is too low to generate any steam at all (for Geis' original model).

After this, Fournier comments that the water for the eruptions must come from deep underground, not just drain into the reservoir from the surface. This is true, but it strengthens Geis' long tube theory and detracts from Rinehart's short tube theory. Fournier states that in 1963 (no reference given), a tracer experiment showed that more than 24 consecutive eruptions were required to clear Old Faithful's reservoir of rhodamine B. This also strengthens Geis' model and again detracts from Rinehart's model. During an eruption, for Geis' model, the pressure in the reservoir increases and some of the water is lost through the inlet channels. After the eruption, this water flows back into the reservoir. Thus, some of the rhodamine B would flow out the inlet channels during the eruption, then back in again during the quiet period. In Rinehart's model, the pressure is lowered during the eruption; the tracer should all be

ejected during an eruption that empties both reservoirs. Fournier then suggests that the "critical column" theory as explained by White (whose experience appears to be limited to short tube geysers where the "critical column" theory applies) is a better mechanism.

Further field tests are available to verify whether or not the "critical column" theory can apply to Old Faithful. The "critical column" theory represents an unstable mechanism--the system periodically exceeds some critical energy level and then erupts. The "steam chamber" theory requires only that the liquid reservoir finally overflow into a high temperature cavity. Pouring cold water into the geyser vent would abort an eruption for a "critcal column" geyser, but might initiate the eruption for a "steam chamber" geyser. Rapidly raising an inserted plunger would abort an eruption for a "steam chamber" geyser and initiate the eruption for a "critical column" geyser; depressing the plunger would have the opposite effect. Adding a soap solution or dropping sand into the vent would have no effect on a "steam chamber" geyser, but might initiate the eruption for a "critical column" geyser. Other disturbances are considered by White (17).

In conclusion, it has been shown that Old Faithful's geyser tube must be fairly long (between 75 and 300 feet) and also that the "critical column" theory applies only to short tube geysers (less than 50 feet).

REFERENCES

1. Allen, E.T., and A.L. Day. "Hot Springs of the Yellowstone National Park." Carnegie Inst. of Washington Publ. 466, 208 (1935).

2. Barth, T.F.W., "Volcanic Geology, Hot Springs and Geysers of Iceland." Carnegie Inst. of Washington Publ., 587, 76 (1950).

3. Bird, R.B., W.E. Stewart, and E.N. Lightfoot. "Transport Phenomena." John Wiley & Sons, New York, 180 (1960).

4. Bloss, F.D., and T.F.W. Barth. "Observations on Some Yellowstone Geysers." Geol. Soc. America Bull., 60, 861 (1949).

5. Bunseman, R.F., "The Components of a Geyser." New Zealand Jour. Sci., 8, 24 (1965).

6. Fenner, C.N., "Bore Hole Investigations in Yellowstone Park." J. Geol., 44, 225 (1936).

7. Fournier, R.O., "Old Faithful: A Physical Model." Science, 163, 304 (1969).

8. Fournier, R.O., and J.J. Rowe. "Estimation of Underground Temperatures from the Silica Content of Water from Hot Springs and Wet-Steam Wells." Am. Jour. Sci., 264, 685 (1966).

9. Geis, F., Jr., "Old Faithful." Science, 151, 223 (1966).

10. Geis, F., Jr., "Old Faithful: A Physical Model." Science, 160, 989 (1968).

11. Golovina, I.F., and N.N. Malov. "On the Theory of Geysers." Akad. Nauk SSSR Izv., ser. geofiz., 7, 616 (1960). (English Trans.).

12. Keenan, J.H., and F.G. Keyes. "Thermodynamic Properties of Steam." John Wiley & Sons, (1936).

13. Marler, G.D., "The Story of Old Faithful Geyser." Yellowstone Interpretive Ser. (1957).

14. Nichols, H.R., and J.S. Rinehart. "Geophysical Study of Geyser Action in Yellowstone National Park." Jour. of Geophysical Res., 72, 4651 (1967).

15. Peale, A.C., "Thermal Springs (of Yellowstone National Park): Old Faithful Geyser." U.S. Geol. Survey of the Territories, 12, 220 (1883).

16. Rinehart, J.S., "Earth Tremors Generated by Old Faithful Geyser." Science, 150, 494 (1965).

17. White, D.E., "Some Principles of Geyser Activity, Mainly from Steamboat Springs, Nevada." Amer. Jour. Science, 265, 641 (1967).